Effects of beta-2 adrenergic receptor agonists in DOK7 congenital myasthenic syndrome

Lisa K J Clausen

A thesis submitted for the degree of Doctor of Philosophy

Pembroke College

University of Oxford

Trinity Term 2015

Abstract

Effects of beta-2 adrenergic receptor agonists in DOK7 congenital myasthenic syndrome

Lisa K J Clausen
Pembroke College, University of Oxford, Trinity Term 2015
A thesis submitted for the degree of Doctor of Philosophy

Congenital myasthenic syndromes (CMS) are a rare group of heterogeneous disorders, characterised by compromised neuromuscular transmission and symptoms of fatiguable muscle weakness. CMS is caused by mutations in genes that affect the structure and function of the neuromuscular junction (NMJ). In about 20% of CMS cases, patients have mutations in the gene *DOK7*; the protein product, DOK7, is crucial for maintaining the dense aggregation of acetylcholine receptor (AChR) clusters at the NMJ. DOK7-CMS patients do not respond to treatment with acetylcholinesterase inhibitors which are the first line treatment for most forms of CMS. Instead, a dramatic response to beta-2 adrenergic receptor (ADRB2) agonists, such as salbutamol, is observed. The aim of this project was to investigate the molecular mechanisms that underlie the beneficial effects of ADRB2 agonists.

Firstly, NMJ functioning was modelled *in vitro* by studying AChR clusters formed on cultured C2C12 mouse myotubes in the presence of WT DOK7. Overexpression of mutant DOK7 led to a significant reduction in the number of AChR clusters, explaining the pathogenic effect of the mutation. Importantly, incubation of myotubes with salbutamol increased the number of AChR clusters and their stability. The results provide the first evidence that ADRB2 agonists directly affect proteins located at the NMJ. However, this disease model suffers from limitations.

The rest of the thesis focussed on developing alternative cell culture models to explore the AChR clustering pathway. The first model combined optogenetics and fluorescence lifetime microscopy to study the effects of ADRB2 activation on AChR cluster stability in single live cells. The second used CRISPR/Cas9 genome editing tools to directly introduce *Dok7* mutations to the genome of C2C12 cells, thereby overcoming some of the drawbacks associated with DOK7 overexpression. Further manipulations of these novel model systems will be used in the future to examine in more detail the molecular events underlying the pathogenic effects of DOK7 mutations and the mechanisms of ADRB2 agonists. *(Word count: ~37,000)*

Acknowledgements

First of all, I would like to express my sincere gratitude to my supervisor Prof. David Beeson. It has been a privilege to work on this project as part of the neurosciences group, and I am thankful for his immense scientific knowledge and his guidance at all stages of my research.

I would like to thank my secondary supervisor Dr. Judith Cossins, who supported me throughout my D.Phil. studies. Her day-to-day supervision in the lab, the teaching provided in a broad range of methods and techniques and her encouragement have been crucial to the completion of this project. I am also grateful for her very useful comments during the writing of my thesis and the many scientific and non-scientific discussions.

I thank the members of the neurosciences group for their everyday advice. A special thank you goes to Dr. Wei Wei Liu for kindly sharing her expertise on cloning.

The experiments, using FLIM and FRET would not have been possible without the help of Dr. Christoffer Lagerholm. I am very grateful for his hands-on support throughout the experiments, his technical expertise and his enthusiasm for the project.

I would further like to acknowledge Muscular Dystrophy UK which funded this project. Moreover, I am thankful for the travel grants received by the Weatherall Institute of Molecular Medicine, Pembroke College and Guarantors of Brain which allowed me to present my research at national and international conferences.

I am greatly indebted to my parents who always supported and encouraged me throughout my studies both back home and abroad.

Finally, I would like to thank Michael Price for his steady love and support along this journey.

Table of contents

List of figures

List of tables

Abbreviations

AAV	Adeno-associated virus
ACh	Acetylcholine
AChE	Acetylcholinesterase
AChR	Acetylcholine receptor
ADRB2	Beta-2 adrenergic receptor
BSA	Bovine serum albumin
CaMKII	Ca^{2+}/calmodulin-dependent protein kinase II
cAMP	Cyclic adenosine monophosphate
Cas	CRISPR associated
CFP	Cyan fluorescent protein
ChAT	Choline acetyltransferase
CHO	Chinese hamster ovary
CMS	Congenital myasthenic syndrome
CRE	cAMP response element
CRISPR	Clustered regularly interspaced short palindromic repeat
DGC	Dystrophin-glycoprotein complex
DMEM	Dulbecco's Modified Eagle's Medium
DNA	Deoxyribonucleic acid
DOK7	Downstream-of-tyrosine-kinase 7
DPAGT1	Dolichyl-phosphate (UDP-N-acetylglucosamine) N-acetylglucosaminephosphotransferase 1 (GlcNAc-1-P transferase)
Dvl	Dishevelled
EGFP	Enhanced green fluorescent protein
EMG	Electromyography
Epac	Exchange protein directly activated by cAMP
EPP	Endplate potential
FCS	Foetal calf serum
FLIM	Fluorescence lifetime imaging microscopy
FOV	Field of view
FRAP	Fluorescence recovery after photobleaching
FRET	Förster resonance energy transfer
GDP	Guanosine diphosphate
GEF	Guanine nucleotide exchange factor
GFPT1	Glutamine-fructose-6-phosphate transaminase 1
GLMM	Generalised mixed effects model
GMPPB	GDP-mannose pyrophosphorylase B
GTP	Guanosine triphosphate
GTPases	Guanosine triphosphatases
HEK	Human embryonic kidney
HS	Horse serum

iPSC	Induced pluripotent stem cell
LB	Lysogeny broth
LRP4	Low-density lipoprotein receptor-related protein 4
MG	Myasthenia gravis
MuSK	Muscle specific kinase
NMJ	Neuromuscular junction
Opto	Optogenetic
PAM	Protospacer adjacent motif
PBS	Phosphate-buffered saline
PREPL	Prolyl-endopeptidase-like
PCR	Polymerase chain reaction
PH	Pleckstrin homology
PKA	Protein kinase A
PKC	Protein kinase C
PTB	Phosphotyrosine-binding
QMG	Quantitative myasthenia gravis score
RNA	Ribonucleic acid
RNAi	RNA interference
SFK	Src family kinase
SH2	Src homology 2
siRNA	Short interfering DNA
SPAD	Single-photon avalanche diode
SSRs	Short sequence repeats
TALEN	Transcription activator-like effector nucleases
TBE	Tris-Borate-EDTA
TCSPC	Time-correlated single photon counting
Tg	Transgenic
TIRFM	Total internal reflection fluorescence microscopy
WLL	White light laser
YFP	Yellow fluorescent protein
ZNF	Zinc finger nuclease
3,4-DAP	3,4-Diaminopyridine

CHAPTER 1

Introduction

Muscle contraction depends on the transmission of action potentials from motor neurons to muscle fibres (reviewed in Ruff, 2011). This neuromuscular transmission occurs at highly specialised chemical synapses, called neuromuscular junctions (NMJs). Large in size and experimentally accessible, the NMJ provides a widely used model system to investigate the general mechanisms of synaptic development and also synaptic dysfunction (Shi et al., 2012). The NMJ is an important target for neurological diseases, including both genetic and autoimmune disorders (Tintignac et al., 2015). Myasthenic disorders cause fatiguable muscle weakness which, if left untreated, may be life-threatening (Rodriguez Cruz et al., 2014). The research topics presented within this thesis focus on a subtype of inherited muscle weakness, DOK7 congenital myasthenic syndrome, and the molecular mechanisms underlying its treatment with beta-2 adrenergic receptor agonists. This introductory chapter gives an overview on the functioning of the neuromuscular synapse, its impairment in congenital myasthenic syndromes and other disorders, and the relevant treatment strategies.

1.1 The neuromuscular junction

1.1.1 Signal transmission at the neuromuscular synapse

Each skeletal muscle fibre receives input from one motor nerve fibre (Wu et al., 2010). When an action potential reaches the nerve terminal, voltage-dependent calcium channels open, and the influx of Ca^{2+} ions causes vesicles containing the neurotransmitter acetylcholine (ACh) to fuse with the presynaptic cell membrane (Ruff, 2011) (Fig. 1.1A).

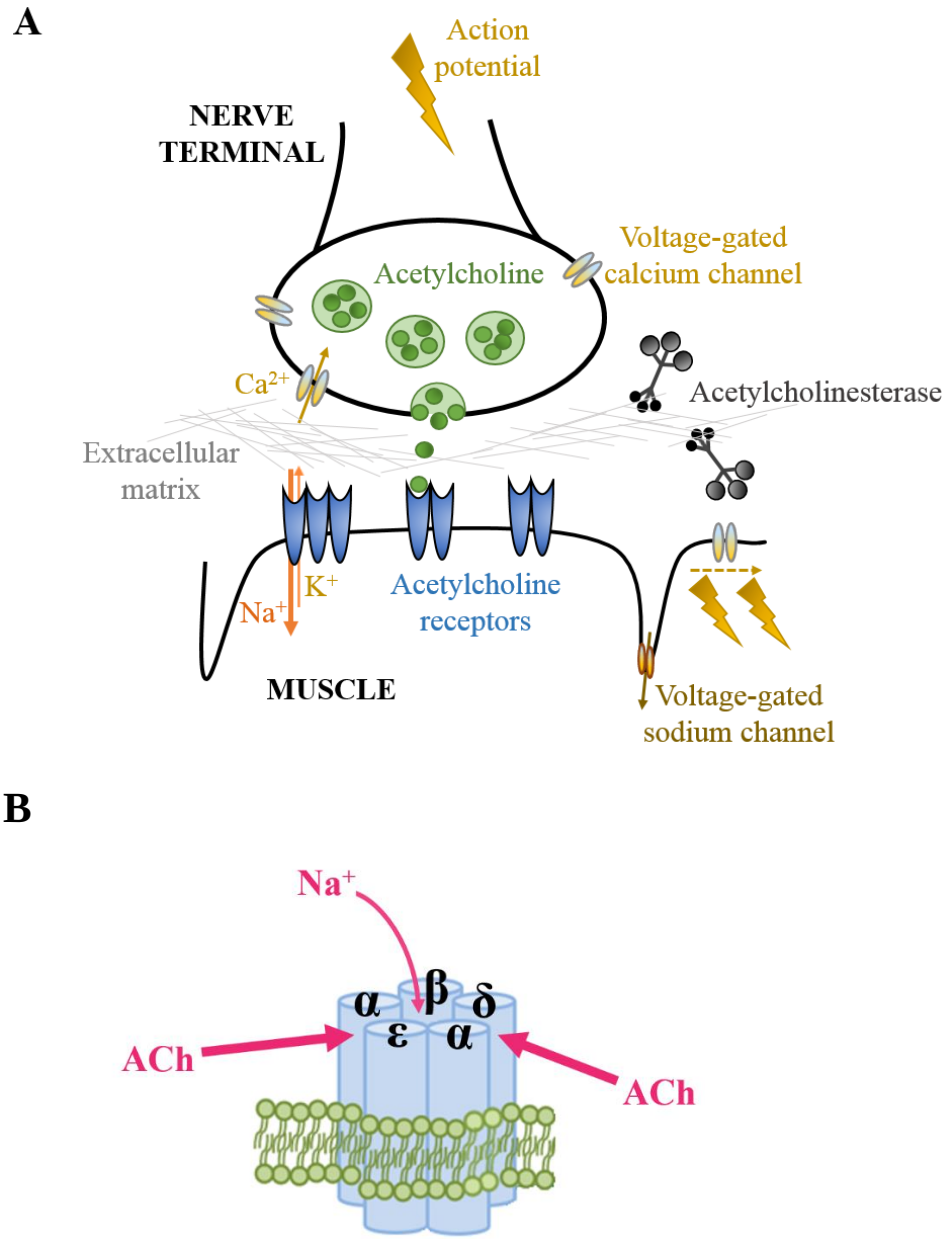

Figure 1.1 Signal transmission at the NMJ. (A) A nerve-derived action potential causes acetylcholine (ACh) to be released from the nerve terminal and to bind to ACh receptors (AChRs) located on the muscle membrane. The resulting influx of sodium ions triggers an endplate potential (EPP) which can then cause an action potential that induces muscle contraction. (B) Pentameric structure of the adult AChR. ACh binds at the interface between the adjacent subunits α-δ and α-ε.

Exocytosis occurs, ACh is released into the 50-80nm-wide synaptic cleft and binds to nicotinic acetylcholine receptors (AChRs) on the motor endplate.

AChRs are large glycoproteins (290kDA) and are highly enriched at the crests of junctional folds (~10,000/μm^2) (Martin, 1994, Shi et al., 2012). Each receptor forms a pentamer and is composed of a ring of the subunits α1, β1, δ, γ in the fetal form, and α1, β1, δ, ε in the adult form (Auerbach, 2015, Unwin, 2005) (Fig. 1.1B). The proteins are encoded by the genes *CHRNA1, CHRNB1, CHRND, CHRNG and CHRNE,* respectively (Schaaf, 2014). Two α1 subunits are separated by a γ or ε subunit and a βδ dimer (2:1:1:1 ratio). AChRs have a large N-terminal extracellular domain for ACh binding, a membrane-spanning pore and an intracellular domain. AChR binds at two sites on opposite sides of the pore at the interface between adjacent subunits (α-δ and α-γ/ε) (Unwin, 2005). This causes a conformational change in the receptor and opening of a cationic channel which allows Na^+ and Ca^{2+} ions to enter and K^+ ions to exit the muscle. Since the net flow of positively charged ions is inward, a localised depolarisation occurs, called the endplate potential (EPPs) (Ruff, 2011). EPPs themselves do not propagate but trigger the opening of voltage-gated Na^+ channels located in the folds of the postsynaptic membrane. This may result in an action potential which travels along the muscle fibres and induces muscle contraction.

Action potentials are generated as an all-or-none response to EPPs, which have to be large enough to exceed the action potential threshold. Normally, the excitatory effect of nerve stimulation is in excess of what is required to generate an action potential. This so called safety factor allows for times when the muscle is under stress, and can be described by the EPP, divided by the voltage difference between the resting potential and the action potential threshold (Ruff, 2011, Wood and Slater, 2001). If the safety factor is larger than one, an EPP triggers an action potential. Amongst other factors, the size of

the nerve terminal, the density of AChRs, the AChR conductance, Na^+ channels, and the quantal content (numbers of synaptic vesicles released) have an influence on the safety factor. Most neuromuscular transmission diseases cause muscle weakness by reducing the safety factor (Ruff, 2011, Wood and Slater, 2001). ACh eventually gets hydrolysed to acetate and choline by acetylcholinesterase (AChE).

1.1.2 Structure and functioning of the neuromuscular synapse

The development and maintenance of the neuromuscular junction depends on a complex interplay of proteins located pre- and postsynaptically (Fig. 1.2). The formation of a dense array of AChRs on the postsynaptic membrane beneath the nerve terminal is a central event in neuromuscular development, and is also essential for maintaining synaptic functioning by enabling efficient signal transduction (Wu et al., 2010).

The agrin-LRP4-MuSK signalling pathway

Studies from the 1970s/80s on synaptic development suggested that motor nerves stimulate the redistribution and accumulation of AChRs on the muscle fibre (Frank and Fischbach, 1979, Burden et al., 1979). The search for nerve-derived factors that affect AChR aggregation led to purification of agrin from the Torpedo electric organ (Godfrey et al., 1984, Nitkin et al., 1987). Agrin is a 225kDa heparin sulphate proteoglycan, synthesised in motor neurons and released into synaptic basal lamina. In cultured muscle cells, agrin stimulated the formation of AChR clusters, associated with the accumulation of other cytoplasmic, membrane and extracellular matrix components, such as acetylcholinesterase and rapsyn (Campanelli et al., 1991, Wallace, 1989). Furthermore, findings on the different agrin splice variants suggested a role of agrin in NMJ development. It was shown that agrin with an eight amino acid insert in the C-terminal at a site called Z is the most active isoform in AChR clustering assays, and that this insert

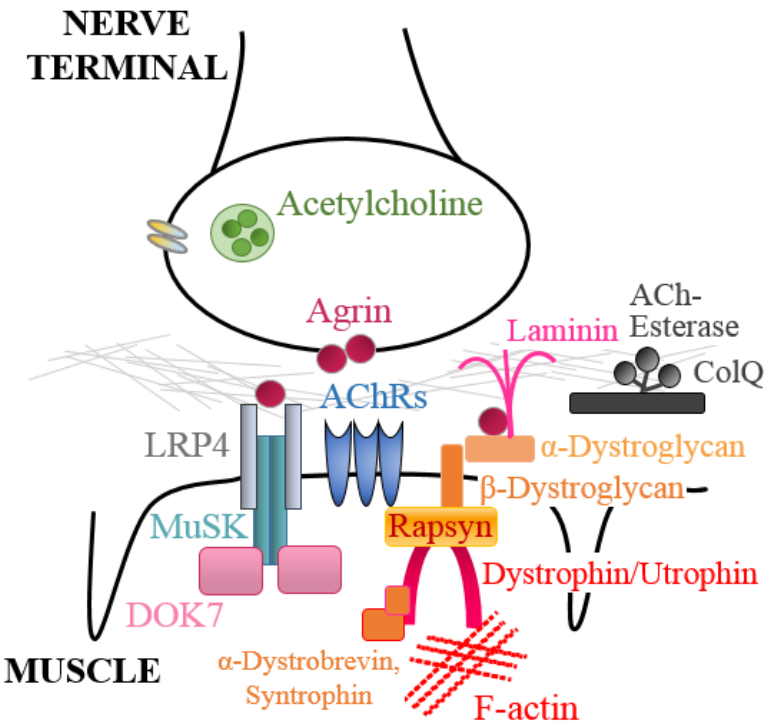

Figure 1.2 Structure of the NMJ. The development and maintenance of the NMJ depends on a complex interplay of proteins located pre- and postsynaptically. Signal transmission depends on the aggregation of AChRs on the postsynaptic membrane. Agrin is a key molecule in the AChR clustering pathway and stimulates MuSK phosphorylation via LRP4. DOK7 acts as a muscle intrinsic activator of MuSK.

is absent in non-neural agrin expressed in myotubes and Schwann cells (Kleiman and Reichardt, 1996, Gesemann et al., 1995). It was also shown, in experiments using isoform-specific mutant mice and nerve-muscle co-cultures, that the non-neural isoforms of agrin are dispensable for synaptogenesis (Burgess et al., 1999). Together, these findings provided support for the "agrin hypothesis", according to which nerve-derived z-agrin induces the aggregation of AChRs (Kleiman and Reichardt, 1996). Neural agrin is henceforth referred to as agrin.

In vivo experiments conducted in Joshua Sanes' laboratory significantly enhanced our understanding of the agrin signalling pathway at the NMJ. Agrin-deficient mice died shortly before birth and showed severe pre- and postsynaptic disorganisation (Gautam et al., 1996). Muscle staining with alpha-bungarotoxin, which specifically binds to AChRs, showed that in muscle tissue from healthy controls each muscle fibre bears one AChR cluster. In muscle from the homozygous agrin mutants, AChR aggregates were present but significantly smaller, and the distribution of clusters was disturbed, with some myotubes showing no or more than one cluster. Moreover, the receptor density was reduced. *In vitro*, impaired AChR clustering could be rescued by incubation of myotubes from agrin-mutant mice with agrin. Antibody staining of neurofilaments and synaptic vesicle proteins revealed a lack of nerve-innervation of the majority of clusters and disturbed axonal branching as well as excessive axon growth (Gautam et al., 1996). Cell culture experiments on neurite outgrowth in CHO cells later suggested that agrin acts as a stop signal that prevents axonal growth and guides presynaptic fibres to the endplates (Chang et al., 1997).

It was shown that agrin affects intracellular kinase activity, such as the phosphorylation of AChRs (Wallace et al., 1991), and that kinase inhibitors prevent agrin-mediated AChR aggregation (Wallace, 1994). The discovery of muscle-specific

kinase (MuSK) led to a greater understanding of how agrin affects NMJ development (Glass et al., 1996). MuSK is expressed in skeletal muscle and upregulated during myotube formation, and was found to be concentrated at NMJs (Valenzuela et al., 1995). Similar to agrin-deficient mice, MuSK knockout mice died at birth and showed severe neuromuscular dysfunction (DeChiara et al., 1996). New-born pups did not breathe and were immobile at birth. Moreover, no arborized nerve terminals but continuous axon growth was observed. Staining of diaphragm muscle showed that no AChR aggregates had formed. Unlike agrin deficient mice, other post- or subsynaptic membrane and basal lamina proteins, such as erbB, dystroglycan, rapsyn, and the laminin-β2/s-laminin subunit, which are usually found at NMJs, were absent.

The findings strongly suggested an interaction of agrin and MuSK, a hypothesis which was further supported by cell culture experiments (Glass et al., 1996). MuSK was shown to be indispensable for agrin-mediated AChR clustering: Cultured muscle cells from MuSK-deficient mice fused into myotubes and showed similar AChR expression levels as control cells, but failed to form AChR clusters in response to incubation with agrin. Further experiments on the interaction of the two proteins demonstrated that agrin induces MuSK tyrosine phosphorylation, but also showed that agrin does not directly bind to MuSK (Glass et al., 1996). The search for a binding partner of agrin led to the finding that agrin causes MuSK activation via binding to transmembrane protein low-density lipoprotein receptor-related protein 4 (LRP4) (Kim et al., 2008). Accordingly, LRP4 deficient mice displayed pre- and postsynaptic defects that resembled those of MuSK deficient mice (Weatherbee et al., 2006). MuSK contains the phosphotyrosine-binding (PTB) target motif Asn-Pro-X-Tyr, encompassing Tyr553 in the juxtamembrane region, which in interaction with a PTB binding domain is used for autophosphorylation and recruitment of downstream signalling molecules (Watty et al., 2000). When released

from the nerve terminal, agrin binds to LRP4 which leads to complex-formation of LRP4 and MuSK (Kim et al., 2008). As a result, MuSK autophosphorylates in its juxtamembrane region at Tyr553. Subsequent phosphorylation of tyrosine residues 750, 754 and 755 in the activation loop of the kinase domain switches MuSK to an active state and is essential for downstream kinase activity (Ghazanfari et al., 2011).

The 43kDa receptor-associated protein rapsyn was purified from Torpedo electric organ around the same time as agrin (Frail et al., 1988). Cell culture and *in vivo* experiments showed that rapsyn co-localises with AChRs and that rapsyn leads to clustering of otherwise diffusely distributed AChRs (Noakes et al., 1993, Froehner et al., 1990). Animal-knockout studies confirmed the importance of rapsyn for AChR aggregation (Gautam et al., 1995). The phenotype of the rapsyn-mutant was similar to the one observed in agrin- and MuSK-mutant mice. Homozygous mutants were weak and died shortly after birth. AChR aggregates were absent from muscle fibres, and cultured myotubes from mutants failed to form AChR clusters in response to agrin. Presynaptic specialisations formed but axons grew excessively. The results indicated that rapsyn is an indispensable molecule in the agrin-LRP4-MuSK signalling pathway. It was shown in subsequent experiments that rapsyn may act as a scaffolding protein that aggregates AChRs and links them to the cytoskeleton (Shi et al., 2012).

Despite striking evidence that nerve innervation drives postsynaptic development and its maintenance via agrin signalling, several observations made in the last decade pointed towards a more complex and dynamic mechanism. It was shown that in the absence of nerve innervation AChR pre-patterning occurs: in embryonic muscle from agrin-deficient mice, AChRs were found to be aggregated (Lin et al., 2001). Moreover, AChR clusters were present in embryonic diaphragm muscle from mouse mutants, whose diaphragm muscles was rendered aneural (Yang et al., 2001, Lin et al., 2001). No AChR

pre-patterning occurred, however, in MuSK or rapsyn mutants. While aneural AChR clusters increased in size as development proceeded, clusters from innervated muscle from agrin-deficient mice dispersed (Lin et al., 2001). These finding led Joshua Sanes to propose a model, according to which postsynaptic differentiation is regulated by both positive and negative signals (Kummer et al., 2006, Sanes and Lichtman, 2001).

Numerous studies have demonstrated a destabilising effect of ACh, which appears to be counteracted by agrin signalling. ACh was found to downregulate AChR gene expression (Sanes and Lichtman, 2001). Moreover, it was shown that animals harbouring a mutation in ChAT, the synthetic enzyme for ACh, showed larger AChR aggregates in late embryonic state than WT animals with active synaptic sites (Misgeld et al., 2002, Brandon et al., 2003). The authors showed that AChR clusters formed on muscles from agrin mutant mice were more stable if the muscle was denervated. The finding that in ChAT-agrin double knockout animals AChR clusters formed, suggested that an important function of agrin is to counteract neurotransmission-mediated dispersal. Further evidence came from cell culture experiments, where agrin prevented the breakdown of AChR clusters, caused by incubation with the cholinergic agonist carbachol (Lin et al., 2005). It has been suggested that the nerve-derived dispersing signal might be mediated via Cdk5, a cytoplasmic serine/threonine kinase (Lin et al., 2005). Cholinergic stimulation activated the cysteine protease calpain, which generated p25 from protein p35, which in turn led to increased activity of Cdk5 (Chen et al., 2007). In cell culture, blocking of Cdk5 or calpain prevented the ACh-mediated breakdown of agrin-induced AChR clusters. There is evidence that rapsyn acts as a calpain inhibitor, mediated through agrin, and exerts a stabilising effect on AChR clusters (Chen et al., 2007). Of note, besides ACh, other molecules such as tyrosine phosphatases have been shown to have a dispersing effect on AChRs. For example Shp2, activated by SIRPα1 in

response to agrin-mediated activation of MuSK, was shown to disperse prepatterned AChR clusters, to reduce the formation of novel AChR clusters and to regulate AChR gene expression (Qian et al., 2008).

The precise apposition of an endplate with a nerve terminal during synaptic development and the enrichment of AChR clusters at synaptic sites therefore depends on both positive and negative signals (Kummer et al., 2006). While MuSK is indispensable for AChR aggregation, agrin appears to play an important role by acting as an 'anti-de-clustering' factor.

The DOK7-MuSK signalling pathway

The question remained how MuSK-dependent AChR aggregates are formed in the absence of agrin or prior to nerve innervation. By investigating muscle from mice which lack motor axons, it was shown that MuSK expression is patterned independently of nerve innervation (Kim and Burden, 2008). In muscle from transgenic mice that express MuSK uniformly along the muscle and lack motor axons, widely scattered NMJs were observed. In the same study it was shown that, *in vivo*, upregulating MuSK expression rescued the lethality of agrin-mutant mice. These findings strongly suggested a muscle-derived molecule that can act as a MuSK activator and promote postsynaptic differentiation. A search for the binding partner for the MuSK PTB domain target motif Asn-Pro-XTyr, encompassing Tyr553 in the juxtamembrane region led to the discovery of a novel key molecule involved in NMJ functioning. Okada et al. (2006) identified downstream-of-tyrosine-kinase-7 (DOK7) as a novel member of the DOK-family of proteins. The N-terminal portion of DOK7 contains a pleckstrin-homology (PH) and a PTB domain, while the C-terminal half contains Src homology 2 (SH2) domain target motifs (Fig. 1.3A).

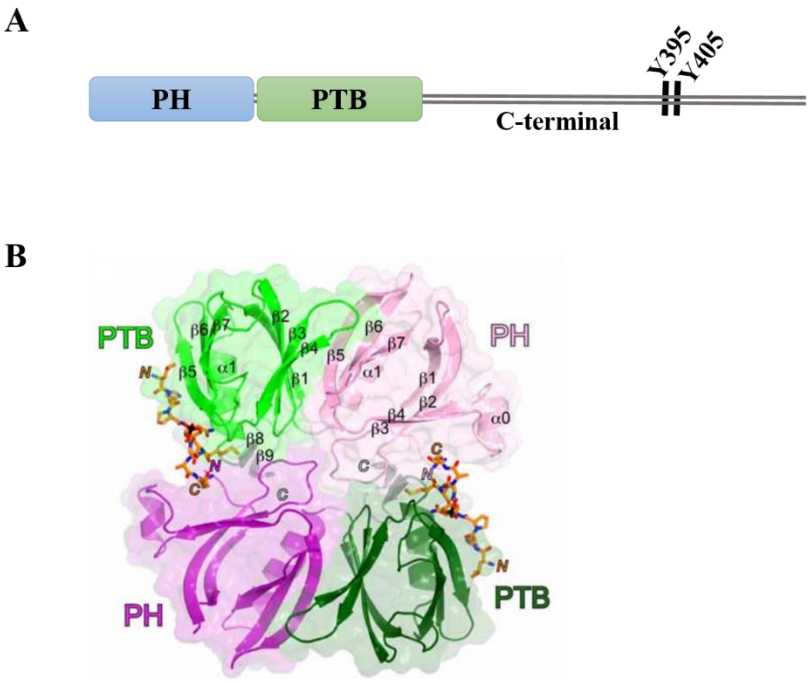

Figure 1.3 DOK7 structure. (A) The N-terminal portion of DOK7 contains a pleckstrin-homology (PH) and a phosphotyrosine-binding (PTB) domain. The C-terminal half contains SH2 target motifs encompassing Tyr395/Tyr405 which are binding sites for CrkII/CrkL. (B) Crystal structure of the DOK7 PH/PTB domains in complex with a phosphopeptide including pTyr553 in MuSK (figure taken from Bergamin et al. (2010)). The structure shows that DOK7 PH-PTB forms a dimeric structural unit, which causes MuSK dimerisation and *trans*-autophosphorylation of tyrosine residues in the MuSK activation loop.

DOK7 is expressed in heart and skeletal muscle, and is enriched at NMJs (Okada et al., 2006). The authors showed that overexpression of DOK7 in C2C12 mouse muscle cells caused tyrosine-phosphorylation of MuSK, which resulted in phosphorylation of the AChR beta-subunit and in the formation of mature "pretzel-like" AChR clusters. No clusters formed in the absence of MuSK. Downregulation of DOK7, using small inferring RNA, suppressed spontaneous MuSK-dependent AChR aggregation and also prevented agrin-induced AChR clustering. DOK7 and MuSK only co-immunoprecipitated when the MuSK tyrosine residue 553 in the PTB target motif was intact, suggesting that DOK7 binds to MuSK via the PTB domain. Results on the crystal structure of DOK7 and further biochemical experiments confirmed that DOK7 selectively binds to phosphorylated Tyr553 in the MuSK juxtamembrane region, and, through dimerization of its PH-PTB domains, brings together two MuSK kinase domains for autophosphorylation of the kinase activation loops (Bergamin et al., 2010) (Fig. 1.3B).

DOK7 knock-out mice were immobile at birth and died (Okada et al., 2006). Similar to MuSK-mutant mice, no AChR clustering could be observed in diaphragm muscle, and axons were abnormally long. Thus, DOK7 appears to act as a muscle-intrinsic activator of MuSK, indispensable for downstream signalling and AChR aggregation.

Of note, in cultured myoblasts, the PTB domain and the COOH-terminal region were found to be dispensable for MuSK activation, whereas in fully differentiated myotubes these domains were required for MuSK activation and AChR clustering (Okada et. al, 2006). This suggests a negative regulatory mechanism that prevents MuSK activation during myotube formation.

Okada et al. generated DOK7 transgenic (Tg) mice, expressing human DOK7-EGFP (Inoue et al., 2009). Myofibres from DOK7-Tg mice had multiple AChR clusters

and the endplate band was wider than in control mice. The finding that AChR aggregation and the accumulation of MuSK transcripts in the central muscle region was increased in DOK7 Tg embryos, but decreased in DOK7 knockout mice, indicated that DOK7 has a role in regulating MuSK localisation. Moreover diaphragm muscle from the Tg mice contained a larger number of NMJs and MuSK phosphorylation was increased compared to WT mice. These findings suggested that DOK7 activates MuSK *in vivo*. Myotubes from DOK7 knockout mice failed to form AChR clusters in response to agrin but exogenous expression of DOK7 restored this function (Inoue et al., 2009).

Not only the PH and the PTB domain, but also the C-terminal region of DOK7 contains functional elements. Mutations which cause ablation of the entire COOH-terminal region, lead to a DOK7 protein that is unable to activate MuSK (Hamuro et al., 2008). Hamuro et al. (2008) identified a chromosome region maintenance 1-dependent nuclear export signal (NES) in the C-terminal of DOK7, which together with the PH domain is required for DOK7 to shuttle between the nucleus and the cytoplasm and to activate MuSK. Moreover, DOK7 has SH2 target motifs in the C-terminal: two Tyr-Xaa-Xaa-Pro motifs encompassing Tyr395 or Tyr405 (Hamuro et al., 2008). Mutation of these residues led to a reduction in MuSK activation and to severely impaired AChR clustering in muscle cultures. The authors identified the adaptor protein CrkII as a binding partner for DOK7, which consists of the SH2 and SH3 domains. CrkII binds to DOK7 via the interaction of its SH2 domain and the DOK7 SH2 target motifs encompassing Tyr395/Tyr405. Similar findings were reported by Hallock et al. (2010) who demonstrated that the DOK7 C-terminal plays a modest role in MuSK phosphorylation and is essential for postsynaptic differentiation. CrkII/CrkL deficient mice died at birth and showed impaired pre- and postsynaptic differentiation with smaller synapses, lack of AChR aggregation and nerve denervation (Hallock et al., 2010).

Thus, it appears that the interplay of nerve derived factors, such as agrin and AChR signalling, and muscle-derived molecules, such as DOK7, mediates synaptogenesis *in vivo*. Figure 1.4 displays a simplified model of DOK7, MuSK and agrin functioning, as proposed by Inoue et al. (2009). DOK7 expressed in the central muscle region activates MuSK, which in turn has an effect on MuSK acting predominantly in the central region of the muscle. Independently of nerve innervation, MuSK activity triggers postsynaptic differentiation. Resulting AChR aggregates which get opposed by a nerve terminal are stabilised via agrin signalling which leads to full activation of MuSK and which counteracts the dispersing effect of ACh. On the other hand, AChR clusters which lack nerve innervation are dispersed.

In a recent study it was shown that overexpression of DOK7 in muscle from agrin-deficient mice caused increased MuSK activation and restored NMJ formation. However, after birth, despite unaltered DOK7-mediated MuSK activation, these NMJs dispersed quickly (Tezuka et al., 2014). This finding suggests a potential role of agrin for postnatal NMJ maintenance in addition to MuSK activation.

Signalling pathways involved in AChR aggregation downstream of MuSK

MuSK activation leads to the stimulation of a large number of downstream signalling cascades which orchestrate AChR aggregation, anchorage to the cytoskeleton and recycling of AChRs (Wu et al., 2010).

The scaffolding protein rapsyn is crucial for MuSK-induced AChR aggregation and stability (Gautam et al., 1995). Rapsyn likely acts via multiple mechanisms and is thought to interact with a number of molecules, such as AChRs (Moransard et al., 2003), beta-dystroglycan (Cartaud et al., 1998, Bartoli et al., 2001), actin (Antolik et al., 2007), the

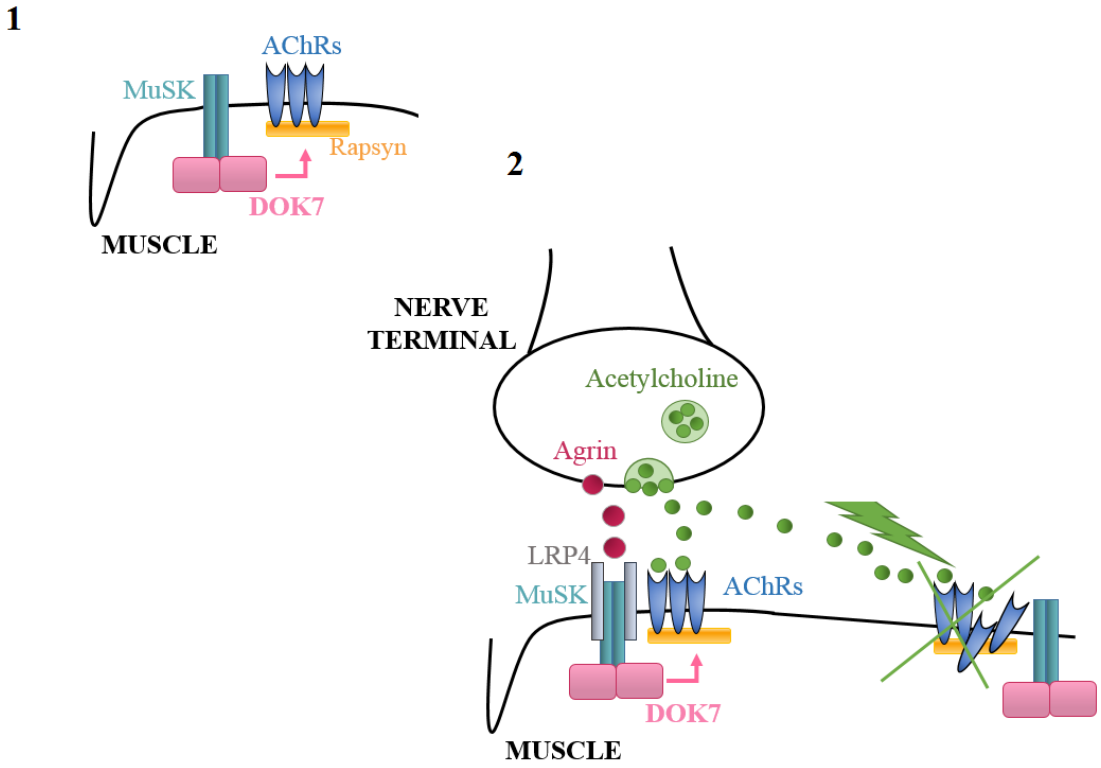

Figure 1.4 Interaction of positive and negative signals during synaptogenesis. (1) DOK7 is expressed in the central muscle region and activates MuSK, which induces AChR aggregation in the central region of the muscle. (2) AChR clusters opposed by a nerve terminal are stabilised through agrin, which fully activates DOK7-primed MuSK and counteracts the effects of ACh. ACh diffuses distantly and leads to the dispersal of clusters that lack nerve innervation (model proposed by Inoue et al. (2009)).

actin cross-linker alpha-actinin (Dobbins et al., 2008), beta-catenin (Zhang et al., 2007), calpain (Chen et al., 2007) and heat-shock protein 90β (Luo et al., 2008). Altogether, there is compelling evidence that rapsyn serves as a bridge between AChRs and cytoskeletal proteins.

Part of these 'anchoring' proteins is the dystrophin-glycoprotein complex (DGC), which is thought to contribute to postsynaptic maturation and NMJ maintenance by anchoring AChR clusters to the extracellular basal lamina and the intracellular cytoskeleton (Banks et al., 2003). The DGC includes alpha-dystroglycan (extracellular) and beta-dystroglycan (transmembraneous), the cytoplasmic actin-binding proteins dystrophin and utrophin and the cytoplasmic proteins alpha-dystrobrevin and syntrophins (Banks et al., 2003). Alpha-dystroglycan binds to agrin and laminin, while beta-dystroglycan may bind to rapsyn and dystrophin/utrophin (Shi et al., 2012). Muscle cells deficient in dystroglycan form less stable AChR clusters in response to agrin incubation (Jacobson et al., 2001, Grady et al., 2000).

In the last two decades, a large number of molecules downstream of MuSK were discovered, and the importance of kinase activity for NMJ development and maintenance emerged. It was shown in cultured muscle cells that agrin stimulates activity of the tyrosine kinases Abl, which was required for agrin-mediated AChR clustering and for MuSK phosphorylation (Finn et al., 2003). Abl kinases were found to be enriched at NMJs and able to engage in reciprocal tyrosine phosphorylation and complex formation with MuSK. It was proposed that Abl kinase activation could induce phosphorylation and activation of members of the Rho family of small guanosine triphosphatases (GTPases), such as Rac and Cdc42, which were previously shown to be important for the clustering of AChRs in muscle cultures (Weston et al., 2000), as well as induce activation of Pak and other targets of activated GTPases (Finn et al., 2003). There is evidence that the

serine-threonine kinase PAK1 is associated with MuSK via dishevelled (Dvl) (Luo et al., 2002) and that PAK1 regulates actin dynamics through phosphorylation of cortactin (Webb et al., 2006).

Both Abl and Src-family kinases (SFKs) can trigger the phosphorylation of the AChR beta subunit in response to agrin which precedes AChR clustering (Borges and Ferns, 2001, Mittaud et al., 2004, Finn et al., 2003). AChR beta-subunit phosphorylation appears to affect the stability of AChR aggregates, although it is not essential for their formation (Borges and Ferns, 2001, Friese et al., 2007). Reduction of SFK functioning in the soleus muscle of mice caused fragmentation of NMJs, and in Src- and Fyn-deficient myotubes, the interaction between AChRs and rapsyn was found to be less stable after the removal of agrin (Sadasivam et al., 2005). Moreover, less alpha-dystrobrevin remained bound to AChRs when compared to control cells and AChR beta-subunit phosphorylation decreased more quickly in the mutant.

A significant amount of research on kinase pathways involved in AChR stability was conducted by Mohammed Akaaboune. A recent study pointed towards an important role of serine/threonine kinases at the NMJ. Skeletal muscle expresses protein kinase A (PKA) and protein kinase C (PKC), and it appears that these kinases exert antagonistic effects on the stability and recycling of AChRs *in vivo* (Martinez-Pena y Valenzuela et al., 2013). It was shown that either the inhibition of PKC or the activation of PKA enhances the recycling of internalised AChRs into synaptic sites and stabilises existing AChRs on the membrane. On the other hand, activation of PKC or inhibition of PKA reduce the recycling of receptors and stimulates the removal of receptors from the membrane. It was shown recently that PKA in interaction with myosin A might regulate AChR recycling and stability through its anchoring at NMJs by rapsyn (Choi et al., 2012).

Moreover, as mentioned above, the intracellular calcium-concentration was shown to have an effect on AChR recycling (Martinez-Pena y Valenzuela et al., 2010). Ca^{2+}/calmodulin-dependent protein kinase II (CaMKII), a serine/threonine protein kinase family member, gets activated by calcium and calmodulin, and appears to mediate the regulation of AChR recycling in response to changes in intracellular calcium levels. Inhibition of CaMKII did not affect internalisation of AChRs on the membrane, but blocked AChR recycling and led to intracellular accumulation of internalized AChRs (Martinez-Pena y Valenzuela et al., 2010).

The discovery of a growing number of kinase pathways advances our understanding of how downstream signalling of MuSK may ultimately lead to AChR stabilisation via rapsyn. It was shown that these kinases can be found enriched in different locations at the NMJ, and that they may act by interacting with AChR subunits directly or with proteins involved in stabilising AChRs (Martinez-Pena y Valenzuela et al., 2013). Future research is required to unravel the precise mechanisms by which kinases affect their targets, and how their signalling cascades interact. Indeed, the studies cited above suggest that NMJ functioning might be regulated by a complex but balanced interplay of kinases.

1.2 Disorders of the neuromuscular junction

The refined structure of the NMJ makes it a target for disease: Mutations in the genes coding for NMJ proteins can cause congenital myasthenic syndrome (CMS), whereas autoantibodies to neuromuscular proteins can result in autoimmune disorders, such as myasthenia gravis (Cruz et al., 2014, Vincent et al., 2012). Most neuromuscular transmission disorders cause symptoms of muscle weakness but only show a beneficial response to specific treatment regimens (Rodriguez Cruz et al., 2014). A differential

diagnosis is therefore crucial. While disease onset with myasthenic features at birth or early infancy can hint towards CMS, a late and rapid disease onset can point towards an autoimmune disorder. On the other hand, autoimmune disorders can be present at birth or early in childhood (Hoff et al., 2007, Yang et al., 2015), and some forms of inherited myasthenia may not manifest until well into adulthood (reviewed in Engel et al. 2015).

In patients with a suspected NMJ disorder, neurophysiological testing usually reveals abnormalities. These are found in both MG and CMS (reviewed in Finlayson et al. 2013a). Single-fibre electromyography (EMG), which is used to record action potentials from individual muscle fibres, often shows abnormal jitter measurement, which results from excessive variation in the time that the EPP requires to reach the action potential threshold. Repetitive nerve stimulation often shows progressive decrease or decrement (>10%) in the amplitude of the muscle action potential at low rates of nerve stimulation (reviewed in Finlayson et al. 2013a). In order to make a differential diagnosis between an autoimmune disorder and CMS, patients undergo testing for autoantibodies.

1.2.1 Myasthenia gravis

Myasthenia gravis (MG) is the most common disorder of the NMJ with a prevalence between 70 and 163 per million (Carr et al., 2010). In ~80% of patients, MG is caused by autoantibodies to the AChR (Lindstrom et al., 1976). AChR antibodies cause loss of AChRs via complement-mediated damage of the postsynaptic membrane (Engel, 1984), increased AChR endocytosis (Heinemann et al., 1977) and sometimes direct AChR block (Burges et al., 1990).

In 10-15% of MG cases, AChR antibodies cannot be detected despite the use of sensitive clustered AChR cell based assays, and patients belong to the group of seronegative MG (reviewed in Koneczny et al., 2014). Up to 64% of these patients are

diagnosed with antibodies to MuSK (Lindstrom et al., 1976, Koneczny et al., 2014). It was shown in cell culture that antibodies from MuSK MG patients can inhibit AChR clustering (Hoch et al., 2001) and disrupt the interaction between MuSK and LRP4 (Koneczny et al. 2013, Huijbers et al. 2013). Moreover, antibodies caused dispersal of agrin-induced clusters and, secondly, dispersal of agrin-independent clusters formed on DOK7-overexpressing cells, suggesting direct MuSK inhibition (Koneczny et al., 2013).

1.2.2 Congenital myasthenic syndrome

If the test for autoantibodies is negative, patients with myasthenic symptoms might suffer from a genetic condition. CMS is a group of inherited neuromuscular disorders caused by mutations in genes that affect proteins located at the NMJ (reviewed in Engel et al., 2015). These are rare conditions with an overall incidence of ca. 1:100,000 and a prevalence in the UK of 9.2 cases per one million children below the age of 18 (Parr et al., 2014). This number only includes genetically confirmed cases and the prevalence is expected to increase since, for many patients with a clinical diagnosis, the underlying mutation(s) have yet to be determined.

CMS is a very heterogeneous group of disorders, with at least 20 affected genes identified (reviewed in Cruz et al., 2014b). Apart from slow-channel syndrome, all types of CMS are autosomal recessive. CMS generally results in a reduced safety factor, but clinical features, age of onset and treatment strategies differ depending on the mutation (reviewed in Engel et al., 2015, Finlayson et al., 2013a). In many cases of CMS, neurophysiological findings combined with phenotypical observations point towards a candidate gene and a genetic diagnosis can be made, confirmed by Sanger sequencing. A broad spectrum of mechanisms have been shown to cause CMS, although it is not clear how particular phenotypes result. Mutations have been found in genes coding for proteins

located presynaptically, synaptically and postsynaptically, and they can affect the development of the NMJ, its maintenance or signal transmission (reviewed in Engel et al., 2015). Next-generation sequencing has revealed novel CMS-causing mutations in genes which are ubiquitously expressed (Belaya et al., 2015, Cossins et al., 2013, Belaya et al., 2012, Senderek et al., 2011). Figure 1.5 depicts the proportion of the most common CMS subtypes, and Table 1.1 lists the differentiating symptoms for these subtypes.

Mutations in the AChR account for the majority of CMS cases. Slow channel syndrome is one of the first described subtypes of CMS (Engel et al., 1982). It can be caused by mutations in any of the four subunits of the adult AChR which leads to altering of the ion channel function (Engel et al., 1999). Slow channel syndrome is characterised by a gain of function which causes prolonged AChR opening. This leads to desensitisation blockade of the receptor, a repetitive compound muscle action potential and cationic overloading of the muscle fibre (Engel et al., 1996b). Ultrastructural studies have shown features of secondary endplate myopathy, such as degenerated junctional folds, which are thought to result from high intracellular Ca^{2+} concentrations (Engel et al., 1996b, Otero-Cruz et al., 2010). The secondary endplate myopathy may account for the commonly observed worsening of symptoms and disease progression.

It was discovered that kinetic defects in the AChR due to mutations in the AChR subunits can cause fast channel CMS (Ohno et al., 1996, Palace et al., 2012). As opposed to slow channel syndrome, the channel openings are abnormally brief.

AChR deficiency syndrome is the most common form of CMS and in most cases caused by mutations in the *CHRNE* gene (Engel et al., 1996a). Endplate studies show a reduction in postsynaptic AChRs, and elongated AChR clusters (Ohno et al., 1997).

Acetylcholinesterase (AChE) is anchored to the synaptic basal lamina by a collagen-like subunit tail encoded by *COLQ*. Mutations is COLQ can lead to a loss of

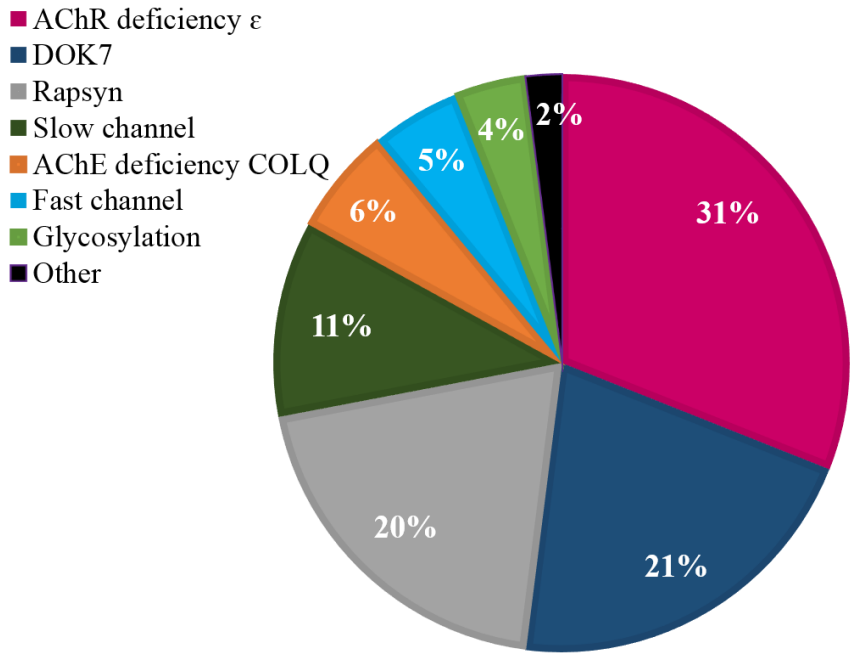

Figure 1.5 Most common subtypes of CMS. Genes coding for proteins located postsynaptically are most commonly affected by mutations (adapted from Finlayson et al. (2013a)).

CMS subtype	Typical age of onset	Typical presenting features	Ocular features	Other features
Slow channel	Variable (birth to adulthood)	Hypotonia or weak neck muscles at birth/infancy, limb weakness, ptosis, difficulties running	Ophthalmoplegia mild-moderate or absent	Autosomal dominant
Fast channel	Birth	Apnoea/respiratory crisis, ptosis, weak cry, poor feeding, choking, may require ventilation at birth	Ophthalmoplegia	Severe weakness
AChR deficiency	Birth or infancy	Ptosis, poor feeding	Ophthalmoplegia	Generally stable course
COLQ	Can be variable	Ptosis, falls, slower movement, poor feeding	Ophthalmoplegia, Slowed pupillary response following constriction to light	Chronic hypoventilation
ChAT	Birth or infancy	Episodic apnoeas	-	May be normal between episodes of apnoea
Rapsyn	Birth/infancy (or milder late-onset phenotype with limb weakness, sometimes ptosis)	Crises, poor feeding, ptosis, contractures, may require ventilation at birth	Strabismus may be convergent or divergent and latent or manifest	Dysmorphic features, Respiratory crisis often resolve in late childhood
DOK7	Early childhood (early symptoms at birth may include poor feeding and stridor)	Normal motor milestones, followed by frequent falls and difficulties walking	May have ptosis, reduced upgaze	Typical limb girdle weakness, tongue muscle wasting, stridor
GFPT1, DPAGT1, ALG2, ALG14	Early childhood	Deterioration in walking, falls, limb weakness, absence of reflexes	Ptosis mild or absent	Little or no facial weakness, tubular aggregates on muscle biopsy
GMPPB	Adolescence-adulthood (early symptoms may be a delay of motor milestones) or early childhood	Wild spectrum of symptoms, limited march tolerance, inability to run and lift weights, difficulties rising from the floor, proximal weakness (upper and lower limb)	-	Myopathic features, elevated creatine kinase levels, lack of facial weakness. Severe cases with congenital muscular dystrophy with brain and eye abnormalities
	Mutations in *GMPPB* can lead to the onset of muscular dystrophy			no demonstrable effect on the neuromuscular junction

Table 1.1 Phenotypical features of the most common subtypes of CMS. Adapted from Finlayson et al. (2013a).

AChE which increases the lifetime of ACh in the synaptic cleft (Ohno et al., 1998). The result is desensitisation of AChRs and prolonged endplate potentials which causes depolarisation blockade and secondary endplate myopathy. A recent study suggests that mutations in the C-terminal of COLQ reduce the interaction of COLQ with MuSK and basal lamina proteins (Arredondo et al., 2014).

Choline acetyltransferase (ChAT) is an enzyme located presynaptically, responsible for the synthesis of acetylcholine from acetyl-CoA and choline. Mutations in *CHAT* can lead to depletion of the AChR vesicle pools and thereby cause CMS (Ohno et al., 2001, Mora et al., 1987).

It was discovered that mutations in *RAPSN* can cause postsynaptic AChR deficiency (Ohno et al., 2002). AChR expression and the number of junctional folds is reduced in rapsyn CMS, and the co-clustering of AChR with rapsyn is impaired. It is important to note, however, that the clinical phenotypes associated with rapsyn CMS and AChR deficiency due to mutations in *CHRNE* differ (Burke et al., 2004).

MuSK CMS is a rare and severe subtype of CMS (Chevessier et al., 2004, Ben Ammar et al., 2013, Maselli et al., 2010). Muscle biopsies revealed a reduced endplate size and simplification of postsynaptic folds. There is evidence that some mutations in MuSK impair the interaction of MuSK and DOK7 (Maselli et al., 2010). In cultured MuSK-deficient myotubes overexpressing the mutant MuSK, co-immunoprecipitation of MuSK and DOK7 was reduced, indicating decreased DOK7 recruitment. Moreover, phosphorylation of MuSK was significantly reduced, and significantly fewer AChR clusters formed on MuSK mutant myotubes in response to agrin incubation. The interaction with LRP4, on the other hand, was normal. The clinical features of MuSK CMS resemble those seen in DOK7 CMS, a subtype of CMS discovered by Beeson et al.

in 2006. DOK7 CMS is one of the most common forms of CMS and the main topic investigated in this thesis. It is therefore discussed separately in section 1.3.

Only recently, mutations in LRP4 were detected, causing moderate-severe CMS (Ohkawara et al., 2014, Selcen et al., 2015). Endplate studies revealed normal junctional fold development but smaller NMJs. MuSK phosphorylation and AChR clustering in response to agrin was reduced in LRP4-mutant myotubes.

Novel subtypes of CMS were discovered in the last few years that affect the glycosylation pathway of proteins (Belaya et al., 2015, Senderek et al., 2011, Cossins et al., 2013, Belaya et al., 2012). In contrast to the disease subtypes discussed above, these affected proteins are ubiquitously expressed, which highlights that CMS can be caused by proteins not solely located at the NMJ. Glycosylation is crucial for protein folding and intracellular transport, and at the NMJ it is required for the enrichment of AChRs and their response to ACh. To date, mutations in five different genes coding for proteins involved in glycosylation have been found to cause CMS: *ALG2*, *ALG14* and *DPAGT1*, which are involved specifically in N-linked protein glycosylation, and *GFPT1* and *GMPPB*, which are involved in several biosynthetic pathways, including N- and O-linked glycosylation (reviewed in Cruz et al., 2014b).

1.3 DOK7 CMS

Our laboratory was the first to discover that *DOK7* mutations underlie a subtype of CMS (Beeson et al., 2006). DOK7 was discovered in 2006 as a key molecule involved in the development and maintenance of the neuromuscular junction (Okada et al., 2006). This prompted screening of genomic DNA within the seven coding exons of *DOK7* in a group of patients with suspected CMS who until then lacked a genetic diagnosis (Beeson et al., 2006). These patients showed a characteristic limb-girdle pattern of weakness and

their disease was previously described as limb-girdle myasthenia (Slater et al., 2006, Beeson et al., 2006, Engel, 2006).

The disease onset in patients with mutations in *DOK7* is usually in early childhood after the development of normal motor milestones, and is characterised by frequent falls and walking difficulties (Beeson et al., 2006). Many affected children have difficulty getting up from the floor and develop a waddling or swaying gait (Klein et al., 2013). Recent studies showed that feeding difficulties and stridor in the neonatal period often precede the diagnosis with DOK7 CMS and can serve as early diagnostic clues (Jephson et al., 2010, Klein et al., 2013). In adolescence and adulthood, patients usually present with proximal weakness of the upper and lower extremities, the trunk and the neck regions. Facial weakness and ptosis are common, but ocular movements are generally unaffected which contrasts with several other CMS subtypes. Wasting of the tongue muscles occurs in about half of the patients and can be a distinguishing feature of DOK7 CMS (Finlayson et al., 2013a). The severity of the disease varies but DOK7 CMS can be life threating due to potential respiratory failure, and some undiagnosed patients deteriorate with disease progression. Early diagnosis and treatment is therefore important.

Muscle biopsies from patients revealed small simplified NMJs (Palace et al., 2007, Selcen et al., 2008, Beeson et al., 2006, Slater et al., 2006). Postsynaptic junctional folds were often degenerated as seen in slow channel syndrome, and the length of the postsynaptic membrane was significantly reduced. Furthermore, absence or degeneration of nerve terminals was common. The density and distribution of AChRs on intact folds was normal and a reduction in AChRs per endplate resulted from the small size of endplates. In DOK7 patients, tubular aggregates are absent, which contrasts with some myopathies and CMS subtypes, but mild myopathic changes may be observed with increased fibre size variability, type I fibre preponderance, type II fibre atrophy and

occasionally internalised nuclei (Palace et al., 2007). Due to the characteristic feature of small simplified NMJs but normal AChR and ACh esterase function (Slater et al., 2006), DOK7 CMS is classified as a synaptopathy rather than a channelopathy (Beeson et al., 2006).

In a recent study, 34 different mutations were identified in a cohort of 72 patients derived from 64 kinships (Cossins et al., 2012). The mutations were located along the gene, highlighting the need for mutational screening of all seven *DOK7* exons. Similar to rapsyn-CMS, a common variant is found in DOK7 patients. In the study cited above, the C-terminal mutation c.1124_1127dupTGCC was present homozygous or in at least one allele in 41 of the 64 kinships (~64%). Only six out of 6092 screened individuals were found to be heterozygous for this variant (http://evs.gs.washington.edu/EVS/). The c.1124_1127dupTGCC mutation results in a frameshift which leads to truncated protein, lacking a large part of the COOH-terminal moeity (from Ala-377 to the COOH terminus). Overexpression of c.1124_1127dupTGCC in C2C12 mouse muscle cells caused a significant reduction in the phosphorylation of MuSK and of the AChR beta-subunit (Beeson et al., 2006). Moreover, many *DOK7* mutations, including c.1124_1127dupTGCC, significantly reduced the number of AChR clusters when overexpressed in cultured mouse muscle cells (Cossins et al., 2012, Beeson et al., 2006).

It was shown in cultured myotubes that missense mutations in the PH or PTB domain reduce MuSK and AChR beta-subunit phosphorylation as well as AChR clustering (Hamuro et al., 2008). The majority of mutations that cause DOK7 CMS occur in the C-terminal region, which highlights the importance of the C-terminal domain for NMJ maintenance. The two SH2 target motifs encompassing Tyr395 and Tyr405 are ablated by the 1124_1127dupTGCC mutation (Hamuro et al., 2008, Hallock et al., 2010).

1.4 Drug treatment of CMS

1.4.1 Signal transmission enhancing drugs

The response of CMS patients to drug treatment depends on the underlying mechanism of the respective syndrome. Treatment of CMS is classically aimed at enhancing neuromuscular transmission (Engel et al., 2003), which may be achieved by different mechanisms. Pyridostigmine acts by inhibiting AChE and prolonging the lifetime of ACh at the endplate. More AChRs are activated by a single quantum, the amplitude of the EPP is increased and the safety margin of transmission is met. 3,4-diaminopyridine (3,4-DAP), on the other hand, is a potassium channel blocker, leading to increased ACh release. Often, these two drugs are used in combination. Pyridostigmine and 3,4-DAP are beneficial to patients with fast channel CMS (Palace et al., 2012) and AChR deficiency due to mutations in *CHRNE* (Ohno et al., 1997). An initial dramatic response may be followed by a decline in the treatment success, which is in line with the destabilising effects of signal transmission discussed earlier. Moreover, most patients with ChAT (Ohno et al., 2001), rapsyn (Ohno et al., 2002) and glycosylation CMS (Belaya et al., 2015) respond well to pyridostigmine, and if needed to 3,4-DAP. However, in slow channel syndrome with prolonged AChR opening, pyridostigmine and 3,4-DAP cause worsening of symptoms since they exacerbate the underlying pathology. Instead, patients benefit from fluoxetine and quinidine which act as open channel blockers (Chaouch et al., 2012). Neurotransmission enhancing drugs also worsen symptoms of patients suffering from mutations in *COLQ* (Mihaylova et al., 2008), and until recently no satisfactory treatment was available. In MuSK CMS, pyridostigmine had no effect (Gallenmuller et al., 2014).

1.4.2 ADRB2 agonists as a novel treatment for CMS

Treatment of DOK7 patients with pyridostigmine and 3,4-DAP either had no effect or caused worsening of symptoms (Beeson et al., 2006). Instead, a dramatic response to ephedrine and salbutamol, which stimulate the beta-2 adrenergic receptor (ADRB2) system, was noticed (Beeson et al., 2006, Palace et al., 2007, Lashley et al., 2010, Liewluck et al., 2011).

Ephedrine, a sympathomimetic amine with α- and β-adrenergic effects, is contained in herbs such as *Ephedra Sinica*, and has been used in traditional Chinese medicine as an anti-asthmatic drug and stimulant for more than 5000 years (Abourashed et al., 2003). In the 1930s, the physician and scientist Henrietta Edgeworth who suffered from MG used ephedrine as treatment for dysmenorrhea and noticed improved muscle strength and reduced fatigability (Edgeworth, 1930). As a result, ephedrine was commonly prescribed for MG, but was later replaced by cholinesterase inhibitors and immunosuppressive therapy. Its prescription is now strictly regulated in many countries (Liewluck et al., 2011). Anecdotally, patients with neuromuscular disorders reported improved strength when being prescribed ephedrine after alternative medication had failed, or when being prescribed ephedrine or salbutamol as treatment for their asthma. The beneficial effects of ADRB2 agonists in DOK7 CMS patients identified from cohort observations has sparked the revival of these drugs for treatment of impaired neuromuscular transmission.

Fatiguable muscle weakness was measured in a cohort of DOK7 patients at baseline and after 6-8 months after drug treatment using the quantitative myasthenia gravis severity score (QMG), which includes scores for components such as ptosis, facial muscles, arm raise time and leg raise time (Lashley et al., 2010). Measurements also included a mobility score for the time walked over a fixed distance or a timed stair climb. Treatment with ephedrine caused a significant, in many cases life-changing, increase in

exercise tolerance, with patients previously wheelchair-bound being able to walk long distances, jump and climb stairs. This remarkable effect has been replicated in a number of patient studies (Burke et al., 2013, Schara et al., 2009). A recent meta-analysis, reviewing the treatment of 122 DOK7 patients from 16 publications, showed significant improvement in 65 of 69 patients treated with salbutamol or ephedrine (Witting and Vissing, 2014). Genetic information was available for 120 patients, of which 96 were either compound heterozygous or homozygous for the common mutation c.1124_1127dupTGCC. Ephedrine was usually prescribed at 0.5 to 1mg/kg/day in children and 100mg/day in adults, while salbutamol was given at 0.1 to 0.3mg/kg/day in children and 6 to 18mg/day in adults. AChE inhibitors improved symptoms in only six out of 66 patients. In some of these patients, the initial benefit was lost, and in 26 out of 66 patients, worsening of symptoms occurred. An interesting observation was that the treatment success with salbutamol and ephedrine is delayed and builds up over weeks and months. A progressive increase in exercise tolerance and decrease in fatiguable muscle weakness can usually be observed within 6-8 months (Lashley et al., 2010, Witting and Vissing, 2014). Salbutamol and ephedrine are generally tolerated well, with occasional cardiac side effects.

Due to the remarkable effects noticed in DOK7 CMS, salbutamol was soon investigated as potential treatment for other NMJ disorders. Indeed, both salbutamol and ephedrine were beneficial in COLQ CMS where, similar to DOK7 CMS, the postsynaptic structures are destabilised (Mihaylova et al., 2008, Chan et al., 2012). Accordingly, symptoms of a slow channel patient who only modestly responded to fluoxetine improved dramatically after combined treatment of fluoxetine and salbutamol (Finlayson et al., 2013).

In AChR deficiency syndrome due to *CHRNE* mutations, combined treatment of pyridostigmine and salbutamol prevented the decline in the treatment response, observed in response to treatment with pyridostigmine alone (Rodriguez Cruz et al., 2015).

Given that DOK7 and MuSK act within the same pathway, it may not be surprising that salbutamol had a dramatic beneficial effect in MuSK CMS (Gallenmuller et al., 2014). This raises the possibility that seronegative MG patients with antibodies to MuSK might respond to ADRB2 agonists. Indeed, in a mouse model of MuSK MG, salbutamol reduced weakness and fragmentation of AChR aggregates (Ghazanfari et al., 2014).

Thus, ADRB2 agonists provide clear benefit to DOK7 CMS patients, but are now also a first line treatment for other CMS subtypes or used in combination with other drugs.

1.5 Objectives and hypothesis

Despite the well-documented effects of ADRB2 agonists in CMS, very little is known about how ADRB2 activation affects NMJ functioning. The aim of this thesis is to shed light on the molecular mechanisms underlying the dramatic effects of ADRB2 agonists in CMS. The work undertaken focuses on DOK7 CMS.

Salbutamol is an activator of ADRB2s. Skeletal muscle expresses a large number of adrenergic receptors predominantly of the beta-2 subtype (Lynch and Ryall, 2008). ADRB2s belong to the class of G-coupled receptors which have a conserved structure of seven transmembrane alpha-helices which form three extracellular and three intracellular loops (Johnson, 2006) (Fig. 1.6). While the third to fifth intramembranous regions are thought to be important for agonist binding, the third intracellular loop is involved in G protein coupling. It is believed that the ADRB2 oscillates between an active and an inactive state and that ADRB2 agonists stabilise the receptor in its active form. A G protein consists of βγ subunits which form a tightly interacting dimer, bound to the

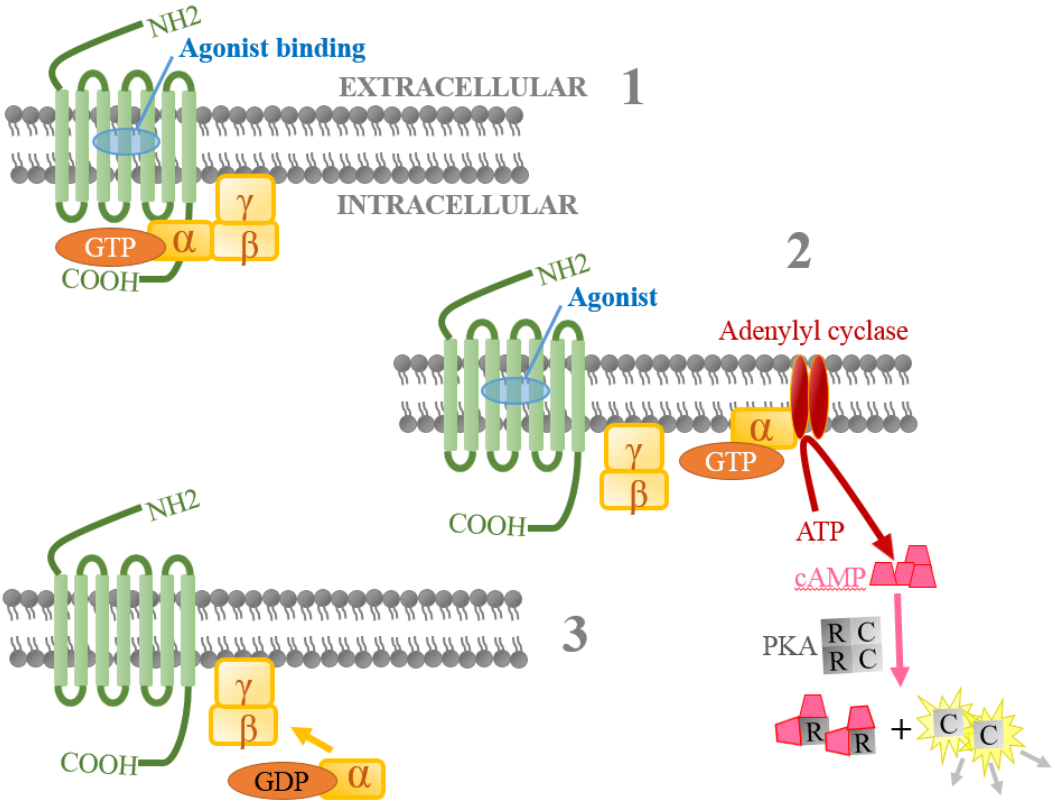

Figure 1.6 ADRB2 functioning. ADRB2s oscillate between an active and an inactive state. (1) ADRB2 agonists bind to the intramembranous region of the receptor. GDP is replaced by GTP, which causes destabilisation of the G protein complex. (2) The α-subunit of the G protein detaches from the βγ-dimer. The subunits of the G protein can then activate downstream signalling pathways, including cAMP/PKA signalling pathways, induced through stimulation of adenylyl cyclase by Gα. (3) If the receptor changes to its inactive state, Gα reattaches to the Gβγ dimer and the G protein binds GDP.

intracellular plasma membrane. In the inactive state, the α-subunit (Gα) of the G protein, remains attached to the Gβγ dimer. G proteins can bind GDP (guanosine diphosphate) or GTP (guanosine triphosphate). If the receptor is activated, GDP is replaced by GTP, which causes destabilisation of the G protein complex. As a result, a conformational change occurs in the protein, Gα detaches, and downstream signalling targets are activated by the α- and βγ-subunits. Gα regulates many second messenger systems, including the cAMP/PKA signalling pathway. Activation of adenylyl cyclase catalyses the conversion of adenosine triphosphate into cAMP. Four molecules of cAMP activate one PKA molecule: If two cAMPs bind to each of the two regulatory subunits of PKA, the catalytic subunits of PKA are activated and can phosphorylate downstream targets.

1.5.1 Hypothesis

It was hypothesised that the ADRB2 signalling cascades directly affect proteins located at the NMJ. Although ADRB2 agonists are well known for their anabolic effects, it is unlikely that these explain the beneficial effects seen in CMS patients (discussed in chapter 4.1). ADRB2 agonists appear to be beneficial to neuromuscular disorders where the endplate structure is disrupted. In DOK7 CMS, this disruption is caused by mutations which impair the DOK7-MuSK signalling pathway. It was proposed that ADRB2-mediated cAMP/PKA second messenger signalling compensates for the partial loss of DOK7 function, thereby exerting a stabilising effect on the postsynaptic structure (Fig. 1.7). This effect could be mediated via multiple mechanisms, including kinase pathways.

To address this hypothesis, the following novel experimental models were developed in this thesis:

- The effects of ADRB2 agonists on AChR clusters formed on cultured mouse muscle cells were explored
- A cell culture model utilising CRISPR/Cas9 genome editing tools was developed
- Single AChR clusters in living cells were studied, utilising novel imaging techniques including optogenetics and fluorescence lifetime microscopy

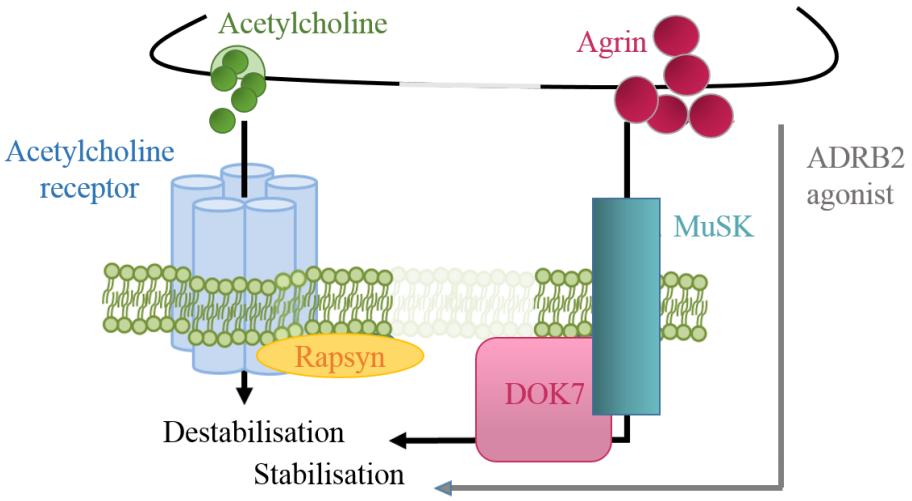

Figure 1.7 Regulation of postsynaptic stability by positive and negative signals. Agrin is a positive signal for AChR cluster stabilisation, while ACh induces dispersal. ADRB2 agonists might compensate for the partial loss of DOK7 signalling and exert a stabilising effect on the endplate structure.

CHAPTER 2

Materials and methods

2.1 Materials

See Table 2.1 and Table 2.2.

Product	Company	Product number
0.5% Trypsin-EDTA (10X)	Invitrogen	15400-054
36% w/v formaldehyde EM, 100 ml	TAAB	F003
Alexa Fluor-594 conjugated bungarotoxin	Invitrogen	B13423
Amersham ECL Western Blotting Detection Reagent	GE Healthcare	RPN2106
Amersham Protran 0.45 NC 300mm*4m 1 roll/PK	Fisher Scientific	10600002
Ampicillin	Sigma-Aldrich	A1593
Antarctic Phosphatase	New England BioLabs Inc.	M0289S
PSA (100x Antibiotic-Antimycotic)	Gibco	15240-062
Bacto Agar	BD	214010
Bacto Tryptone	BD	211705
Bacto Yeast Extract	BD	212750
BamH1	New England BioLabs Inc.	R0136S
BbsI enzyme	New England BioLabs Inc.	R0539S
Boric acid	Sigma-Aldrich	B6768
BSA (bovine serum albumin)	Sigma-Aldrich-Aldrich	A7906
Countess automated cell counter	Invitrogen	C10227
Dimethyl sulphoxide, dehydrated	VWR Chemicals	23500.260
Distel High Level Disinfectant	Tristel	TM305
DMEM	Sigma-Aldrich-Aldrich	D6429-6X500ML
DNA Polymerase I, Large (Klenow) Fragment	New England BioLabs Inc.	M0210S
Dynabeads MyOne Streptavidin T1	Invitrogen	65601

Dynabeads Protein G for Immunoprecipitation 5ml	Invitrogen	10004D
E. coli JM109	Promega	P9751
EDTA	Fluka	03690
Epicentre QuickExtract DNA Extraction Solution	Cambio	QE09050
FCS (foetal calf serum)	Gibco	10270-106
FujiFilm RX NIF autoradiography film	Fuji	12705325
Geneticin Selective Antibiotic (G418 Sulfate)	Invitrogen	11811-031
Halt Phosphatase Inhibitor Cocktail	Invitrogen	78420
HEPES	Sigma-Aldrich	H3375
Horse serum	Sigma-Aldrich	H1138-500ml
HyperLadder™ 1kb	Bioline	BIO-33026
Ibidi µ-Dish 35 mm, high glass bottom	Thistle Scientific	IB-81158
ICI-118,551	Enzo Life Sciences, Inc.	BML-AR104-0010
KpnI enzyme	New England BioLabs Inc.	R0145S
MegaMix~Blue PCR master mix	Microzone	2MMB-25
NaCl AnalaR NORMAPUR	VWR	27810.364
NaCl solution	Sigma-Aldrich	S5150-1L
NcoI enzyme	New England BioLabs Inc.	R0193S
NEB PCR Cloning kit	New England BioLabs Inc.	E1202S
Neon Transfection System 100 µL Kit	Invitrogen	MPK10096
NuPAGE 4-12% Bis-Tris gel, 10-well, box of 10	Invitrogen	NP0321BOX
NuPAGE LDS Sample Buffer (4X)	Invitrogen	NP0008
NuPAGE MOPS SDS running buffer (20x)	Invitrogen	NP0001
NuPAGE Sample Reducing Agent (10X)	Invitrogen	NP0004
NuPAGE transfer buffer (20x)	Invitrogen	NP00061
Oxoid Phosphate Buffered Saline Tablets	Thermo Scientific	BR0014G
pGEM-T Easy Vector System I	Promega	A1360
Pierce BCA Protein Assay Kit	Thermo Scientific	23227
Pierce IP Lysis Buffer	Thermo Scientific	87788
Polybrene	Insight Biotechnology Ltd	sc-134220
Protease inhibitor cocktail	Sigma-Aldrich	P8340-5ML
Puromycin	Sigma-Aldrich	P8833-25MG

QIAprep Spin Miniprep Kit	Qiagen	27104
QIAquick gel extraction kit	Qiagen	28706
QIAquick PCR purification kit	Qiagen	28104
Roche Genopure Plasmid Maxi Kit	Roche	3143422001
Salbutamol sulphate	Sigma-Aldrich	PHR1053-1G
SeeBlue Plus2 Pre-stained Protein Standard	Invitrogen	LC5925
T4 DNA ligase	New England BioLabs Inc.	M0202S
T4 Polynucleotide kinase	New England BioLabs Inc.	M0201S
Tris-HCl	Invitrogen	15567-027
Triton X-100	Sigma-Aldrich	T8532
Trizma base	Sigma-Aldrich	T1503
Tween 20	Sigma-Aldrich	P1379-250ML
UltraPure Agarose	Invitrogen	15510-027 10975-035
VisionWorks LS Image Acquisition Software	UVP	97-0186-03
XbaI enzyme	New England BioLabs Inc.	R0145S
XhoI enzyme	New England BioLabs Inc.	R0146S
XL10-Gold Ultracompetent Cells	Agilent	200315
α-Bungarotoxin, [^{125}I]	PerkinElmer	NEX126050UC
α-Bungarotoxin, Biotin-XX Conjugate	Invitrogen	B1196

Table 2.1 List of materials and reagents.

Antibody name	Company	Product number
Anti rMuSK antibody	R&D system	AF562
Anti-MuSK antibody	Abcam	ab5619 (discontinued)
Anti-Phosphotyrosine Antibody, clone 4G10	Merck-Millipore	05-321
Dok-7 Antibody (H-284)	Santa Cruz	sc-50463
HRP-conjugated anti-goat	Dako	P044901-2
HRP-conjugated anti-mouse	Dako	P044701-2
HRP-conjugated anti-rabbit	Dako	P044801-2
mAb124 anti-AChR beta	Provided by Sokrates Zartos	mAb124
Musk antibody H-300	Santa Cruz	sc33204

p-AchRβ1 Antibody (Tyr 390)	Santa Cruz	sc-17087
β2-AR Antibody (H-73)	Santa Cruz	sc-9042

Table 2.2 List of antibodies.

2.2 Recipes of buffers and other solutions

See Table 2.3.

Buffer/solution name	**Formulation**
Electrophoresis gels	1.5% or 0.7% UltraPure Agarose in 1% TBE (see below)
LB (lysogeny broth) agar solution for agar plates	2.5g NaCl, 2.5g Bacto Tryptone, 1.25 g Bacto Yeast Extract, 3.75g Bacto Agar in a total of 250ml dH_2O (autoclaved)
LB (lysogeny broth) medium	5g NaCl, 5g Bacto Tryptone, 2.5g Bacto Yeast Extract in a total of 500ml dH_2O (autoclaved)
Lysis buffer	1ml Tris-HCl, 1M, pH 7.5, 2ml NaCl solution, 5M, 0.2ml EDTA, 0.5M, 1ml 1% Triton X-100, 95.8ml dH_20
PBS (phosphate-buffered saline)	10 phosphate buffered saline tablets in total of 1L dH_2O (autoclaved)
PBS-Tween	100 phosphate buffered saline tablets, 10ml Tween 20 in a total of 10L dH_2O
TBE (Tris-Borate-EDTA) electrophoresis buffer 5x	54g Trizma base, 22.5g boric acid In a total of 1L dH_2O, 20ml 1mM EDTA, 0.5M
Annealing buffer	100µl Tris pH 7.5-8, 1M 100µl NaCl, 5M 20µl EDTA, 500mM, 780µl dH_20

Table 2.3 Recipes of buffers and other solutions.

2.3 Cell culture

C2C12 myoblasts and Phoenix-ECO cells were purchased from ATCC, HEK293T cells were purchased from ECACC. Cells were passaged using 0.5% Trypsin-EDTA, diluted 1:10 in PBS. Cells were washed once with PBS and incubated in Trypsin-EDTA (3.5ml/T175 flask) for 5min at 37°C. Cells were transferred to a 30ml universal and centrifuged in growth medium (5ml/T175 flask) for 5min at 1200g at room temperature. Pelleted cells were resuspended in growth medium and counted, using a Countess automated cell counter.

C2C12 cells were maintained in DMEM, supplemented with 15% FCS and with 1% PSA. C2C12 cells were differentiated in DMEM supplemented with 10% horse serum or 2% FCS, or a combination of both. Differentiation media were supplemented with PSA. The medium was changed daily or every second day (0.5-1ml/24-well, 1-2ml/6-well). Phoenix-ECO and HEK293T cells were maintained in DMEM, supplemented with 10% FCS and PSA.

All cell lines were cultured at 37°C and 5.5% CO_2.

2.4 Production of agrin

Neural agrin was produced by transfection of HEK293T cells with plasmid DNA containing full length human agrin or soluble short rat agrin (plasmid kindly donated by the late Dr. Werner Hoch). HEK293T sells were seeded at $2x10^6$ cells in a T75 flask. The following day, cells were transfected with 18µg plasmid DNA, using polyethyleneimine and 20% glucose. The following morning, the transfection solution was replaced with 7ml HEK cell medium, and cells were left for incubation for further two days. The medium was centrifuged at 1200g for 10min at room temperature, aliquoted and frozen at -20°C. A fresh aliquot was used for each experiment and thawed shortly before use.

To determine a suitable agrin concentration for AChR cluster induction, a titration experiment was conducted for each batch of agrin.

2.5 AChR clustering assay

C2C12 myoblasts were seeded at a concentration of $6x10^4$-$1x10^5$ or $3x10^5$-$4x10^5$ in 24- or 6-well plates, respectively. Cells were left to grow for 48 hours to reach 100% confluency. Differentiation of myoblasts into myotubes was induced by growth factor depletion. Cells were cultured in differentiation medium for 5-10 days until myotubes formed. The protocol was optimised for each cell line.

C2C12 cells overexpressing DOK7 form AChR clusters in the absence of agrin (Okada et al., 2006). To induce clustering of AChRs in C2C12 WT cells, myotubes were incubated with soluble or full length rat agrin for 16h unless otherwise stated. Cells were washed three times for 5min in differentiation medium to remove agrin.

AChR clusters were visualised by incubation of myotubes with Alexa Fluor-594 conjugated alpha-bungarotoxin, diluted 1:500 in differentiation medium, for 1h at 37°C. Cells were washed three times for 5min in the dark with differentiation medium and fixed in differentiation medium, supplemented with 3% paraformaldehyde for 20min at room temperature in the dark. The fixing solution was removed and the cells were stored in PBS (1ml/24 well) at 4°C.

Images of myotubes were aquired using an Olympus IX71 fluorescence microscope at 20x magnification, using Simple PCI software (purchased from Digital Pixel). At least 20 microscopic fields per experimental condition were selected in the bright field to ensure the presence of AChR myotubes without selecting for areas with AChR clusters. Images in the red fluorescence channel were acquired and analysed manually using the

software Volocity (Improvision). Only clusters longer than 3µm (or 5µm for AChR dispersion experiments) were included in the statistical analysis.

Application of treatment solutions, microscopy and image analysis were carried out blinded.

2.6 Production of retrovirus and retroviral infection

DOK7- or ADRB2-encoding cDNA was cloned into the retroviral expression vector pBabe puro EGFP and transfected into the Phoenix-ECO cells.

Phoenix-ECO cells were seeded at $2x10^6$ in T25 tissue culture flasks. The following day, cells were transfected, using a mix of 12µg DNA in a final volume of 16µl (in dH_20), 3.75µl polyethyleneimine, 5.25µl sterile filtered 20% glucose and 2.5 ml growth medium. Cells were transferred to a T75 flask the following day and incubated in 7ml of growth medium for another two days. The medium was harvested and centrifuged for 10min at 1200g at room temperature to remove cell debris. 1ml aliquots were stored at -80°C and thawed shortly before each infection. Equipment used for handling retrovirus or for cells recently infected with retrovirus was decontaminated with Distel Laboratory Disinfectant for at least 15min before disposal.

C2C12 myoblasts were seeded at $3x10^5$ in T25 tissue culture flasks and infected with 1ml retrovirus and 1µl of polybrene (8µg/ml) the following night. The next day, cells were reseeded in a T75 or T175 flask depending on the density and left to grow in growth medium for one day. To select for infected cells, the medium was then supplemented with 1µg/ml puromycin dihydrochloride, and cells were kept under selection during further passaging.

2.7 Electroporation of C2C12 cells

For electroporation of C2C12 myoblasts, a Neon transfection system was used. C2C12 myoblasts were trypsinised, centrifuged and resuspended in PBS for counting. The required number of cells was centrifuged and the pellet was resuspended in Neon resuspension buffer at a concentration of $1x10^7$ cells/ml. 120µl of cell suspension was mixed with the DNA of interest and transferred into a 100µl transfection tip. Cells were electroporated by applying one pulse of 1400mV for 30ms and then incubated in PSA-free growth medium. The following day, the medium was changed to growth medium, supplemented with PSA.

2.8 Cell surface ^{125}I-α-bungarotoxin binding

AChR surface expression was quantified by ^{125}I-α-bungarotoxin binding (Fig. 2.1). C2C12$^{DOK7\ c.1124_27dupTGCC}$ motubes were incubated with salbutamol sulphate in differentiation medium for 22h. The cells were washed twice with differentiation medium and were incubated with 10^6cpm/ml ^{125}I-α-bungarotoxin and 1mg/ml BSA for 30min. After three washes with PBS, the cells were lysed with 250µl lysis buffer and the radioactivity was counted with a γ-counter.

2.9 MuSK pulldown for MuSK tyrosine-phosphorylation experiments

C2C12 cells were seeded into 6-well plates at a concentration of $4x10^5$cells/well. Myoblasts were differentiated into myotubes, and two wells per condition were used for the immunoprecipitation of MuSK.

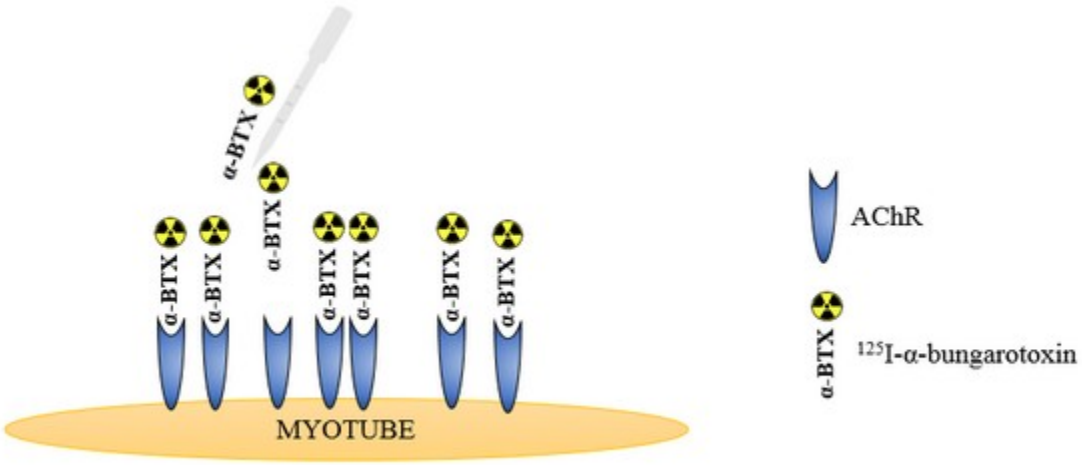

Figure 2.1 Schematic of cell surface ^{125}I-α-bungarotoxin binding. C2C12 myotubes were incubated with 10^6cpm/ml ^{125}I-α-bungarotoxin and 1mg/ml BSA for 30min. Cells were washed three times in PBS, lysed and the radioactivity was counted with a γ-counter.

2.9.1 C2C12 WT cells

Myotubes were serum-starved overnight by incubation in serum-free medium (DMEM, supplemented with PSA) and the following morning incubated with 0, 1, 5, 10 or 50µM salbutamol sulphate in serum-free medium for 6h. For the agrin control condition, cells were incubated with short rat agrin, diluted 1:100, for 6h. Cells were washed three times with serum-free medium and lysed with 500µl/well lysis buffer, supplemented with 1:100 protease inhibitor cocktail and 1:100 Halt phosphatase inhibitor cocktail under agitation at 4°C. After 15min, the cells were scraped off the plate and the lysate for each treatment condition was transferred to an Eppendorf tube. The lysates were subjected to brief pipetting and vortexing and centrifuged for 10min at 12000g at 4°C. Each supernatant was transferred to a new Eppendorf tube and mixed with 20µl AF562 anti rMuSk antibody. As a negative control, the immunoprecipitation was performed without adding the MuSK antibody. All tubes were left to rotate overnight at 4°C. The following morning, 50µl protein G magnetic beads per condition were transferred to an Eppendorf tube and washed twice, once with PBS and once with Pierce IP lysis buffer, using a magnetic rack. The lysates were then added to the beads and left for incubation for 60min at 4°C under rotation of the tubes. The beads were washed six times with 500µl Pierce IP lysis buffer and resuspended in 8.6µl NuPAGE sample reducing agent and 21.4µl NuPAGE LDS sample buffer. The samples were either frozen at -20°C or immediately incubated for 5min at 95°C and subjected to SDS-PAGE using NuPAGE 4-12% Bis-Tris 10-well gels and NuPAGE MOPS SDS Running Buffer. The samples were placed into the magnetic rack and 10µl supernatant per condition was loaded into the wells of a gel. Each sample was run twice to be able to probe separately for MuSK and MuSK tyrosine phosphorylation. SeeBlue Plus2 Prestained Standard was used as a marker. The gel was transferred to nitrocellulose blotting membranes using

NuPAGE Transfer Buffer. After the transfer, the nitrocellulose membranes were incubated in 50ml blocking solution, containing 5% BSA in PBS-Tween overnight at 4°C.

MuSK was detected by incubation with Musk antibody H-300 for 1h at room temperature, diluted 1:1000. MuSK tyrosine phosphorylation was detected with Anti-Phosphotyrosine Antibody clone 4G10, diluted 1:800 for 1h at room temperature. The membranes were washed in PBS Tween for ca 30min under agitation. Primary antibody was detected with HRP-conjugated secondary antibody, diluted at 1:1000 for 1h at room temperature and ECL western blotting detection reagents. All antibody solutions were prepared in PBS-Tween, supplemented with 3% BSA.

2.9.2 C2C12$^{DOK7\ WT}$ and C2C12$^{DOK7\ c.1124_27dupTGCC}$ cells

The same protocol was applied to C2C12$^{DOK7\ WT}$ and C2C12$^{DOK7\ c.1124_27dupTGCC}$ cells with the following changes: Myotubes were incubated in salbutamol sulphate in differentiation medium for a duration of 20h. Instead of using whole cell lysate, MuSK was pulled down from the cell surface after the drug treatment by incubation with 50µl Anti-MuSK antibody (Abcam) in 500µl differentiation medium/well for 1h at room temperature under gentle agitation. After three washes with PBS, the cells were lysed and the lysates were added to the dynabeads as described above. MuSK was detected by incubation with AF562 anti rMuSk antibody for 1h at room temperature, diluted 1:500.

2.10 AChR pulldown for AChR beta-subunit tyrosine phosphorylation experiments

2.10.1 C2C12 WT and CRISPR/Cas9 genome edited cells

Myotubes were plated on 6-well plates at a concentration of 4x10^{5}cells/well. Myoblasts were differentiated into myotubes and one well per condition was used for the

pulldown. Treatment solutions for 4h incubation of the cells were prepared in serum free medium (DMEM), whereas treatment solutions for 24h incubation were prepared in differentiation medium.

After the treatment, the cells were washed three times with differentiation medium and incubated with 1ml/well α-Bungarotoxin Biotin-XX Conjugate diluted 1:500 for 1h at 37°C (Fig. 2.2). The cells were then washed three times with differentiation medium and lysed with 500µl/well lysis buffer, supplemented with 1:100 protease inhibitor cocktail and 1:100 Halt phosphatase inhibitor cocktail under gentle rocking of the 6-well plate at 4°C. After 20min, the cells were scraped off the plate and each lysate was transferred to an Eppendorf tube for centrifugation for 12min at 12000g at 4°C.

For the pulldown, 50µl magnetic streptavidin-coupled beads per condition were transferred to an Eppendorf tube and washed twice with PBS, using a magnetic rack. The supernatant of each lysate was mixed with an aliquot of dynabeads and incubated for 30min at room temperature under gentle rotation of the tubes. The beads were washed three times with 800µl of PBS, resuspended with a mix of 38.5µl NuPAGE LDS sample buffer and 15.3µl NuPAGE sample reducing agent and frozen at -20°C. Aliquots were thawed at room temperature and incubated for 5min at 95°C. The tubes were placed into the magnetic rack and the supernatant was subjected to SDS-PAGE using NuPAGE 4-12% Bis-Tris 10-well gels and NuPAGE MOPS SDS Running Buffer. 15µl supernatant per condition was loaded into the wells of each gel. Each sample was run twice to be able to probe separately for the AChR beta-subunit and for AChR beta-subunit tyrosine phosphorylation. SeeBlue Plus2 Prestained Standard was used as a marker. The gel was transferred to nitrocellulose blotting membranes using NuPAGE Transfer Buffer. The nitrocellulose membranes were then incubated in 50ml of blocking solution, containing 5% BSA in PBS-Tween over night at 4°C. The AChR beta subunit was detected by

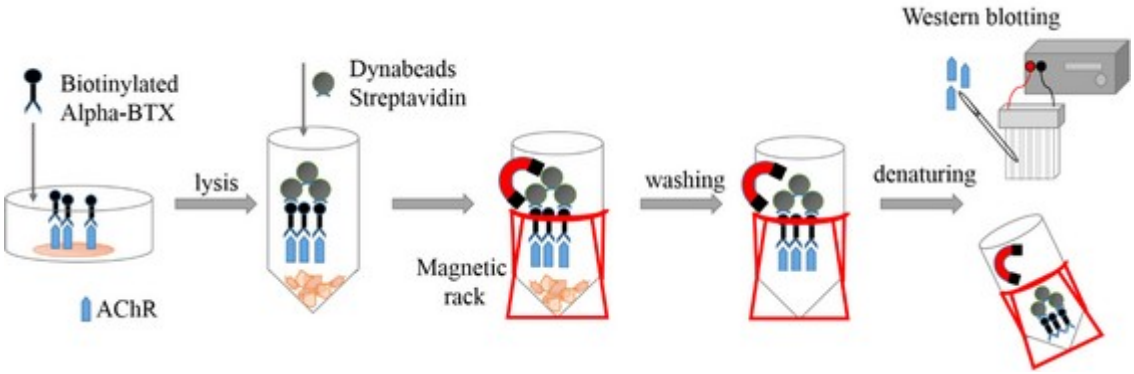

Figure 2.2 Schematic of an alpha-bungarotoxin pulldown experiment. C2C12 myotubes were incubated with biotinylated alpha-bungarotoxin which binds to AChRs. The cells were lysed, centrifuged and the supernatant was incubated with streptavidin dynabeads which bind to the biotinylated alpha-bungarotoxin. The beads were washed and resuspended in sample buffer and reducing agent. After denaturing the sample, the tubes were placed into the magnetic rack and the supernatant was subjected to SDS page and western blotting.

incubation of the membrane with mAb124 anti-AChR beta antibody for 1h at room temperature, diluted 1:3000. AChR beta-subunit tyrosine phosphorylation was detected with p-AChRβ1 Tyr390 antibody, diluted 1:100 at 4°C overnight under gentle agitation.

The membranes were washed in PBS Tween for ca 30min under agitation. Primary antibody was detected with HRP-conjugated secondary antibodies, diluted at 1:1000 for 1h at room temperature and ECL western blotting detection reagents. All antibody solutions were prepared in PBS-Tween, supplemented with 3% BSA.

2.10.2 C2C12$^{DOK7\ WT}$ and C2C12$^{DOK7\ c.1124_27dupTGCC}$ cells

The same protocol was applied to C2C12$^{DOK7\ WT}$ and C2C12$^{DOK7\ c.1124_27dupTGCC}$ myotubes with the following changes: Salbutamol sulphate was applied at a concentration of 0, 1, 10 or 50μM diluted in differentiation medium for 22h.

The supernatant of each lysate was mixed with an aliquot of dynabeads and incubated for 60min at 4°C under gentle rotation of the tubes.

The AChR beta-subunit was detected by incubation of the membrane with mAb124 anti-AChR beta antibody for 1h at room temperature, diluted 1:1000. AChR beta-subunit tyrosine phosphorylation was detected with Anti-Phosphotyrosine Antibody clone 4G10, diluted 1:800 for 1h at room temperature.

2.11 Western blot of ADRB2

C2C12^{ADRB2} and C2C12 WT myoblasts were plated on 6-well plates at a concentration of 4x10^{5}cells/well. The following day, cells were lysed with 200μl lysis buffer/well, supplemented with 1:100 protease inhibitor cocktail for 15min under agitation at 4°C. The cells were scraped off the plate and each lysate was transferred to an Eppendorf tube for centrifugation for 12min at 12000g at 4°C. The protein

concentration was determined, using a Pierce BCA Protein Assay Kit, and 8µg protein was mixed with 4x NuPAGE LDS sample buffer and 10x NuPAGE sample reducing agent to achieve a total volume of 20µl (in lysis buffer). The samples were incubated for 5min at 95°C and subjected to SDS-PAGE, using NuPAGE 4-12% Bis-Tris 10-well gels and NuPAGE MOPS SDS Running Buffer. SeeBlue Plus2 Prestained Standard was used as a marker. Gels were transferred to nitrocellulose blotting membranes using NuPAGE Transfer Buffer. Membranes were incubated in 50ml blocking solution, containing 5% milk powder in PBS Tween overnight. A band corresponding to the ADRB2 was detected by incubation of the immunoblot with 1:800 β2-AR Antibody (H-73) overnight at 4°C. A second blot was probed with 1:5000 anti-alpha tubulin antibody for 1h at room temperature. The membranes were washed in PBS Tween for ca 30 minutes under agitation. Primary antibody was detected with HRP-conjugated secondary antibodies, diluted at 1:1000 for 1h at room temperature and ECL western blotting detection reagents. All antibody solutions were prepared in PBS Tween, supplemented with 3% milk powder.

2.12 FLIM-FRET experiments

A stable C2C12 cell line overexpressing opto-ADRB2 was created by electroporation of C2C12 WT myoblasts with 2µg DNA and subsequent selection with 1mg/ml Geneticin selective antibiotic for 14 days. For overexpression of the FRET sensor, C2C12 WT myoblasts or C2C12 myoblasts overexpressing opto-ADRB2 were electroporated with 10µg of the FRET sensor construct. After the electroporation with the sensor, cells were seeded into an Ibidi cell culture dish. All electroporations were performed as described in section 2.7.

2.12.1 Microscopic setup for FLIM-FRET experiments

The FLIM measurements were performed on an inverted Leica SP8 laser-scanning microscope that had been extended with a TCSPC upgrade from PicoQuant (Berlin, Germany) (Fig. 2.3). This TCSPC upgrade consisted of a 440nm pulsed laser excitation source with a repetition rate of 40 MHz (LDH-P-C-440 B; PicoQuant, Berlin, Germany) and laser driver (PDL 800-B, PicoQuant, Berlin, Germany), two external SPADs (Single-photon avalanche diodes, Micro Photon Devices, Bolzano, Italy), and TCSPC electronics (PicoHarp 300, PicoQuant, Berlin, Germany). All measurements were done with a 63X, 1.2 NA water-immersion microscope objective and zoom settings, such that the projected pixel size in the image was 200x200nm.

Only the donor fluorescence was collected by utilising a 483/32nm fluorescence bandpass emission filter and a 50/50 beamsplitter. The collected TCSPC data was collected and analysed using Picoquant SymPhoTime software.

For the FRET measurements, bright fluorescent cells were selected by visual inspection through the ocular (excitation bandpass filter 470/40nm, dichroic mirror 510nm, emission longpass filter 515nm) to ensure high expression of the sensor.

For the light activation of opto-ADRB2, a tuneable pulsed white light laser (WLL, tuneability range of 470-670nm) was used, tuned to 504nm at laser power setting of 70% corresponding to a power of ~1mW at the back aperture of the objective. Laser activation was done by scanning a region of interest of 10x10μm^2 (50x50 pixels) at scan speed of 100 Hz with line average of 4 corresponding to a 20s total activation time.

2.12.2 Analysis of FLIM-FRET experiments

Quantitative FLIM-FRET analysis was done using Picoquant SymPhoTime software. In this analysis, the collected TCSPC histogram, N(t), was curve fit with a time

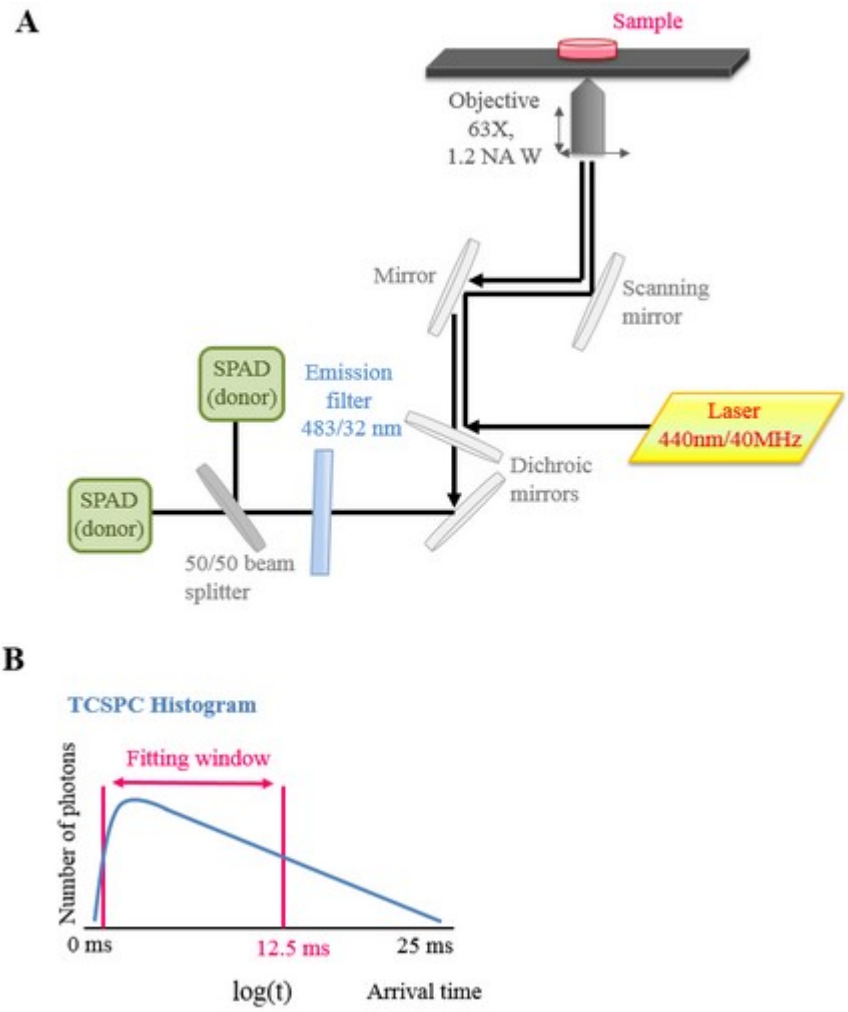

Fig. 2.3 Schematic of the microscopic setup for FLIM/FRET experiments. (A) The FLIM measurements were performed on an inverted Leica SP8 laser-scanning confocal microscope that also incorporates PicoQuant TCSPC components. Fluorescence excitation in this setup was achieved with a pulsed 440nm laser operating at 40Mhz. This laser is coupled into the microscope via an optical fibre and is subsequently focussed to a diffraction limited spot, in this case by a 63X 1.2 NA water immersion objective. The fluorescence emission in the case of FLIM measurements in this setup was collected by two external single photon avalanche photodiodes (SPADs), where the signal was first filtered with a single fluorescence emission bandpass filter (483/32nm) that only passed the fluorescence emission from the FRET donor mTurquoise2, and was then split evenly between the two detectors with a 50/50 beam splitter. (B) Schematic of a TCSPC histogram in which the number of photons (N(t)) is plotted versus the log of the photon arrival time (t) for a single laser pulse of 1/40 MHz=25ms. The rise of the N(t) corresponds to the arrival of the excitation pulse at the sample while the decay of the TCSPC contains information about the fluorescence lifetime of the emitting fluorescent species. In the simplest case for a fluorophore that has only a single lifetime (e.g. mTurquoise2, donor only), the slope of the decay curve N(t) versus log(t) plot is equal to the lifetime τ, i.e. $N(t)=A\ \exp^{-t/\tau}$, where A is the amplitude of the TCSPC histogram. In more complicated cases, such as in the case of the full cAMP sensor, the decay curve is best fitted to more than one components, e.g. $N(t)=A_1\ \exp^{-t/\tau 1} + A_2\ \exp^{-t/\tau 2}$, as was the case here. In these more complicated scenarios is it is customary to report on the average fluorescent lifetime, τ_{avg}, which in our case was intensity weighted averaged.

range of about 0 to 12.5ms to either a single exponential decay, $N(t)=A\ exp^{-t/\tau}$, in the case of control measurements with the donor fluorophore mTurquoise2 only, or, in the case of experiments with the cAMP sensor (*mTurq2Del-EPAC(dDEPCD)Q270E-td_black_cp173Venus(d) EPAC-S^{H189})*, to a double exponential decay, $N(t)=A_1\ exp^{-t/\tau 1} + A_2\ exp^{-t/\tau 2}$. The here reported fluorescence lifetime values are subsequently the intensity weighted averaged lifetime values.

Qualitative FLIM-FRET analysis of time-lapse FLIM data was also done in Picoquant SymPhoTime software. FAST-FLIM images were generated by the software after which a false colour scheme of blue to red was applied to illustrate changes in lifetime in response to an increase in cAMP upon laser activation of the opto-ADRB2 construct. The false colour scheme ranged from 2.5 to 4ns.

2.12.3 Time-lapse imaging of AChR cluster stability upon light activation of opto-ADRB2

Time-lapse imaging of myotubes with AChR clusters that had been labelled with Alexa Fluor-594 conjugated alpha-bungarotoxin was performed on an inverted Leica SP8 confocal microscope equipped with an automated stage and using a 63X 1.2 NA water immersion objective. All images were acquired using the Leica LAS software using the .lif format. For excitation, the WLL was tuned to 594nm, and a typical power setting of 5-10% corresponding to 75-150µW at the back aperture of the objective was used, with a typical scan speed of 400Hz and a zoom setting corresponding to a projected pixel size in the image of 200x200nm. Fluorescence emission was collected on an internal HyD detector with an optical bandpass setting of 600-670nm. In these experiments, a simultaneous transmission light image on an internal PMT detector was collected in order to also visualise the cell morphology.

Time lapse imaging experiments were done by acquisition of three z-planes spaced one micron apart with an acquisition rate of one image stack per 20min for a duration of about 12h and in at least 10 field of views (FOVs of 1024x1024 pixels corresponding to about 200x200µm), where each FOV contained at least one differentiated myotube that had labelled AChR clusters. In these experiments, opto-ADRB2s on specific myotubes were activated in about half of the FOVs by use of a tuneable pulsed WLL (tuneability range of 470-670nm) tuned to 504nm at laser power setting of 70% corresponding to a power of ~1mW at the back aperture of the objective. Laser activation in each instance was done by scanning a region of interest of 10x10µm^2 (50x50 pixels) at a scan speed of 100 Hz with a line average of 4, corresponding to a total activation time of 20s.

2.12.4 Analysis of time-lapse intensity images of AChR cluster stability

Time-lapse image sequences of AChR clusters were rendered by using the Fiji distribution of ImageJ (http://fiji.sc/Fiji). Raw Leica .lif format images were imported in Fiji by use of a BioFormat plug-in. Subsequently, effects of z-drift and or cell motility were minimized by flattening of the acquired three adjacent z-planes to a single image plane by use of the Maximum Intensity Projection command.

2.13 Cloning

2.13.1 Transformation of JM109 competent cells

Transformation of JM109 competent cells was performed by mixing 40µl JM109 competent cells with 2µl of ligation reaction mix, or, for maxi-preparation, with 1µl miniprep DNA or 1µl maxiprep DNA (diluted 1:10). The reaction mix was incubated on ice for 10min, followed by heat-shock for 45s at 42°C and 2min on ice. 500µl LB medium

was added and the reaction was incubated for 1h at 37°C under agitation. After centrifugation for 3min at 5000g, the pellet was resuspended in 150µl supernatant and plated on agar plates (LB agar, supplemented with ampicillin 1:1000 (100mg/ml stock solution prepared in dH_2O)) at 37°C overnight. Colonies were picked and grown overnight in 3ml LB medium, supplemented with 3µl ampicillin (100mg/ml stock solution). Bacteria were centrifuged for 3min at 12000g and DNA was purified using a QIAprep Spin Miniprep Kit according to the manufacturers' instructions.

2.13.2 Cloning of tagged *ADRB2* into pBabe puro EGFP

First, *ADRB2* was cloned into pGEM-T Easy. *ADRB2*-pCMV-Sport vector was digested with restriction endonucleases NcoI and NotI to yield an *ADRB2* gel fragment that was gel purified, using a QIAquick Gel Extraction Kit. *DOK7*-pGEM-T Easy vector was digested with NcoI and NotI, and the backbone gel fragment was gel purified. The pGEM-T Easy backbone was ligated with *ADRB2*, using T4 ligase. After transformation of JM109 bacteria, plasmid DNA was obtained using a QIAprep Spin MiniPrep Kit.

Secondly, an HA tag and a myc tag were inserted at the N-terminus of *ADRB2*. To do this, two complementary oligonucleotides were designed so that, when annealed, they form a linker that encodes an HA and a myc tag. Overhangs corresponded to an NcoI restriction site at each end. First, each oligonucleotide was phosphorylated at the 5', using T4 Polynucleotide kinase at 37°C for 1h, followed by heat inactivation for 10min at 70°C. 10µg of each oligonucleotide was mixed with 2µl annealing buffer and 4µl dH_2O. The Eppendorf tube containing the mix was placed in a beaker with boiling water and left to cool down to room temperature to promote annealing of the oligonucleotides.

Miniprep DNA of *ADRB2* in pGEM-T Easy was linearised by digestion with NcoI, and the mix was purified using a QIAquick PCR purification kit. Purified *ADRB2* in pGEM-T Easy was phosphatased, using Antarctic phosphatase and ligated with the linker

containing the HA tag and the myc tag. After transformation of XL10-Gold ultracompetent cells, plasmid DNA was obtained using a QIAprep Spin MiniPrep Kit.

Next, tagged *ADRB2* was cloned into the mammalian expression vector pcDNA 3.1/ Hygro(+). *ADRB2* in pGEM-T Easy was excised, using BamHI and NotI. pcDNA 3.1/ Hygro(+) vector was digested with BamHI and NotI. After gel purification, the two fragments were ligated, and after transformation of JM109 bacteria, plasmid DNA was obtained using a QIAprep Spin MiniPrep Kit. Maxiprep DNA was prepared, using a Roche Genopure Plasmid Maxi Kit according to the manufacturers' instructions.

Tagged *ADRB2* was also cloned into pBabe puro EGFP. *ADRB2* in pcDNA 3.1/ Hygro(+) was digested with BamHI and XhoI, and after purification, using a QIAquick PCR purification kit, the ends were blunt ended using DNA Polymerase I, Large (Klenow) Fragment. The reaction was then gel purified. pBabe puro EGFP was linearised by digestion with XhoI, purified, using a QIAquick PCR purification kit, and blunt ended as described above. After purification, the product was phosphatased and gel purified. A ligation with tagged *ADRB2* was set up. Sequencing using primer pBabe F confirmed correct insertion of *ADRB2* into pBabe puro EGFP (see Table 2.4 for sequencing primers). Maxiprep DNA was prepared by using a Roche Genopure Plasmid Maxi Kit.

Oligonucleotide F	CATGGGGATCCATGAAGACTATCATTGCTTTGAGCTA CATTTTCTGTCTGGTTTTCGCCGACGAACAAAAACTTA TTTCTGAAGAAGATCTAGC
Oligonucleotide R	CATGGCTAGATCTTCTTCAGAAATAAGTTTTTGTTCGT CGGCGAAAACCAGACAGAAAATGTAGCTCAAAGCAA TGATAGTCTTCATGGATCCC
pBabe F	CCCCGTCTCTCCCCCTTGAA
ADRB2 F	GGCCGCCCATATTCTTATGAAA
ADRB2 F2	ATCATGGGCACTTTCACCCTC
ADRB2 R	TGGAAGGCAATCCTGAAATCTGGG

Table 2.4 Oligonucleotides and sequencing primers used for cloning of tagged *ADRB2* into pBabe puro EGFP.

2.13.3 CRISPR/Cas9 cloning

For the generation of C2C12$^{CRISPR\ Dok7\ c.1124_27dupTGCC}$ and C2C12$^{CRISPR\ Dok7\ c.1504_1505insTA}$ the same protocol was followed:

Guide and target oligonucleotides were purchased from Integrated DNA Technologies. The complementary forward and reverse strands of the guide oligonucleotide sequences were annealed for both guides A and B. Each strand was resuspended at 100µM in dH_2O, and 1µl top and 1µl bottom strand were mixed with 1µl T4 Polynuclease Kinase reaction buffer and 1µl T4 Polynuclease Kinase (total volume of 10µl). The reaction mix was placed into a thermal cycler with the following programme: 30min at 37°C, 5min at 95°C, ramp cool to 25°C over a period of 45min. The reaction mix was diluted 1:100 in dH_2O for subsequent ligation with the pX335 plasmid.

3µg pX335 plasmid was digested with BbsI restriction enzyme for 3h at 37°C in a total volume of 10µl. The digest was phosphatased for 30min at 37°C, followed by heat-inactivation for 5min at 65°C. The sample was gel purified alongside an undigested control, using a 0.7% agarose gel and a QIAquick gel extraction kit.

100ng BbsI cut plasmid was ligated with 2µl of the diluted annealed guide oligonucleotide A or B, using T4 DNA ligase (total volume of 10µl). After transformation of JM109 competent cells, colonies were grown and the DNA was purified using a QIAprep Spin Miniprep Kit according to the manufacturers' instructions. Test digestion reactions of the miniprep DNA with BbsI restriction enzyme were set up, to confirm that the ligation was successful. When cloned into the plasmid, the oligonucleotides remove the BbsI restriction site and the enzyme should not cut. This could be confirmed through gel purification of the test digests and sequencing of the miniprep DNA with primer HU6F (ACTATCATATGCTTACCGTAAC).

In order to be able to express both guide A and guide B oligonucleotides from the same plasmid, guide oligonucleotide B, along with the HU6 promoter and tracrRNA, was cloned into the pX335 plasmid containing guide A. Guide oligonucleotide B was amplified from plasmid pX335 using AccuPrime polymerase (PCR forward primer: GCCATCTAGAGAGGGCCTATTTCCCATGAT, PCR reverse primer: GCCAGGTACCGTCTGCAGAATTGGCGCACG), and the amplicon was gel purified. The amplicon was then subcloned into the vector pMiniT, using a NEB PCR Cloning kit. For the subcloning, gel purified guide B was mixed with 1µl pMiniT vector and 5µl master mix, provided with the cloning kit. The reaction mix was left at room temperature for 15min, followed by 2min on ice and transformation of JM109 competent cells. Cell colonies were grown and plasmid DNA was purified using a QIAprep Spin Miniprep Kit according to the manufacturers' instructions. Sequencing with an upstream sequencing PCR primer provided by the NEB PCR cloning kit identified clones in which guide B has been inserted into the vector. To excise guide B plus HU6 promoter and tracrRNA, miniprep DNA was digested with KpnI and XbaI restriction enzymes at 37°C overnight, and the mix was gel purified. Digested guide B was ligated with plasmid pX335 containing guide A that had also been digested with KpnI and XbaI at 4°C overnight, using T4 DNA ligase with an insert to backbone ratio of 2:1. After transformation of JM109 competent cells, colonies were grown and plasmid DNA was purified using a QIAprep Spin Miniprep Kit. A test digest of miniprep DNA with KpnI and XbaI confirmed that guide B was successfully inserted into the backbone and maxiprep DNA was prepared, using the Roche Genopure Plasmid Maxi Kit according to the manufacturers' instructions. The guides within the final construct were sequenced with a Guide A forward primer (TTGCTGGCCTTTTGCTCACATGT) and a Guide B reverse primer (GTAACGGGTACCGTCTGCAG).

To create the C2C12$^{\text{CRISPR } Dok7 \text{ c.1124_27dupTGCC}}$ cell line, C2C12 myoblasts were electroporated with a mix of 10µl target oligonucleotide (10µM) and 5µg pX335 plasmid containing the guide sequences. To create the C2C12$^{\text{CRISPR } Dok7 \text{ c.1504_1505insTA}}$ cell line, myoblasts were electroporated with a mix of 20µl target oligonucleotide (10µM) and 10µg pX335 plasmid containing the guide sequences. Electroporated cells were left in PSA-free medium for one day and were then incubated in growth medium, supplemented with 1mg/ml Geneticin selective antibiotic for selection of cells for 72h.

After selected cells were cloned by limiting dilution, colonies were maintained in standard growth medium in 6-well plates. Cells were passaged by washing the cells once with PBS and incubation in 100µl trypsin for 5min. 1ml of medium was added to the cells and 100µl cells were directly transferred into a new well of a 6-well plate without centrifugation.

DNA from each colony was extracted for screening for the mutation. Cells were washed in PBS once and incubated in 100µl Trypsin-EDTA for 5min. 1ml of growth medium was added and the cells were transferred to an Eppendorf tube. After centrifugation, the cell pellet was resuspended in 100µl QuickExtract extraction solution, and the sample was incubated for 6min at 65°C and for 2min at 98°C. For the c.1124_27dupTGCC mutation, extracted DNA from the modified region was amplified, using 1124TestF and 1124R primer, and in a second PCR, 1124F and 1124R primer (Table 2.5). For the c.1504_1505insTA mutation, extracted DNA from the modified region was amplified, using 1504TestF and 1504R primer, and in a second PCR, 1504F and 1504R primer. 10µl forward primer was mixed with 10µl reverse primer (1µg/µl) and 60µl dH_2O. For the PCR reaction, 2µl of this primer mix was mixed with 1µl DNA extract and 80µl MegaMix-Blue. The following cycling parameters were chosen: 3min at 95°C (1x), 30s at 95°, 30s at 55°C, 20s at 72°C (35x), 3min at 72°C (1x). The PCR

product was gel-purified, using a 1.5% agarose gel and a QIAquick gel extraction kit. PCR primers were also used for sequencing of the PCR products.

Primers used for screening of CRISPR/Cas9 controls are also listed in Table 2.5.

1124TestF	CGGTTCTCTGCTCAGTCTGCCTG
1124F/Control F	AGGCAGCCACTCCTCTTACTCTGGCA
1124R	GCGCAGGCTTCGAGGTGTGTCA
1504TestF	GTGGCGGACTCAAAGTAAAGCTA
1504F	GACGCTGCGCTGCCGAGTCCATC
1504R/Control R	GCTAGGGCCCCTCTTCCCCTGTC

Table 2.5 List of primers used for screening of monoclonal cell colonies for *Dok7* c.1124_27dupTGCC and *Dok7* c.1504_1505insTA and for screening of WT *Dok7* controls.

2.14 Statistics

A significance level of 0.05 was selected for all statistical analyses.

2.14.1 Analysis of the number and length of AChR clusters

Differences in the number and length of AChR clusters were statistically analysed, using the Software RStudio for Windows (RStudio, Inc., version 0.98.1074).

In the analysis of cluster numbers, the response data are counts with no fixed maximum which can be modelled using a Poisson distribution (Mize et al., 1999). ANOVAS and nonparametric tests do not provide a sensible approach for the analysis of count data since statistical assumptions may be violated and random effects are disregarded (Bolker et al., 2009). A widely used method for the analysis of count data is fitting a generalised mixed effects model (GLMM), which combines the properties of two regression models (Bolker et al., 2009). As a type of generalised linear model, the GLMM "generalises" ordinary linear regression by allowing the response variable to be other than normally distributed (e.g. Poisson distributed). Secondly, as a type of mixed

effect model, the GLMM incorporates both fixed and random effects. In many of the AChR clustering experiments reported in this thesis, application of ADRB2 agonists at different concentrations or the expression of a particular DOK7 mutation is the explanatory variable of interest and can be interpreted as a fixed effect. Since experimental results are usually pooled from several experiments and variation between cultured cell samples is common, this variation based on performing separate experiments is incorporated in the model as a random effect. Thus, a Poisson generalised mixed effects model was fitted, with cluster counts as the response variable, drug concentration (or mutation) as a fixed effect coded as a categorical variable, and with experiment as a random intercept (R package MASS, function glmmPQL).

Differences between mean cluster counts were tested for significance by performing a Wald t-test, which tests the null hypothesis that the predicting variable has no effect, thus comparing the test-statistic to zero. When more than two groups were compared, the results were Bonferroni-corrected. The number of clusters in 20 microscopic fields was counted, and the mean number per microscopic field was calculated. This was repeated N number of times as stated in the respective figure legend. Of note, when Poisson regression models are fitted for the analysis of count data, the Poisson mean representing an expected count has to be positive in value. Therefore, the logarithm of the mean count is modelled, and the results of the significance test are on a log scale accordingly (logarithm to the base *e*). For straight forward interpretation of the results, the data were unlogged and the "raw" cluster numbers were visualised in a second bar chart.

For the analysis of cluster lengths, the data were log-transformed to achieve normal distribution (logarithm to the base *e*). A linear mixed effects model was fitted with log length as the response variable, concentration as a fixed effect coded as a categorical

variable, and experiment as a random intercept (R package nlme, function lme). Differences between cluster lengths were tested for significance by performing Wald t-tests (Bonferroni-corrected). For straight forward interpretation of the results, the data were unlogged and the "raw" cluster lengths were visualised in a second bar chart.

2.14.2 Analysis of ^{125}I-α-bungarotoxin surface binding

For the analysis of ^{125}I-α-bungarotoxin surface binding, a Poisson generalised mixed effects model was fitted, with radioactive counts as the response variable, salbutamol concentration as a fixed effect coded as a categorical variable, and with experiment as a random intercept (R package MASS, function glmmPQL). Differences in AChR surface expression were tested for significance by performing a Wald t-test (Bonferroni-corrected). For straight forward interpretation of the results, the data were unlogged and the "raw" number of radioactive counts were visualised in a second bar chart.

2.14.3 Analysis of FLIM data

FLIM data was statistically analysed, utilising GraphPad Prism software (version 6.01 for Windows, GraphPad Software, La Jolla California USA, www.graphpad.com). Each dataset was tested for normal distribution by performing a D'Agostino-Pearson Omnibus normality test. If the data passed the test for normal distribution, either an unpaired t-test was chosen (for comparison of two groups) or a one-way ANOVA with Dunnett's multiple comparisons test (for comparison of more than two groups to a reference group). If the data violated the assumption of normality or the sample size was too small for the application of the normality test, a non-parametric test was chosen. Either a Mann-Whitney test (for comparison of two groups) or a Kruskal-Wallis test with Dunn's multiple comparisons test (for comparison of more than two groups to a reference group) was performed.

Time course data were analysed with a non-parametric test for paired data. Either a Wilcoxon matched-pairs signed rank test (comparison of two time points) or a Friedman test with Dunn's multiple comparisons test (comparison of more than two time points to a reference group/time point) was chosen.

2.15 List of cell lines created throughout the current project

C2C12$^{DOK7\ WT}$	Stable C2C12 cell line overexpressing DOK7 WT (retroviral infection)
C2C12$^{DOK7\ c.1124_27dupTGCC}$	Stable C2C12 cell line overexpressing DOK7 c.1124_27dupTGCC (retroviral infection)
C2C12^{ADRB2}	Stable C2C12 cell line overexpressing ADRB2 (retroviral infection)
C2C12$^{WT\text{-}ADRB2+Epac}$	C2C12 cell line transiently overexpressing the FRET sensor (electroporation)
C2C12$^{opto\text{-}ADRB2+Epac}$	C2C12 cell line stably overexpressing opto-ADRB2 (electroporation) and transiently overexpressing the FRET sensor (electroporation)
C2C12$^{CRISPR\ Dok7\ c.1124_27dupTGCC}$	Stable C2C12 cell line expressing DOK7 c.1124_27dupTGCC (CRISPR/Cas9-edited)
C2C12$^{CRISPR\ Dok7\ c.1504_1505insTA}$	Stable C2C12 cell line expressing DOK7 c.1504_1505insTA (CRISPR/Cas9-edited)
Control 7-11	CRISPR/Cas9 control cell lines (transfected with pX335 plasmid DNA only, no gene editing)
(C2C12 WT	untransfected C2C12 WT cells)

CHAPTER 3

Cell culture disease model for DOK7 CMS

3.1 Modelling NMJ functioning and dysfunction *in vitro*

The aim of this thesis is to investigate the effects of ADRB2 agonists on the postsynaptic structure of the NMJ *in vitro*. As described earlier, the interaction of agrin, MuSK and DOK7 leads to the aggregation of AChRs on the muscle membrane (Okada et al., 2006). Modelling the AChR clustering pathway in a cell culture system requires the use of muscle cells which have the ability to differentiate into muscle-like fibres. In the current study, the mouse myoblast cell line C2C12 was used. This cell line was originally derived from 2-month old mice of the C2H strain by selective serial passaging of myoblasts 70h after crush injury of the thigh muscle of the mice (Yaffe and Saxel, 1977). Growth factor deprivation of confluent C2C12 cells causes the fusion of myoblasts into myotubes, which resemble the skeletal muscle fibres that develop *in vivo.* In the experiments described within this thesis, AChR cluster formation in C2C12 myotubes was induced via two different methods: by agrin incubation or overexpression of DOK7 (Fig. 3.1).

Induction of AChR clustering by incubation with agrin

Myotube cultures lack nerve innervation and thus the nerve-derived signals that are involved in stimulating AChR aggregation *in vivo.* As described earlier, it was shown that incubation of cultured myotubes with neural agrin causes the formation of AChR clusters (Campanelli et al., 1991). By contrast, NMJs *in vivo* where AChRs are enriched in a central endplate band opposed by a nerve terminal (Wu et al., 2010), agrin incubation of cultured myotubes stimulates the formation of several aggregates along the muscle

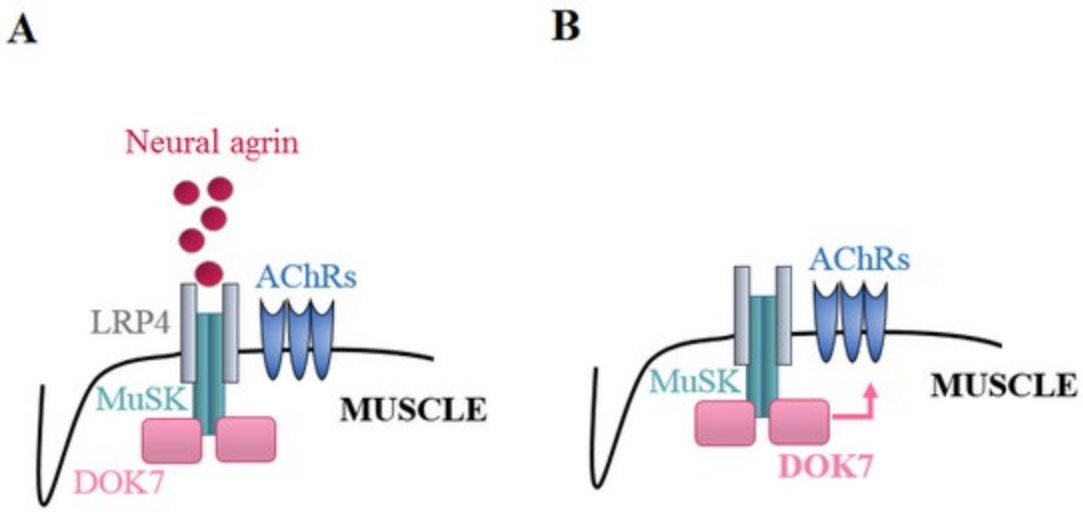

Figure 3.1 AChR cluster induction in cultured C2C12 cells. (A) Clusters form on C2C12 myotubes, incubated with agrin. Agrin induces MuSK activation via binding to Lrp4, which leads to recruitment of DOK7. (B) In cells overexpressing DOK7, clusters form in the absence of agrin. DOK7 acts as a muscle-intrinsic MuSK activator.

fibre. In the experiments described in subsequent chapters, full length human agrin or soluble short rat agrin was used. Different agrin isoforms have been found to be expressed by neural tissue (Ferns et al., 1993). Rat agrin has three sites of alternative splicing, referred to as x, y and z (in order from the N-terminus), with one or more possible inserts at each site. Our agrin construct for the short soluble rat agrin contains the truncated C-terminus of agrin with a 12 amino acid insert at the x-splice site, a four amino acid insert at the y-splice site and an eight amino acid insert at the z-splice site (Fig. 3.2). This truncated form of agrin has been shown to be sufficient to induce AChR clustering in C2C12 cells (Ferns et al., 1993). Fig. 3.3 shows the results from a titration experiment in which C2C12 myotubes were incubated with 1:50, 1:100, 1:200, 1:500 or 1:1000 short rat agrin for 16h. Cells were left untreated in a 'no agrin' negative control to ensure that AChR cluster formation was due to incubation with agrin. AChR clusters were visualised by labelling with Alexa Fluor-594 conjugated bungarotoxin, which specifically binds to AChRs (Young et al., 2003). Cells were fixed, and images of ~20 microscopic fields per condition were taken with a fluorescence microscope at 20x magnification. The average number and length of AChR clusters from these images were then analysed, using the software Volicity and the statistical program RStudio. Only clusters that were in focus and larger than 3µm in length were included in the analysis. The results show that incubation of cells with short rat agrin induced AChR clusters of similar length in a dilution-dependent manner. A very low level of clusters were observed in the negative control condition (average of 2.4 clusters per microscopic field).

For each type and batch of agrin, a titration experiment was conducted. In subsequent experiments in which the effects of ADRB2 agonists on agrin-induced AChR clusters were explored, a concentration that induced about half maximum clustering was chosen. This was done in order to be able to detect subtle potential changes in the number

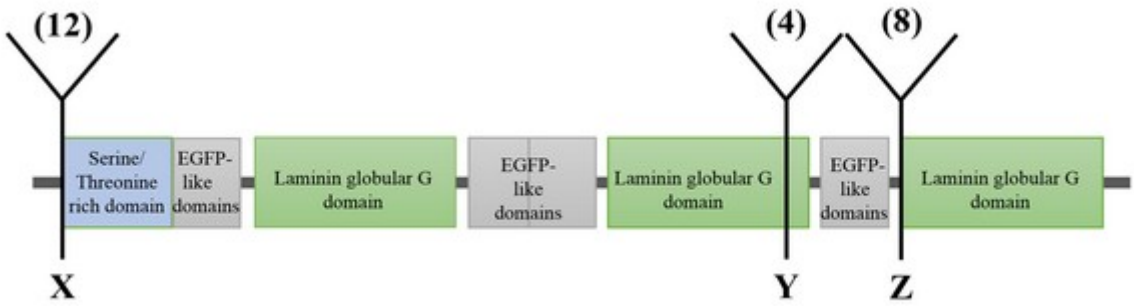

Figure 3.2 Schematic of the truncated agrin protein. Depicted is the soluble short rat agrin with a 12 amino acid insert at the x-splice site, a four amino acid insert at the y-splice site and an eight amino acid insert at the z-splice site (adapted from Ferns et al., 1993).

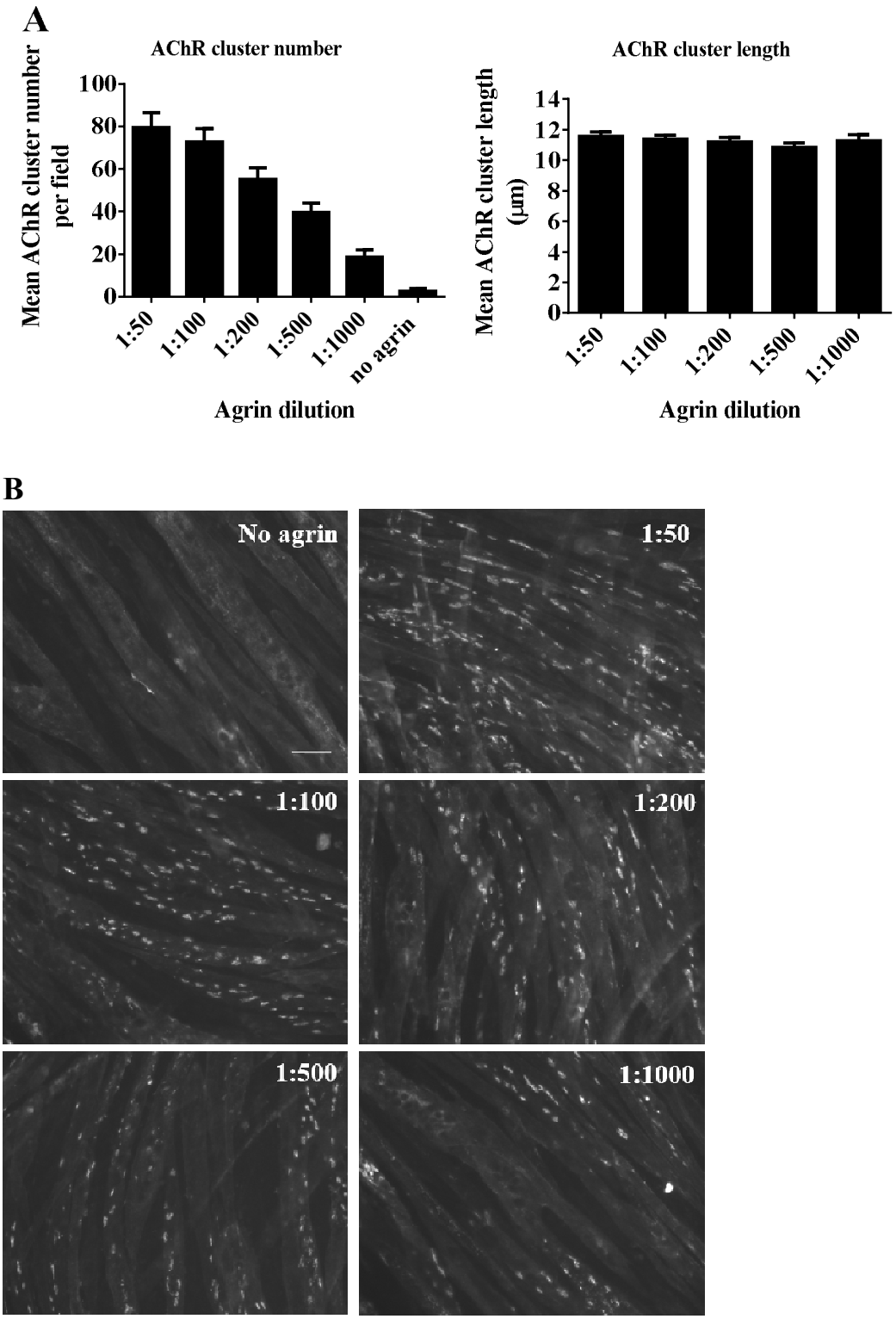

Figure 3.3 Agrin titration. C2C12 cells were incubated with short rat agrin diluted at 1:50, 1:100, 1:200, 1:500 or 1:1000 for 16h. (A) The average number and length of AChR clusters was determined for each dilution. (B) Representative microscopic images of cells treated with agrin as indicated. AChR clusters detected by incubation with Alexa Fluor-594 conjugated bungarotoxin appear as white lines on the myotubes. N=1. Scale bar=50μm. Error bars indicate the standard error of the mean.

of clusters that might otherwise be undetectable due to maximal cluster stimulation.

Induction of AChR clustering by DOK7 overexpression

Alternatively, AChR cluster formation in C2C12 myotubes can be induced in the absence of agrin by overexpression of DOK7 (Okada et al., 2006). Since it was shown that some mutations in *DOK7* impair the efficiency of AChR clustering (Beeson et al., 2006), this model can help determine the pathogenicity of *DOK7* variants identified in gene screens (Cossins et al., 2012). The use of this method requires that the majority of C2C12 myoblasts are transfected with WT or mutant DOK7 expression constructs before differentiation into myotubes. Therefore, the pBabe/puro retroviral expression system was used which ensures nearly 100% infection efficiency and allows for the generation of stable cell lines (Morgenstern and Land, 1990). The pBabe vector provides the viral packaging signal, transcription and processing elements, and the gene of interest, while the packaging cell line Phoenix-ECO provides the viral structural proteins Gag, Pol and Env. Transfection of Phoenix-ECO cells leads to the generation of high-titre, replication-incompetent virus which can be harvested from the medium and used to infect the C2C12 cells.

It was shown in our laboratory that the common DOK7 frameshift duplication mutation c.1124_27dupTGCC causes a significant decrease in the number of AChR clusters when overexpressed in C2C12 cells compared to cells overexpressing WT DOK7 (Beeson et al., 2006). A stable cell line overexpressing c.1124_27dupTGCC was therefore considered to provide a suitable disease model of DOK7 CMS, which could then be utilised to investigate the effects of ADRB2 agonists on the AChR clustering pathway.

First, a stable C2C12 cell line overexpressing DOK7 c.1124_27dupTGCC was generated. The methodological steps are depicted in Fig. 3.4. Retrovirus was produced

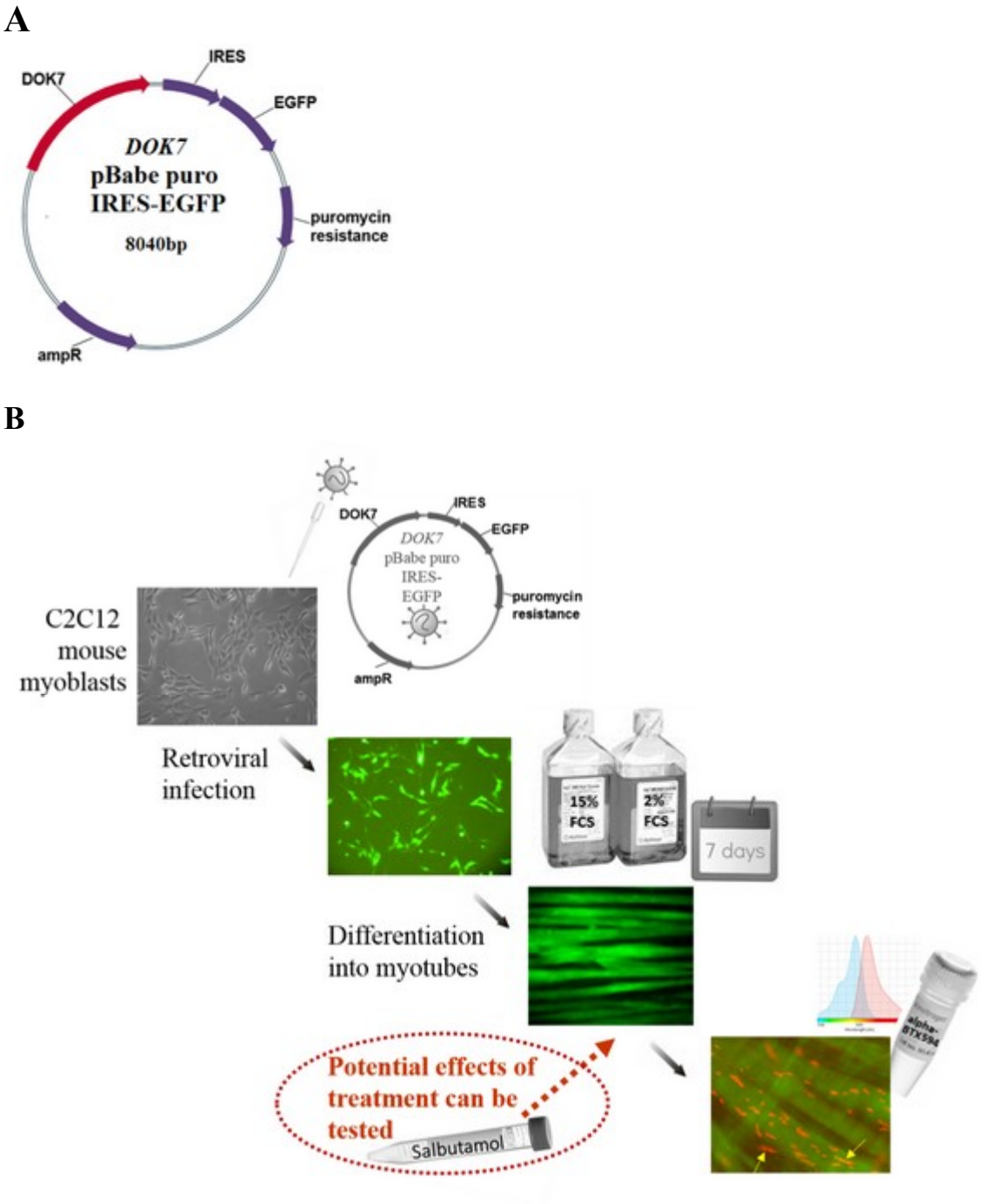

Figure 3.4 Schematic of the DOK7 overexpression disease model. (A) Map of the plasmid *DOK7* pBabe puro IRES-EGFP. Phoenix-ECO cells were transfected with WT or mutant *DOK7* pBabe puro IRES-EGFP plasmid DNA to generate retrovirus. (B) C2C12 myoblasts were infected with retrovirus, selected with puromycin and differentiated into myotubes. AChR clusters were visualised with Alexa Fluor-594 conjugated bungarotoxin and analysed (clusters appear as red lines on the myotubes, two of which are indicated by yellow arrows). This protocol was used to explore the effects of different *DOK7* mutations on AChR clustering, and also to investigate the effects of ADRB2 agonist treatment on AChR clusters in cells overexpressing either mutant or WT DOK7.

by transfection of Phoenix-ECO cells with plasmid DNA containing *DOK7* WT or c.1124_27dupTGCC (available in our laboratory). The plasmids were generated by cloning of human DOK7-encoding cDNA into pBabe puro EGFP, which has an internal ribosomal entry site upstream of enhanced green fluorescent protein (EGFP) such that DOK7 and EGFP are expressed as two separate proteins (Cossins et al., 2012). C2C12 myoblasts were infected with retrovirus, and the puromycin-resistance gene in the pBabe-vector allowed for selection of cells. The resulting stable cell lines are henceforth referred to as C2C12$^{DOK7\ \mathrm{WT}}$ and C2C12$^{DOK7\ \mathrm{c.1124_27dupTGCC}}$.

To confirm that the c.1124_27dupTGCC mutation reduces AChR clustering, myoblasts from the two cell lines were differentiated into myotubes by serum-starvation, and AChR clusters formed on the myotubes were visualised with Alexa Fluor-594 conjugated bungarotoxin. The average number and length of clusters were analysed for both WT and mutant cells, using the software Volocity and the statistical programme RStudio. A Poisson generalised mixed effects model was fitted with cluster counts as the response variable, cell line (WT vs. mutant) as a fixed effect, and with experiment as a random intercept (see chapter 2.14.1 for details on the statistical analysis). The difference in the mean AChR cluster count between WT and mutant cells was determined and tested for significance. Using this model, the logarithm to the base *e* of the mean cluster count is modelled, and the results of the significance test are on an ln scale accordingly. In addition to plotting the ln mean cluster numbers, the data were back-transformed (un-logged) and shown in a second bar graph.

For the analysis of cluster lengths, a linear mixed effects model was fitted with ln length as the response variable, cell line as a fixed effect coded as a categorical variable, and experiment as a random intercept. The data were log-transformed to achieve normal distribution (logarithm to the base *e*). The difference in the mean AChR cluster length

between WT and mutant cells was determined and tested for significance. The data were un-logged and the "raw" cluster lengths were visualised in a second bar chart.

As expected from previous studies (Beeson et al. 2006, Cossins et al. 2012), the results show that significantly fewer clusters formed on C2C12$^{DOK7\ c.1124_27dupTGCC}$ cells when compared to C2C12$^{DOK7\ WT}$ cells (~82.5% reduction, $p<0.00005$) (Fig. 3.5). Moreover, the length of AChR clusters was significantly reduced (~30% reduction, $p=0.001$). The stable cell line C2C12$^{DOK7\ c.1124_27dupTGCC}$ was used in further experiments to investigate the effects of ADRB2 agonists on AChR cluster formation and stability in chapter 4.

3.2 The DOK7 overexpression model as a tool to determine the pathogenicity of *DOK7* variants

In a recent meta-analysis of cases of DOK7 CMS, Vitting and Vissing (2014) reviewed data from 16 publication describing the treatment response of DOK7 patients. In 96 out of 120 patients the *DOK7* mutation c.1124_27dupTGCC was identified in at least one allele. Some patients are homozygous for this common frameshift mutation, however, the majority of patients are compound heterozygote (Cossins et al., 2012). The *DOK7* gene is highly polymorphic with the occurrence of many rare variants, and therefore it is important for a genetic diagnosis, with implications for prognosis, prenatal diagnosis and treatments, to determine the pathogenicity of a variant found in a patient gene screen. In an extensive mutational analysis on a cohort of 72 patients from 64 different kinships 34 mutations were identified (Cossins et al., 2012). These mutations were located throughout the *DOK7* gene (Fig. 3.6). 27 variants likely to be non-pathogenic were identified. Since DOK7 CMS is recessively inherited, it is often difficult to differentiate between a rare polymorphism and pathogenic nucleotide changes.

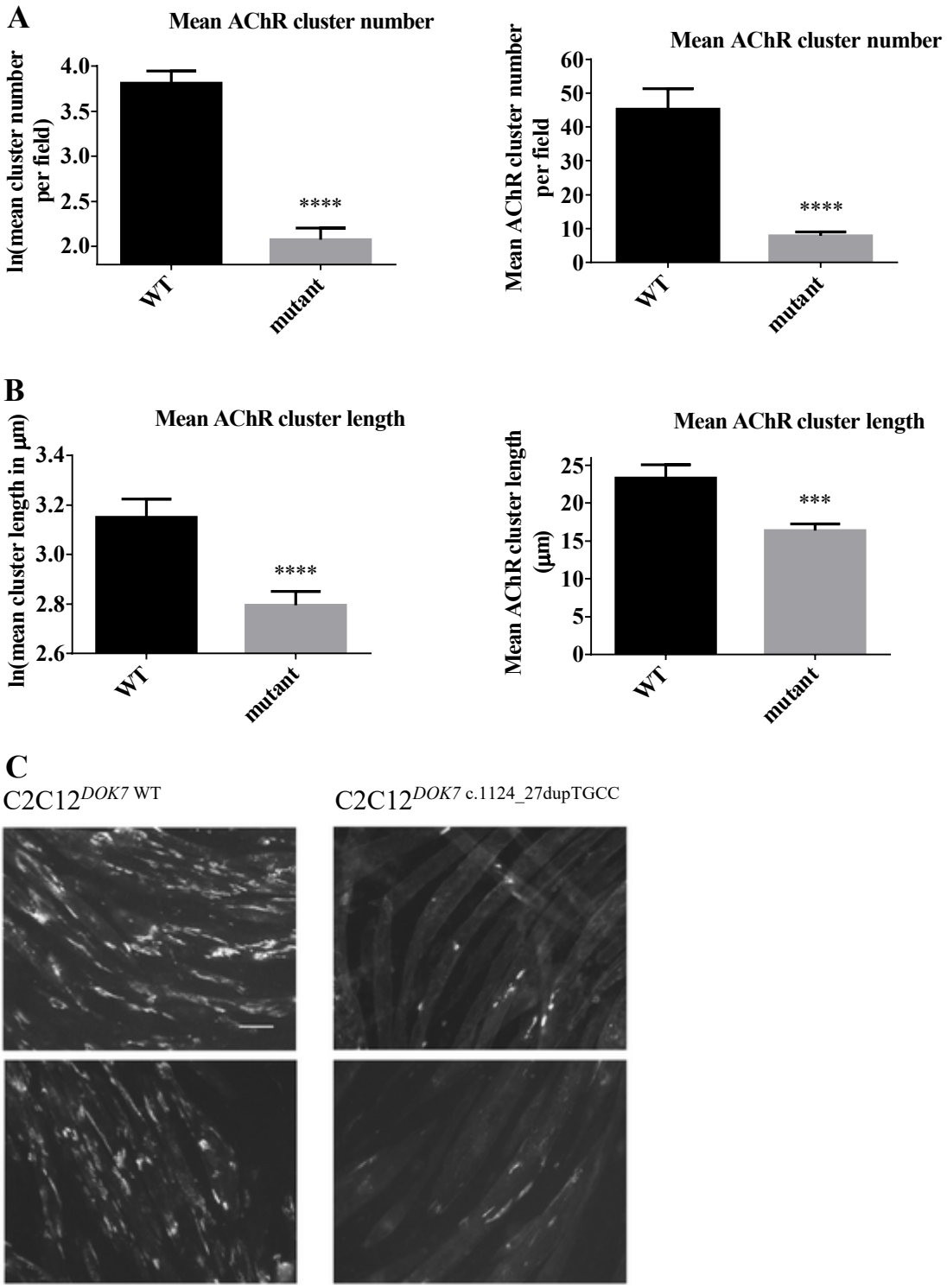

Figure 3.5 Effects of overexpression of DOK7 c.1124_27dupTGCC on AChR clustering. In C2C12$^{DOK7\ c.1124_27dupTGCC}$ myotubes, (A) the number (difference=1.74, SE=0.13, p<0.00005) and (B) the length (difference=0.36, SE=0.09, p=0.001) of AChR clusters were significantly reduced when compared to C2C12$^{DOK7\ WT}$ cells. (C) Representative microscopic images of C2C12$^{DOK7\ WT}$ and C2C12$^{DOK7\ c.1124_27dupTGCC}$ cells N=5. Scale bar=50µm. Error bars indicate the standard error of the mean. ***p≤0.001 ****p≤0.0001.

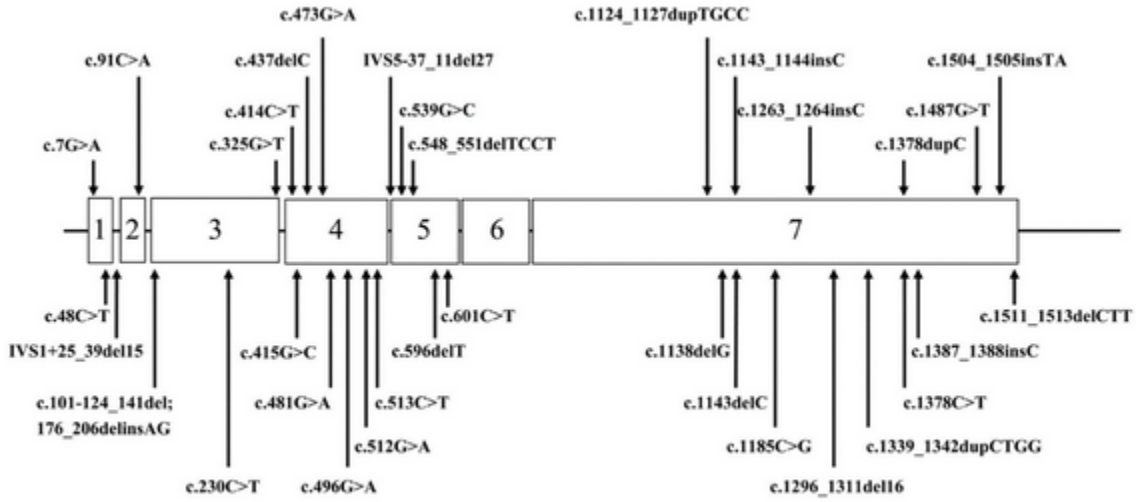

Figure 3.6 Location of *DOK7* mutations. Depicted is a schematic diagram of *DOK7*, showing the exons and positions of 34 different mutations identified in a cohort of 72 patients with suspected CMS (figure taken from Cossins et al., 2012).

Overexpression of a DOK7 variant in C2C12 cells can lead to impaired AChR clustering as observed with the common mutation c.1124_27dupTGCC, and this would indicate that the variant affects DOK7 functioning and may be pathogenic.

Using the DOK7 overexpression model as a functional assay to explore potential pathogenicity, 3 recently identified *DOK7* variants were investigated: *DOK7* c.85C>G, *DOK7* c.1061C>T and *DOK7* c.1340_1354del15 (Fig. 3.7). Each of the variants was found in just one allele of one patient with suspected CMS.

The patient harbouring *DOK7* c.85C>G is a 57 year-old female with symptoms of progressive limb-girdle weakness, mild ptosis but normal ocular motility and wasting of the tongue muscle.

The patient harbouring *DOK7* c.1061C>T is a 27 year-old female. Onset of symptoms occurred at the age of 5, characterised by difficulties walking, frequent falls and weakness in the arm muscles. Later respiratory symptoms occurred and the patient required external ventilation for several weeks. No ocular, facial or bulbar symptoms could be observed. Neurophysiological testing revealed ~20% decrement and increased jitter and block on single fibre EMG. The patient reported fatigue throughout the day, showed symptoms of limb girdle weakness, instability of the hips, and she found it easier to stand with her legs crossed. Signs of tongue wasting were reported.

The patient harbouring *DOK7* c.1340_1354del15 is a 2 year-old male with symptoms of hypotonia. Moreover, abnormalities in single fibre EMG and myopathic EMG changes had been reported.

Constructs for the generation of retrovirus were generated by Dr. Wei Wei Liu, a postdoctoral researcher in our laboratory, and kindly provided for the functional studies. The AChR clustering assays were carried out as described above. The results show that *DOK7* c.85C>G, *DOK7* c.1061C>T and *DOK7* c.1340_1354del15 did not significantly

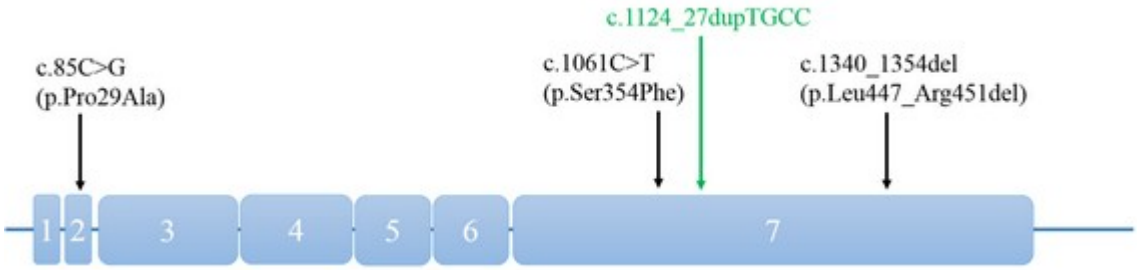

Figure 3.7 Location of novel *DOK7* mutations. Depicted is a schematic diagram of *DOK7*, showing the exons and positions of three novel *DOK7* mutations in relation to the common frameshift mutation c.1124_27dupTGCC.

affect the number of AChR clusters when compared to cells overexpressing WT DOK7 (p=0.5, p=0.7, and p=0.47, respectively) (Fig. 3.8). Moreover, no effects on the length of AChR clusters could be observed (data not shown).

3.3 Discussion

The DOK7 overexpression model could provide a useful tool for investigating the effects of ADRB2 agonists *in vitro*. The majority of DOK7 patients are homozygous or compound heterozygous for the mutation c.1124_27dupTGCC, and overexpression of this mutation in C2C12 cells drastically reduced the number of AChR clusters. Since this reduction therefore at least partly reflects the disruption of the endplate structure seen in patients, these mutant cells were generated to study the effects of salbutamol and other ADRB2 agonists on the DOK7-MuSK signalling pathway (see chapter 4).

The DOK7 overexpression model was also utilised to investigate three novel, previously uncharacterised *DOK7* variants found in suspected CMS patients. The three variants investigated are rare and were therefore candidates for pathogenic variants. The results from the AChR clustering assay, however, suggest no effects on the functioning of DOK7 for any of these three variants.

Pathogenic variants that are located upstream of *DOK7* c.1124_27dupTGCC have been shown to disrupt AChR clustering in this experimental set-up (Cossins et al., 2012, Hamuro et al., 2008). In the mutational analysis by Cossins et al. (2012), 9 out of 11 missense mutations identified in the N-terminus of DOK7 caused a significant reduction in the number of AChR clusters when overexpressed in C2C12 cells. DOK7 c.85C>G is located in the PH domain of the DOK7 N-terminus, and therefore, if it was pathogenic, a decrease in the number of AChR clusters would be expected. Since this was not observed, *DOK7* c.85C>A could be an as yet unidentified rare single-nucleotide polymorphism that

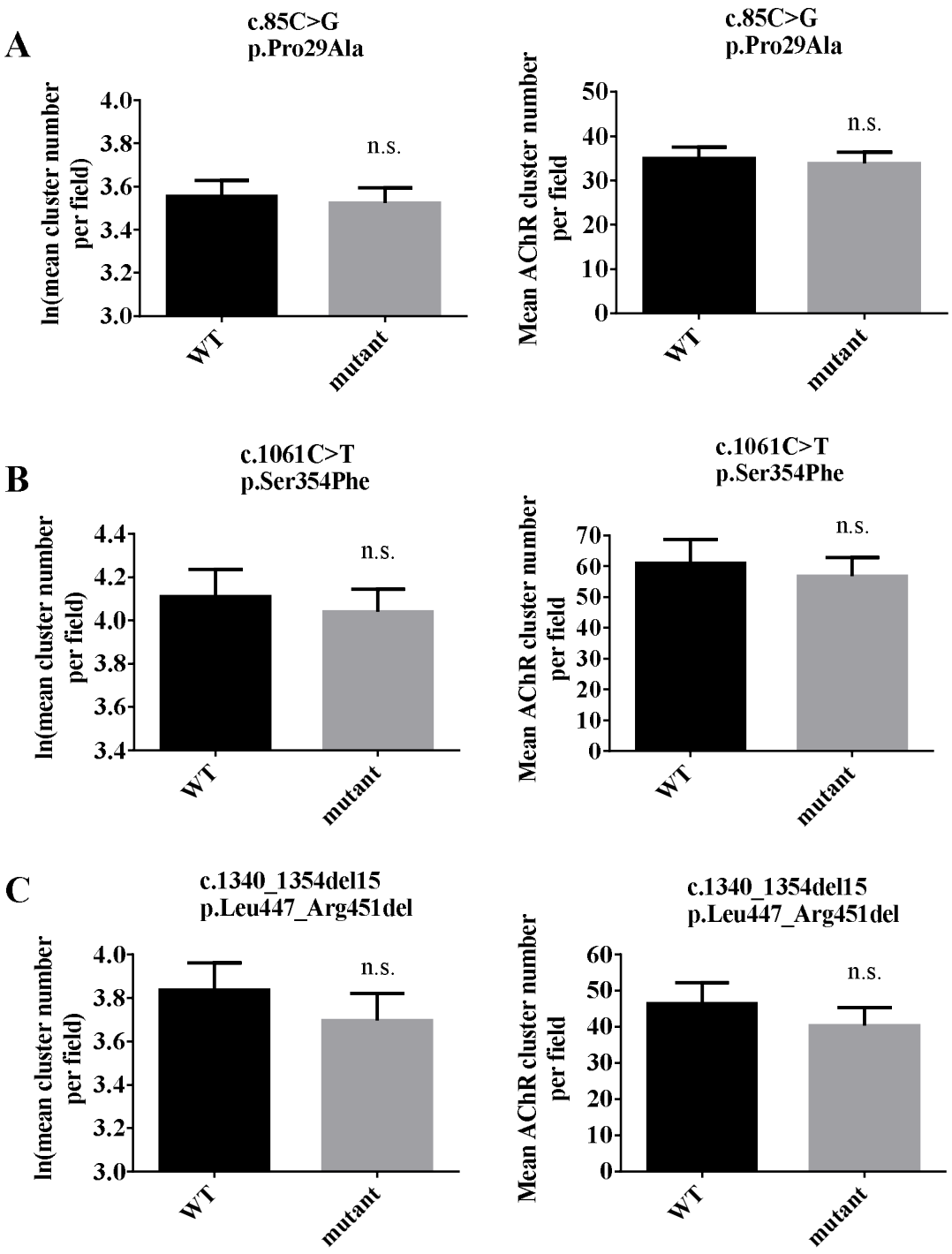

Figure 3.8 Effects of novel *DOK7* mutations on AChR clustering. Overexpression of (A) *DOK7* c.85C>G (difference=0.03, SE=0.05, p=0.5), (B) *DOK7* c.1061C>T (difference=0.07, SE=0.16, p=0.7) or (C) *DOK7* c.1340_1354del15 (difference=0.14, SE=0.18, p=0.47) did not affect the number of AChR clusters formed when compared to cells overexpressing WT DOK7. All N=3. Error bars indicate the standard error of the mean. n.s.p>0.05.

is not pathogenic. Alternatively, it may have effects on DOK7 functioning which we were unable to detect by using the AChR clustering assay. In a further experiment, MuSK phosphorylation levels could be investigated which were previously shown to be reduced in C2C12 myotubes overexpressing mutations in the PH or PTB domain (Hamuro et al., 2008). Moreover, potential effects of *DOK7* c.85C>A could be investigated by using information from the recently identified crystal structure of DOK7 (Bergamin et al., 2010). It was shown that some mutations in the N-terminal region of DOK7 were predicted to affect the structure of the protein, preventing DOK7 dimerisation or impairing binding to MuSK (Cossins et al., 2012, Bergamin et al., 2010). In the experimental set-up here, the mutation is overexpressed in C2C12 cells, but one cannot exclude the possibility that it causes reduced DOK7 expression levels *in vivo*. Genetic testing revealed the variant c.54+25_54+39del15 in intron 1 as the second allele which affects splicing. The patient was therefore diagnosed with DOK7 CMS.

In the patient harbouring the c.1061C>T variant, no other *DOK7* mutation was identified. Therefore, further DNA screening was performed and mutations in *COLQ* were identified. Variant c.1061C>T is therefore considered to be non-pathogenic. No other variant could be detected in the patient, harbouring *DOK7* c.1340_1354del15, suggesting that this variant is also a rare non-pathogenic variant.

The results presented above highlight the importance of functional assays that help determine the pathogenicity of variants. If such assays point towards a non-pathogenic variant, further DNA screening may be performed which, in the case of the patient with the c.1061C>T variant, led to the identification of disease-causing mutations and a precise genetic diagnosis (here COLQ CMS).

It is important to note that the currently used AChR clustering assay does not always provide a clearcut answer when utilised to determine the pathogenicity of rare

variants. It was observed that mutations located towards the C-terminus of DOK7 do not appear to affect AChR clustering when overexpressed in C2C12 cells. These mutations are usually located downstream of two domains in the COOH-terminal region which have been reported to be important for DOK7 functioning: the nuclear export signal (NES) sequence (amino acid 240-249) and the SH2 target motifs encompassing Tyr395 and Tyr405 (Hamuro et al., 2008). *DOK7* c.1124_27dupTGCC encodes a truncated protein lacking the COOH-terminal region from Ala377 and significantly reduced AChR clustering, while a *DOK7* mutation that leads to ablation of the COOH-terminal region from Pro421, thus leaving the SH2 target motifs intact, did not affect AChR clustering (Hamuro et al., 2008). These results suggest that the C-terminal domain downstream of the SH2 target motifs is dispensable for AChR clustering *in vitro*. Nevertheless, in a number of DOK7 patients with a confirmed genetic diagnosis, one allele is located 3' of the SH2 target motifs towards the end of the C-terminal region (Muller et al., 2007, Cossins et al., 2012). This suggests that there are domains in this region which have a role in DOK7 functioning which cannot be investigated using the DOK7 overexpression model. Therefore, further research is needed in order to develop a functional assay that helps determine the pathogenicity of variants located towards the end of the *DOK7* gene. This issue is addressed in chapter 6, by developing an alternative cell culture disease model for studying *DOK7* mutations utilising CRISPR/Cas9 genome editing.

CHAPTER 4

Effects of ADRB2 agonists on the AChR clustering pathway

4.1 Introduction

The beneficial effects of ADRB2 agonists on muscle strength in patients suffering from DOK7 CMS are well documented in a number of clinical papers as described in chapter 1. However, little is known about the underlying molecular mechanisms. A potential direct effect on neurotransmission has been proposed as an explanation and was studied by Engel et al. (Milone and Engel, 1996, Sieb and Engel, 1993). Microelectrode experiments on canine intercostal muscle endplates showed that ephedrine at 100μM increased the quantal content of the endplate potential by 21% and the probability of quantal release by 16% (Sieb and Engel, 1993). The amplitude of the miniature endplate potential and the channel conductance were significantly reduced, suggesting decreased postsynaptic responsiveness to ACh. Results on the effects of ephedrine and salbutamol on AChR channel kinetics investigated by single channel patch-clamp recordings in adult rat hindlimb lumbrical muscles showed short-lived AChR channel blocking effects at high drug concentrations of 10 to 100μM (Milone and Engel, 1996). These effects however, cannot account for the increase in muscle strength seen in patients, where serum concentrations peak at about 0.5μM after a single oral dose of 25mg ephedrine.

Instead, it has been proposed that ADRB2 agonists might act by increasing muscle mass. Clenbuterol for example is a popular performance enhancing drug amongst some body builders due to its anabolic and lipolytic effects when taken at high dose. Numerous studies on humans and animals have demonstrated anabolic effects of ADRB2 agonists even at low doses and highlighted their potential for the treatment of muscle-wasting

disorders and age-related weakness (Lynch and Ryall, 2008). For example, formoterol and salmeterol induced significant muscle hypertrophy in rats after four weeks of treatment at doses of less than 25μg/kg^{-1}/day^{-1} (Ryall et al., 2006). A similar effect was observed when formoterol was tested in a mouse model of Duchenne muscular dystrophy, the *mdx* mouse (Harcourt et al., 2007). Although anabolic effects might counteract secondary muscle atrophy in DOK7 CMS and add some long term beneficial effects, they unlikely explain the dramatic although slow response to ADRB2 agonists. Patients who discontinue the treatment or reduce the dose show rapid worsening of symptoms which argues against anabolic effects as a primary mechanism (Lashley et al., 2010). Moreover, ephedrine and salbutamol appear to be particularly beneficial to CMS subtypes, characterised by disruption of the endplate structure (Webster et al., 2013, Finlayson et al., 2013, Liewluck et al., 2011), which suggests a more specific mechanism than general anabolic effects which would be equally beneficial to all types of muscle weakness.

As shown in chapter 3, some *DOK7* mutations, such as DOK7 c.1124_1127dupTGCC, cause a significant reduction in the number of AChR clusters when overexpressed in C2C12 cells. The main objective of this chapter was therefore to investigate the effects of ADRB2 agonists on the AChR clustering pathway and to test whether ADRB2 agonists have the potential to increase the number of AChR clusters.

Not only the effects of salbutamol but also other ADRB2 agonists were explored. During the last century, a number of different beta-2 selective adrenergic agonists were developed, with the aim to effectively and safely treat asthma. Salbutamol was discovered in the 1960s as a bronchial-selective noncatechol sympathomimetic drug with fewer cardiac side-effects than previously prescribed compounds such as isoproterenol (Tattersfield, 2006). Salbutamol is a short-acting ADRB2 agonist with rapid onset of action and a duration of action between four and six hours. In the 1990s, formoterol and

salmeterol were marketed as longer acting beta-2 selective adrenergic agonists with a duration of action of up to 12 hours. Long-acting ADRB2 agonist do not only bind to the active sites of ADRB2s, but have a long lipophilic side-chain that binds to an exosite (i.e. a secondary binding site on the ADRB2), which promotes repetitive active-site binding (Foye et al., 2008). Fig. 4.1 shows the chemical structures of salbutamol, salmeterol, formoterol and XA-01-NZ86, and the corresponding cAMP EC50 values in CHO cells. The values show that all compounds are selective agonists for beta-2 but not beta-1 adrenergic receptors, since a much higher concentration is required to elicit a half-maximum response of the beta-1 receptor. In the treatment of asthma, long acting ADRB2 agonists have the advantage of providing relief of persistent symptoms overnight, whilst salbutamol is indicated in the event of acute asthma attacks which require rapid intervention. This newer generation of ADRB2 agonists was also shown to have advantages in studies on muscle wasting. The drug dose required to increase muscle strength in ageing rats or *mdx* mice was considerably lower and associated with fewer side effects, such as fatigue (Harcourt et al., 2007, Ryall et al., 2006). Nevertheless, in clinical practice, salbutamol is the first choice treatment for DOK7 CMS, mainly due to its high safety profile in children.

A novel ADRB2 agonist with great potential for the treatment of muscle weakness was recently developed by Novartis (patent application available through WIPO PATENTSCOPE WO2013035047). This compound named XA-01-NZ86 shows increased beta-2 affinity compared to formoterol and, importantly, selective action on skeletal muscle over cardiac and smooth muscle. XA-01-NZ86 might therefore be more effective in the treatment of muscle weakness and is expected to be associated with fewer cardiac side-effects. In a study conducted by Novartis, rats were treated with formoterol or with XA-01-NZ86 subcutaneously for 28 days (0.003 to 0.03mg/kg/day and 0.01 to

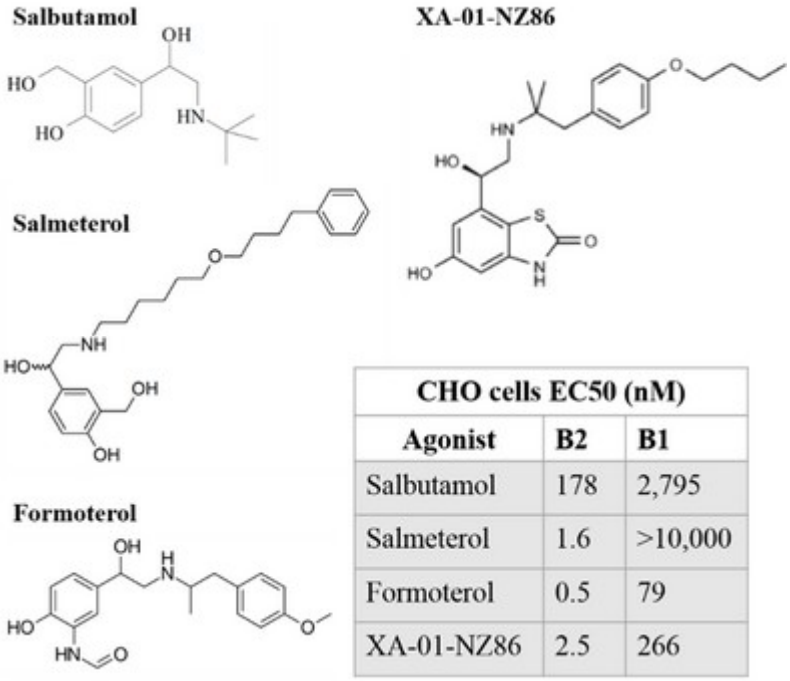

CHO cells EC50 (nM)		
Agonist	**B2**	**B1**
Salbutamol	178	2,795
Salmeterol	1.6	>10,000
Formoterol	0.5	79
XA-01-NZ86	2.5	266

Figure 4.1 Chemical structures and cAMP EC50 data of salbutamol, salmeterol, formoterol and XA-01-NZ86 (B2=beta-2 adrenergic receptor, B1=beta-1 adrenergic receptor, data provided by Novartis).

0.1mg/kg/day, respectively). To measure the effect of the drugs, the weight of the gastrocnemius and soleus muscles and of the heart were measured. While formoterol caused muscle hypertrophy and heart mass increase to the same extent, XA-01-NZ86 had minimal impact on the heart even at the highest concentration of 0.1mg/kg/day (plasma concentration of ca 2nM). At the lowest concentration of 0.01mg/kg/day (plasma concentration of ca 0.2nM), XA-01-NZ86 significantly increased skeletal muscle mass by 11 %. In line with these findings, XA-01-NZ86 treatment was associated with a significantly smaller increase in the heart rate in rats and rhesus monkeys.

In the current study it was tested whether the different ADRB2 agonists exert similar effects on AChR clustering in C2C12 myotubes. A collaboration with researchers from Novartis was established, who provided us with samples of salbutamol, salmeterol, formoterol fumarate, and XA-01-NZ86.

Moreover, it was studied whether salbutamol affects the stability of AChR clusters. Finally, potential pathways were investigated by which salbutamol might affect AChR clustering.

4.2 Effects of ADRB2 agonists on AChR clustering

The effects of ADRB2 agonists were investigated on both agrin-induced clusters and on clusters formed in DOK7-overexpressing cells (see chapter 3, Fig. 3.1).

After the drug treatment of C2C12 myotubes, AChR clusters were visualised by staining with Alexa Fluor-594 conjugated alpha-bungarotoxin, and the number of clusters was analysed. The difference in the ln mean AChR cluster count between untreated and treated cells was determined for each drug concentration and tested for significance (see chapter 2.14.1 for details on the statistical analysis). In addition to plotting the ln mean

cluster numbers, the data were back-transformed (un-logged) and shown in a second bar graph.

4.2.1 Effects of salbutamol sulphate

For the salbutamol treatment of myotubes, salbutamol sulphate was chosen since it dissolves easily in growth medium. 10mM stock solutions were prepared fresh before each experiment.

In a first experiment, the effects of salbutamol sulphate on AChR cluster formation were tested in C2C12 WT cells. C2C12 myoblasts were differentiated into myotubes, and AChR clusters were induced by incubation with 1:100 short rat agrin for 16h overnight. Salbutamol sulphate was applied to the cells simultaneously with agrin for 16h at concentrations of 0, 0.1, 1, 10 or 50µM. The results show a moderate significant increase in the number of AChR clusters at 1, 10 and 50µM ($p=0.003$, $p=0.012$, and $p=0.008$, respectively) (Fig. 4.2). Cluster numbers did not significantly differ from untreated cells after treatment with 0.1µM salbutamol ($p>0.99$). To ensure that cluster formation was due to agrin-incubation, cells were left untreated in a 'no agrin' control condition. Significantly fewer clusters were observed in the negative control condition in the absence of agrin when compared to agrin-treated cells ($p<0.00005$).

It was hypothesised that salbutamol affects AChR clustering by feeding into the agrin-dependent clustering pathway and/or by stabilising clusters on the membrane. To confirm that salbutamol itself does not induce clusters, the effect of salbutamol sulphate incubation was investigated in the absence of agrin. As a positive control, cells were treated with 1:100 short rat agrin for 16h to ensure that the myotubes are in healthy condition, capable of forming clusters. As hypothesised, when C2C12 WT myotubes were treated with 0.1, 1 or 6µM salbutamol sulphate for 16h, no significant increase in

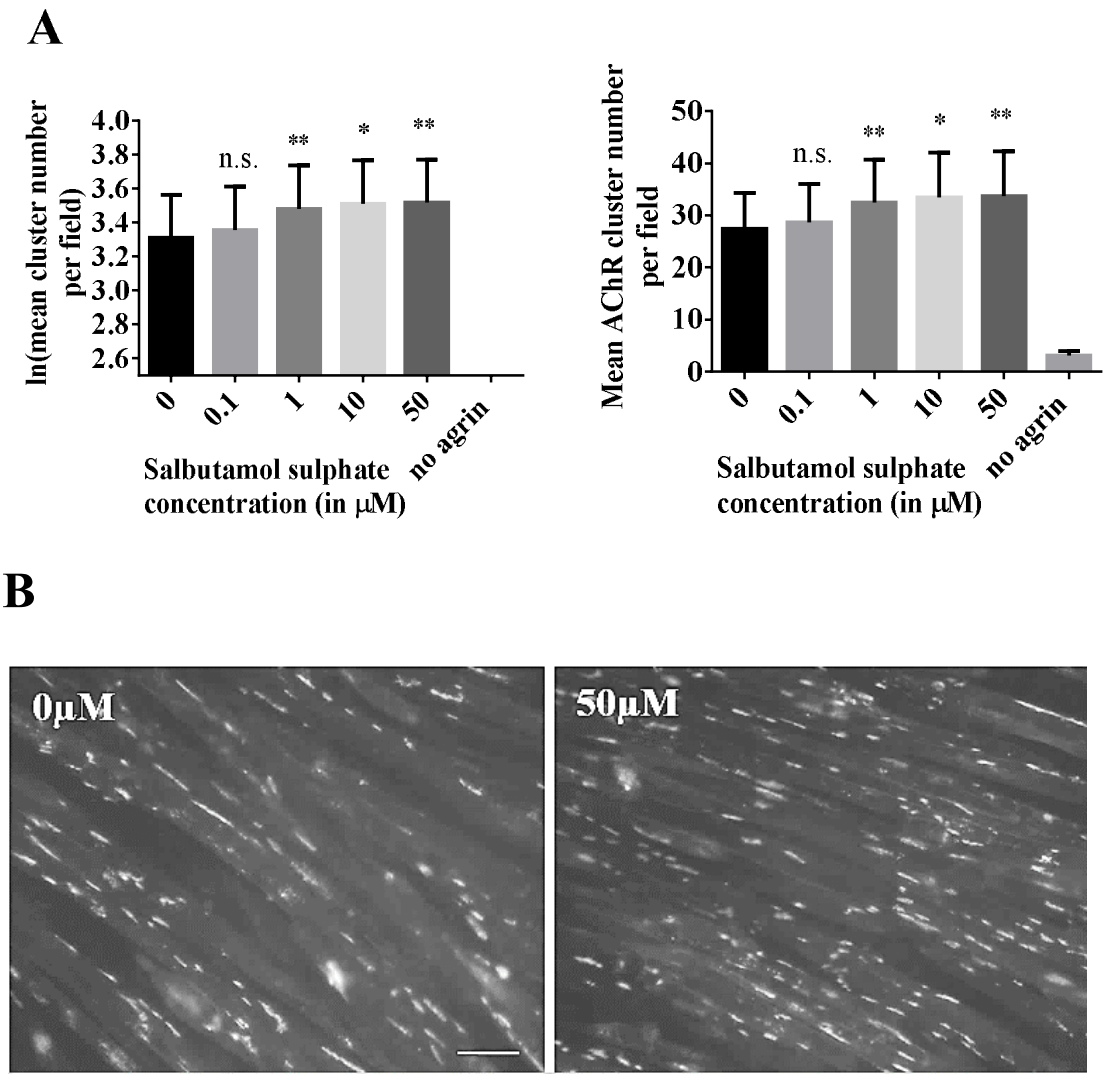

Figure 4.2 Effects of salbutamol on AChR clustering in C2C12 WT cells. Salbutamol sulphate was applied for 16h simultaneously with short soluble rat agrin. (A) 1, 10 and 50μM but not 0.1μM salbutamol caused a significant increase in the number of AChR clusters (difference=0.17, SE=0.05, p=0.003, difference=0.2, SE=0.07, p=0.012, difference=0.26, SE=0.07, p=0.008, and difference=0.05, SE=0.05, p>0.99, respectively; agrin negative control: difference=2.19, SE=0.16, p<0.00005). (B) Representative microscopic images of untreated and salbutamol-treated myotubes (both agrin-treated). N=4. Scale bar=50μm. Error bars indicate the standard error of the mean. n.s.p>0.05, *p≤0.05, **p≤0.01.

the number of clusters occurred ($p>0.99$, $p=0.5$, and $p>0.99$, respectively) (Fig. 4.3). The small trend towards increased clustering in salbutamol treated cells in the absence of agrin could potentially be explained by a stabilising effect of salbutamol on spontaneously forming clusters. Significantly more clusters formed in the positive control condition in the presence of agrin ($p<0.00005$).

It was hypothesised that salbutamol exerts its effect on AChR clustering through the activation of ADRB2s. Therefore, it was investigated whether overexpression of ADRB2s in C2C12 cells would cause a larger increase in AChR clustering in response to salbutamol. To address this question, the ADRB2 was cloned into a retroviral expression vector, and C2C12 myoblasts were infected with retrovirus. Cells stably overexpressing ADRB2s are henceforth referred to as C2C12^{ADRB2}. To confirm overexpression of ADRB2s, a western blot was performed. C2C12^{ADRB2} and C2C12 WT myoblasts were lysed and 8µg protein were subjected to SDS PAGE. For C2C12^{ADRB2} cells, a band corresponding to the ADRB2 was detected by incubation of the immunoblot with 1:800 anti-ADRB2 antibody overnight (Fig. 4.4A). Endogenous ADRB2s in C2C12 WT cells could not be detected. Probing the blot with anti-alpha tubulin antibody showed that equal amounts of protein had been loaded on the gel.

Overexpression of ADRB2s in C2C12 cells did not increase the effect of salbutamol on AChR cluster numbers (Fig. 4.4B). When C2C12^{ADRB2} myotubes were incubated with 0.1, 1, 5 or 10µM salbutamol sulphate for 16h during agrin-incubation, no increase in the number of AChR clusters could be observed when compared to untreated cells ($p>0.99$, $p=0.64$, $p>0.99$, and $p>0.99$, respectively).

In DOK7 patients, the effect of salbutamol and ephedrine on muscle strength builds up within weeks and months. Mimicking synaptic functioning *in vitro* for the investigation of treatment is challenging since the time window for treatment application

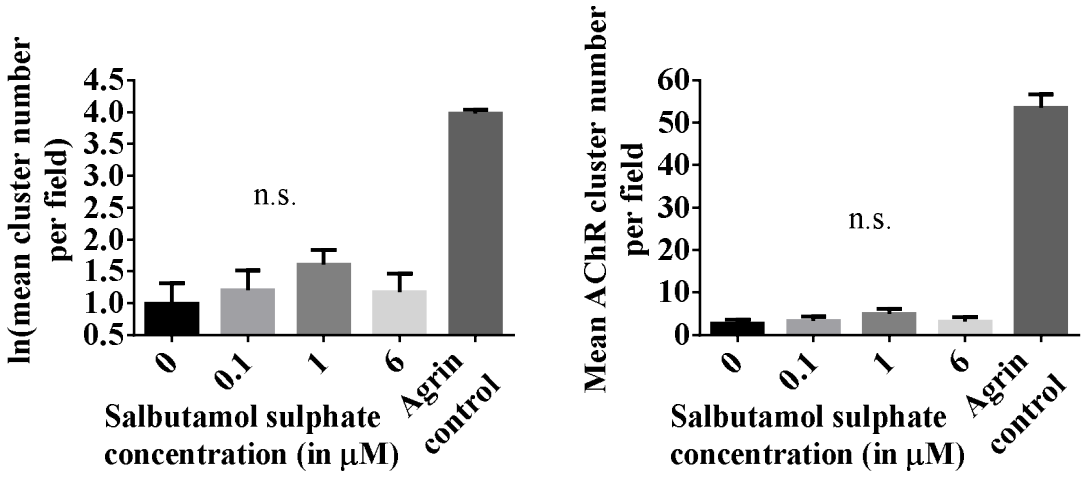

Figure 4.3 Effects of salbutamol on AChR cluster formation in the absence of agrin. Salbutamol sulphate was applied to C2C12 WT myotubes at 0, 0.1, 1 or 6μM for 16h. Salbutamol did not increase the number of AChR clusters when compared to untreated cells (difference=0.21, SE=0.44, $p>0.99$, difference=0.61, SE=0.4, $p=0.5$, and difference=0.17, SE=0.43, $p>0.99$, respectively; agrin positive control: difference=2.98, SE=0.32, $p<0.00005$). Error bars indicate the standard error of the mean. n.s.$p>0.05$.

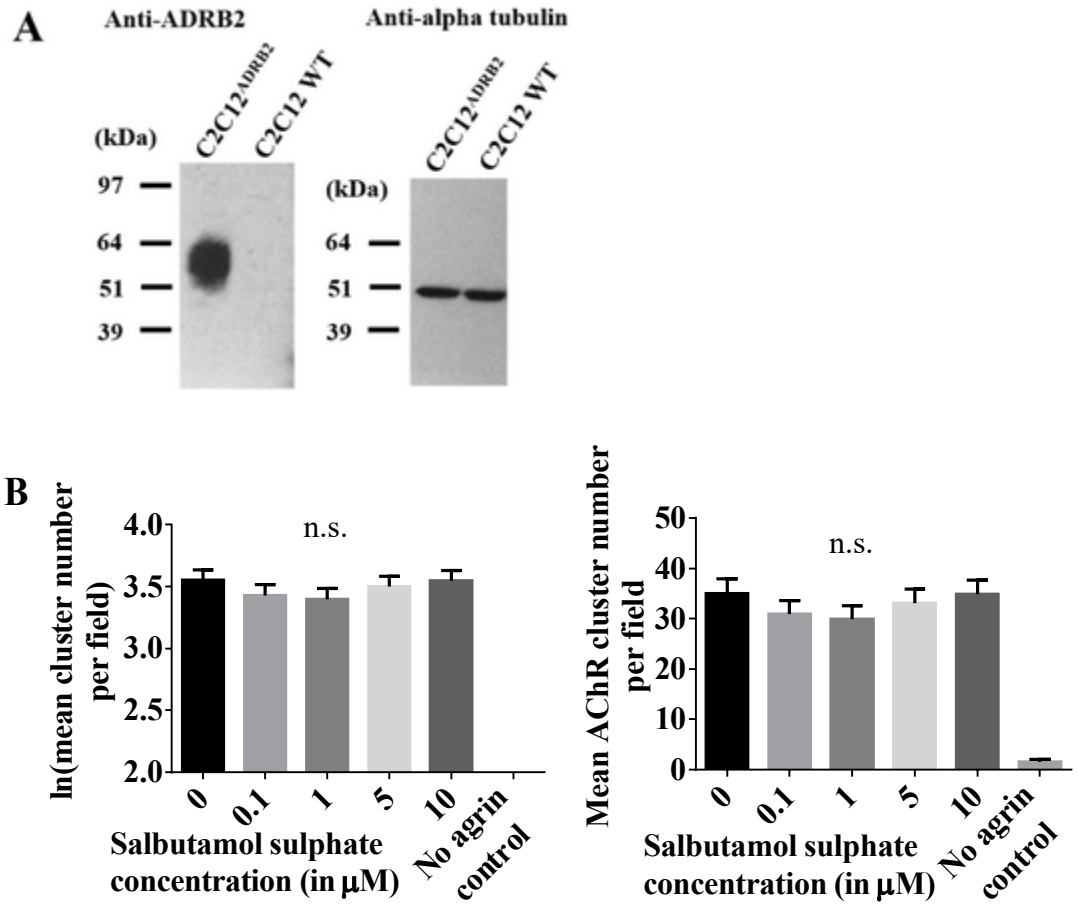

Figure 4.4 Expression of ADRB2 in C2C12 cells. (A) Western blot of ADRB2. Whole-cell lysate from C2C12^{ADRB2} and C2C12 WT myoblasts was subjected to SDS Page. A band corresponding to the ADRB2 was detected for C2C12^{ADRB2} cells by probing with 1:800 anti-ADRB2 antibody overnight. (B) No increase in the number of AChR clusters occurred in response to incubation with 0.1, 1, 5 or 10µM salbutamol sulphate (difference=0.12, SE=0.1, p>0.99, difference=0.16, SE=0.1, p=0.64, difference=0.004, SE=0.1, p>0.99, and difference=0.05, SE=0.1, p>0.99). N=2. Error bars indicate the standard error of the mean. n.s.p>0.05.

is limited. It is not possible to investigate the effects of salbutamol on myotubes over a long period of time since the cells deteriorate within days after fusion of myoblasts. In order to maximise the duration of the treatment, C2C12 WT cells were incubated with salbutamol for 6-8 days during the differentiation of myoblasts into myotubes. The medium was replaced every other day. AChR clustering was induced by incubation of myotubes with soluble short rat agrin for 16h (salbutamol present). The results suggest a detrimental effect of sustained salbutamol incubation on the number of clusters even at low concentrations of 0.1 and 1μM ($p=0.04$, and $p=0.01$, respectively; no agrin control: $p<0.00005$) (Fig. 4.5A). Sustained salbutamol treatment also reduced the numbers of spontaneously forming AChR clusters in the absence of agrin incubation ($p=0.17$ and $p=0.03$, respectively; agrin positive control: $p<0.00005$) (Fig. 4.5B).

The results presented so far suggested that salbutamol has an effect on the formation of agrin-induced AChR clusters in C2C12 WT cells. Next, it was investigated whether salbutamol affects AChR clustering in DOK7-mutant cells. This was addressed by studying the DOK7-mediated clustering pathway in the absence of agrin. C2C12 myoblasts were infected with retrovirus, containing WT or mutant *DOK7* (c.1124_1127dupTGCC). A preliminary experiment was conducted in which $C2C12^{DOK7\ WT}$ myotubes were treated with 0, 0.1, 1, 5 or 10μM salbutamol sulphate for 16h (Fig. 4.6). Although the results suggested a small increase in the number of clusters ($p=0.02$, $p=0.78$, $p=0.03$, and $p=0.02$, respectively), DOK7 mutant cells were considered to provide a better disease model. In $C2C12^{DOK7\ WT}$ cells, a large number of AChR clusters form due to continuous DOK7 signalling, and subtle differences caused by ADRB2 agonist treatment are more likely to go unnoticed. A preliminary experiment was performed in which $C2C12^{DOK7\ c.1124\_27dupTGCC}$ myotubes were treated with 0, 0.1, 1, 5 or 10μM salbutamol sulphate for 16h (Fig. 4.7). No significant effect with treatment could

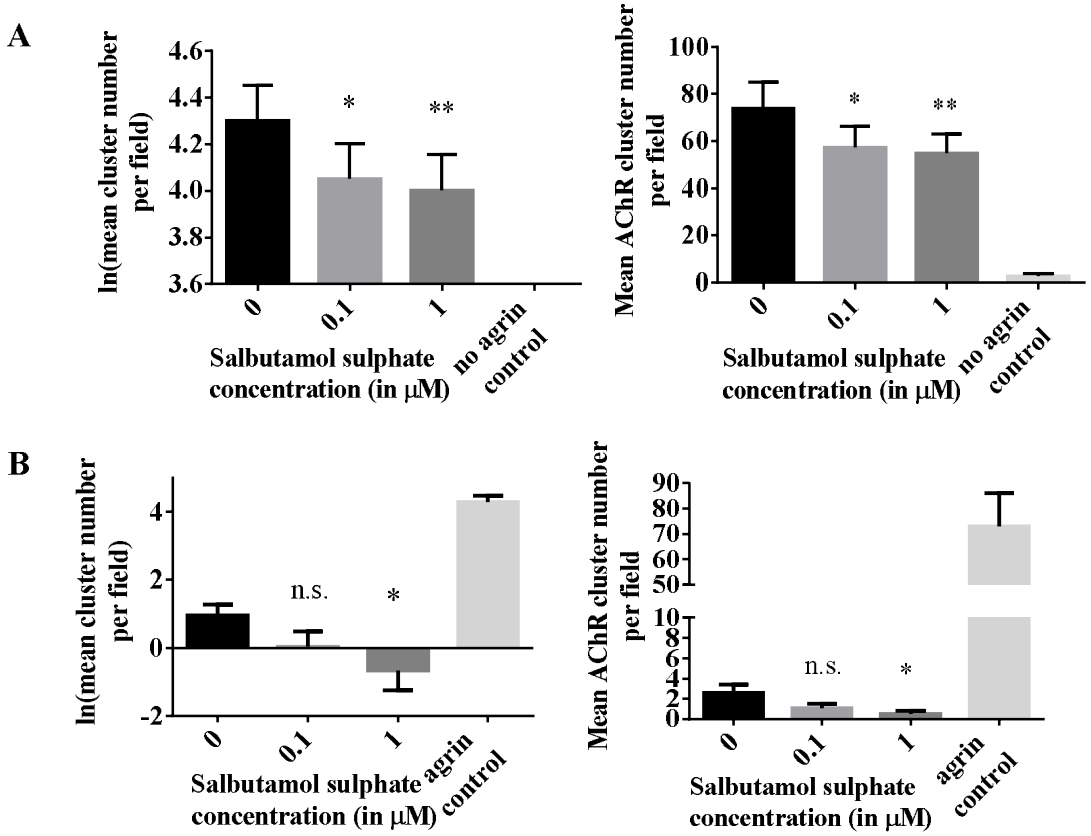

Figure 4.5 Effects of sustained salbutamol application on AChR clustering. C2C12 WT cells were incubated with 0, 0.1, or 1μM salbutamol sulphate during differentiation. (A) Salbutamol significantly reduced the number of agrin-induced clusters when compared to untreated cells (difference=0.25, SE=0.1, p=0.04, and difference=0.3, SE=0.1, p=0.01; negative no agrin control: difference=3.32, SE=0.41, p<0.00005). (B) Sustained salbutamol treatment reduced spontaneous AChR clustering in the absence of agrin (difference=0.92, SE=0.48, p=0.17 and difference=1.61, SE=0.62, p=0.03, respectively; agrin positive control: difference=3.34, SE=0.26, p<0.00005). N=3. Error bars indicate the standard error of the mean. n.s.p>0.05, *p≤0.05, **p≤0.01.

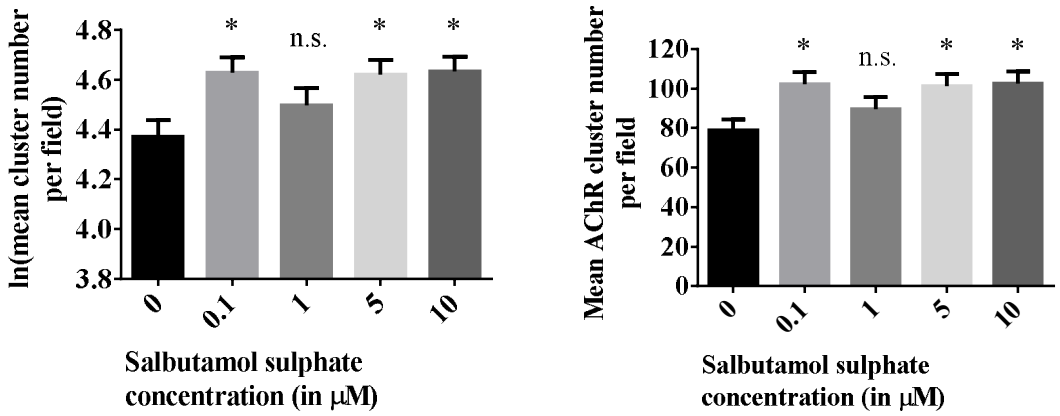

Figure 4.6 Effects of salbutamol treatment on AChR clustering in C2C12$^{DOK7\ WT}$ cells. Incubation of myotubes with 0.1, 1, 5 or 10μM salbutamol sulphate for 16 hours caused a small increase in the number of clusters (difference=0.26, SE=0.09, p=0.02, difference=0.13, SE=0.1, p=0.78, difference=0.25, SE=0.09, p=0.03, and difference=0.26, SE=0.09, p=0.02, respectively). N=1. Error bars indicate the standard error of the mean. n.s.p>0.05, *p≤0.05.

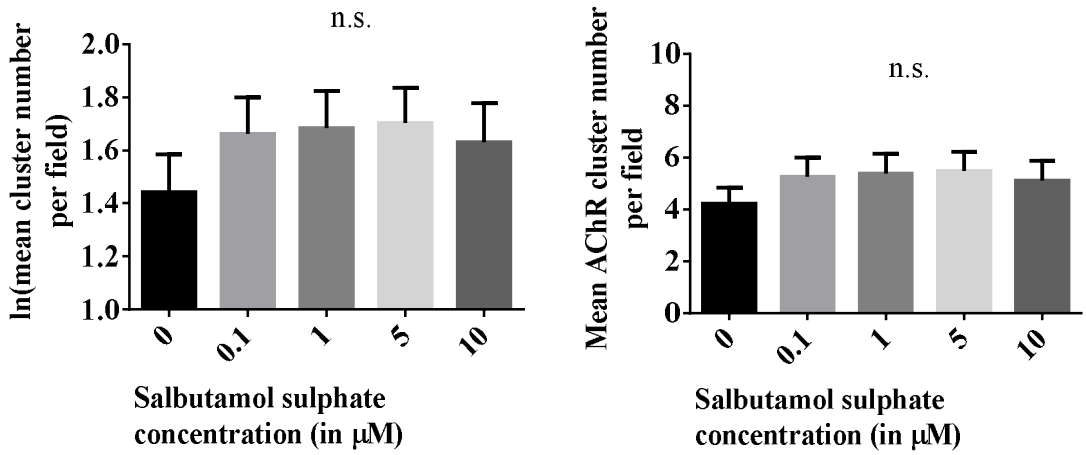

Figure 4.7 Effects of 16h salbutamol treatment on AChR clustering in C2C12$^{DOK7\ c.1124_27dupTGCC}$ cells. No significant effect on the number of clusters occurred at concentrations of 0.1, 1, 5 or 10μM (difference=0.22, SE=0.2, p>0.99, difference=0.24, SE=0.2, p=0.92, difference=0.26, SE=0.2, p=0.74, and difference=0.19, SE=0.21, p>0.99, respectively). N=1. Error bars indicate the standard error of the mean. n.s.p>0.05.

be observed (p>0.99, p=0.92, p=0.74, and p>0.99, respectively). However, it is important to note that baseline cluster numbers (condition '0μM') were very low with an average of 4.2 clusters per microscopic field, which might have an effect on the ability of salbutamol to exert a stabilising effect during cluster formation.

A variable for potential change in the protocol is the treatment duration. Previously applying salbutamol overnight for 16h, the treatment duration was now increased to a total of 22h. The effects of salbutamol sulphate treatment on AChR cluster numbers in C2C12$^{DOK7\ c.1124_27dupTGCC}$ myotubes were tested at concentrations of 0.01, 0.1, 1, 5, 10 and 50μM (Fig. 4.8). A significant dose-dependent increase in the number of clusters was observed (Fig. 4.8A). 0.01 and 0.1μM salbutamol sulphate caused a similar increase in AChR clustering (p=0.001 and p=0.00002, respectively). 1 and 5μM caused a further increase in clustering (p<0.00005 and p<0.00005, respectively), whereas a slight decrease in the treatment response was found at 10μM (p<0.00005). The largest increase in AChR clustering was obtained after incubation with 50μM salbutamol sulphate (increase of 99%, p<0.00005). The length of AChR clusters was also analysed, and the difference in the ln mean AChR cluster length between untreated and treated cells was determined for each concentration and tested for significance (see chapter 2.14.1 for details on the statistical analysis). No significant effect of salbutamol sulphate on the length of clusters was observed (p=0.64, p=0.45, p>0.99, p>0.99, p>0.99, and p=0.12, respectively) (Fig. 4.8B).

It is important to note that baseline levels of AChR cluster numbers in the absence of treatment can vary considerably between stable cell lines, i.e. between retroviral infections (between ~5 and 15 clusters per field). Variation also often occurs between experiments on cells from the same batch. Therefore, the experiment was repeated, using both different batches of cells and virus.

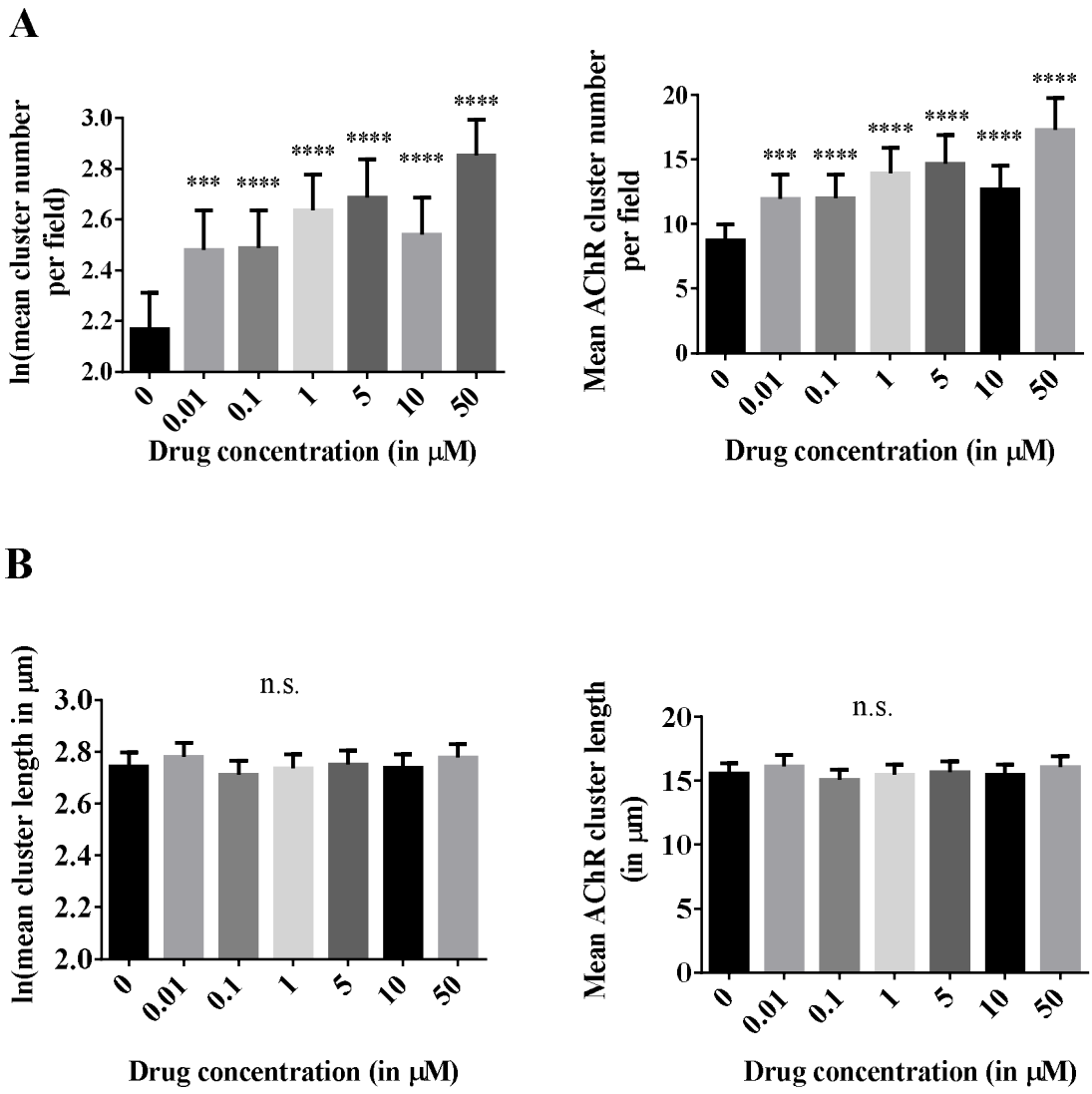

Figure 4.8 Effects of salbutamol sulphate on AChR clustering in C2C12$^{DOK7\ c.1124_27dupTGCC}$ cells. Myotubes were incubated with 0.01, 0.1, 1, 5, 10 or 50μM salbutamol sulphate for 22h. (A) Salbutamol sulphate treatment induced a significant increase in the number of clusters at all concentrations tested (difference=0.31, SE=0.08, p=0.001, difference=0.32, SE=0.07, p=0.00002, difference=0.47, SE=0.05, p<0.00005, difference=0.52, SE=0.07, p<0.00005, difference=0.37, SE=0.06, p<0.00005, and difference=0.68, SE=0.05, p<0.00005, respectively). (B) No significant effect on the length of clusters was observed (difference=0.04, SE=0.02, p=0.64, difference=0.03, SE=0.02, p=0.45, difference=0.01, SE=0.01, p>0.99, difference=0.01, SE=0.02, p>0.99, difference=0.01, SE=0.02, p>0.99, and difference=0.03, SE=0.01, p=0.12, respectively). N=12. Error bars indicate the standard error of the mean. n.s.p>0.05 ***p≤0.001, ****p≤0.0001.

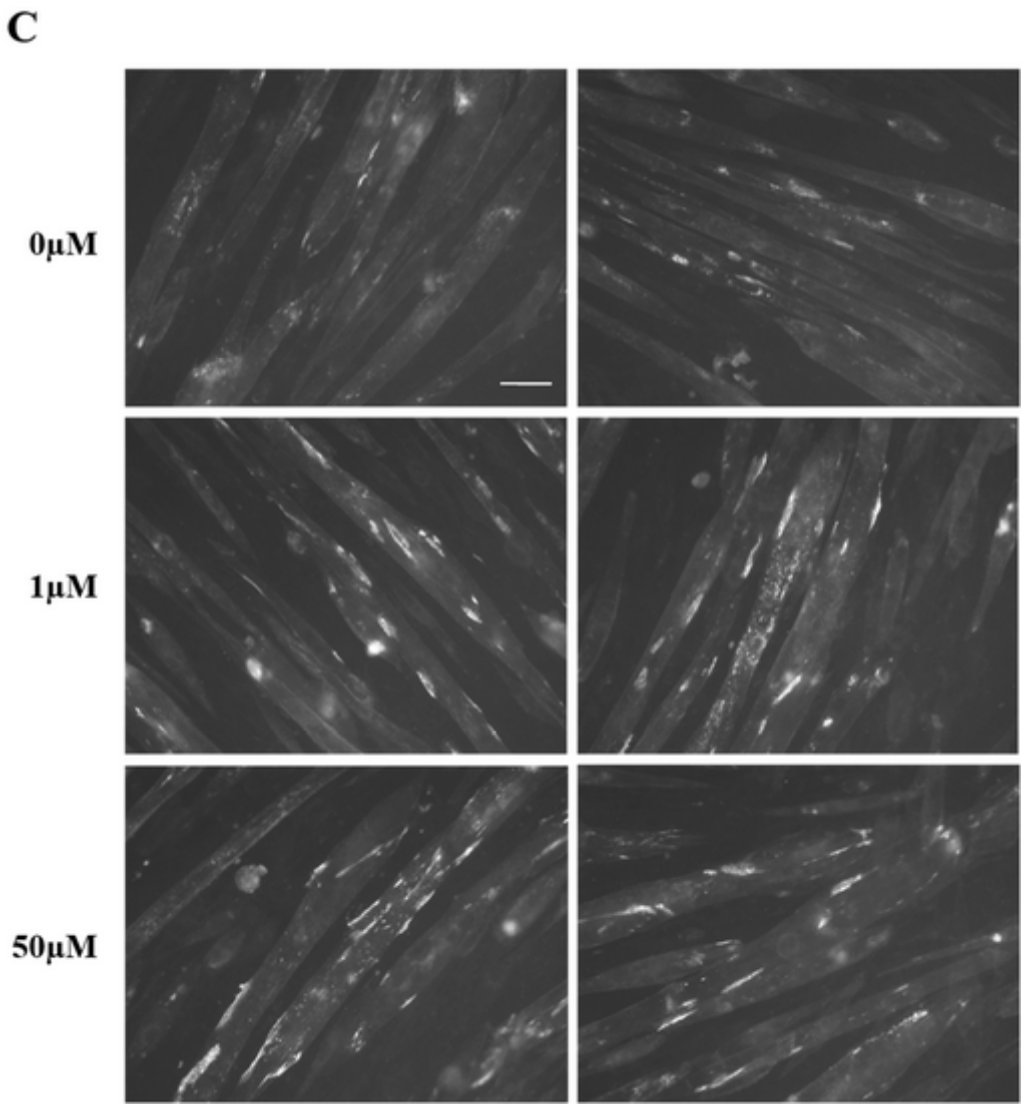

Figure 4.8 (continued) (C) Representative microscopic images of C2C12$^{DOK7\ c.1124_27dupTGCC}$ myotubes treated with salbutamol sulphate as indicated. Scale bar=50µm.

4.2.2 Effects of additional ADRB2 agonists: a collaboration with Novartis

C2C12$^{DOK7\ c.1124\text{-}27dupTGCC}$ myotubes were treated with the respective ADRB2 agonist for 22h. All drugs were reconstituted in DMSO to gain 10mM stock solutions, which were then frozen at -20°C. Further dilutions were prepared with growth medium before each experiment.

XA-01-NZ86

Myotubes were incubated with the agonist XA-01-NZ86 at a concentration of 0, 0.01, 0.1, 0.5, 1, 10 and 50µM. The drug treatment significantly increased the number of AChR clusters, especially when applied at low concentrations (Fig. 4.9). 0.01, 0.1 and 0.5µM caused a dose-dependent increase in the number of cluster (all $p<0.00005$). 0.5µM XA-01-NZ86 was most effective, causing an increase in the number of clusters by 82%. A further increase in the dose, however, caused a reduction in the treatment response. While 1µM agonist still significantly increased clustering ($p<0.00005$), no significant difference could be observed at a concentration of 10µM XA-01-NZ86 ($p>0.99$). Cells treated with 50µM agonist died during the incubation period and detached from the bottom of the plate. Solutions with a higher drug concentration contained a higher percentage of DMSO. Since this might account for the cell death observed at 50µM, a control experiment was performed in which cells were treated with the same amount of DMSO in the absence of XA-01-NZ86. No cell death was observed in cells treated with DMSO alone (data not shown).

It was hypothesised that XA-01-NZ86 exerts its effects by activating ADRB2s expressed in the myotubes, which leads to downstream signalling events that affect AChR clustering. To confirm this hypothesis the experiment was repeated but in the presence of ICI-118,551, a selective ADRB2 antagonist. Cells were incubated with 0, 0.1, or 0.5µM

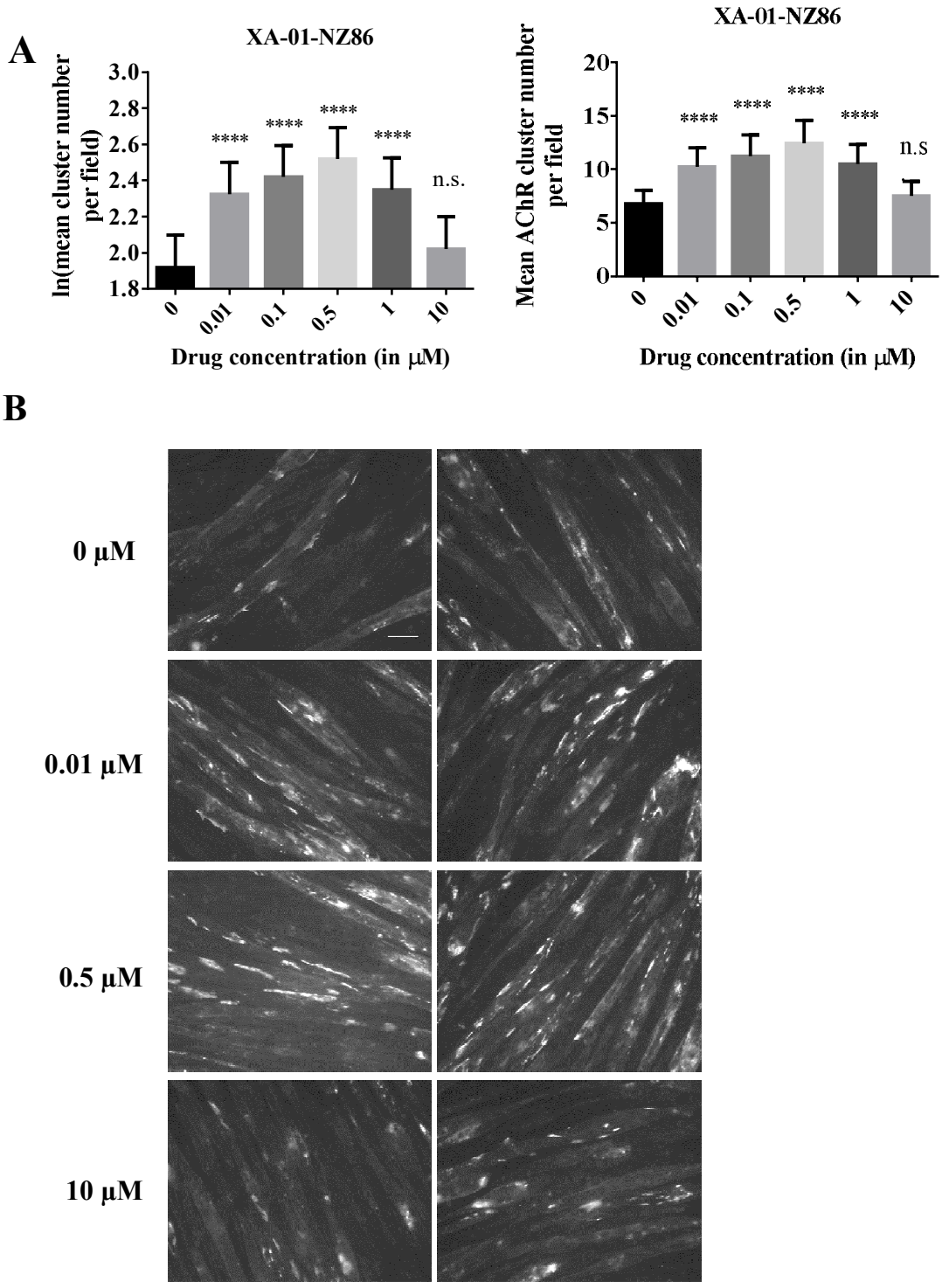

Figure 4.9 Effects of XA-01-NZ86 on AChR clustering in C2C12$^{DOK7\ c.1124_27dupTGCC}$ cells. Myotubes were incubated with 0.01, 0.1, 0.5, 1, 10 or 50μM XA01N286 for 22h. (A) A significant increase in the number of clusters was observed at 0.01, 0.1, 0.5 and 1μM (difference=0.41, SE=0.09, p<0.00005, difference=0.5, SE=0.09, p<0.00005, and difference=0.6, SE=0.09, p<0.00005, and difference=0.43, SE=0.1, p<0.00005, respectively), but not 10μM (difference=0.1, SE=0.11, p=1.67). (B) Representative microscopic images of C2C12$^{DOK7\ c.1124_27dupTGCC}$ myotubes treated with XA-01-NZ86 as indicated. N=4. Scale bar=50μm. Error bars indicate the standard error of the mean. n.s.p>0.05, ****p≤0.0001.

XA-01-NZ86 only, or with a mix of 0, 0.1, or 0.5µM XA-01-NZ86 and 1µM ICI-118,551. As shown earlier, 0.1 and 0.5µM XA-01-NZ86 significantly increased the number of AChR clusters (both $p<0.00005$) (Fig. 4.10A). This effect was abolished when the ADRB2 inhibitor was applied (both $p<0.00005$). Fig.4.10B shows the number of AChR clusters plotted for each concentration of XA-01-NZ86 in the presence versus absence of ICI-118,551. Incubation of the cells with ICI-118,551 alone did not affect the number of AChR clusters when compared to cells left untreated (comparison '0µM': $p=0.53$). In cells treated with 0.1 or 0.5µM XA-01-NZ86, simultaneous incubation with ICI-118,551 led to the formation of significantly fewer AChR clusters when compared to cells treated with XA-01-NZ86 alone (comparison '0.1µM' and '0.5µM' both $p=0.005$). The results suggest that blocking of ADRB2s prevented the agonist-mediated effects on AChR clustering and that XA-01-NZ86 increases the formation of clusters.

Formoterol fumarate

Cells were incubated with 0, 0.1, 1, 10 or 50µM of the agonist formoterol fumarate. 0.1, 1 and 10µM caused a similar significant increase in the number of AChR clusters ($p=0.01$, $p=0.01$, and $p=0.01$, respectively) (Fig. 4.11). The largest increase was achieved with 50µM formoterol fumarate (34% increase, $p<0.00005$).

Salmeterol

The effects of salmeterol on AChR clustering were tested at concentrations of 0, 0.01, 0.1, 1 and 10µM. The response pattern was similar to that observed for XA-01-NZ86 incubation, with low concentrations being most effective in raising the number of AChR clusters (Fig. 4.12). The greatest difference in the cluster number between treated and untreated cells was achieved with a concentration of 0.01µM (54% increase, $p<0.0005$). 0.1, 1 and 10µM also significantly increased the number of clusters ($p<0.0005$, $p<0.0005$, and $p=0.03$, respectively), although a slight decrease in the

A

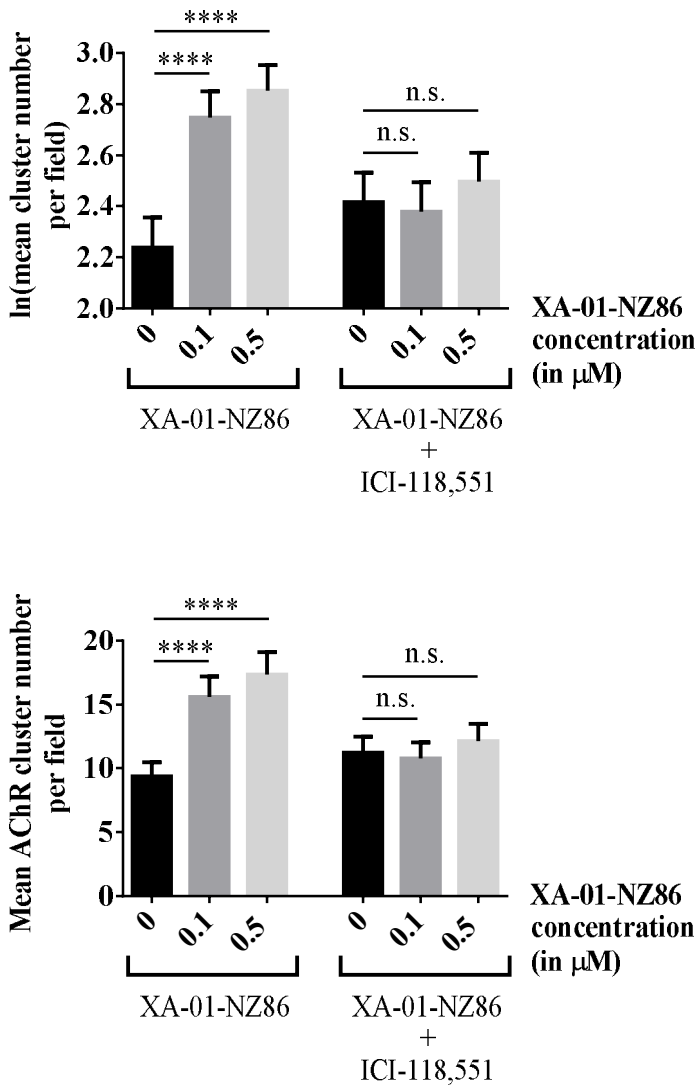

Figure 4.10 Blocking of XA-01-NZ86-mediated effects by inhibition of ADRB2s in C2C12$^{DOK7\ c.1124_27dupTGCC}$ myotubes. For 22h, cells were incubated with 0, 0.1, or 0.5μM XA-01-NZ86 only, or with a mix of XA-01-NZ86 and 1μM ICI-118,551. (A) Agonist treatment significantly increased the number of AChR clusters (difference=0.51, SE=0.12, p<0.00005, and difference=0.62, SE=0.12, p<0.00005, respectively). This effect was abolished through simultaneous incubation with the ADRB2 inhibitor (difference=0.04, SE=0.13, t-test p>0.99, and difference=0.08, SE=0.12, p>0.99, respectively). N=2. Error bars indicate the standard error of the mean. n.s.p>0.05, ***p≤0.001, ****p≤0.0001.

B

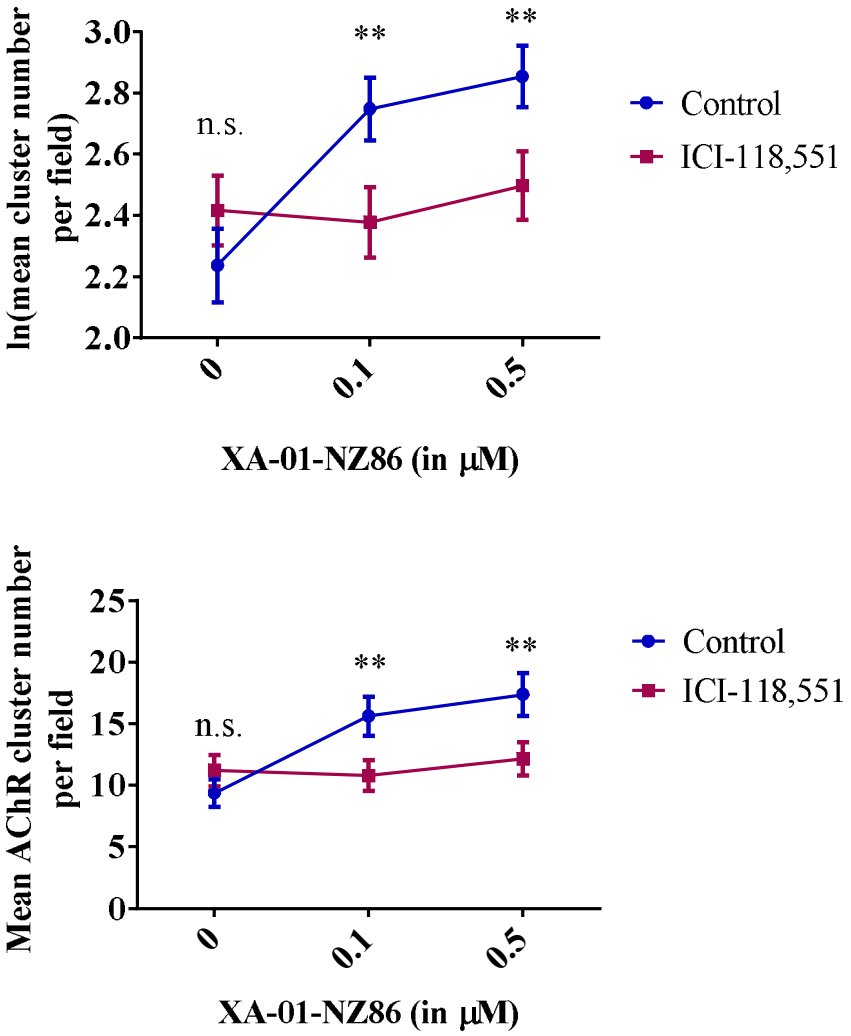

Figure 4.10 (continued) (B) Incubation of the cells with the ADRB2 inhibitor ICI-118,551 did not have a significant effect on the number of AChR clusters in the absence of XA-01-NZ86 treatment ('0µM': difference=0.18, SE=0.13, p=0.53). In cells treated with 0.1 or 0.5µM XA-01-NZ86, simultaneous incubation with ICI-118,551 led to the observation of significantly fewer AChR clusters when compared to cells treated with XA-01-NZ86 alone ('0.1µM': difference=0.37, SE=0.12, p=0.005, and '0.5µM': difference=0.36, SE=0.11, t-test p=0.005). N=2. Error bars indicate the standard error of the mean. n.s.$p>0.05$, **$p\leq0.01$.

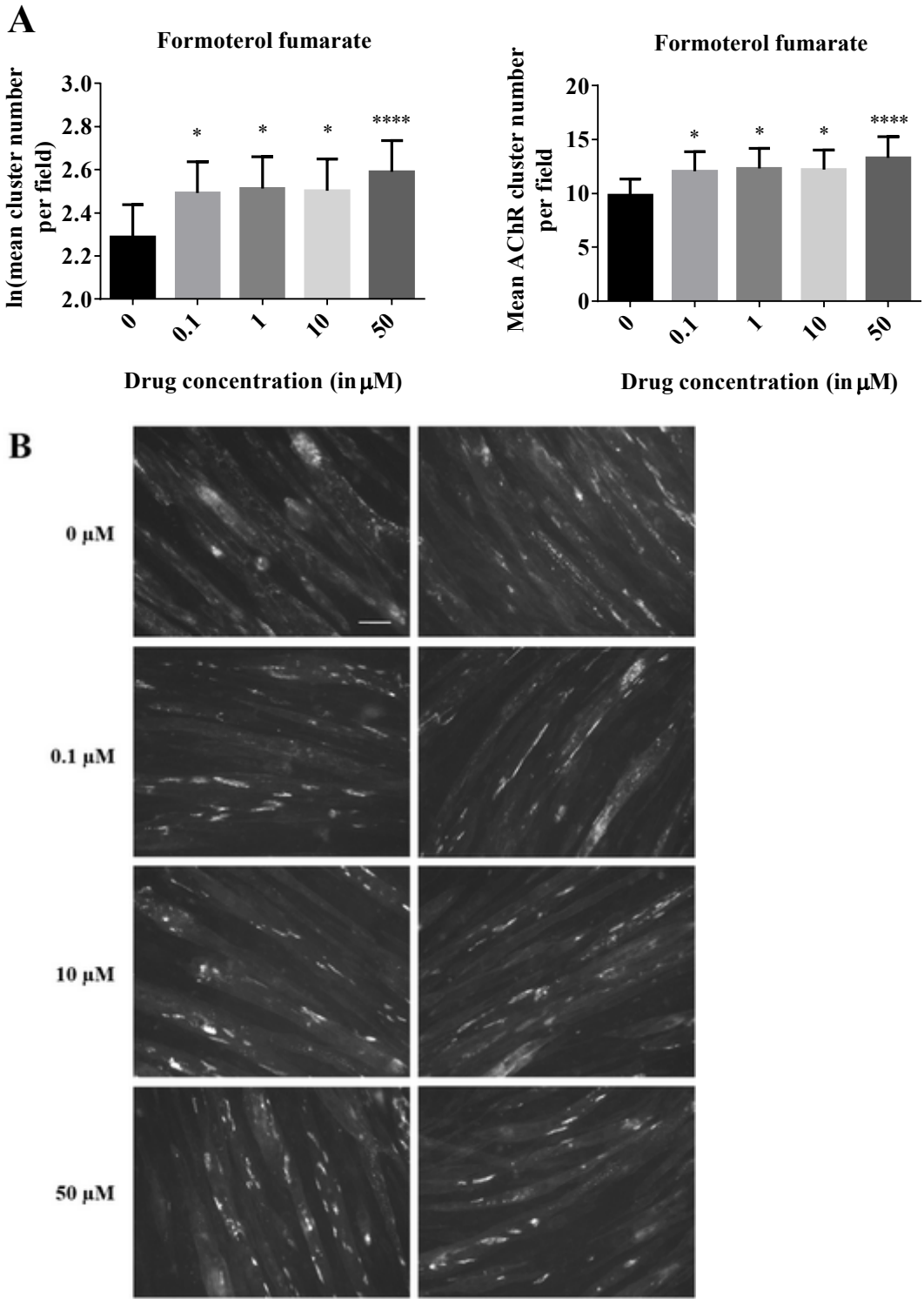

Figure 4.11 Effects of formoterol fumarate on AChR clustering in C2C12$^{DOK7\ c.1124_27dupTGCC}$ cells. Myotubes were incubated with 0.1, 1, 10 or 50µM formoterol fumarate for 22h. (A) A significant increase in the number of clusters occurred (difference=0.2, SE=0.07, p=0.01, difference=0.22, SE=0.07, p=0.01, and difference=0.21, SE=0.07, p=0.01, and difference=0.3, SE=0.07, p<0.00005, respectively). (B) Representative microscopic images of C2C12$^{DOK7\ c.1124_27dupTGCC}$ myotubes treated with formoterol fumarate as indicated. N=5. Scale bar=50µm. Error bars indicate the standard error of the mean. *p≤0.05, ****p≤0.0001.

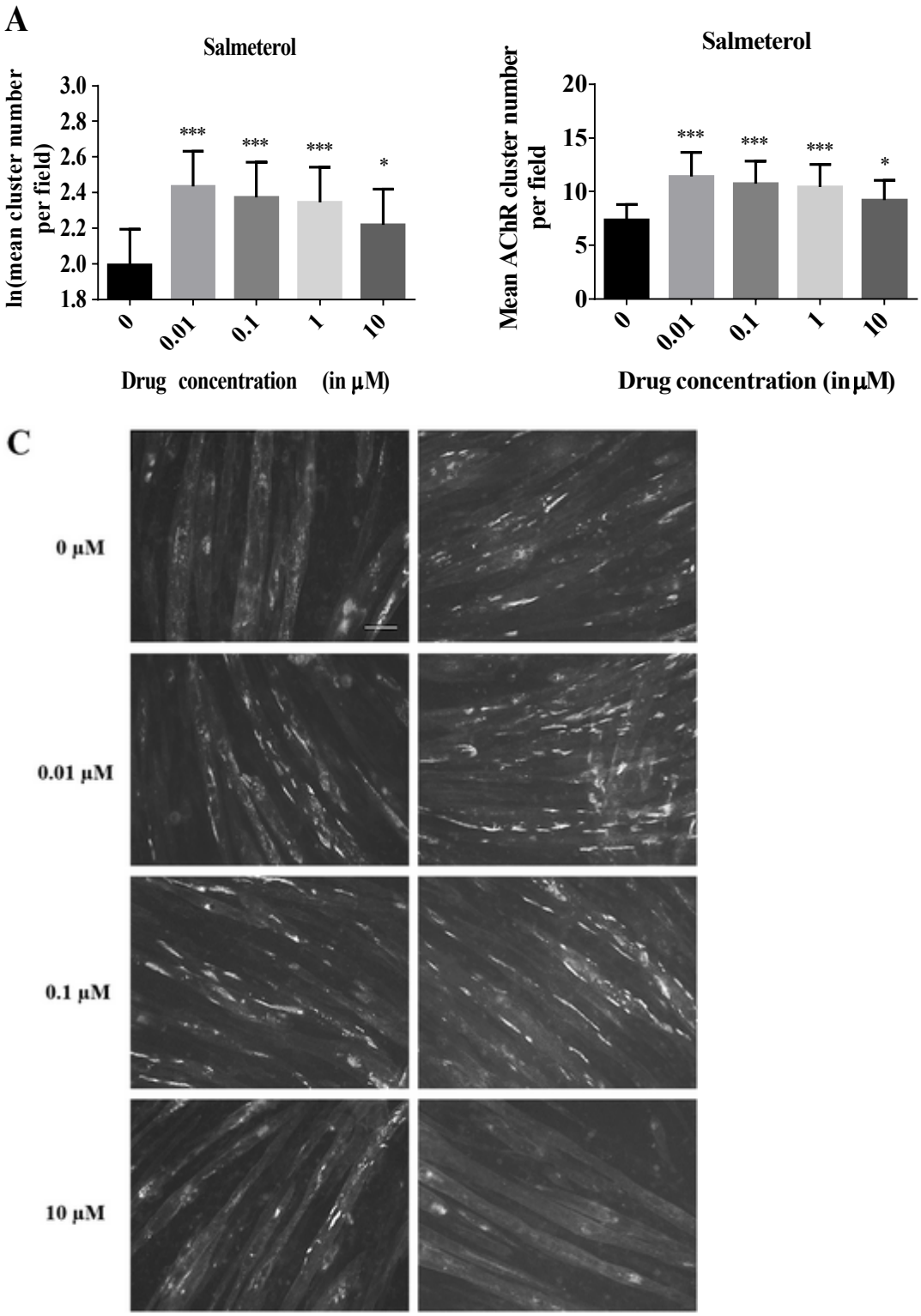

Figure 4.12 Effects of salmeterol on AChR clustering in C2C12$^{DOK7\ c.1124_27dupTGCC}$ cells. Myotubes were incubated with 0.01, 0.1, 1, 10 or 50µM salmeterol for 22h. (A) 0.01, 0.1, 1, and 10µM caused a significant increase in the number of AChR clusters (difference=0.44, SE=0.08, p<0.0005, difference=0.38, SE=0.08, p<0.0005, difference=0.35, SE=0.08, p<0.0005, and difference=0.23, SE=0.08, p=0.03 respectively) (B) Representative microscopic images of C2C12$^{DOK7\ c.1124_27dupTGCC}$ myotubes treated with salmeterol as indicated. N=5. Scale bar=50µm. Error bars indicate the standard error of the mean. *p≤0.05, **p≤0.01, ***p≤0.001, ****p≤0.0001.

treatment response was observed. Cells treated with 50µM salmeterol died during the incubation period and detached from the plate.

Salbutamol

Finally, the effects of salbutamol were tested at concentrations of 0, 0.1, 1, 10 and 50µM. Similar results as with salbutamol sulphate were expected, and indeed, a dose dependent increase in the number of AChR clusters was observed (Fig. 4.13). 0.1, 1 and 10µM caused a similar highly significant increase in clustering (all $p<0.00005$), while 50µM caused the greatest difference in the mean cluster number when compared to untreated cells (146% increase, $p<0.00005$).

The results show that all ADRB2 agonists tested increased the number of AChR clusters. Salbutamol had the largest effect (145% increase), followed by XA-01-NZ86 (82%), salmeterol (54%) and formoterol fumarate (34%). XA-01-NZ86 and salmeterol were most effective at low concentrations (0.5 and 0.01µM), while salbutamol caused the largest increase at 50µM.

Results on cluster lengths were only reported for C2C12 WT cells, although they were analysed in every experiment. Despite an occasional trend towards reduced cluster lengths, overall, no noteworthy differences in cluster size occurred in response to salbutamol treatment.

4.3 Effects of salbutamol on AChR cluster stability

The experiments presented above suggest that ADRB2 agonists have an effect on both agrin-induced and DOK7-mediated AChR clusters. The observed increase in the number of AChR clusters might be due to a stabilising effect of ADRB2 agonists on

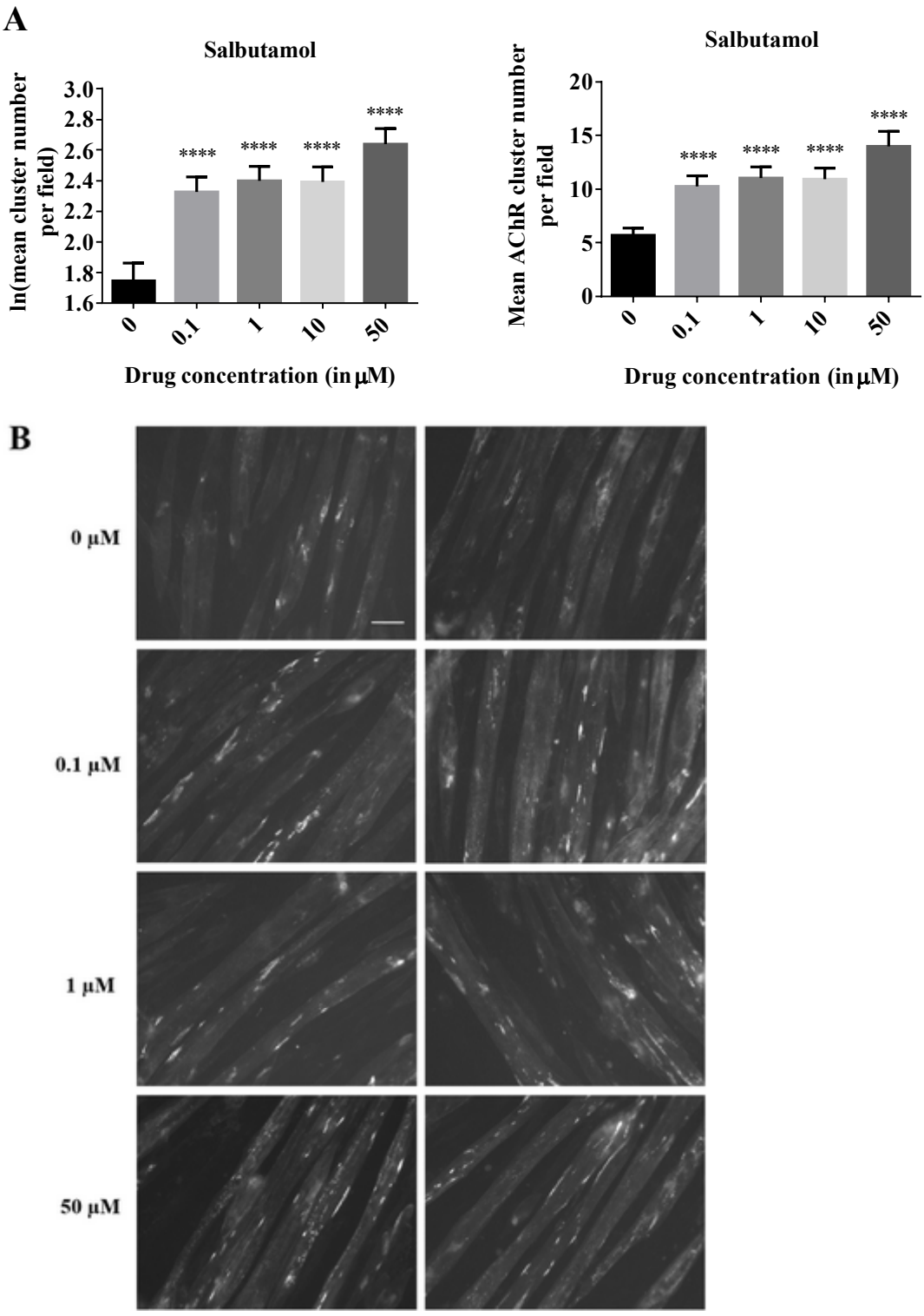

Figure 4.13 Effects of salbutamol on AChR clustering in C2C12$^{DOK7\ c.1124_27dupTGCC}$ cells. Myotubes were incubated with 0.1, 1, 10 or 50µM salbutamol for 22h. (A) A dose dependent increase in the number of clusters was observed (difference=0.58, SE=0.13, p<0.00005, difference=0.66, SE=0.12, p<0.00005, difference=0.65, SE=0.12, p<0.00005, difference=0.9, SE=0.13, p<0.00005). (B) Representative microscopic images of C2C12$^{DOK7\ c.1124_27dupTGCC}$ myotubes treated with salbutamol as indicated. N=3. Scale bar=50µm. Error bars indicate the standard error of the mean. n.s.p>0.05, ****p≤0.0001.

forming clusters. To explore this hypothesis in more detail, experiments on the stability of AChR clusters were conducted by studying the effects of salbutamol on dispersing clusters. C2C12 WT myotubes, where cluster formation can be induced by agrin, provides a suitable model for such experiments. It was hypothesised that clusters induced by incubation with soluble short rat agrin will break down when agrin is removed. Accordingly, a reduction in cluster numbers over time was expected.

A time course experiment was performed in which clusters were induced with 1:500 soluble short rat agrin for 16h. Agrin was removed, and the cells were washed three times in differentiation medium. The cells were then left in differentiation medium for 6, 12 or 22h, and the number and length of clusters were compared to cells fixed and stained directly after 16h of agrin treatment ('0h'). The results confirmed significant dispersal of AChR clusters in a time-dependent manner (6h: $p=0.02$, 12h: $p=0.001$, and 22h: $p<0.00005$) (Fig. 4.14A). After 22h, only very few clusters remained and images of myotubes resembled those from the 'no agrin' control condition. A trend towards smaller clusters was observed (6h: $p=0.86$, 12h: $p=0.88$, and 22h: $p=0.06$) (Fig. 4.14B). The finding that a reduction in cluster lengths did not reach statistical significance might be explained by the fact that only clusters larger than 5µm in length were included in the analysis. This threshold was chosen in order to be able to detect a decrease in average-sized clusters, and therefore to prevent smaller clusters, which are the result of larger clusters breaking down, to increase the cluster count.

To investigate whether salbutamol has an effect on dispersing clusters, cells were incubated with 0, 1, 10 or 50µM salbutamol sulphate after agrin wash-off and left in the respective treatment solution for 6, 12 or 22h. For each treatment duration, the cluster number for salbutamol treated cells was compared to the number for untreated cells ('0µM'). The results showed that 6h after agrin-wash off, significantly more clusters

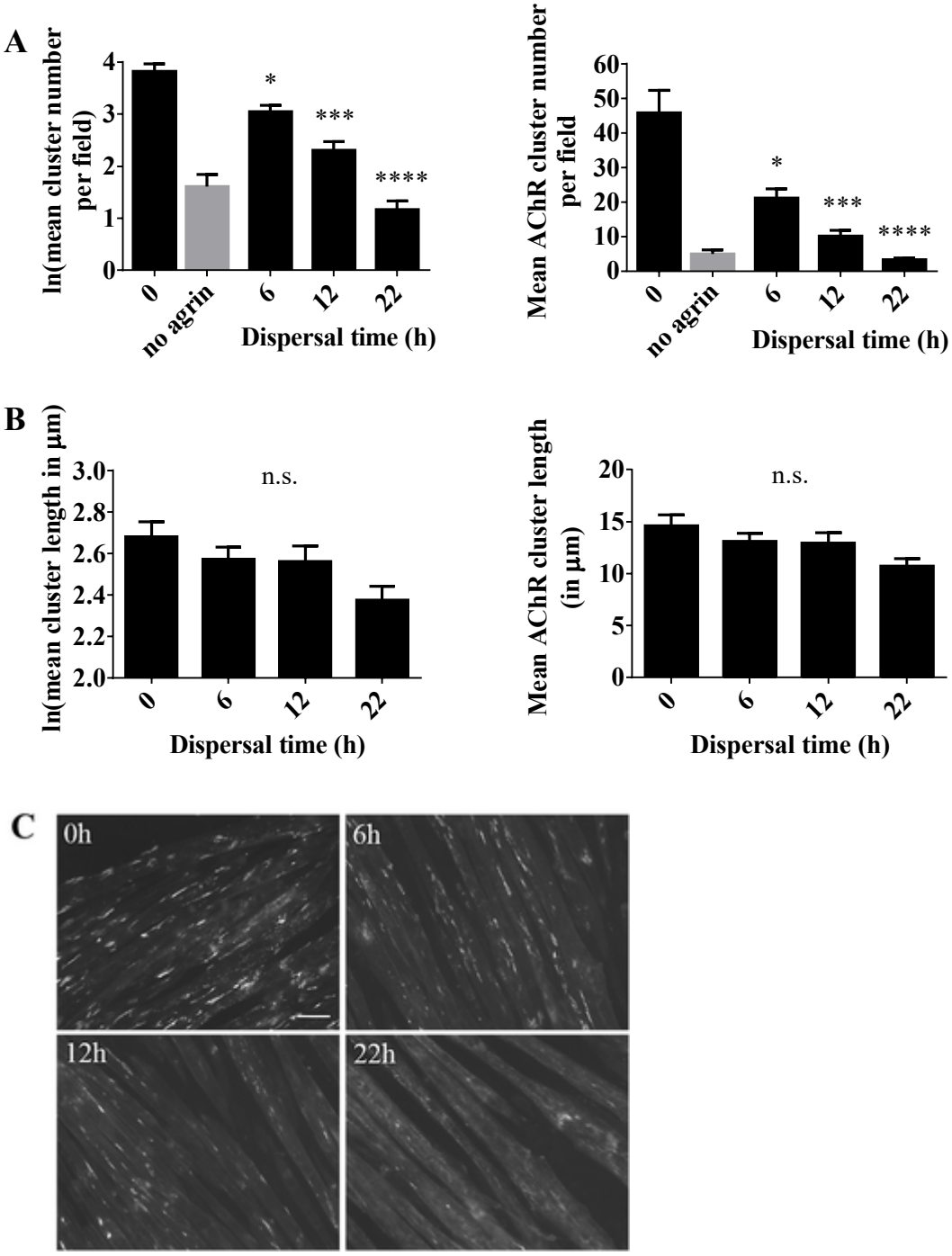

Figure 4.14 Dispersal of AChR clusters in C2C12 WT cells as a result of agrin wash-off. After incubation with soluble short rat agrin, cells were washed to remove agrin and left for 0, 6, 12 or 22h in differentiation medium for dispersal of AChR clusters. (A) The number of AChR clusters was significantly reduced in a time-dependent manner (6h: difference=0.77, SE=0.19, p=0.02, 12h: difference=1.51, SE=0.21, p=0.001, and 22h: difference=2.66, SE=0.21, p<0.00005) (B) A non-significant trend towards reduced cluster lengths occurred (6h: difference=0.11, SE=0.09, p=0.86, 12h: difference=0.12, SE=0.1, p=0.88, and 22h: difference=0.31, SE=0.1, p=0.06) (C) Representative microscopic images of cells acquired 0, 6, 12 and 22h after agrin wash-off. Scale-bar=50µm. Error bars indicate the standard error of the mean. N=3 (6 and 22h), N=2 (0 and 12h). n.s.p>0.05, *≤0.05, ***p≤0.001, ****p≤0.0001.

remained on myotubes incubated with salbutamol ($p=0.03$, $p=0.0006$, and $p=0.02$, respectively; no agrin control: $p<0.00005$) (Fig. 4.15). Salbutamol had a similar effect on clusters 12h after agrin wash-off ($p>0.99$, $p<0.00005$, and $p=0.98$, respectively; no agrin control: $p<0.00005$) and 22h after agrin wash-off ($p>0.99$, $p<0.00005$, and $p=0.98$, respectively; no agrin control: $p<0.00005$). The most likely explanation for these results is that ADRB2 agonists increase the stability of AChR clusters. To confirm that this effect is mediated through ADRB2 signalling, the experiment was repeated in the presence of the ADRB2 inhibitor ICI-118,551. First, a titration experiment was performed, in which C2C12 WT myotubes were treated with soluble short rat agrin for 16h. After the removal of agrin, AChR clusters were left for dispersal for 22h. Cells were either incubated with the inhibitor only or with a mix of inhibitor and 10µM salbutamol (Fig. 4.16). Salbutamol was applied at 10µM since at this concentration the most clusters remained in the previous experiment. A stabilising effect of salbutamol on dispersing clusters could still be observed in the presence of 100, 200, 300 and 500nM ICI-118,551 ($p=0.05$, $p=0.0005$, $p=0.06$, and $p=0.01$, respectively). When the inhibitor was applied at a concentration of 1µM, no increase in cluster numbers occurred with salbutamol ($p=0.85$).

Having determined 1µM ICI-118,551 as a suitable concentration to block ADRB2 signalling, the dispersion experiment described above was repeated. AChR clusters were induced by incubation of C2C12 WT myotubes with soluble agrin overnight and left to disperse for 6, 12 or 22h. For each treatment duration, the number of AChR clusters for salbutamol-treated cells was compared to the cluster number for untreated cells ('0µM'). In the presence of 1µM ICI-118,551, salbutamol sulphate (1, 10 or 50 µM) did not have an effect on the number of AChR clusters after agrin-wash off (6h: $p=0.47$, $p=0.47$, and $p=0.3$, 12h: $p=0.06$, $p>0.99$, and $p=0.08$, and 22h: $p>0.99$, $p>0.99$, and $p>0.99$) (Fig. 4.17).

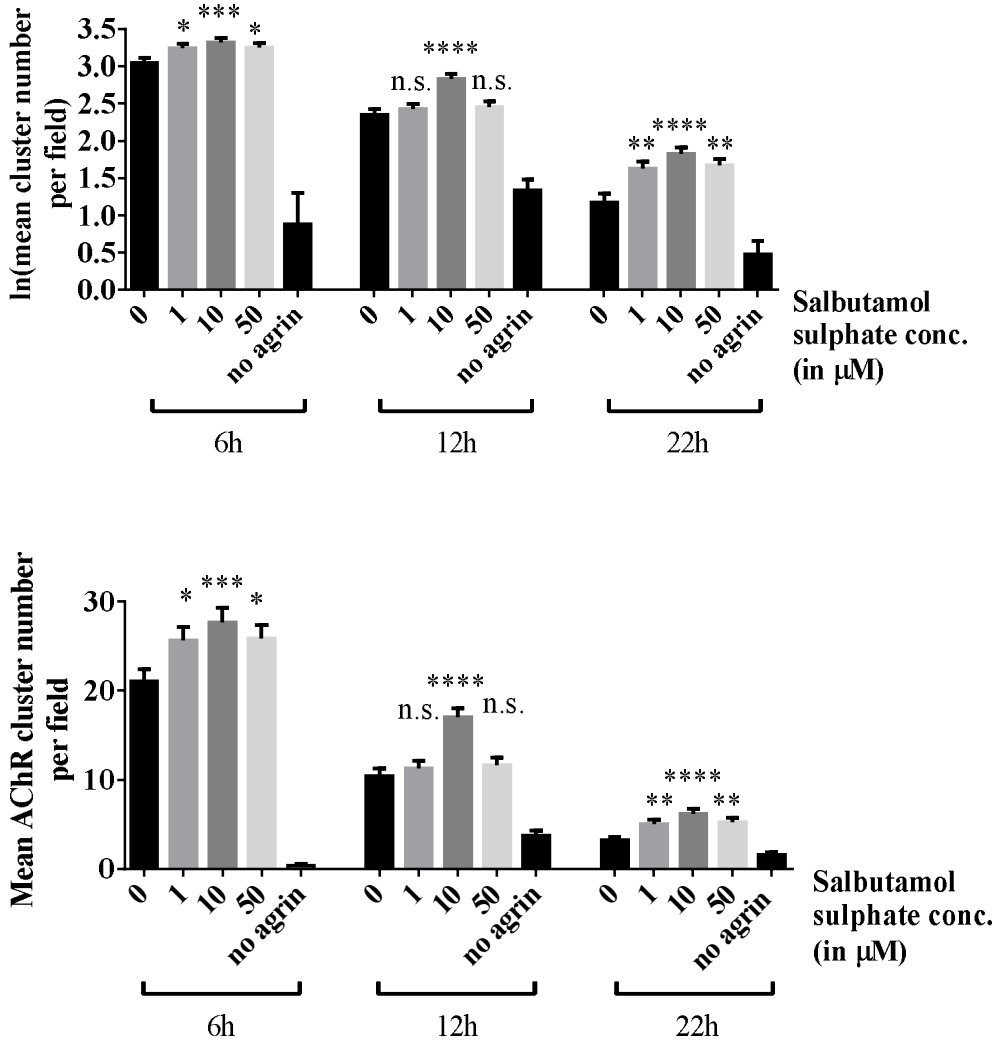

Figure 4.15 Effects of salbutamol on AChR clusters after agrin wash-off. Clusters were induced by incubation of myotubes with 1:500 soluble short rat agrin. After agrin was removed, AChR clusters were left to disperse for 6, 12 or 22h in the absence or presence of 1, 10 or 50μM salbutamol sulphate. Significantly more clusters remained in salbutamol treated cells after a dispersal time of 6h (difference=0.2, SE=0.07, p=0.027, difference=0.27, SE=0.07, p=0.0006, and difference=0.2, SE=0.07, p=0.02, respectively; no agrin control: difference=3.92, SE=0.43, p<0.00005), 12h (difference=0.08, SE=0.11, p>0.99, difference=0.49, SE=0.1, p<0.00005, and difference=0.11, SE=0.11, p=0.98, respectively; no agrin control: difference=1.01, SE=0.16, p<0.00005) and 22h (difference=0.08, SE=0.11, p>0.99, difference=0.49, SE=0.1, p<0.00005, and difference=0.11, SE=0.11, p=0.98, respectively; no agrin control: difference=1.01, SE=0.16, p<0.00005). N=3 (6 and 22h), N=2 (12h). Scale-bar=50μm. Error bars indicate the standard error of the mean. n.s.p>0.05, *p≤0.05, **p≤0.01, ***p≤0.001, ****p≤0.0001.

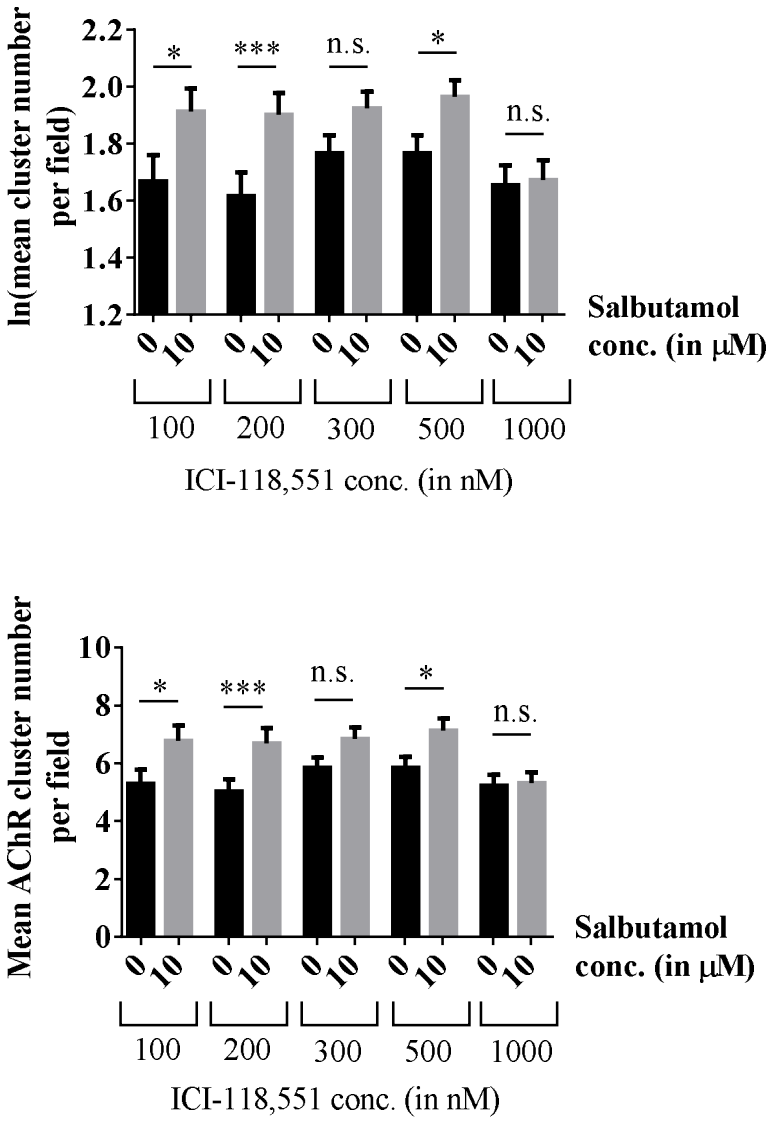

Figure 4.16 Titration of ICI-118,551. C2C12 WT myotubes were incubated with soluble short rat agrin for 16h. After agrin wash-off, AChR clusters were left for dispersal for 22h in the presence of 100, 200, 300, 500 or 1000nM of the ADRB2 inhibitor ICI-118,551. At 100, 200, 300 and 500nM inhibitor, 10μM salbutamol caused an increase in AChR cluster numbers (difference=0.22, SE=0.12, p=0.05, difference=0.29, SE=0.08, p=0.0005, difference=0.16, SE=0.08, p=0.06, and difference=0.2, SE=0.08, p=0.01, respectively), whereas 1000nM ADRB2 inhibitor blocked the salbutamol-mediated effect (difference=0.02, SE=0.09, p=0.85). N=3 (100nM) and N=5 (200, 300, 500 and 1000nM). (Error bars indicate the standard error of the mean. n.s.p>0.05, *p≤0.05, ***p≤0.001.

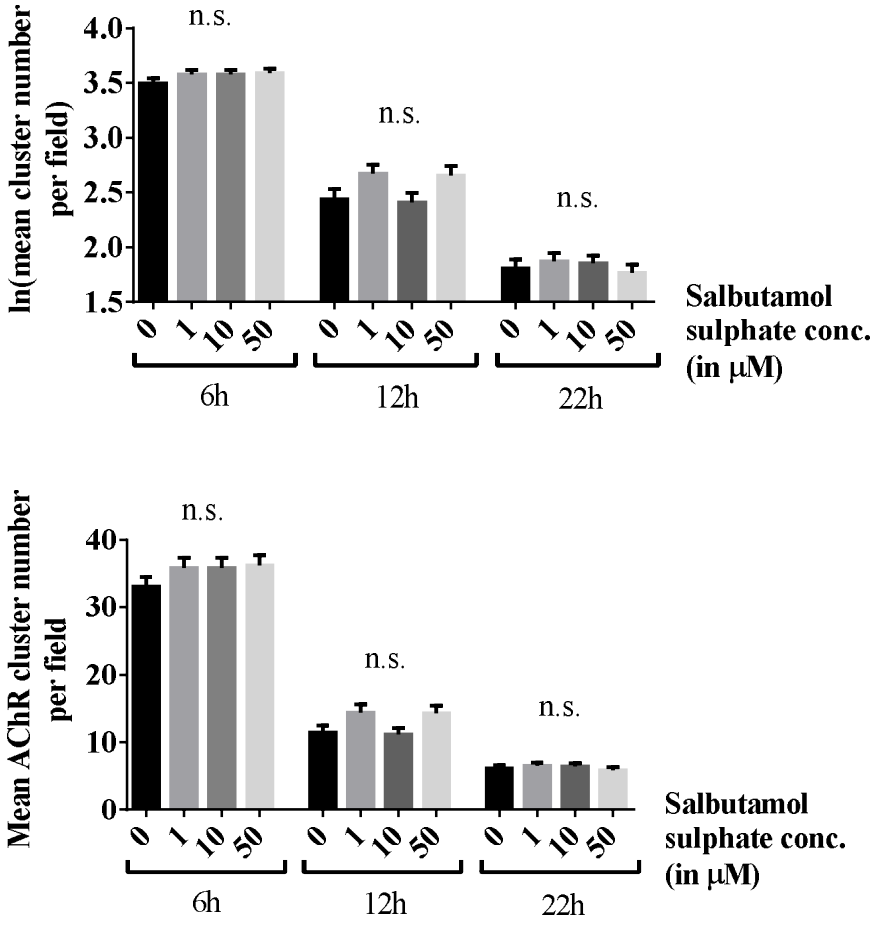

Figure 4.17 Blocking of the effects of salbutamol on AChR clusters after agrin wash-off by inhibition of ADRB2s. C2C12 WT myotubes were incubated with short rat agrin overnight. After agrin wash-off, AChR clusters were left for dispersal for 6, 12 or 22h, during which myotubes were incubated with a mix of 0, 1, 10 or 50μM salbutamol sulphate and 1μM ICI-118,551. The ADRB2 inhibitor abolished the stabilising effect of salbutamol on AChR clusters and no difference occurred between salbutamol-treated and untreated cells (6h: difference=0.08, SE=0.06, p=0.47, difference=0.08, SE=0.06, p=0.47, and difference=0.09, SE=0.06, p=0.3, 12h: difference=0.23, SE=0.1, p=0.06, difference=0.03, SE=0.1, p>0.99, and difference=0.22, SE=0.1, p=0.08, and 22h: difference=0.06, SE=0.11, p>0.99, difference=0.04, SE=0.11, p>0.99, and difference=0.04, SE=0.11, p>0.99) (Fig. 4.16). N=3 (6h), N=2 (12h and 22h). Error bars indicate the standard error of the mean. n.s.p>0.05.

The results suggest that ADRB2 agonists have a stabilising effect on agrin-induced AChR clusters in C2C12 WT cells where the AChR clustering pathway is intact. Next, this effect was investigated in C2C12$^{DOK7\ c.1124_27dupTGCC}$ cells, in which the number of AChR clusters is significantly reduced and where the postsynaptic structure might be less stable. Such an experiment is challenging since the mutant *DOK7* cell line is based on overexpression of DOK7. Unlike in WT cells where signalling events responsible for clustering of AChRs can be abolished by agrin wash-off, in C2C12$^{DOK7\ c.1124_27dupTGCC}$ cells, DOK7 continuously stimulates cluster-inducing signalling cascades.

By taking advantage of the positive and negative signals that regulate synaptic development and the maintenance of the neuromuscular synapse, a novel experimental setup was developed to study the effects of salbutamol on cluster dispersal in *DOK7*-mutant cells. As described earlier in chapter 1, neural activity has been indicated as a negative regulator which disperses the postsynaptic apparatus (Lin et al., 2005, Kummer et al., 2006). Lin et al. (2005) demonstrated that the cholinergic agonist carbachol disperses agrin-induced AChR clusters formed on C2C12 myotubes. To replicate this finding, C2C12 WT myotubes were incubated with soluble short rat agrin for 16h to induce clustering. After agrin wash-off, cells were incubated with 0.1, 1 or 5mM carbachol for 6h. The number of clusters was significantly reduced in carbachol-treated cells compared to untreated cells (all $p<0.00005$) (Fig. 4.18A). At 0.1mM, carbachol reduced the number of clusters by about 64% from an average of 36 to 13 clusters per microscopy field. Cluster lengths were also significantly reduced in carbachol-treated cells ($p<0.00005$, $p=0.007$, and $p=0.0003$, respectively) (Fig. 4.18B). It is important to note that even in the absence of carbachol (condition '0mM') some clusters will have broken down during the 6h period due to time-correlated dispersal after agrin-wash off (as shown in the time-course experiments reported above). However, the results

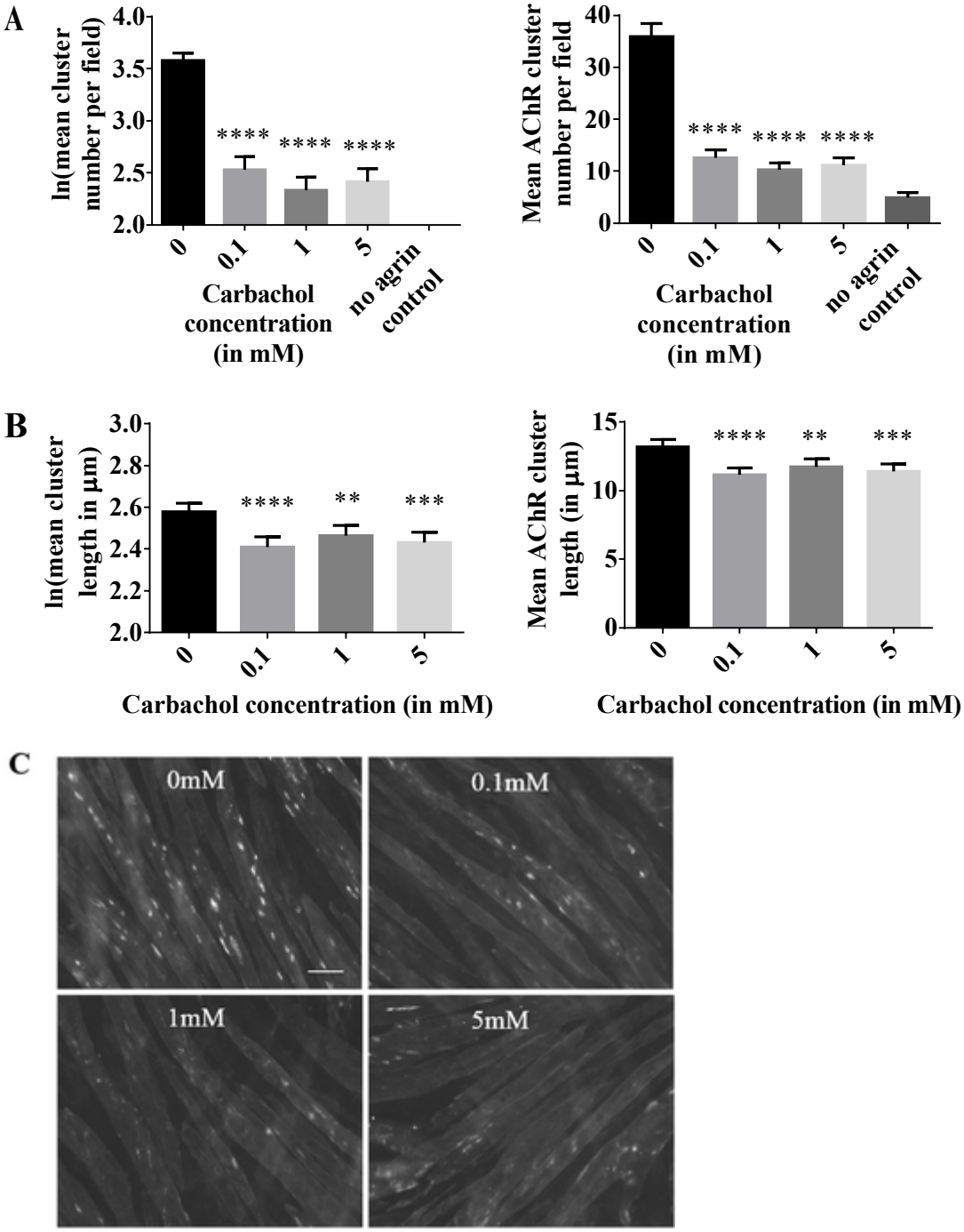

Figure 4.18 Effects of carbachol on AChR clusters in C2C12 WT cells. After cluster induction with short rat agrin for 16h, cells were treated with 0, 0.1, 1 or 5mM carbachol for 6h. (A) Carbachol caused a significant reduction in the number of AChR clusters (difference=1.05, SE=0.14, $p<0.00005$, difference=1.25, SE=0.15, $p<0.00005$, and difference=1.17, SE=0.14, $p<0.00005$, respectively; no agrin control: difference=2, SE=0.21, $p<0.00005$) and (B) in the length of clusters (difference=0.17, SE=0.04, $p<0.00005$, difference=0.12, SE=0.04, $p=0.007$, and difference=0.15, SE=0.04, and $p=0.0003$, respectively). (C) Representative microscopic images of cells treated with carbachol as indicated. N=3. Scale bar=50µm. Error bars indicate the standard error of the mean. **$p\leq0.01$, ***$p\leq0.001$, ****$p\leq0.0001$.

suggested that treatment with carbachol accelerates this process.

A similar effect was observed in C2C12$^{DOK7\ c.1124_27dupTGCC}$ cells, where 6h treatment with 0.5µM carbachol significantly reduced the number of AChR clusters by 63% ($p<0.00005$) and also the length of clusters ($p=0.0003$) (Fig. 4.19). To investigate the effects of salbutamol on AChR cluster stability in C2C12$^{DOK7\ c.1124_27dupTGCC}$ cells, the following experimental setup was chosen. In the first treatment condition, cells were incubated in 1, 5, or 50µM salbutamol sulphate for 22h in order to replicate the previous findings. Salbutamol significantly increased AChR cluster numbers at all treatment concentrations tested, when compared to untreated cells (all $p<0.00005$) (Fig. 4.20). In the second treatment condition, cells were incubated with salbutamol for 22h, however, for the last 6h of the treatment, 0.5mM carbachol were added (16h salbutamol, 6h salbutamol + carbachol). Comparing untreated cells with cells incubated with carbachol only, the results confirmed that carbachol significantly reduces the number of clusters (comparison of treatment conditions '0µM': $p<0.00005$). The salbutamol treatment before and during the application of carbachol significantly increased the number of AChR clusters when compared to cells treated with carbachol only (all $p<0.00005$). Overall, the number of clusters in cells treated with a mix of salbutamol and carbachol was lower than the cluster numbers for cells treated with salbutamol only, suggesting that salbutamol did not abolish the effects of carbachol. In order to directly investigate whether salbutamol partially prevents the carbachol-induced breakdown of AChR clusters, cells were not pre-treated with salbutamol sulphate but incubated for 6h with a mix of 5µM salbutamol sulphate and carbachol. The results showed that significantly more clusters remained in the presence of salbutamol when compared to cells treated with carbachol only (comparison indicated by a dashed line, $p=0.006$). This suggests that salbutamol has a stabilising effect on AChR clusters.

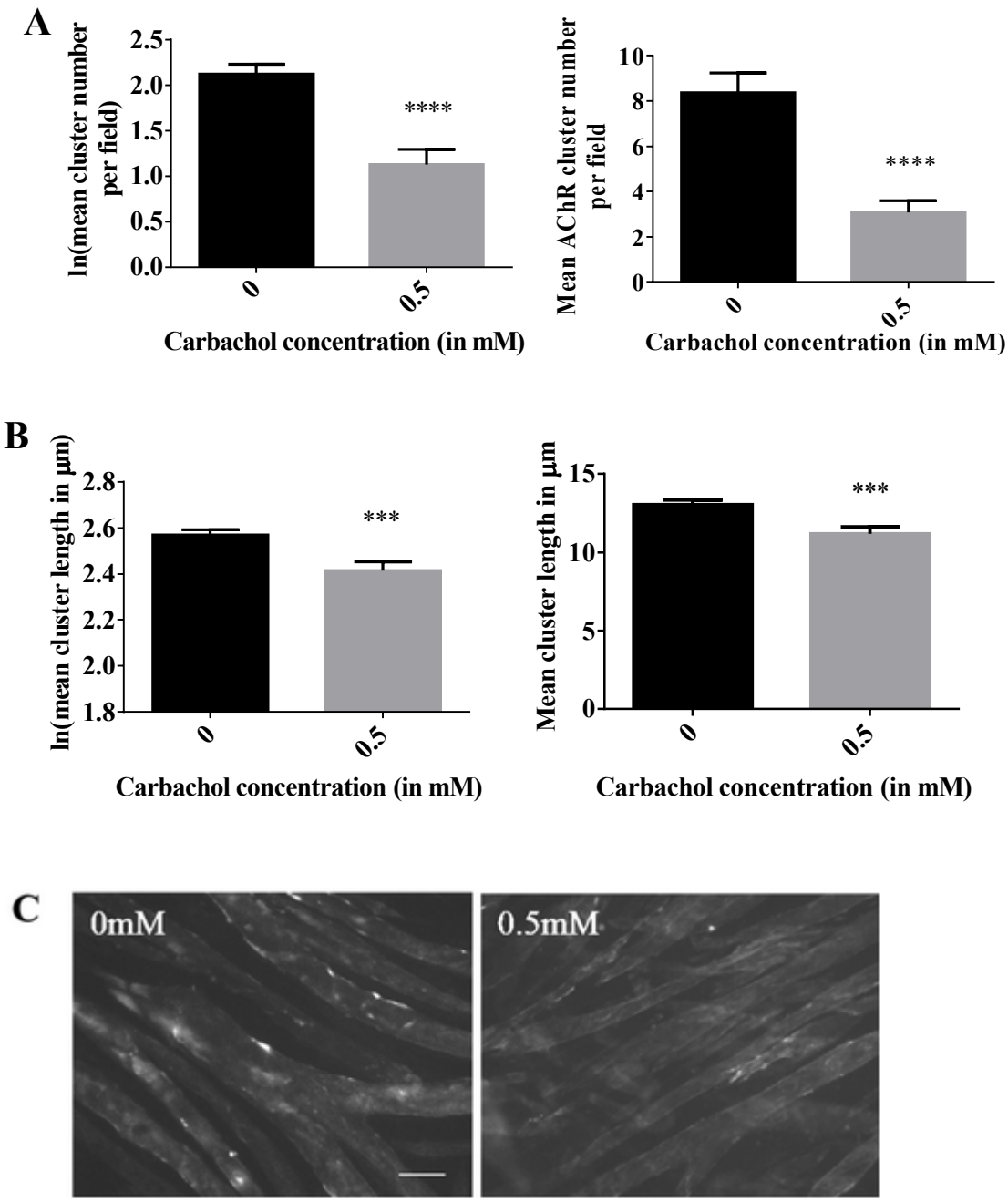

Figure 4.19 Effects of carbachol on AChR clusters in C2C12$^{DOK7\ c.1124_27dupTGCC}$ cells. Myotubes were treated with 0.5mM carbachol or were left untreated. (A, B) Carbachol caused a significant reduction in the number of AChR clusters (difference=1, SE=0.18, $p<0.00005$) and in the length of clusters (difference=0.15, SE=0.04, $p=0.0003$) when compared to untreated cells. (C) Representative microscopic images of cells treated with carbachol as indicated. N=3. Scale bar=50µm. Error bars indicate the standard error of the mean. ***$p\leq0.001$, ****$p\leq0.0001$.

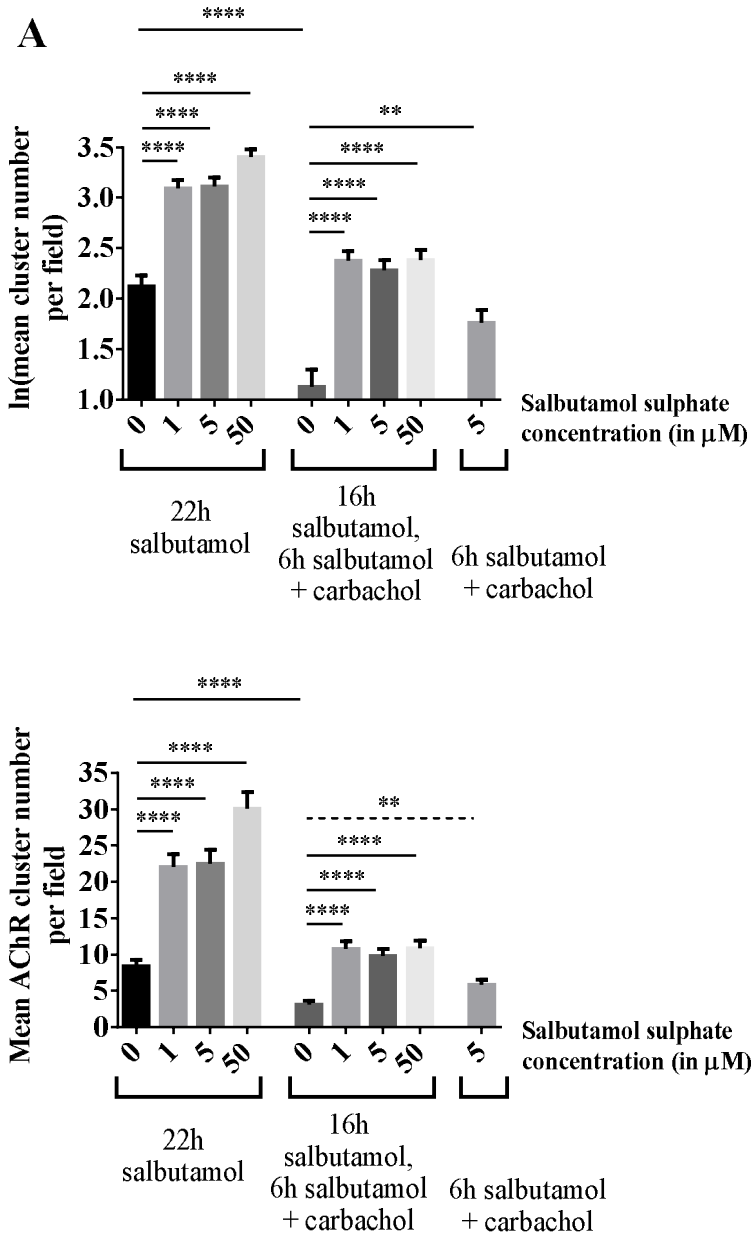

Figure 4.20 Effects of salbutamol on carbachol-treated C2C12$^{DOK7\ c.1124_27dupTGCC}$ cells. (A) In the first treatment condition, cells were treated with salbutamol sulphate for a duration of 22h. 1, 5 and 50µM salbutamol significantly increased the number of AChR clusters in a dose-dependent manner (difference=0.97, SE=0.11, p<0.00005, difference=0.99, SE=0.11, p<0.00005, and difference=1.28, SE=0.11, p<0.00005). In the second treatment condition, cells were incubated with 0, 1, 10 or 50µM salbutamol sulphate for 22h. For the last 6h of the treatment, 0.5mM carbachol was added. Carbachol significantly reduced the number of clusters (comparison of the two treatment conditions '0µM': difference=1, SE=0.19, p<0.00005). The number of clusters was significantly higher in salbutamol-treated cells (difference=1.25, SE=0.18, p<0.00005, difference=1.15, SE=0.18, p<0.00005, and difference=1.26, SE=0.18, p<0.00005, respectively). Thirdly, more clusters remained when 5µM salbutamol was applied during the treatment with carbachol for 6h (no 16h pre-treatment with salbutamol) (comparison indicated by a dashed line, difference=0.63, SE=0.2, p=0.006). N=3. Error bars indicate the standard error of the mean. **p≤0.01, ****p≤0.0001.

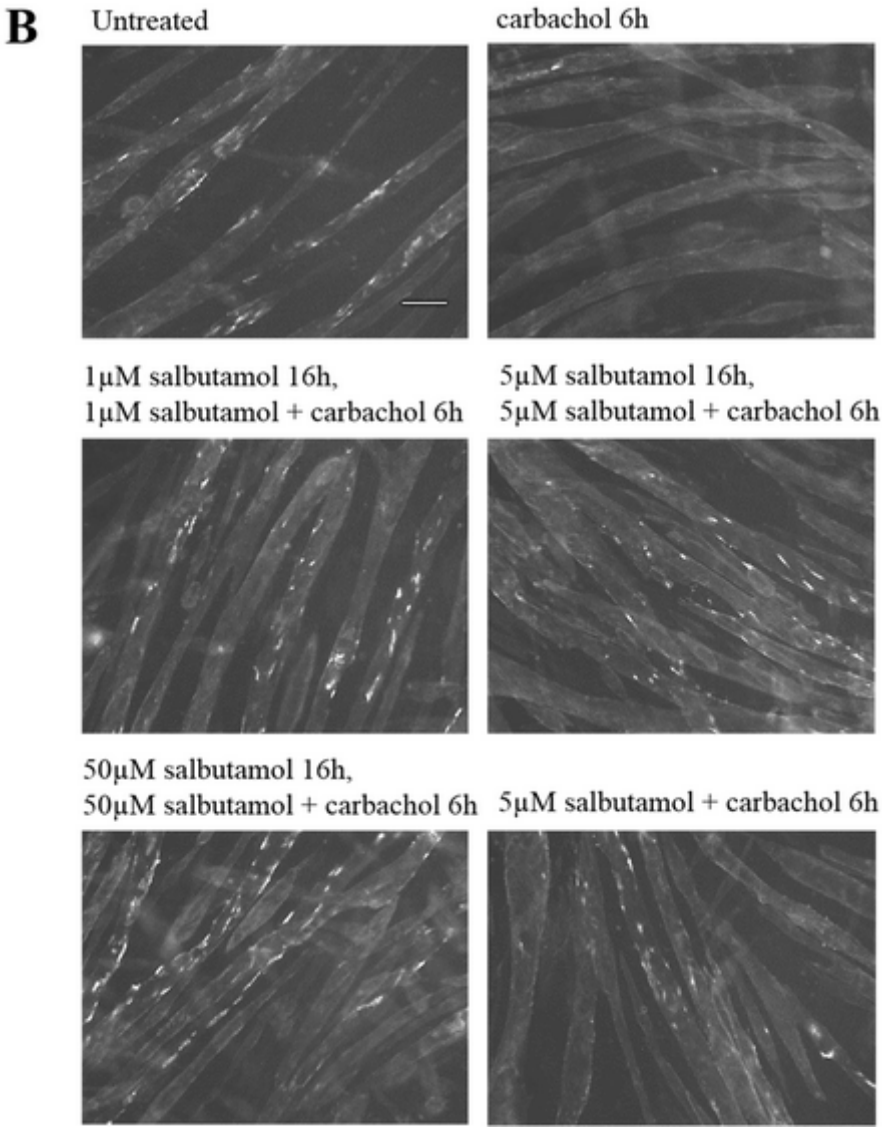

Figure 4.20 (continued) (C) Representative microscopic images of C2C12$^{DOK7\ c.1124_27dupTGCC}$ cells, treated with carbachol and salbutamol sulphate as indicated. Scale bar=50μm.

It has to be kept in mind that in cells overexpressing DOK7, the continuous DOK7 signalling might exert an antagonistic effect on cluster dispersal even in the c.1124_27dupTGCC mutant. In C2C12$^{DOK7\ WT}$ cells, DOK7 signalling seems to eliminate the effect of carbachol (Fig. 4.21).

In summary, the results suggest that ADRB2 agonists affect the formation of AChR clusters, which might be mediated by a stabilising effect on the clusters. The following experiments aimed at investigating the underlying mechanisms of these effects in more detail.

4.4 Potential mechanisms underlying the effects of salbutamol on AChR clustering

4.4.1 Effects of salbutamol treatment on AChR surface expression in C2C12$^{DOK7\ c.1124_27dupTGCC}$ cells

First, it was investigated whether ADRB2 agonists affect AChR surface expression. C2C12$^{DOK7\ c.1124_27dupTGCC}$ cells were differentiated into myotubes and treated with 0.1, 1, 10 or 50µM salbutamol sulphate for 22h. AChR surface expression was determined by ^{125}I-α-bungarotoxin surface binding, and the radioactive count obtained for each treatment condition was compared to the count for untreated cells (see chapter 2.14.2 for details on the statistical analysis). Incubation with 0.1µM salbutamol sulphate caused a significant 17% increase in AChR surface expression ($p=0.001$) (Fig. 4.22). Higher concentrations did not have a significant effect on AChR expression levels ($p=0.08$, $p>0.99$, and $p>0.99$, respectively).

Despite the small increase in AChR surface expression, it is questionable whether this mechanism alone is responsible for the effects of ADRB2 agonists observed *in vivo* and *in vitro*. Therefore, experiments were conducted to test whether salbutamol feeds into the AChR clustering pathway by affecting the phosphorylation of MuSK or the AChR

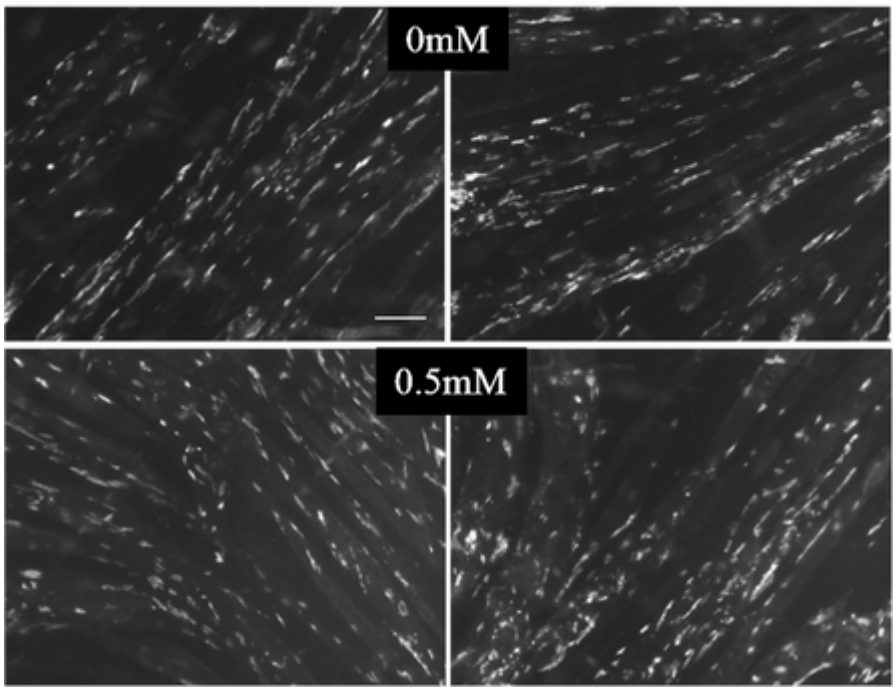

Figure 4.21 Representative microscopic images showing the effect of carbachol on AChR clusters in C2C12$^{DOK7\ WT}$ cells. Myotubes were treated with 0.5mM carbachol for 6h or left untreated. No dispersal of clusters could be observed. Scale bar=50µm.

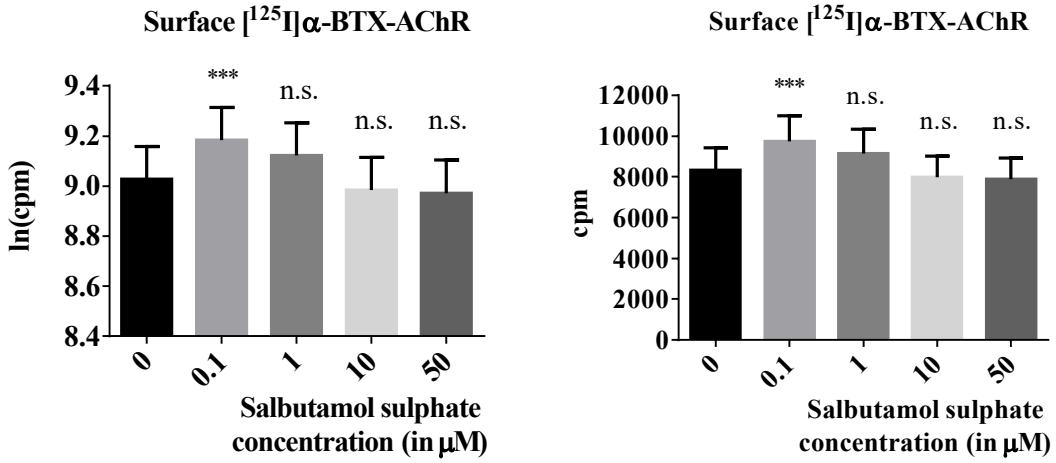

Figure 4.22 Effects of salbutamol on AChR surface expression. C2C12$^{DOK7\ c.1124_27dupTGCC}$ myotubes were treated with 0.1, 1, 10 or 50µM salbutamol sulphate for 22h, and AChR surface expression was determined by ^{125}I-α-bungarotoxin binding. Salbutamol treatment caused a significant increase in AChR surface expression at 1µM (difference=0.16, SE=0.04, p=0.001), whereas higher concentrations did not have a significant effect (difference=0.09, SE=0.04, p=0.08, difference=0.04, SE=0.04, p>0.99, and difference=0.06, SE=0.05, p>0.99, respectively). N=3. Error bars indicate the standard error of the mean. n.s.p>0.05, ***p≤0.001

beta-subunit.

4.4.2 Effects of salbutamol treatment on MuSK tyrosine-phosphorylation

Tyrosine phosphorylation of MuSK is an early key event in the AChR clustering pathway. A potential effect of salbutamol sulphate treatment on MuSK tyrosine-phosphorylation was first investigated in C2C12 WT cells. C2C12 myoblasts were differentiated into myotubes and serum-starved overnight (DMEM, supplemented with 1% PSA). The cells were then treated with 0, 1, 5, 10 or 50µM salbutamol sulphate for 6h. As a positive control, cells were incubated with short rat agrin, diluted 1:100 for 6h, which was expected to significantly increase in MuSK phosphorylation. MuSK was pulled down from whole-cell lysate by incubation with 1:50 rMuSk antibody (AF562, R&D system) overnight, followed by incubation with protein G coupled magnetic beads for 1h. As a negative control, the immunoprecipitation was performed without adding the MuSK antibody. MuSK was detected with 1:1000 Musk antibody H-300 (Santa Cruz), and MuSK tyrosine-phosphorylation was detected with 1:800 Anti-Phosphotyrosine Antibody clone 4G10. The MuSK blot showed a large number of unspecific bands, and no band could clearly be identified as MuSK (blot not shown). However, the tyrosine-phosphorylation blot strongly suggested that MuSK was successfully immunoprecipitated (Fig. 4.23). MuSK bands were detected at ~97kDa. No band occurred in the negative control in which no MuSK antibody was used during the immunoprecipitation. Increased phosphorylation could be observed in the agrin positive control, confirming the specificity of the detected bands. Evaluating the phosphorylation bands alone by eye, no significant increase in MuSK phosphorylation with salbutamol sulphate could be observed.

It is possible that in WT C2C12 cells where the AChR clustering pathway is intact, subtle changes in MuSK phosphorylation in response to salbutamol treatment are missed.

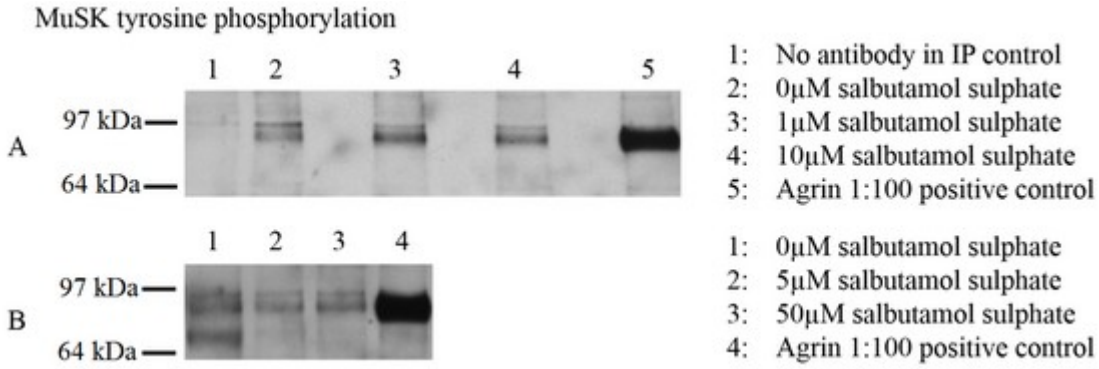

Figure 4.23 Effects of salbutamol on MuSK tyrosine phosphorylation in C2C12 WT cells. C2C12 WT myotubes were serum starved overnight and incubated with 0, 1, 5, 10 or 50μM salbutamol sulphate for 6h. MuSK was immunoprecipitated by pulldown from whole cell lysate with 1:50 Anti rMuSK antibody (R&D system) overnight. The samples were subjected to SDS PAGE and bands corresponding to MuSK (~97kDa) were detected by probing with 1:800 Anti-Phosphotyrosine Antibody clone 4G10. Phosphorylation blots from two different experiments (A and B) are shown.

Therefore, it was investigated next whether salbutamol increases MuSK tyrosine-phosphorylation in cells overexpressing the DOK7 mutation c.1124_27dupTGCC. The experiment was also performed on cells overexpressing WT DOK7. C2C12$^{DOK7\ c.1124_27dupTGCC}$ and C2C12$^{DOK7\ WT}$ cells were differentiated into myotubes and treated with 10µM salbutamol sulphate, diluted in differentiation medium, for a duration of 20h. In order to be able to detect MuSK, the immunoprecipitation protocol was optimised. Instead of using whole cell lysate, MuSK was pulled down from the cell surface with 1:1000 Anti-MuSK antibody (Abcam) for 1h and was later detected with 1:500 Anti rMuSK antibody (R&D system). MuSK could now be identified (Fig. 4.24).

No difference in MuSK tyrosine-phosphorylation could be observed in C2C12$^{DOK7\ c.1124_27dupTGCC}$ or in C2C12$^{DOK7\ WT}$ cells in response to salbutamol treatment.

4.3.3 Effects of salbutamol treatment on AChR beta-subunit tyrosine phosphorylation

It was shown in cultured muscle cells that downstream signalling of MuSK in response to agrin-incubation leads to tyrosine-phosphorylation of the beta-subunit of the AChR and subsequently to clustering of the receptors (Wallace et al., 1991, Ferns et al., 1996). AChR beta-subunit phosphorylation has since been established as a marker for AChR clustering (Borges et al., 2008). Therefore, it was investigated whether incubation of C2C12 cells with ADRB2 agonists might have an effect on the phosphorylation of the AChR beta-subunit.

To explore this hypothesis, C2C12 WT myotubes were incubated with salbutamol either in the presence of soluble short rat agrin or full length human agrin. Agrin was applied at low concentrations diluted 1:1000 to prevent saturation of beta-subunit phosphorylation, thus allowing for the detection of small potential differences caused by salbutamol treatment. In order to investigate the effects of salbutamol on baseline AChR

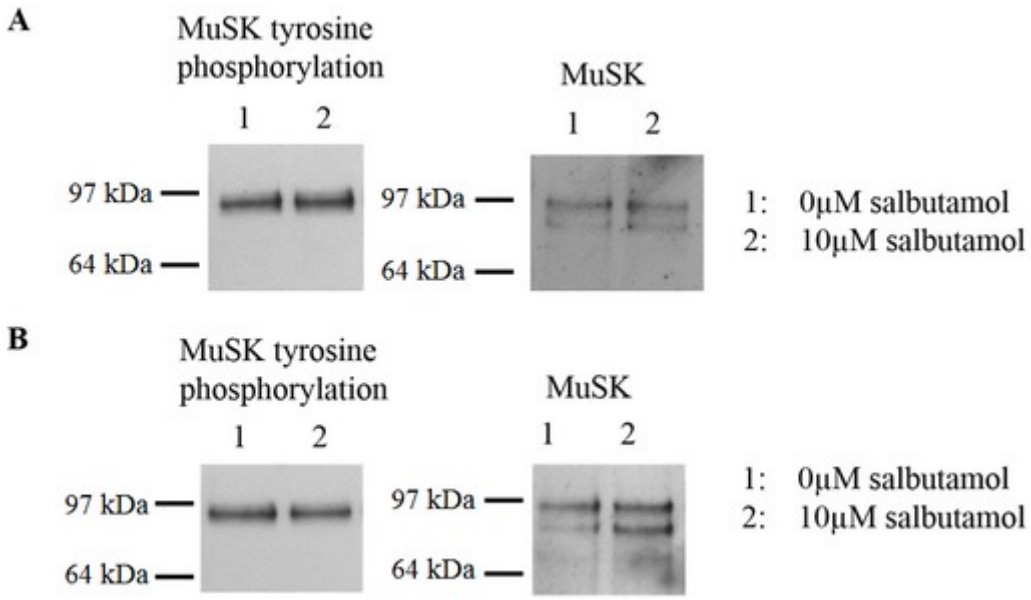

Figure 4.24 Effects of salbutamol on MuSK tyrosine phosphorylation in DOK7-overexpressing cells. (A) C2C12$^{DOK7\ c.1124_27dupTGCC}$ and (B) C2C12$^{DOK7\ WT}$ cells were incubated with 10µM salbutamol sulphate for 22h. MuSK was immunoprecipitated by pulldown from the cell surface with 1:1000 Anti-MuSK antibody (Abcam). The samples were subjected to SDS Page and bands corresponding to MuSK (~97kDa) were detected by probing with 1:500 Anti rMuSK antibody (R&D system) and with 1:800 Anti-Phosphotyrosine Antibody clone 4G10. N=3 (C2C12$^{DOK7\ c.1124_27dupTGCC}$), N=2 (C2C12$^{DOK7\ WT}$).

beta-subunit phosphorylation, salbutamol was applied in the absence of agrin in a further condition. In a first experiment (Fig. 4.25A), C2C12 WT myotubes were incubated with 1:1000 short rat agrin or with a mix of 1:1000 short rat agrin and 50µM salbutamol sulphate (band 1 and 2). In two further conditions, cells were left untreated, or were incubated with 50µM salbutamol sulphate only (band 3 and 4). Since less AChR beta-subunit tyrosine phosphorylation was expected in the absence of agrin, the untreated condition served as a negative control. All treatment solutions were prepared in serum-starved medium (DMEM) and were applied for a duration of 4h. AChRs were pulled down from the cell surface by incubation with α-Bungarotoxin Biotin-XX Conjugate and subsequent incubation of the cell lysate with streptavidin-coupled dynabeads. Bands corresponding to the AChR beta-subunit (~48kDa) were detected by incubation of the immunoblots with 1:3000 mAb124 anti-AChR beta antibody and with 1:100 p-AChRβ1 AChR beta-subunit tyrosine-phosphorylation antibody. In the absence of agrin treatment (band 3, 4) less phosphorylation was detected than in agrin-treated cells (band 1, 2). No increase in AChR beta-subunit tyrosine-phosphorylation could be observed in agrin-treated or -untreated cells in response to salbutamol treatment. The experiment was repeated using full length human agrin (Fig. 4.25B), however, no differences in phosphorylation occurred.

Alterations were made to the protocol in order to investigate whether salbutamol has an effect on AChR beta-subunit tyrosine phosphorylation if the duration of the agrin and salbutamol treatment is increased. For a duration of 24h, C2C12 WT myotubes were treated with 1:1000 short rat agrin (band 1), 1:1000 short rat agrin and 50µM salbutamol sulphate (band 2), 1:1000 full length human agrin (band 3) or 1:1000 full length human agrin and 50µM salbutamol sulphate (band 4) (Fig. 4.26). All treatment solutions were prepared in differentiation medium. No effect of salbutamol incubation on AChR beta-

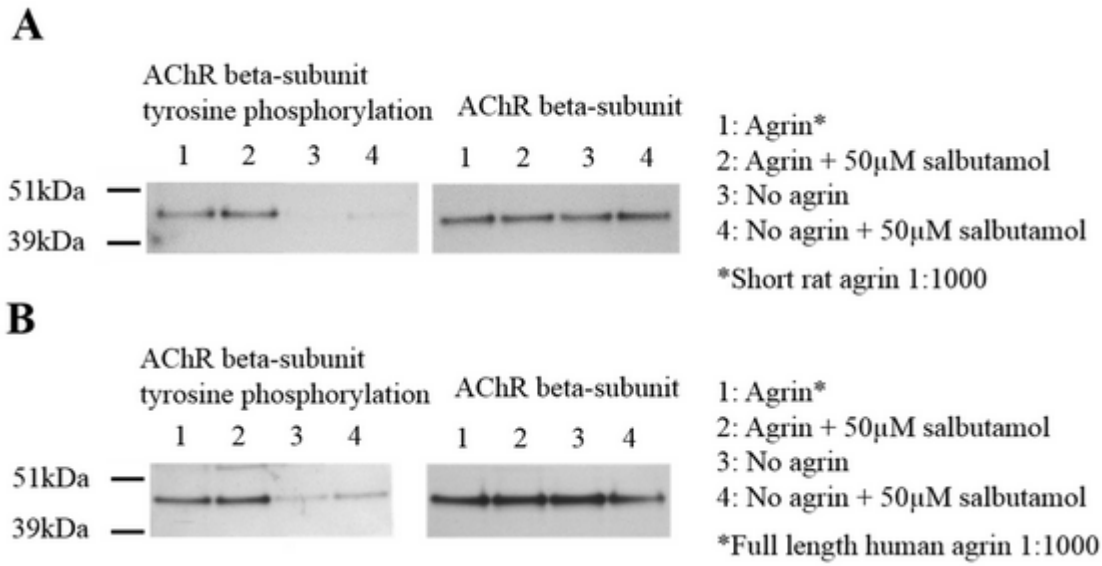

Figure 4.25 Effects of salbutamol on AChR beta-subunit tyrosine phosphorylation in C2C12 WT cells. (A) C2C12 WT myotubes were treated for 4h with 1:1000 short rat agrin (band 1) or with short rat agrin and 50µM salbutamol sulphate (band 2). The effects of salbutamol on baseline phosphorylation levels in the absence of agrin were tested by leaving the cells untreated (band 3) or incubating them with 50µM salbutamol sulphate (band 4). AChRs were pulled down with α-Bungarotoxin Biotin-XX Conjugate, and the samples were subjected to SDS Page. Bands corresponding to the AChR beta-subunit (~48kDa) could be detected with 1:3000 mAb124 anti-AChR beta and 1:100 p-AChRβ1 Tyr390 antibody. (B) The experiment was repeated, using 1:1000 full length human agrin. N=3.

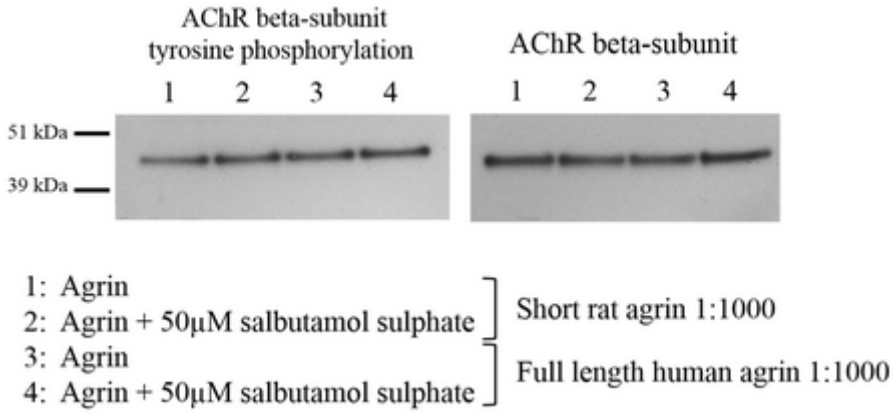

Figure 4.26 Effects of salbutamol on AChR beta-subunit tyrosine phosphorylation in C2C12 WT cells. C2C12 WT myotubes were incubated for 24h with 1:1000 short rat agrin (band 1), 1:1000 short rat agrin and 50µM salbutamol sulphate (band 2), 1:1000 full length human agrin (band 3) or 1:1000 full length human agrin and 50µM salbutamol sulphate (band 4). AChRs were pulled down with biotin-XX α-bungarotoxin, and the samples were subjected to SDS Page. Bands corresponding to the AChR beta-subunit (~48kDa) could be detected with 1:3000 mAb124 anti-AChR beta and 1:100 p-AChRβ1 Tyr390 antibody. N=3.

subunit tyrosine phosphorylation could be observed.

Next, it was investigated whether salbutamol treatment affects AChR beta-subunit tyrosine phosphorylation in C2C12$^{DOK7\ c.1124_27dupTGCC}$ cells (Fig. 4.27A). The experiment was also conducted in C2C12$^{DOK7\ WT}$ cells (Fig. 4.27B). Salbutamol was applied to myotubes at concentrations of 0, 1, 10 or 50µM in differentiation medium for a duration of 22h (no agrin present). AChRs were pulled down from the cell surface by incubation with α-Bungarotoxin Biotin-XX Conjugate and subsequent incubation of the cell lysate with streptavidin-coupled dynabeads. Bands corresponding to the AChR beta-subunit (~48kDa) were detected by incubation of the immunoblots with 1:1000 mAb124 anti-AChR beta antibody and with 1:500 anti Phosphotyrosine clone 4G10 antibody. No increase in phosphorylation in response to salbutamol was observed in C2C12$^{DOK7\ c.1124_27dupTGCC}$ or in C2C12$^{DOK7\ WT}$ cells.

4.5 Discussion

The aim of this chapter was to investigate the effects of ADRB2 agonists on AChR clustering in C2C12 cultures. Our results provide tangible evidence that ADRB2 agonists directly affect proteins located at the NMJ. It was shown that salbutamol application during the incubation of C2C12 WT cells with agrin aids the formation of AChR clusters. Secondly, salbutamol and other ADRB2 agonists significantly increased the number of clusters that form on C2C12 myotubes, overexpressing mutant DOK7.

The effects of salbutamol as a short-acting ADRB2 agonist were investigated, but also the effects of formoterol fumarate, salmeterol and the novel compound XA-01-NZ86, which are long-acting agonists. All compounds tested significantly increased the number of AChR clusters formed on DOK7-mutant C2C12 myotubes. While a dose

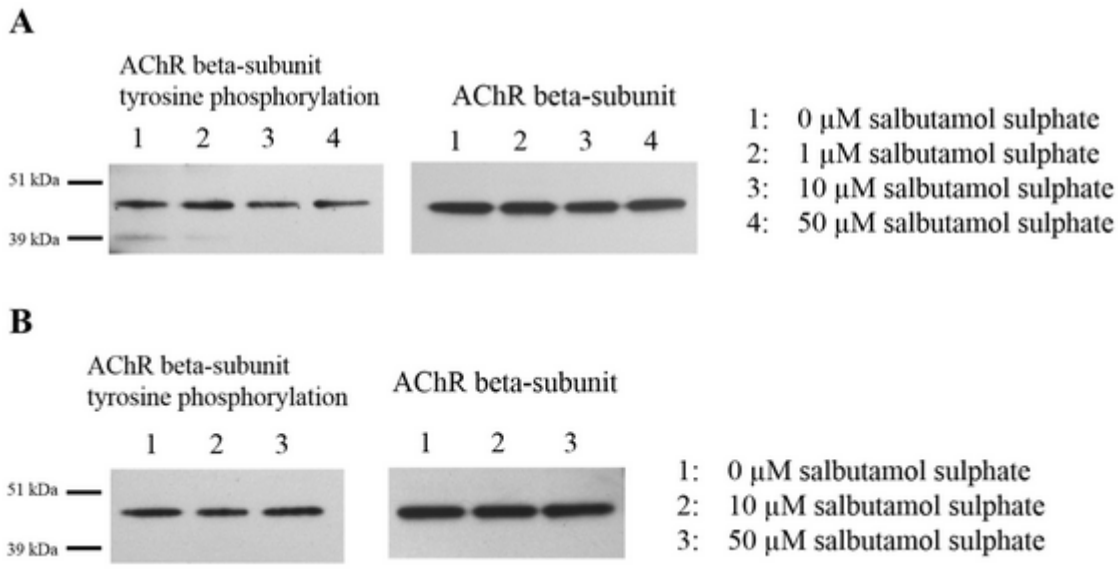

Figure 4.27 Effects of salbutamol on AChR beta-subunit tyrosine phosphorylation in DOK7-overexpressing cells. (A) C2C12$^{DOK7\ c.1124_27dupTGCC}$ myotubes were treated with 0, 1, 10 or 50µM salbutamol sulphate for 22h. AChRs were pulled down with α-Bungarotoxin Biotin-XX Conjugate, and the samples were subjected to SDS Page. Bands corresponding to the AChR beta-subunit (~48kDa) could be detected with 1:1000 mAb124 anti-AChR beta and 1:500 anti Phosphotyrosine clone 4G10 antibody. (B) The experiment was repeated in C2C12$^{DOK7\ WT}$ myotubes, using salbutamol at concentrations of 0, 10 and 50µM. N=3 (C2C12$^{DOK7\ c.1124_27dupTGCC}$), N=2 (C2C12$^{DOK7\ WT}$).

dependent increase in clustering occurred with salbutamol, salmeterol and XA-01-NZ86 were most effective at low concentrations. This is in line with the EC50 data (Fig. 4.1), which show that the longer acting ADRB2 agonists elicit a half-maximum response at lower concentrations than salbutamol. Cell death occurred in response to salmeterol and XA-01-NZ86 at a concentration of 50µM. This finding is in line with the results from a study on the metabolic and pro-apoptotic effects of high concentrations of salmeterol (Duranti et al., 2011). The authors showed that 24h treatment of C2C12 myoblasts with 10µM salmeterol caused a 40% reduction in the number of viable cells and increased cell death 3.5 times when compared to control cells. 48h treatment of myotubes with salmeterol induced apoptosis. On the other hand, formoterol fumarate was found to be most effective at increasing the cluster number at high concentrations, and no cell death was observed at 50µM.

In the current study, salbutamol caused the largest increase in the number of AChR clusters, followed by XA-01-NZ86. Therefore, long acting ADRB2s were not found to be generally more effective, and there was no correlation between the increase in clustering caused by a drug and its potency according to the EC50 value. It is important to keep in mind that the EC50 data are based on experiments using CHO cells and not muscle cultures. Furthermore, experimental variability might complicate the comparison of different agonists. When using C2C12 cells infected with retrovirus, the time-window for conducting experiments is limited. With increasing passage number, myoblasts differentiate less well into myotubes. Therefore, the experiments on the four agonists were performed on cell populations resulting from various infections and differing in age. The quality of the cells might have an influence on the response to drug treatment, although, this needs to be investigated further. Moreover, there was variation in the baseline level of AChR clustering in the absence of treatment with ADRB2 agonists,

which could also affect the results. Indeed, salbutamol failed to elicit an effect on clustering if the average cluster number at baseline was below ~5 clusters (data not shown).

The finding that some agonists bring about changes in neuromuscular proteins at lower concentrations than others could have clinical implications. It is unclear whether the ability of an agonist to affect the AChR clustering pathway *in vitro* relates to the effect the drug has on muscle strength in patients. Clinical trials are needed in which the effects of different agonists are compared in patient cohorts. Due to its muscle-specific action and long-acting effects, XA-01-NZ86 might provide an alternative to treatment with salbutamol.

Salbutamol appears to be beneficial to neuromuscular disorders characterised by disruption of the endplate structure, such as DOK7/COLQ CMS or MuSK MG. Therefore, experiments were performed to explore whether salbutamol has a stabilising effect on the postsynaptic structure. The results are in line with the model proposed by Joshua Sanes, suggesting that synaptic maturation and maintenance is regulated by positive and negative nerve-derived signals (Kummer et al., 2006). In line with the results presented by Lin et al. (2005), it could be shown that agrin-induced AChR clusters disperse in a time-dependent manner if agrin is removed. However, in the presence of salbutamol significantly more clusters remained. Since it was shown earlier that salbutamol is not capable of inducing clusters in the absence of agrin, the most likely explanation is that ADRB2 agonists act as a positive signal and increase the stability of AChR clusters on the membrane. In a further experimental setup, C2C12 cells were treated with 0.1mM of the cholinergic agonist carbachol for 6h after the removal of agrin. Neurotransmission was previously shown to act as a negative dispersing signal at the NMJ (Kummer et al. 2006), and indeed, carbachol reduced the AChR cluster number by

about 64% when compared to untreated cells. Similar numbers have been reported by Lin et al. (2005) after 5h incubation with carbachol. We used carbachol to study AChR cluster stability in cells overexpressing DOK7, where clusters form in the absence of agrin. In cells overexpressing WT DOK7, carbachol failed to decrease the AChR cluster number, suggesting that the continuous DOK7 signalling counteracts the dispersing effects of cholinergic activity. In the DOK7 mutant, where the clustering pathway is disrupted, carbachol reduced the number of clusters by 63%. When 5µM salbutamol was added during the carbachol-induced dispersal of clusters, more clusters remained, which could suggest that salbutamol exerts a positive, stabilising signal that counteracts dispersal. It has to be kept in mind that in this experiment using DOK7-overexpressing cells, the larger cluster number in salbutamol-treated cells could, in theory, be caused by increased cluster induction rather than by a reduction in dispersal. This could be addressed in future experiments.

The results on the effects of ADRB2 agonists on AChR clustering are in line with recent finding on the effects of salbutamol in a mouse model of MuSK MG (Ghazanfari et al., 2014). Daily injections of mice with IgG from anti-MuSK positive patients for a duration of two weeks induced whole-body muscle weakness. Sections of the diaphragm muscles showed a reduction in the number of AChR-stained endplates per microscopic field, and endplates were fragmented into small AChR clusters. Mice treated with salbutamol during the injection period were significantly stronger and showed less fragmentation of AChR clusters.

Several mechanisms were investigated by which ADRB2 agonists might affect AChR clustering. A potential effect of salbutamol on AChR surface expression in DOK7 mutant cells was investigated which would provide an explanation for an increase in the number of AChR clusters in response to ADRB2 agonists. It was previously reported that

12h treatment of embryonic chick muscle myotubes with 1µM isoprotenerol significantly increased the surface expression of AChRs (Blosser, 1983). However, in a study using TE671 cells, no significant effect of 10µM salbutamol on AChR surface expression was found (Li et al., 1996). In the current study, a small significant increase in AChR surface expression in response to salbutamol treatment at 0.1µM was observed, but not at the higher concentrations tested. Given that the effect was small and that there was some variability in the results, other pathways than AChR surface expression are likely to be affected by ADRB2 agonists.

No effect of salbutamol on MuSK tyrosine phosphorylation could be observed in cells overexpressing WT or mutant DOK7. This suggests that salbutamol might exert its effects further downstream within the AChR clustering pathway. Tyrosine phosphorylation of the AChR beta-subunit precedes AChR clustering and is induced by agrin-mediated downstream signalling of MuSK (Borges and Ferns, 2001). We were interested in investigating a potential link between ADRB2 activation and AChR beta-subunit phosphorylation. Several studies suggested that AChR beta-subunit phosphorylation regulates the anchoring of AChRs to the cytoskeleton and is involved in stabilising the endplate structure. It was shown in mouse myotubes that AChR beta-subunit phosphorylation in response to agrin-incubation reduces the extractability of AChRs in low-detergent extraction buffer (Borges and Ferns, 2001, Friese et al., 2007). A potential underlying mechanism could be that ADRB2 agonists act on the downstream cAMP-dependent protein kinase (PKA) type I signalling pathway. It was shown that in response to adrenergic signalling, PKA activates the proto-oncogene tyrosine kinase SRC (Armaiz-Pena et al., 2013). Src-family kinases play a role in the stabilisation of AChR clusters and are involved in MuSK and AChR beta-subunit phosphorylation (Mittaud et al., 2004). Transfection of mice soleus muscle with kinase-inactive Src constructs

resulted in endplate fragmentation, characterised by the disassembly of AChR pretzels and disturbed topology of nerve terminals and synaptic nuclei (Sadasivam et al., 2005). Agrin-induced AChR clusters formed on myotubes from Scr and Fyn double mutant mice dispersed more quickly than clusters from control cells when agrin was removed (Smith et al., 2001). Moreover, after agrin wash-off, AChR beta-subunit phosphorylation decreased more quickly in the mutant and the interaction of AChRs with rapsyn was less stable (Sadasivam et al., 2005). It was shown that more rapsyn is associated with AChRs when the beta-subunit is phosphorylated (Borges et al., 2008). In the current study, however, no effect of salbutamol on AChR beta-subunit phosphorylation could be observed in C2C12 WT cells or in cells overexpressing WT or mutant DOK7. It is important to note that while AChR beta-subunit phosphorylation is an established marker for AChR clustering, it is not essential: chick myotubes expressing mutant mouse AChRs that lack any tyrosine residues in the cytoplasmic domain of the beta-subunit still formed AChR clusters in response to agrin (Meyer and Wallace, 1998). This finding was replicated in experiments using Sol8 mouse myotubes overexpressing AChRs that either lacked all tyrosine residues or Tyr390 only, which is sufficient for abolishing AChR beta-subunit phosphorylation (Borges and Ferns, 2001). Although reduced in numbers, AChR clusters formed in the mutants. When agrin was removed, the clusters dispersed at the same rate as clusters formed on WT cells. Moreover, mice lacking all three tyrosine residues in the main intracellular loop of the AChR beta-subunit had smaller NMJs and reduced AChR surface expression but did not show signs of weakness when compared to control mice (Friese et al., 2007). Thus, since AChR beta-subunit phosphorylation is dispensable for AChR cluster formation, a different mechanism might underlie the observed effects of salbutamol on AChR clustering.

A potential mechanism could be a direct interaction of ADRB2-mediated PKA signalling with rapsyn. Recent studies suggested that AChR localisation and recycling is regulated by a complex of AChR, myosin Va and PKA type I (Roder et al., 2008). Inhibition of myosin Va caused reduced metabolic stability and increased internalisation of AChRs. PKA co-localises with myosin Va, and its inhibition significantly reduced AChR stability (Roder et al., 2010). It has been suggested that myosin-Va captures the recycling carriers for AChRs near the membrane and regulates the activation of PKA by capturing PKA and AChRs in a microdomain of subsynaptic cAMP (Rudolf et al., 2011). Recent evidence emerged that rapsyn may be responsible for accumulating PKA in proximity to the NMJ (Choi et al., 2012).

The Crk-kinase pathway has recently been identified as important for postsynaptic differentiation (Hallock et al., 2010, Hamuro et al., 2008). DOK7 does not only stimulate MuSK kinase activity via its N-terminal region but also stimulates signalling downstream of MuSK. Phosphorylation of DOK7 leads to the recruitment of the proteins v-crk sarcoma virus CT10 oncogene homolog (Crk) and Crk-like (CrkL) to phosphorylation sites on the C-terminal of DOK7 (Tyr396 and Tyr406). Crk and CrkL were shown to be enriched at the NMJ. While DOK7 phosphorylation is dispensable for MuSK and AChR beta-subunit phosphorylation, mutations in the tyrosine residues caused impaired AChR clustering in cultured DOK7-overexpressing myotubes (Hallock et al., 2010). Mice deficient in muscle-specific Crk and CrkL died shortly after birth and had smaller simplified NMJs, often with defective nerve-innervation. In DOK7 CMS, DOK7 C-terminal mutations which cause truncated protein and thus prevent Crk/CrkL binding, lead to a very similar phenotype (Beeson et al., 2006). Further research is needed to explore a potential link between ADRB2 activation and the activation of the Crk-kinase pathway.

Furthermore, cAMP signalling in response to ADRB2 activation could have an effect on transcription at the NMJ. Some genes coding for proteins expressed at the NMJ, such as MuSK, possess a cAMP response element (CRE)-like element in the promotor, and their expression is regulated by cAMP (Kim et al., 2005).

Therefore, a number of different pathways exist, which could be affected by ADRB2 signalling (Fig. 4.28). Salbutamol and other ADRB2 agonists might act via multiple mechanisms, which together could affect the stability of the endplate structure. Further research is needed to explore these potential pathways in greater detail.

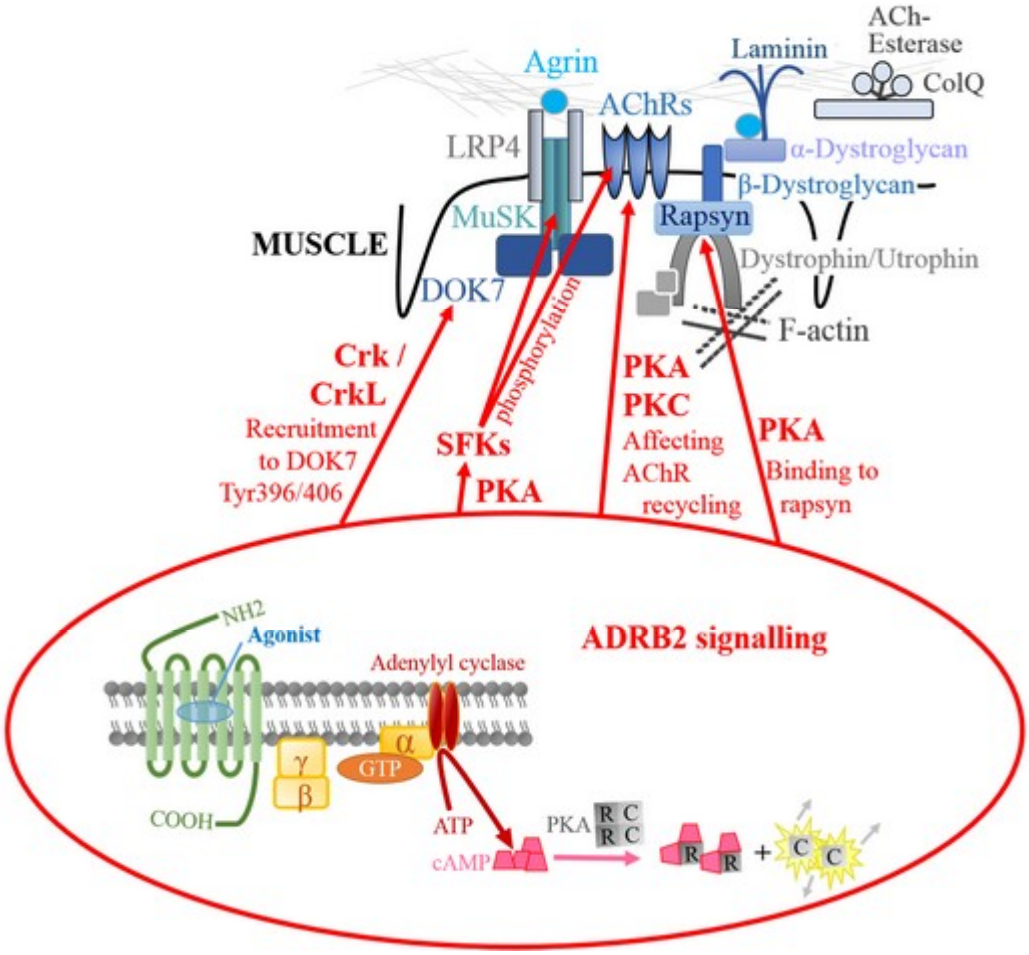

Figure 4.28 Potential pathways underlying the effects of ADRB2 agonists on synaptic stability (see text for details)

CHAPTER 5

Effects of ADRB2 activation on cAMP signalling and synaptic stability

5.1 Introduction

It was shown in chapter 4 that ADRB2 agonists are capable of increasing the number of AChR clusters formed on C2C12 myotubes overexpressing DOK7 c.1124_1127dupTGCC. Secondly, the results suggested that ADRB2 agonists have a stabilising effect on the dispersal of agrin-induced AChR clusters. Since both effects could be abolished by simultaneous application of an ADRB2 inhibitor, second messenger signalling of the receptors appears to be the underlying mechanism. The current chapter aimed at investigating the activation of ADRB2s and subsequent cAMP signalling in C2C12 myotubes in more detail by utilising novel fluorescence microscopy tools.

Agonist treatment of cultured myotubes likely stimulates a large number of ADRB2s expressed in the cell sample. In the AChR dispersion experiments described earlier, a population of cells was treated with an agonist and the average number of remaining AChR clusters was compared to the average number of clusters obtained for a population of myotubes left untreated. The aim of the current chapter was to develop a novel experimental setup that allows for targeted activation of a subset of ADRB2s and that enables us to monitor the breakdown of single AChR clusters. An optogenetic variant of ADRB2 was used, which gives precise optical control over receptor activation and thus downstream signalling. This optogenetic receptor, henceforth referred to as opto-ADRB2, was recently engineered by Karl Deisseroth and colleagues, who created a functional chimeric receptor by replacing the intracellular loops of the

light-sensitive G-coupled receptor rhodopsin with those of the beta-2 adrenergic receptor (Airan et al., 2009) (Fig. 5.1). The result is a photoreceptor which signals through an adrenoreceptor-specific pathway, achieved by coupling between light-induced conformational changes in the transmembrane region of rhodopsin and the intracellular region of ADRB2 (Kim et al., 2005). In the current study, a stable cell line overexpressing opto-ADRB2 was created in order to be able to activate receptors in a small region of a selected myotube by laser stimulation. The advantage of this novel setup is that single dispersing AChR clusters in proximity to activated ADRB2s could be compared to AChR clusters on neighbouring myotubes in the absence stimulation (Fig. 5.2). Such an experiment crucially depends on being able to determine whether opto-ADRB2s have been successfully activated. Since stimulation of ADRB2 leads to an increase in the generation of cAMP (Johnson, 2006), we first developed a method that allows for the measurement of cAMP signalling in C2C12 myotubes to validate the opto-ADRB2 construct in this cell line.

5.2 Investigation of the dynamics of cAMP signalling in C2C12 myotubes

Different tools are commercially available to measure cAMP levels, such as competition enzyme-linked immuoassays, luciferase reporter constructs and radioimmunoassays. However, when performed in our laboratory in C2C12 cultures, neither enzyme-linked immunoassays nor a luciferase reporter assay proved to be sensitive enough to reliably detect agonist-induced changes in cAMP levels (data not shown). The results were variable, and no consistent dose-response relationship could be observed. Besides limited sensitivity, conventional cAMP assays have several other limitations. They fail to give insights into the dynamics of ADRB2 second messenger signalling (Borner et al., 2011). Rapid increases in cAMP levels and changes over time

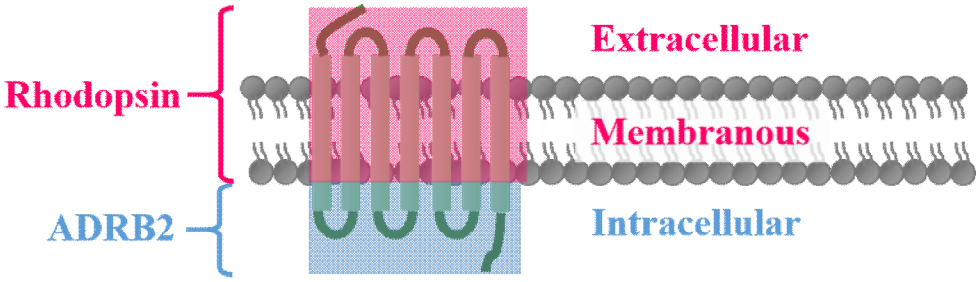

Figure 5.1 Schematic of opto-ADRB2. The intracellular loops of rhodopsin have been replaced with those of the ADRB2.

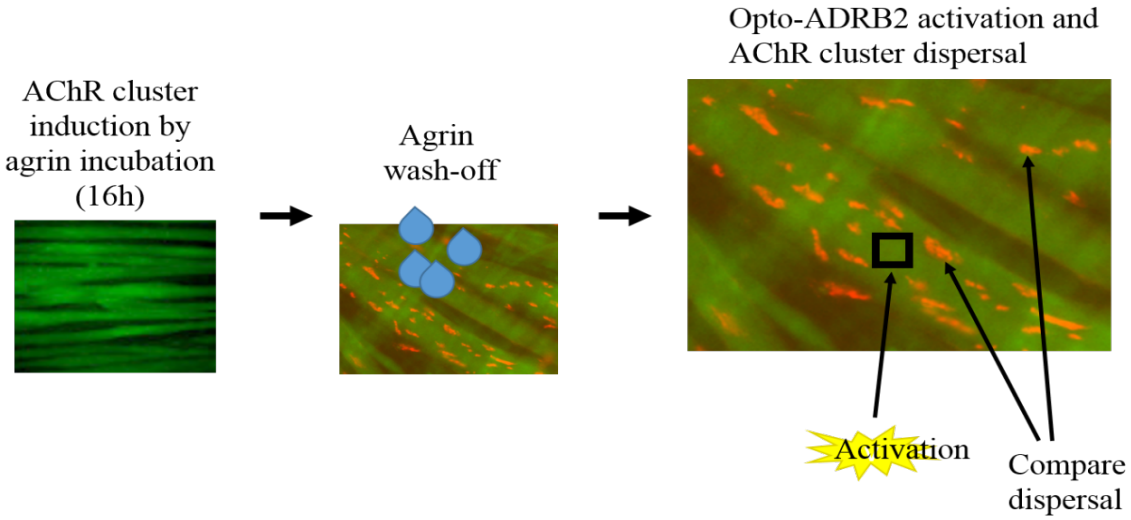

Figure 5.2 Schematic of a novel AChR cluster dispersion experiment. After agrin-mediated AChR cluster induction, agrin was washed off, and a defined region on a C2C12 myotube was subjected to light stimulation to activate opto-ADRB2s. A time course experiment was set up to study dispersal of clusters adjacent to the activation area vs. dispersal of clusters on a different myotube that had undergone no stimulation.

cannot be detected. Also, cAMP concentrations can only be determined for a batch of cultured cells at a chosen time point. Conventional cAMP assays are therefore not suitable for the measurement of cAMP changes in intact living cells such as differentiating C2C12 myoblasts, and they cannot be used to investigate cAMP changes in single cells. As a result, little is known about the temporal and spatial dynamics of cAMP signalling in myotubes. To overcome these methodological concerns, an experimental setup which enables the detection of dynamic changes in cAMP levels in single C2C12 myotubes was developed in collaboration with the recently established Wolfson Imaging Centre Oxford.

Fluorescence microscopy techniques have improved dramatically over the last few decades and can be utilised to study molecular interactions in live single cells at high temporal and spatial resolution. The foundations for such experiments were laid in 1946 by the German physicist Theodor Förster who discovered the phenomenon of nonradiative energy transfer (Förster, 1948). Today known as Förster-resonance energy transfer (FRET), Förster's observation was developed further to monitor the distance between two fluorescent chromophores forming a so called FRET donor/acceptor pair (Sekar and Periasamy, 2003). Energy transfer can be observed if a sample of cells expressing the FRET pair is exposed to light of a specific wavelength that is directly absorbed by the donor fluorophore but not by the acceptor fluorophore. As a result, the donor absorbs a photon of light and transitions to an electronic excited state (Fig. 5.3). If a matching acceptor fluorophore is in close proximity to the donor (r~1-10 nm), the resulting excitation energy can be transferred from the donor to the acceptor by non-radiative energy transfer, after which the acceptor transitions to an excited electronic state. Finally, the acceptor relaxes to its ground state and emits light at a wavelength specific for the emission spectrum of the acceptor. If the donor and the acceptor are far

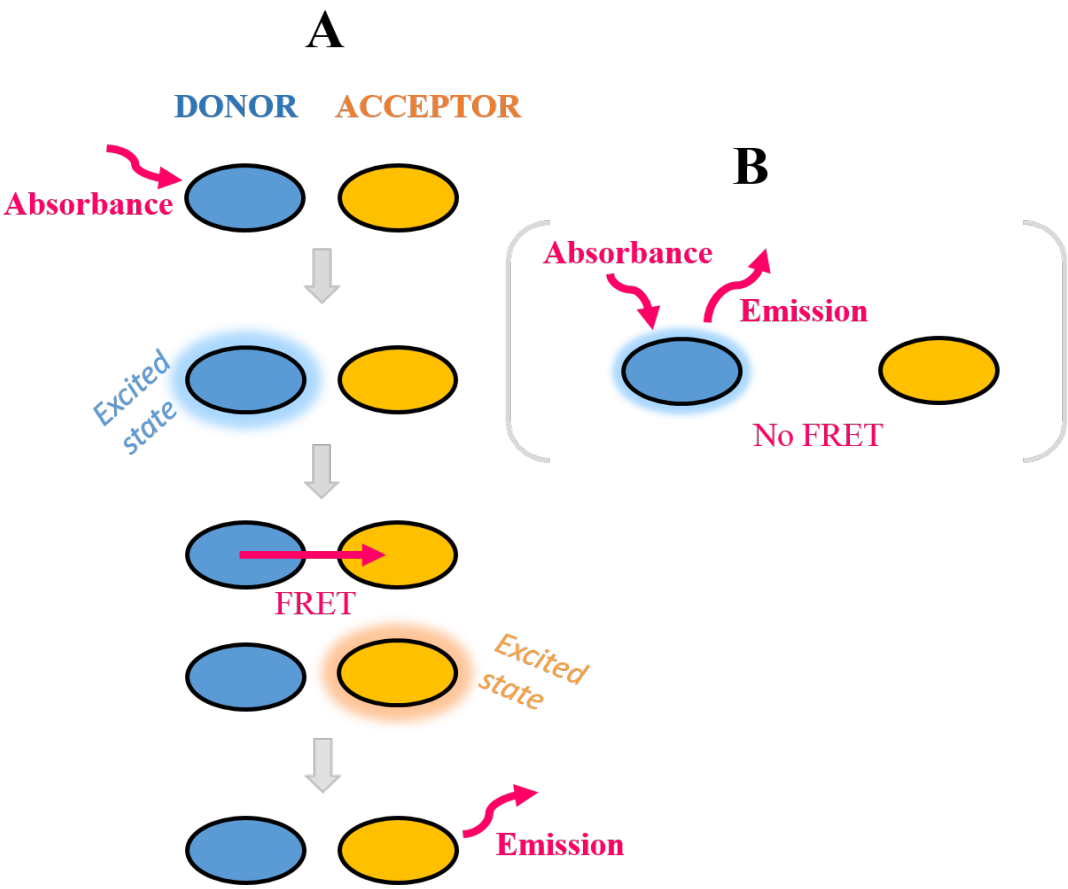

Figure 5.3 Basic principle of FRET. (A) The donor fluorophore is excited by a photon and transfers energy to an acceptor fluorophore as it returns to the ground state. The excited acceptor drops to the ground state and emits a photon. (B) FRET only occurs if the donor and acceptor are in close proximity.

apart from each other, little energy transfer can occur and the emission spectrum is influenced mainly by the characteristics of the donor (Fig. 5.3B). The FRET efficiency *E* therefore depends on the following parameters:

$$E = \frac{1}{1 + (r/R_0)^6}$$

with *r* being the distance between the donor and acceptor and R_0 being the Förster distance. R_0 describes the distance at which the energy transfer efficiency is 50% which depends on physical parameters of the donor-acceptor pair.

FRET can be used to investigate protein interactions and protein conformations but also to detect signalling events (Sekar and Periasamy, 2003). Changes in second messenger levels such as intracellular calcium or cAMP can be measured by expression of a FRET sensor (Borner et al., 2011). Kees Jalink developed the first exchange protein directly activated by cAMP (Epac)-based FRET construct which can be used as a cAMP indicator (Ponsioen et al., 2004). Epac belongs to the group of guanine nucleotide exchange factors (GEFs). It is an activator of the Ras superfamily small GTPase Rap, which oscillates between an inactive guanosine diphosphate (GDP)-bound and an active guanosine triphosphate (GTP)-bound state (Gloerich and Bos, 2010). Activation of Epac initiates the exchange of GDP for GTP. The regulatory region of Epac serves an auto-inhibitory function in which the C-terminal cyclic nucleotide-binding domain sterically hinders Rap from binding to the catalytic region (Rehmann et al., 2008, Metrich et al., 2010). Upon cAMP binding, Epac undergoes a conformational change such that the regulatory subunit bends towards the back of the catalytic site, thus negating the autoinhibition and allowing Rap to bind. This cAMP-mediated conformational change makes Epac a highly sensitive tool to measure cAMP signaling when being combined with FRET imaging. In Epac-based FRET sensor constructs, a high-affinity variant of Epac is sandwiched between two fluorophores (Fig. 5.4). The

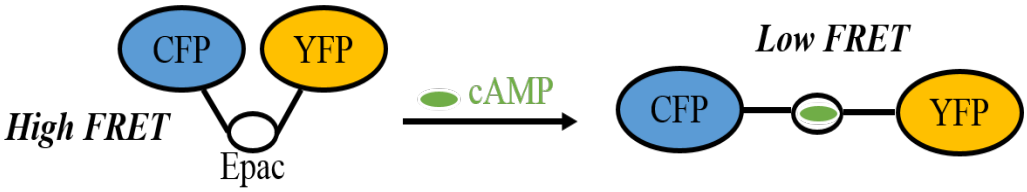

Figure 5.4 Basic principle of an Epac-based FRET sensor. Binding of cAMP causes a conformational change in Epac, which decreases the energy transfer from the donor to the acceptor fluorophore.

most commonly used donor and acceptor pair is cyan fluorescent protein (CFP) and yellow fluorescent protein (YFP), although more efficient variants are constantly being developed (Klarenbeek et al., 2015). The conformational change in Epac in response to cAMP binding increases the distance between the donor and the acceptor, and a decrease in energy transfer efficiency occurs.

FRET can be measured quantitatively either by conventional fluorescence microscopy by measuring the variation of fluorescence intensity of the donor and acceptor fluorophore pair, or by fluorescence lifetime imaging microscopy (FLIM) which records the fluorescence decay rate of the donor (Becker, 2012, Raspe et al., 2015). The fluorescence lifetime τ, measured in nanoseconds, describes the average time the donor fluorophore remains in its excited state before transitioning to the ground state either by emission of a photon or in case of FRET by non-radiative transfer of the excited state energy to a nearby acceptor. τ is commonly determined by time-correlated single photon counting, TCSPC (Wahl et al., 2008, Becker, 2012). In this set-up, a conventional laser-scanning microscope has been further equipped with a pulsed excitation laser source, single photon counting detectors (e.g. single photon counting avalanche photo-diodes (SPADs)), and timing electronics such that the time between the sample excitation by a pulsed-excitation laser source and the arrival of the emitted photon at the detector can be recorded on a pixel-to-pixel basis. By repetition of these measurements it is possible to record the distribution of arrival times, and subsequently a histogram of photon counts over arrival times is calculated. Each histogram is fitted to an exponential function, which describes the fluorescence lifetime decay. The time constant τ from this decay function is the fluorescence lifetime. In order to visually display different lifetimes, the microscopic images obtained through TCSPC are colour-coded.

FLIM provides an excellent tool for the measurement of cAMP signalling in C2C12 cells due to its high sensitivity to cAMP changes and its *in*sensitivity to fluctuations in excitation intensity and dye concentration (Hum et al., 2012). If an Epac-based FRET sensor is expressed in a sample of cells and the intracellular cAMP concentration is low, energy transfer occurs between the donor and the acceptor and the fluorescence lifetime of the donor is short. A decrease in FRET however, caused by enhanced cAMP signalling, will increase the fluorescence lifetime of the donor.

For experiments described below, C2C12 myoblasts were electroporated with a fourth-generation Epac-based FRET sensor, developed and kindly provided by Kees Jalink (Klarenbeek et al., 2015). The sensor construct consists of the CFP variant mTurquoise2, characterised by increased brightness and photostability and a reported single exponential life-time of τ=4.0ns (Goedhart et al., 2012), a dark non-emitting circular permuted venus YFP acceptor variant which allows for the detection of a larger part of the donor spectrum in lifetime measurements, thus increasing the brightness, and finally a high affinity version of Epac.

Expression of this FRET sensor in C2C12 cells was used to control for successful opto-ADRB2 activation in the dispersion experiment outlined above. It also enabled us to study the dynamics of cAMP signalling following activation of endogenous ADRB2s by salbutamol and other ADRB2 agonists. Treatment of C2C12 cells with ADRB2 agonists was expected to cause activation of ADRB2 expressed in the cells. This assumption was tested by measuring changes in intracellular cAMP levels following agonist application. The detection of cAMP signalling also helped to address the following issues arising from previous experiments. Little is known about the temporal dynamics of cAMP signalling following ADRB2 stimulation. In chapter 4, the ADRB2 agonist-induced changes in AChR cluster numbers and the stabilisation of dispersing

clusters were measured after 22 and 6h, respectively. Since desensitisation effects are likely to occur in the presence of an agonist, one might expect cAMP levels to plateau and/or decrease before the end of this incubation period (Sher and Clementi, 1984, Krupnick and Benovic, 1998).

Moreover, it is not known whether the different agonists tested in chapter 4 induce similar changes in cAMP levels at the concentrations shown to affect AChR clustering. The novel agonist XA-01-NZ86 increased cluster numbers at a lower concentration than salbutamol sulphate. Using the FRET sensor, it was tested whether this finding is linked to differences in the ability of these agonists to raise cAMP levels at low drug concentrations.

In summary, this chapter describes the validation of novel fluorescence imaging and optogenetic tools for investigating the effects of ADRB2 signalling on synaptic stability. First, experiments were conducted to validate the use of a FRET sensor in C2C12 cells. Subsequently, preliminary results on the dynamics of cAMP signalling in response to ADRB2 agonist application and on the effects of light-driven opto-ADRB2 stimulation on AChR cluster dispersal are presented.

5.3 Validation of the FRET sensor as a tool to measure cAMP signalling in C2C12 myotubes

In order to detect cAMP levels, the fourth generation Epac-based FRET sensor *mTurq2Del-EPAC(dDEPCD)Q270E-td_black_cp173Venus(d) EPAC-S^{H189} Amp*, which was kindly provided by Kees Jalink (Klarenbeek et al., 2015), was used.

C2C12 myoblasts were electroporated with 10µg of the sensor construct before each experiment. To investigate the effects of targeted ADRB2 activation, a stable C2C12 cell line expressing opto-ADRB2 was created by electroporation with 2µg DNA

and subsequent selection with 1mg/ml neomycin for two weeks. Similar to WT cells, these cells were electroporated with 10µg of the FRET sensor construct before each experiment. C2C12 cells expressing the sensor construct are henceforth referred to as C2C12$^{\text{WT-}ADRB2\text{+Epac}}$. C2C12 cells expressing opto-ADRB2 and the sensor construct are referred to as C2C12$^{\text{opto-}ADRB2\text{+Epac}}$.

For the FRET measurements, bright fluorescent cells were selected by visual inspection through the ocular to ensure high expression of the sensor. Fluorescence excitation was achieved using a 440nm pulsed laser.

First, baseline cAMP levels were investigated in C2C12$^{\text{WT-}ADRB2\text{+Epac}}$ cells and compared to C2C12$^{\text{opto-}ADRB2\text{+Epac}}$. Measurements were taken in the myoblast state of the cells two days after electroporation with the FRET sensor. The results suggest low cAMP levels in the absence of ADRB2 stimulation (both mean τ=2.7ns, SEM=0.03), and the fluorescence lifetimes were similar in the two cell lines ($p=0.54$) (Fig. 5.5).

The sensitivity of the FRET sensor was tested by stimulating endogenous ADRB2s. C2C12$^{\text{WT-}ADRB2\text{+Epac}}$ and C2C12$^{\text{opto-}ADRB2\text{+Epac}}$ cells were treated with 50µM salbutamol sulphate. Measurements were taken before and 5min after agonist incubation. In both cell lines a significant increase in cAMP levels was observed after the treatment ($p=0.0003$ and $p<0.0001$, respectively) (Fig. 5.6).

Next, it was investigated whether cAMP levels change during the differentiation of C2C12 myoblasts into myotubes. Since the differentiation of myoblasts into myotubes takes between six and nine days, it was crucial to test whether the cells would still show sufficient expression of the sensor construct after this many days following transfection. A sample of C2C12$^{\text{WT-}ADRB2\text{+Epac}}$ cells was observed over a total of nine days and lifetime measurements were taken on day 2 after electroporation with the sensor (myoblast state), day 6 (intermediate state) and day 9 (myotube state).

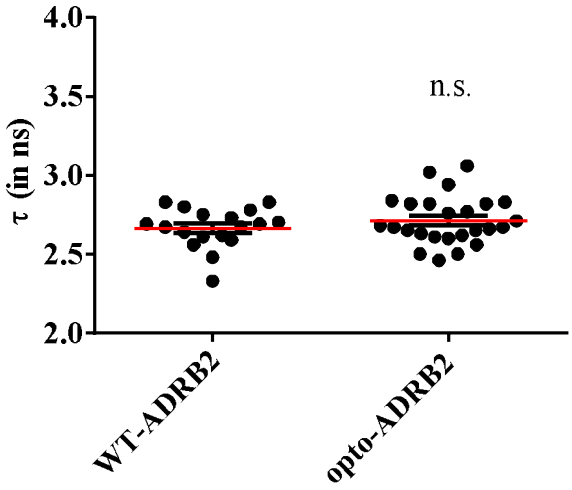

Figure 5.5 Comparison of the fluorescence lifetime in C2C12$^{\text{WT-}ADRB2\text{+Epac}}$ and C2C12$^{\text{opto-}ADRB2\text{+Epac}}$ myoblasts two days after electroporation with the FRET sensor. No difference in cAMP levels occurred between the two cell lines in the absence of ADRB2 stimulation (difference=0.05ns, Mann-Whitney test p=0.54). N=18 (C2C12$^{\text{WT-}ADRB2\text{+Epac}}$), N=25 (C2C12$^{\text{opto-}ADRB2\text{+Epac}}$). Error bars indicate the standard error of the mean. n.s. p>0.05.

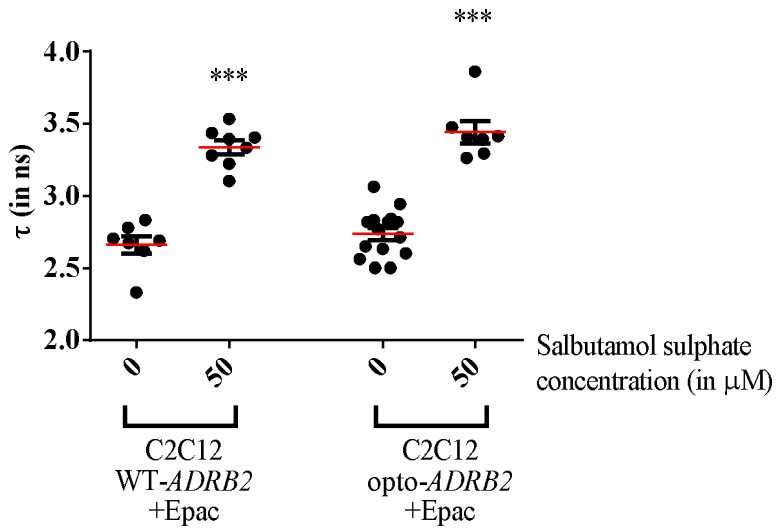

Figure 5.6 Salbutamol treatment of C2C12$^{\text{WT-}ADRB2\text{+Epac}}$ and C2C12$^{\text{opto-}ADRB2\text{+Epac}}$ two days after electroporation with the FRET sensor. 5min of incubation with 50µM salbutamol sulphate significantly increased cAMP levels in both cell lines (difference=0.68ns, Mann-Whitney test p=0.0003, and difference=0.7ns, Mann-Whitney test p<0.0001, respectively). N=7 ('0µM' C2C12$^{\text{WT-}ADRB2\text{+Epac}}$ and '50µM' C2C12$^{\text{opto-}ADRB2\text{+Epac}}$), N=8 ('50µM' C2C12$^{\text{WT-}ADRB2\text{+Epac}}$), N=15 ('50µM' C2C12$^{\text{opto-}ADRB2\text{+Epac}}$). Error bars indicate the standard error of the mean. ***p≤0.001.

Expression of the sensor construct was still observed in the myotube state of the cells, and the results suggested no significant change in cAMP levels during differentiation ($p=0.58$) (Fig. 5.7A). To investigate if changes occur in myotubes after day 9, the fluorescence lifetime was measured in a different cell sample on day 10 and 12. A significant increase was measured on day 12 ($p=0.0009$) (Fig. 5.7B). The same time course experiment was conducted for C2C12$^{\text{opto-}ADRB2\text{+Epac}}$ cells. As before, no statistically significant differences in the mean fluorescence lifetime occurred between day 2, 6 and 9 ($p=0.14$), although a trend towards higher cAMP levels on day 9 was observed (Fig 5.8A).

To test whether cAMP changes can still be detected if cAMP baseline levels are elevated, the same sample of C2C12$^{\text{opto-}ADRB2\text{+Epac}}$ cells was subjected to agonist treatment on day 9, and the lifetimes were measured before and after 5min of agonist incubation. 50µM salbutamol sulphate caused a detectable increase in cAMP levels ($p=0.009$) (Fig. 5.8B).

The results presented so far were obtained by measuring different cells that were electroporated at the same time as each other. Reproducibility of this technique is crucial since different experiments will need to be compared. To test this, two separate electroporations with the sensor constructs were performed using cells that originate from the same culture flask. The cells from each electroporation were then seeded into a different dish and measured on day 2 after the electroporation in the myoblast state of the cells. No significant variability between dishes was observed for C2C12$^{\text{WT-}ADRB2\text{+Epac}}$ or C2C12$^{\text{opto-}ADRB2\text{+Epac}}$ cells ($p=0.74$ and $p=0.37$, respectively) (Fig. 5.9A,B). The experiment was repeated for C2C12$^{\text{WT-}ADRB2\text{+Epac}}$ myotubes on day 8 after electroporation with the sensor, and the lifetimes of 4 different cell samples were compared in the myotube state. No significant difference between dishes was observed

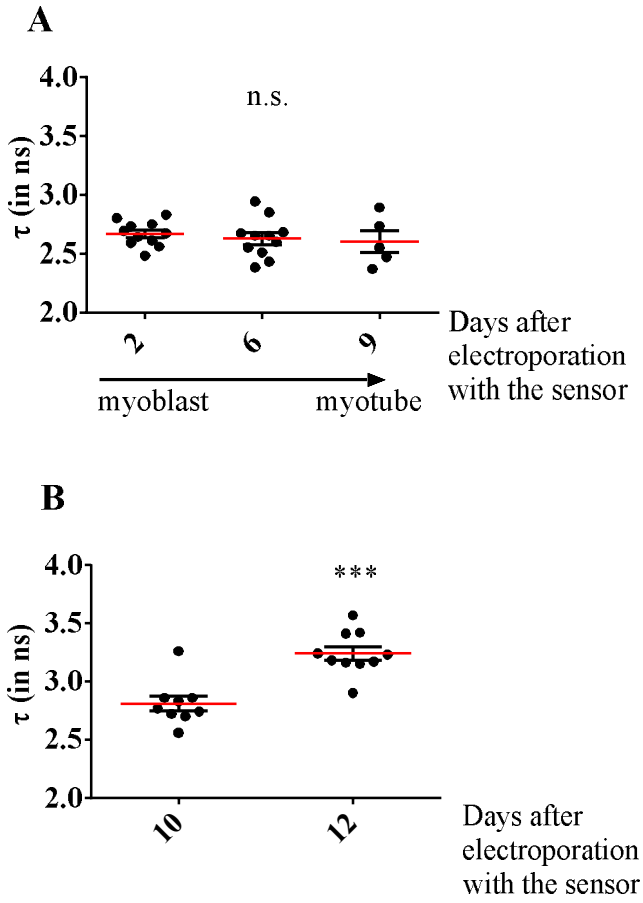

Figure 5.7 Changes in cAMP levels during the differentiation of C2C12$^{WT\text{-}ADRB2+Epac}$ myoblasts into myotubes. (A) The fluorescence lifetime was measured in cells of the same cell culture dish on day 2, 6 and 9 after electroporation with the FRET sensor. No significant change in cAMP levels was observed (Kruskal-Wallis test p=0.58). (B) The fluorescence lifetime was measured in C2C12$^{WT\text{-}ADRB2+Epac}$ myotubes on day 10 and 12 after electroporation with the FRET sensor (different dish than in 14A). cAMP levels were significantly higher on day 12 (difference=0.43ns, Mann-Whitney test p=0.0009). N=11 (2 and 6 days), N=5 (9 days), N=9 (10 days), N=10 (12 days). Error bars indicate the standard error of the mean. n.s. p>0.05, *** p≤0.001.

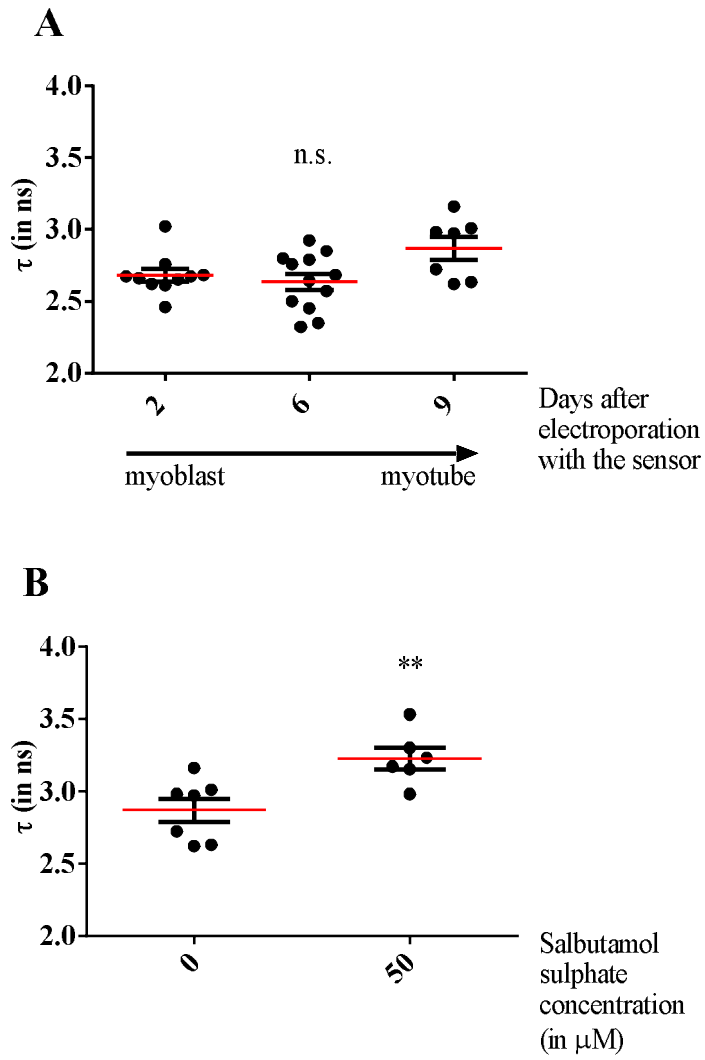

Figure 5.8 Changes in cAMP levels during the differentiation of C2C12$^{opto\text{-}ADRB2}$+Epac myoblasts into myotubes. (A) The fluorescence lifetime was measured in cells of the same cell culture dish on day 2, 6 and 9 after electroporation with the FRET sensor. No significant differences in cAMP levels occurred during the differentiation of cells (Kruskal-Wallis test p=0.14). N=10 (2 days), N=12 (6 days), N=7 (9 days). (B) The same cells from day 9 were treated with 50μM salbutamol sulphate. cAMP levels significantly increased after 5min of agonist incubation (difference=0.36ns, Mann-Whitney test p=0.009). N=7 ('0μM'), N=6 ('50μM'). Error bars indicate the standard error of the mean. n.s. p>0.05, **p≤0.01.

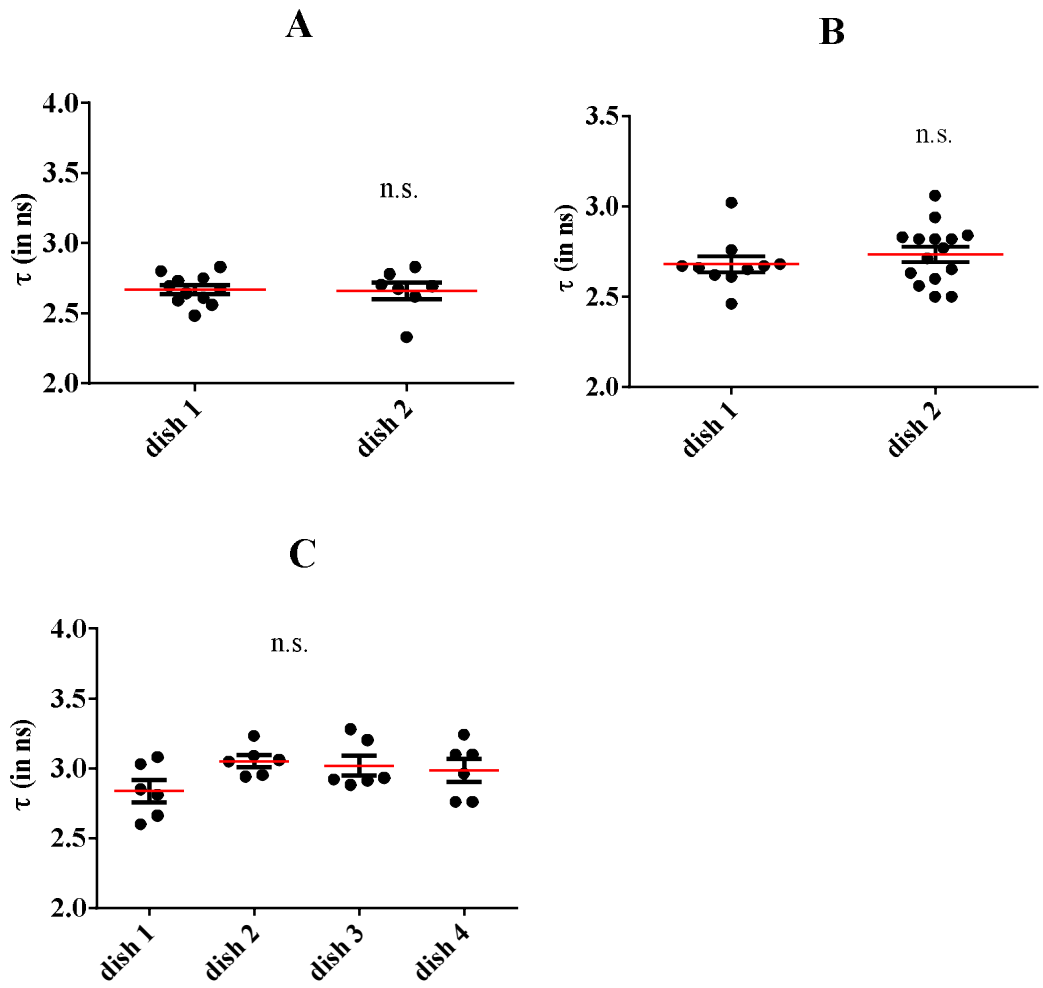

Figure 5.9 Variability in the fluorescence lifetimes between cell culture dishes. Cells from each electroporation with the FRET sensor were seeded into a different dish and the fluorescence lifetime was measured on day 2 after electroporation. (A) No significant differences in cAMP levels were observed between two dishes in C2C12$^{WT\text{-}ADRB2+Epac}$ cells (difference=0.01ns, Mann-Whitney test p=0.74). N=11 (dish 1) and N=7 (dish 2). (B) No differences occurred between two dishes in C2C12$^{opto\text{-}ADRB2+Epac}$ cells (difference=0.06ns, Mann-Whitney test p=0.37). N=10 (dish 1), N=15 (dish 2). (C) Four dishes of C2C12$^{WT\text{-}ADRB2+Epac}$ cells were compared in the myotube state on day 8 after the electroporation with the FRET sensor. No differences in cAMP levels occurred (Kruskal-Wallis test p=0.22). All N=6. Error bars indicate the standard error of the mean. n.s. p>0.05.

(p=0.22) (Fig. 5.9C).

5.4 Effects of agonist-mediated activation of endogenous ADRB2 on cAMP signalling

The results suggest that *mTurq2Del-EPAC(dDEPCD)Q270E-td_black_cp173Venus(d) EPAC-S^{H189} Amp* is a sensitive tool to detect changes in cAMP levels in C2C12 cells. Therefore, the effects of salbutamol sulphate and XA-01-NZ86 treatment on cAMP signalling were investigated in C2C12$^{\text{WT-}ADRB2\text{+Epac}}$ myotubes. Experiments were conducted on day 8 after electroporation with the sensor, and measurements were taken before and 5min after agonist incubation. At a concentration of 10µM, salbutamol sulphate caused a significant increase in cAMP levels (p=0.002). Treatment with 10µM XA-01-NZ86 increased the cAMP levels, however, the results did not reach statistical significance (p=0.07) (Fig. 5.10A and B). A larger increase was observed in response to drug treatment at a concentration of 1µM. While salbutamol sulphate increased the average lifetime by 0.32ns at this concentration (p=0.009) (Fig. 5.10C), the largest increase (0.42ns) was achieved with XA-01-NZ86 (p=0.007) (Fig. 5.10D). Figure 5.10E,F depicts representative colour-coded microscopic images of cells obtained through TCSPC before and after agonist stimulation, illustrating the increase in cAMP levels.

In order to test whether changes in cAMP levels can be detected if baseline levels are higher, the experiment was repeated on day 11 after electroporation with the sensor. At this stage, agonist incubation with 1µM salbutamol sulphate did not increase ADRB2 signalling (p=0.92) (Fig. 5.11). Treatment with 1µM XA-01-NZ86, on the other hand, significantly increased the average lifetime by 0.17ns (p=0.02).

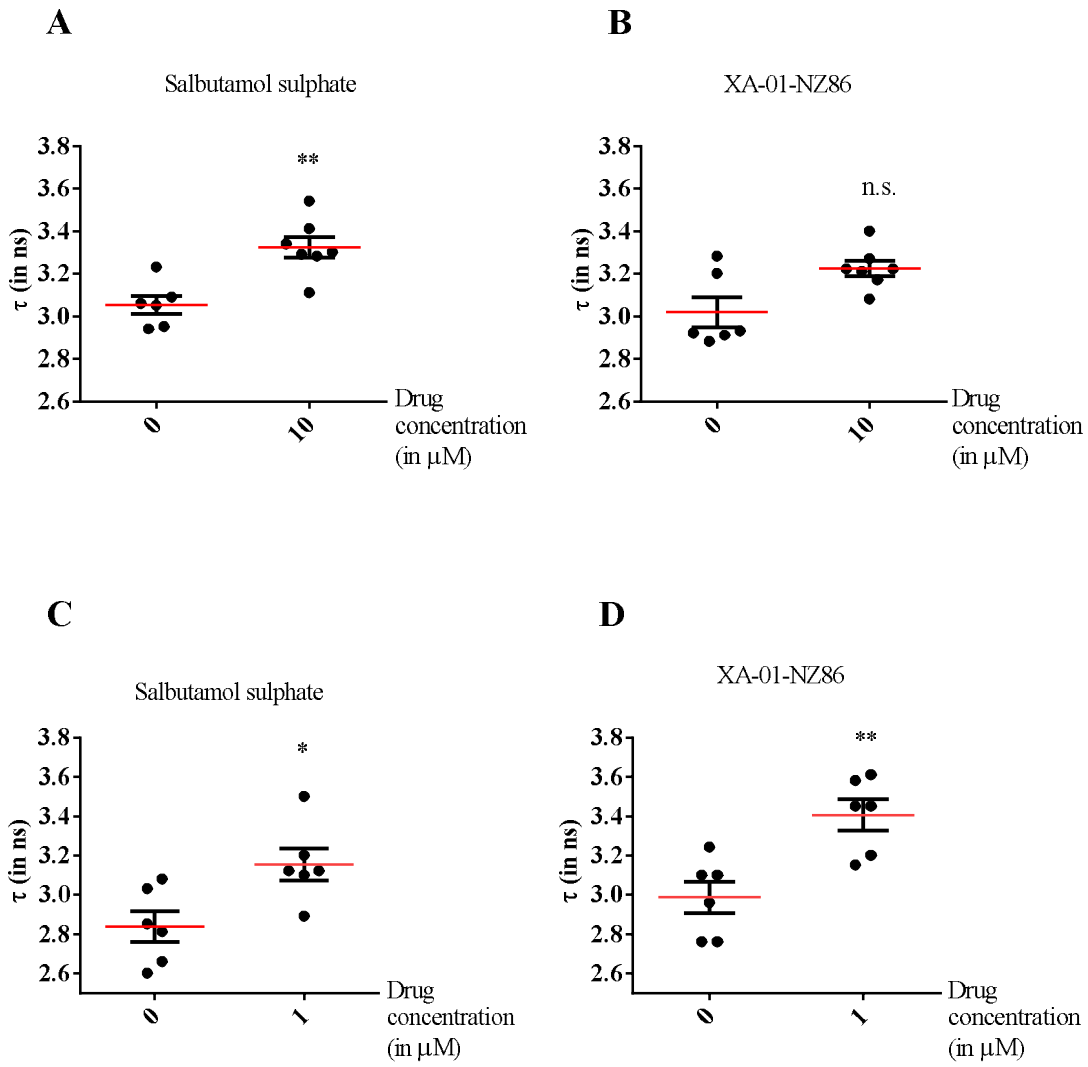

Figure 5.10 Effects of agonist-mediated activation of endogenous ADRB2 on cAMP levels in C2C12$^{WT\text{-}ADRB2+Epac}$ myotubes. Measurements were taken before and after 5min of incubation with salbutamol sulphate or XA-01-NZ86 on day 8 after electroporation with the FRET sensor. (A) At 10µM, salbutamol sulphate significantly increased cAMP levels (difference=0.27ns, Mann-Whitney test p=0.002). N=6 ('0µM'), N=7 ('10µM'). (B) No significant difference occurred with 10µM XA-01-NZ86 (difference=0.2ns, Mann-Whitney test p=0.07). N=6 ('0µM'), N=7 ('10µM') (C) Lowering the dose of the drugs to 1µM caused a larger increase in cAMP levels. Salbutamol sulphate raised the fluorescence lifetime by 0.32ns (Mann-Whitney test p=0.009). N=6 ('0µM'), N=7 ('10µM'). (D) Incubation with 1µM of XA-01-NZ86 raised the lifetime by 0.42ns (Mann-Whitney test p=0.007). Both N=6. Error bars indicate the standard error of the mean. n.s.p>0.05, *p≤0.05, ** p≤0.01.

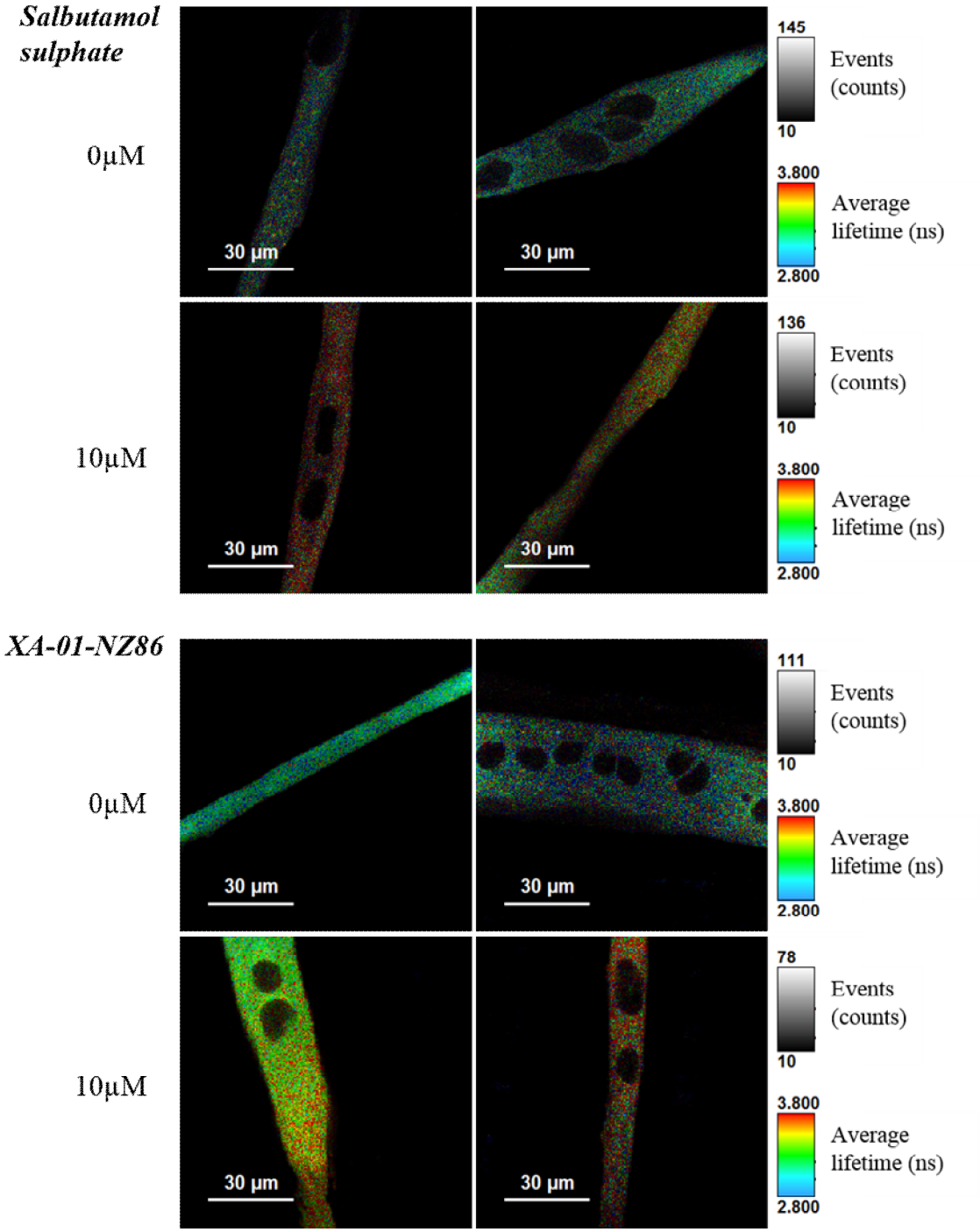

Figure 5.10 (continued) (E) Representative microscopic colour-coded images of C2C12$^{\text{WT-}ADRB2\text{+Epac}}$ myotubes obtained through TCSPC before and after 5min of incubation with 10µM salbutamol sulphate or XA-01-NZ86 on day 8 after electroporation with the FRET sensor. The shift in colour towards bright green/red illustrates the rise in cAMP levels.

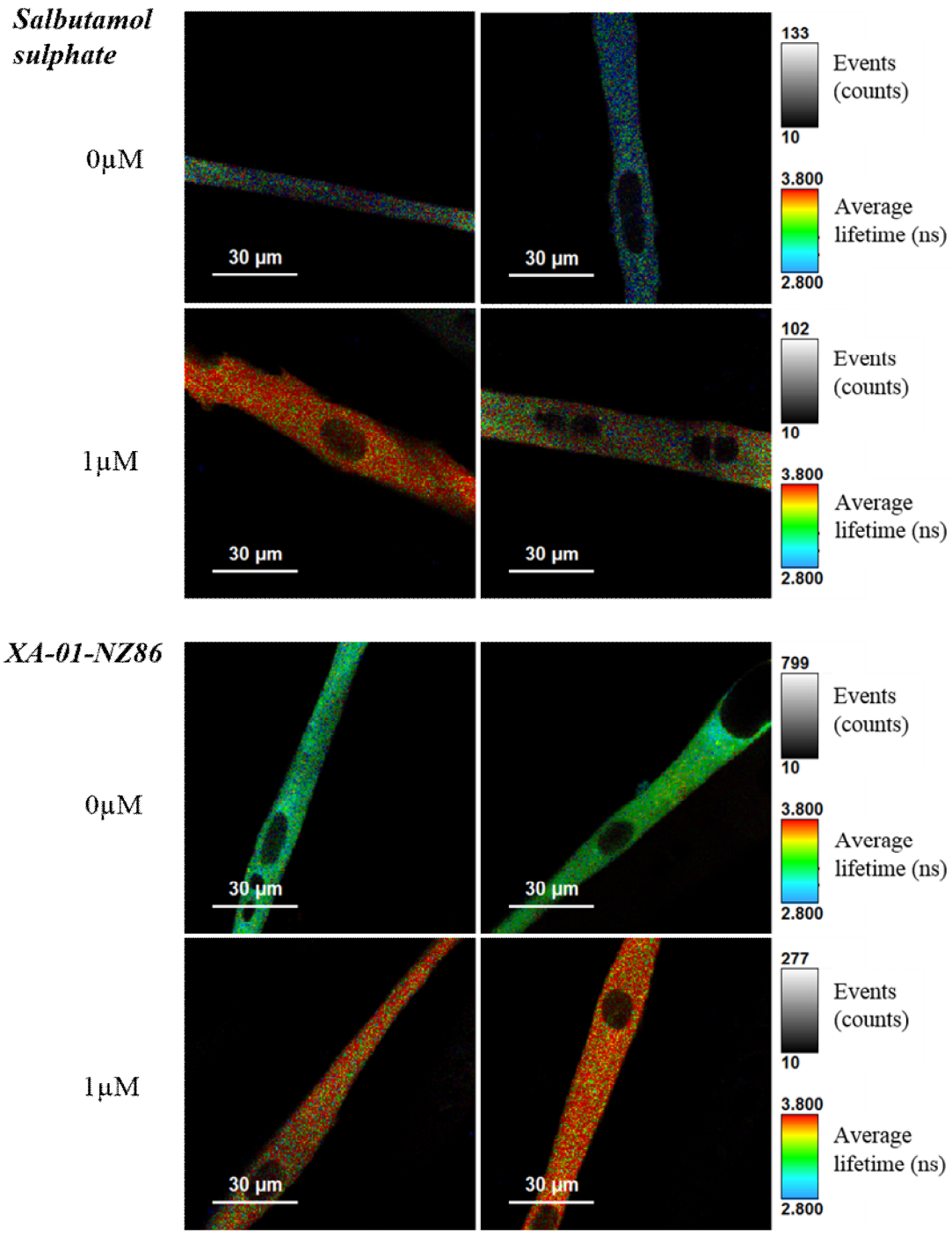

Figure 5.10 (continued) (F) Representative microscopic colour-coded images of C2C12$^{\text{WT-}ADRB2\text{+Epac}}$ myotubes obtained through TCSPC before and after 5min of incubation with 1µM salbutamol sulphate or XA-01-NZ86 on day 8 after electroporation with the FRET sensor. The shift in colour towards red illustrates the rise in cAMP levels.

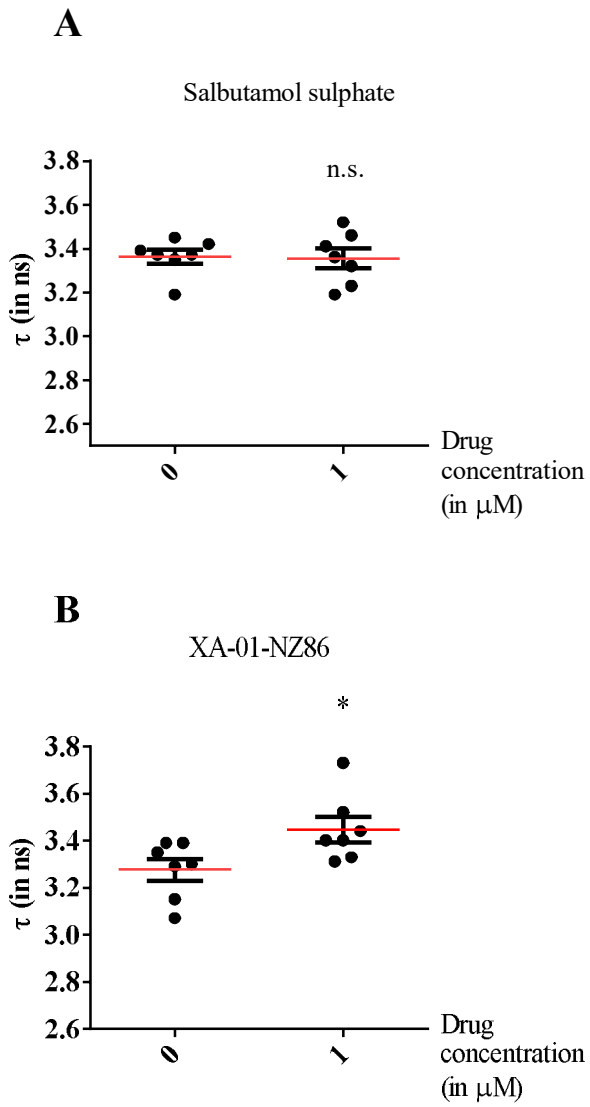

Figure 5.11 Effects of agonist-mediated activation of endogenous ADRB2 on cAMP levels in C2C12$^{WT\text{-}ADRB2+Epac}$. Measurements were taken before and after 5min of incubation with 1μM salbutamol sulphate or 1μM XA-01-NZ86 on day 11 after electroporation with the FRET sensor. (A) No significant increase in cAMP levels was observed in response to salbutamol sulphate treatment (difference=0ns, Mann-Whitney test p=0.92). Both N=7. (B) XA-01-NZ86 caused a moderate increase in cAMP signalling (difference=0.1ns, Mann-Whitney test p=0.02). Both N=7. Error bars indicate the standard error of the mean. n.s.>0.05, *p≤0.05.

In order to shed light on the dynamics of cAMP signalling in C2C12 cells after agonist incubation, a time course experiment was devised in which cAMP levels were monitored over a period of several hours (Fig. 5.12). When using the microscope in the FLIM acquisition mode it is not possible to mark positions for the measurement of several cells over time, and so three separate experiments were conducted, in each of which one cell was chosen for the time course measurements. Data obtained for the three cells were pooled. A further technical challenge was the determination of cAMP levels before stimulation, since the agonist could not be applied without changing the field of view. Therefore, the lifetimes of 8-10 cells per experiment were measured before stimulation in order to estimate the baseline cAMP levels of the cells chosen for the stimulation (Fig. 5.12B). The baseline measurements from the three experiments were pooled. After adding 10µM salbutamol sulphate, a myotube was selected, and measurements were taken every 2min over a time period of 2h48min (84 lifetime measurements in total) (Fig. 5.12A). As expected from previous experiments, a high mean fluorescence lifetime of the donor was observed after agonist incubation (τ=3.28ns, first time point), whilst the baseline mean lifetime of the donor in cells measured before agonist application was significantly lower, with τ=2.8ns (p=0.01) (Fig. 5.12C). Within 2h48min, the mean lifetime decreased by 0.44ns, reaching an average of 2.85ns (last time point). At this point, the lifetime did not significantly differ from the mean lifetime measured in unstimulated cells (p=n.s.). This suggested that cAMP levels returned to baseline levels. The large difference in lifetimes between the first and last time point (0.44ns) did not reach statistical significance (p=0.25), however, this is very likely due to the small sample size.

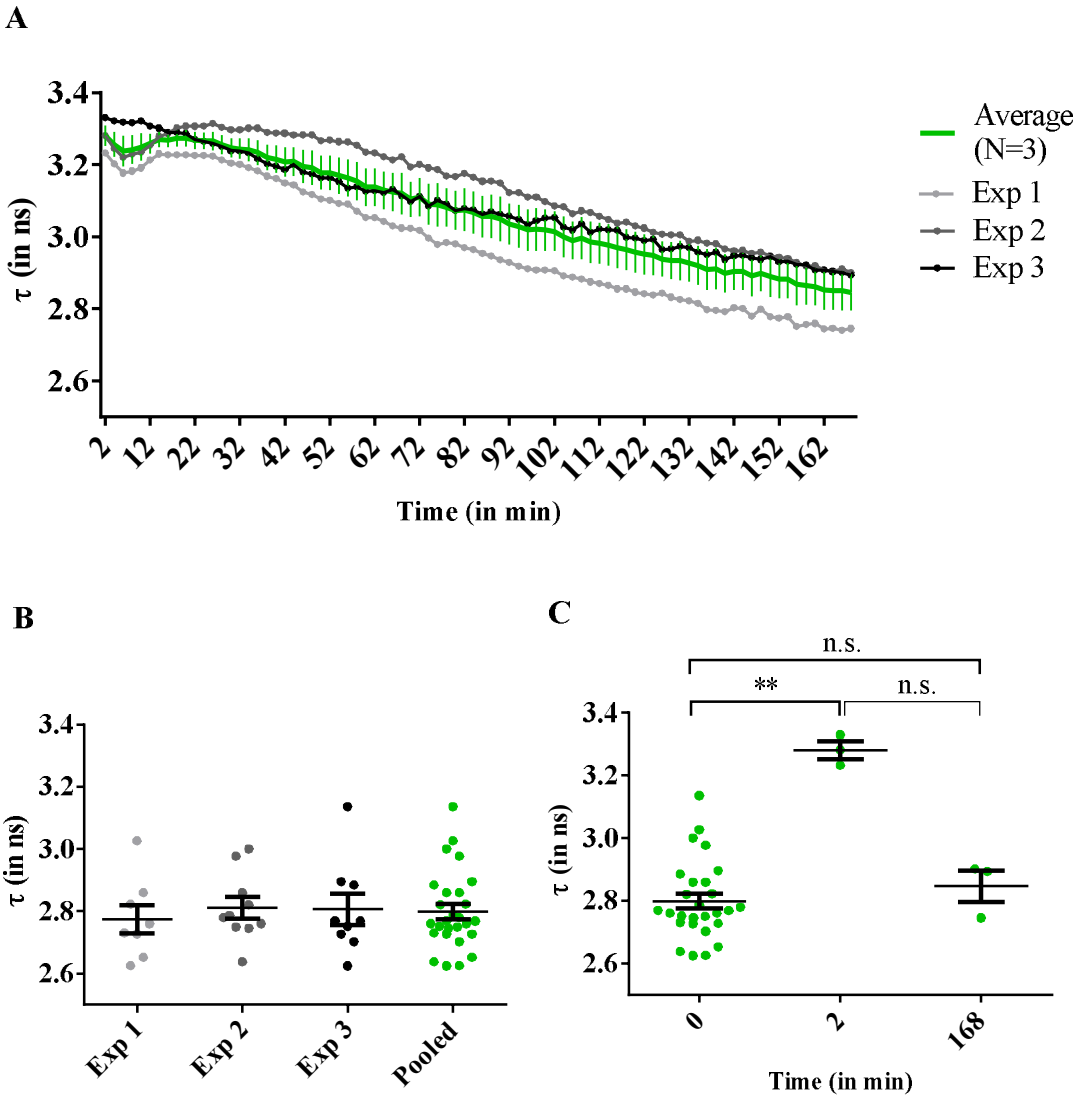

Figure 5.12 Temporal dynamics of cAMP signalling in C2C12$^{WT\text{-}ADRB2+Epac}$ myotubes in response to agonist-mediated activation of ADRB2s. (A) After application of 10µM salbutamol sulphate, lifetime measurements were taken every 2min for a duration of 2h48min. The graphs for Exp 1, 2 and 3 each depict lifetime measurements for one cell, and the results for the three cells were pooled to obtain an average curve (in green). (B) 8-10 cells/experiment were measured before agonist application to estimate cAMP baseline levels. N=27 ('Pooled', in green) (C) Salbutamol sulphate incubation led to a significantly higher average donor lifetime when compared to baseline levels (Kruskal-Wallis test with Dunn's multiple comparisons test p=0.01). Within 2h48min, the mean lifetime of the donor decreased from 3.28ns (SEM=0.03, 2min) to 2.85ns (SEM=0.05, 168min) (Wilcoxon test p=0.25). By the end of the time course (168min), the average lifetime did not significantly differ from the lifetime measured in untreated cells at baseline (Kruskal-Wallis test with Dunn's multiple comparisons test p=n.s.). Error bars indicate the standard error of the mean. n.s.>0.05, **p≤0.01.

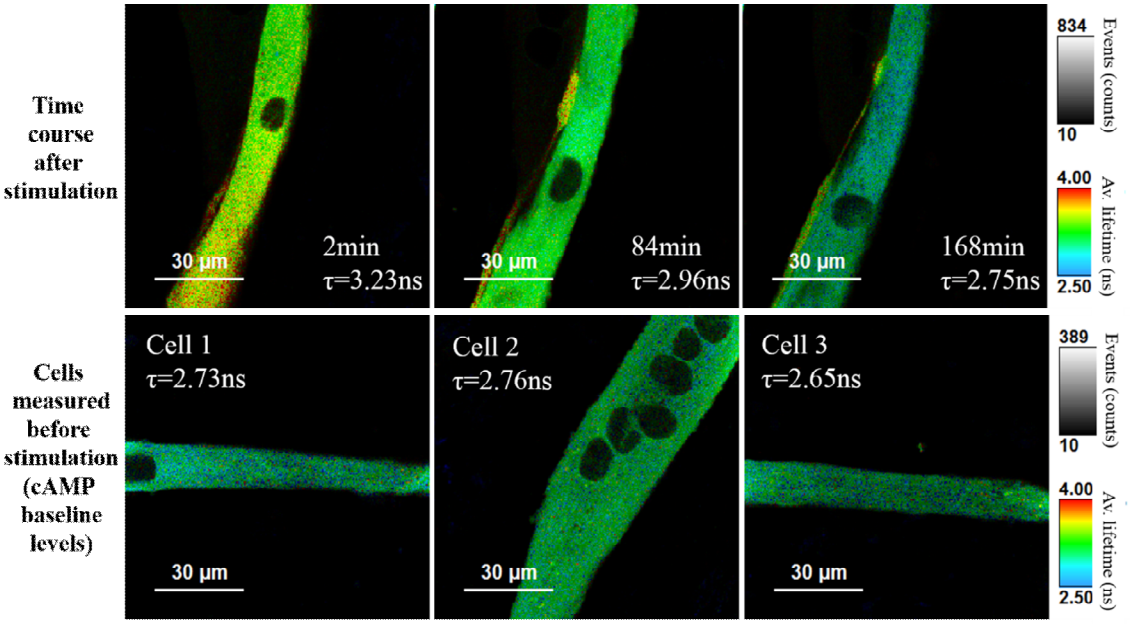

Figure 5.12 (continued) (D) Representative microscopic colour-coded images of C2C12$^{\text{WT-}ADRB2\text{+Epac}}$ cells obtained through TCSPC. After stimulation, cAMP levels decrease significantly within 2h48min (top row) and reach levels similar to those measured in cells before agonist application (bottom row). Images in the top row display the same cell, which moved during the incubation time.

5.5 Effects of light-driven ADRB2 activation on cAMP signalling in C2C12 cells

For the AChR dispersion experiments it was important to explore whether opto-ADRB2s overexpressed in C2C12 cells can be activated by 504nm laser stimulation, and whether light-driven ADRB2 activation brings about similar changes in cAMP levels as agonist-mediated activation. Therefore, ten C2C12$^{\text{opto-}ADRB2\text{+Epac}}$ cells were selected on day 3 or 4 after electroporation with the sensor (myoblast state) and the average donor lifetime was determined for each cell (referred to as time point 'pre'). Six of these cells were then subjected to 504nm laser activation by scanning a region of interest of 10x10µm^2 (50x50 pixels). After the activation, 15 images of each cell were taken over a total time period of 750s (12min 30s). The average lifetime at each time point was compared to the lifetime before stimulation. In stimulated cells, the mean donor lifetime increased from τ=2.81ns ('pre') to τ=2.98ns (last time point, $p<0.0001$) (Fig. 5.13A). In unstimulated control cells, no significant increase in the average lifetime occurred ($p=0.29$). The experiment was repeated in C2C12$^{\text{opto-}ADRB2\text{+Epac}}$ myotubes on day 8 after electroporation with the sensor (myotube state), and similar results were obtained (Fig. 5.13B). In stimulated cells, the mean donor life-time increased from τ=2.7ns ('pre') to τ=2.95ns ($p<0.0001$), whereas in unstimulated control cells, no significant increase in the average lifetime occurred ($p=0.15$). Figure 5.14 depicts colour-coded microscopic images of cells obtained through TCSPC before and after laser activation of opto-ADRB2, illustrating the increase in cAMP levels. The images demonstrate that the change in cAMP levels after activation occurred quickly, with the largest change in lifetimes being measured at the first time point at 50s. In myotubes, one can observe that the change in the lifetime is delayed in an area further away from the area of stimulation, suggesting that cAMP increases locally and then spreads throughout the cell (Fig. 5.14C).

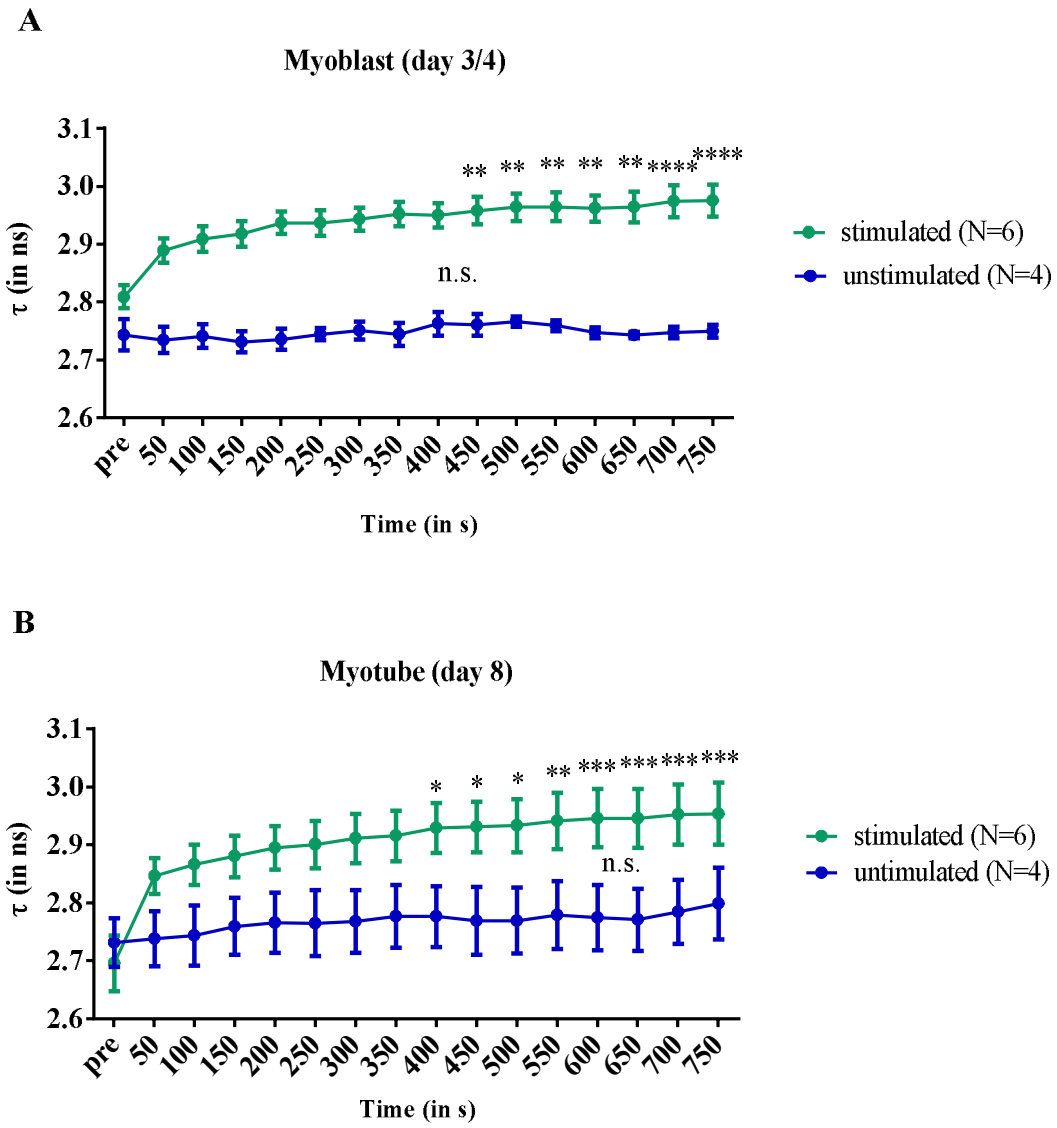

Figure 5.13 Effects of light-driven ADRB2 activation on cAMP signalling in C2C12$^{opto\text{-}ADRB2+Epac}$ cells. (A) In myoblasts, 504nm laser stimulation increased the average donor lifetime by 0.17ns (comparison of 'pre' and 750s, difference=0.17ns, Friedman test with Dunn's multiple comparisons test, p<0.0001), whereas no increase was observed in unstimulated control cells (comparison of 'pre' and 750s difference=0.008ns, Friedman test, p=0.29) (B) In myotubes, light activation increased the average donor lifetime by 0.26ns (comparison of 'pre' and 750s, Friedman test with Dunn's multiple comparisons test, p<0.0001). No increase occurred in unstimulated control cells (comparison of 'pre' and 750s, difference=0.02ns, Friedman test, p=0.15). The lifetime from each time point was statistically compared to baseline ('pre'). Only significant comparisons are indicated. Error bars indicate the standard error of the mean. n.s.>0.05, *p≤0.05, **p≤0.01, ***p≤0.001, ****p≤0.0001.

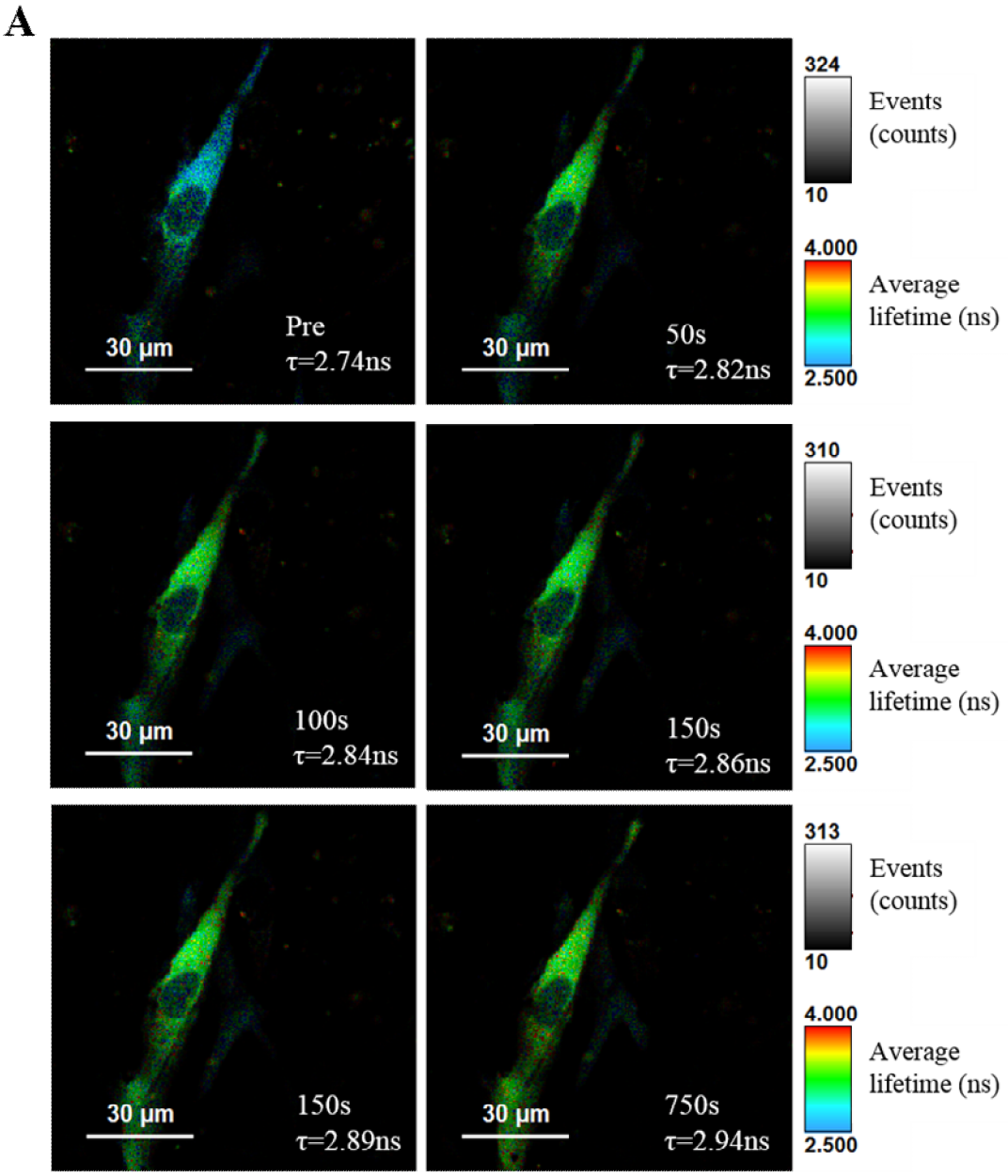

Figure 5.14 Representative microscopic images showing the effects of light-driven ADRB2 activation on cAMP signalling in C2C12$^{opto\text{-}ADRB2+Epac}$ cells. (A) Displayed are colour-coded images obtained through TCSPC on day 3 after electroporation with the sensor (myoblast state of the cells) before and after laser stimulation.

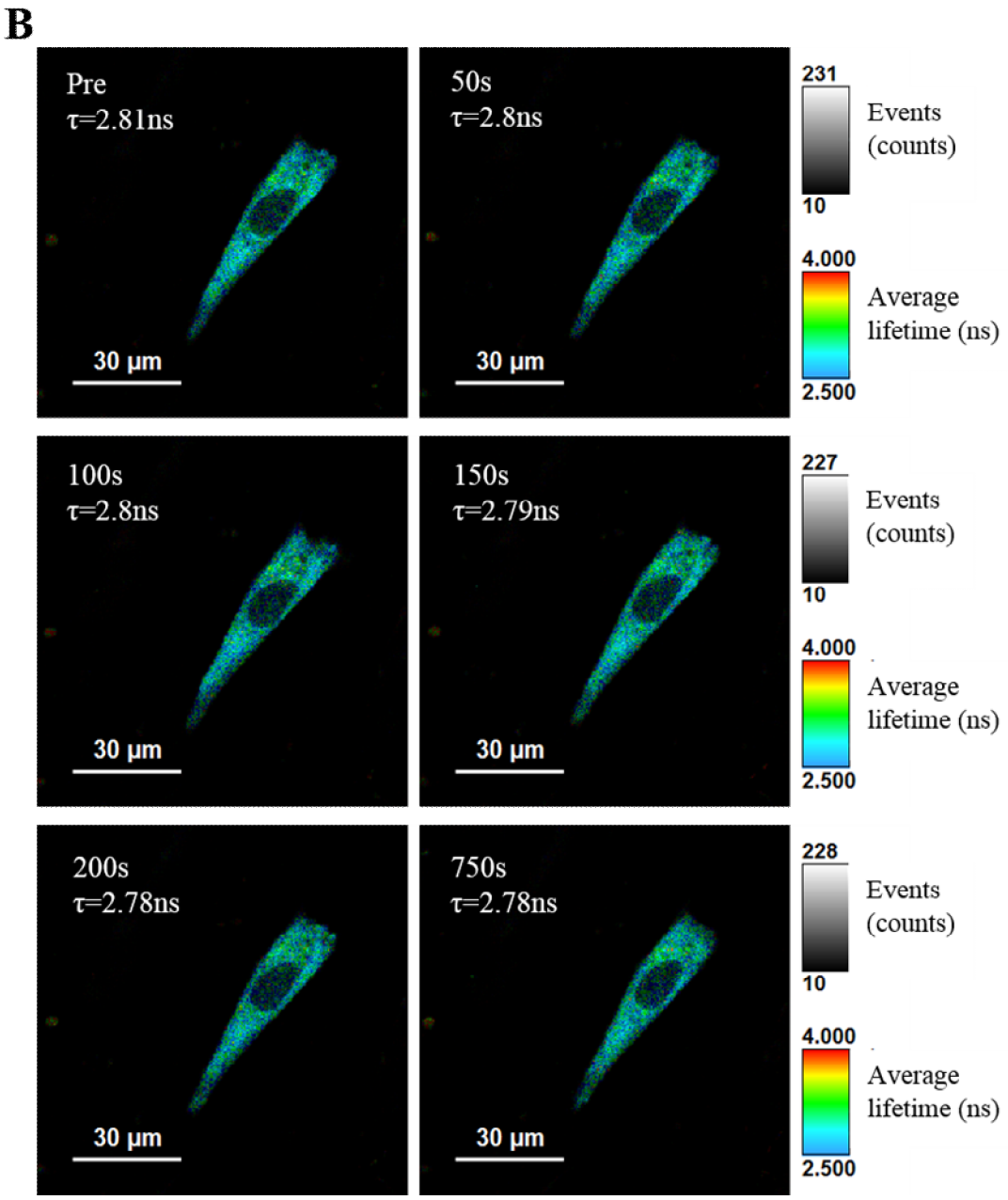

Figure 5.14 (continued) (B) Displayed are microscopic colour-coded images of a C2C12$^{\text{opto-}ADRB2\text{+Epac}}$ myoblast obtained through TCSPC on day 3 after electroporation with the sensor in the absence of laser stimulation (time course only).

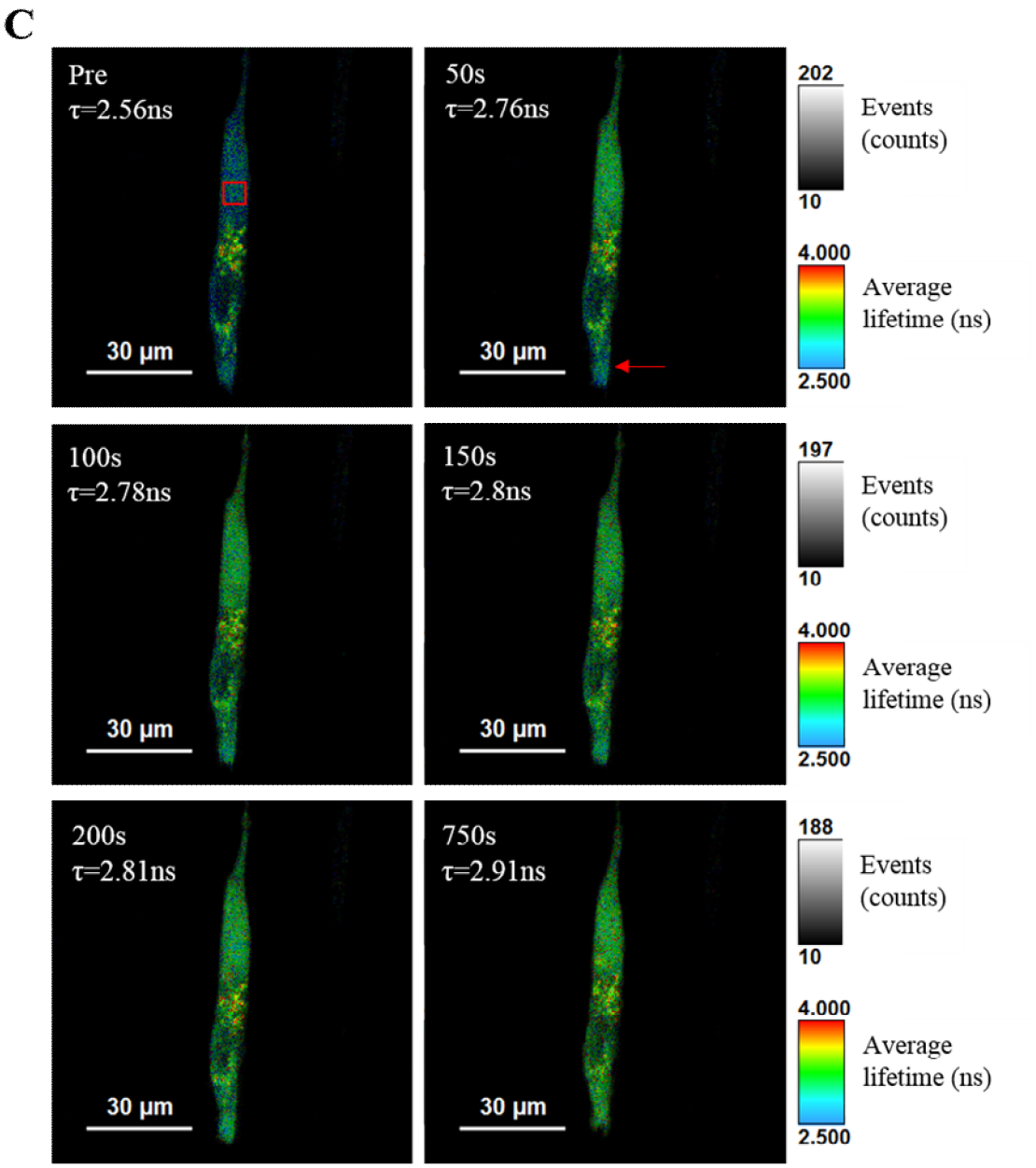

Figure 5.14 (continued) (C) Displayed are microscopic colour-coded images of a C2C12$^{\text{opto-}ADRB2\text{+Epac}}$ myotube obtained through TCSPC on day 8 after electroporation with the sensor before and after laser stimulation. The red square shows the area of laser stimulation. Paying attention to the bottom of the myotube (red arrow), one can see that the change in the average lifetime in this area is delayed, suggesting that cAMP increases in the area of stimulation and then spreads throughout the cell.

D

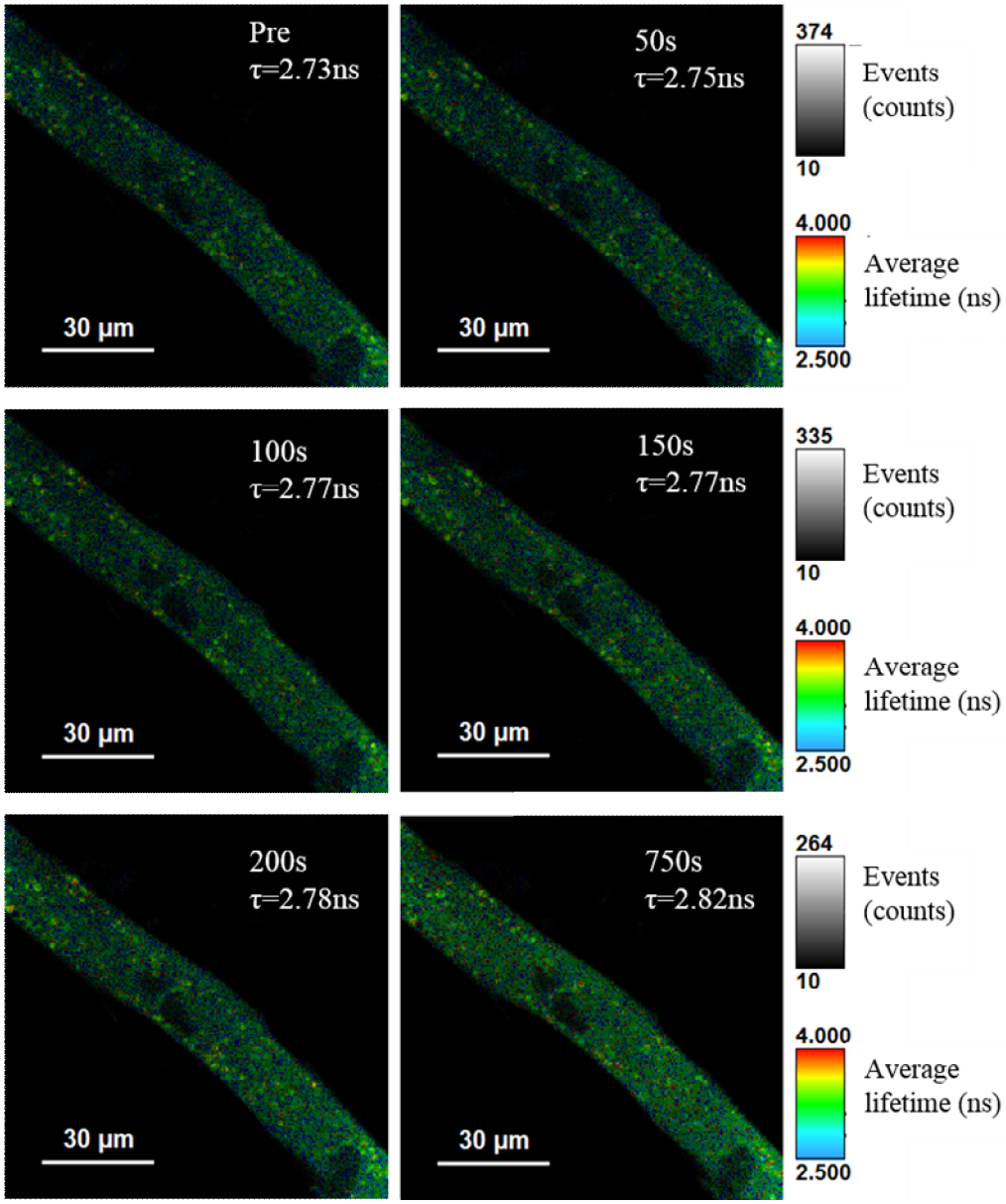

Figure 5.14 (continued) (D) Displayed are microscopic colour-coded images of a C2C12$^{\text{opto-}ADRB2\text{+Epac}}$ myotube obtained through TCSPC on day 8 after electroporation with the sensor in the absence of laser stimulation (time course only).

5.6 Effects of light-driven ADRB2 activation on AChR cluster stability

The results confirm that opto-ADRB2s respond to light stimulation. For the first time, it is possible to study cAMP signalling in live single C2C12 myotubes through optical control of ADRB2s. This set-up allowed us to study the effects of targeted ADRB2 activation on AChR cluster stability. Based on the results presented in chapter 4, we hypothesised that clusters formed on myotubes subjected to opto-ADRB2 stimulation would show less dispersion than clusters formed on unstimulated myotubes.

C2C12 cells expressing opto-ADRB2 (no sensor) were differentiated into myotubes, and AChR clustering was induced by 16h incubation with 1:500 short soluble rat agrin. After agrin wash-off, cells were stained with 1:500 Alexa Fluor-594 conjugated bungarotoxin. Ten myotubes within the same dish with each one or more AChR clusters were chosen and the positions were marked for a time course experiment. 5 of the myotubes were subjected to 504nm laser activation by scanning a region of 10x10μm^2 (50x50 pixels) adjacent to the AChR cluster(s). The remaining myotubes were left unstimulated. Pictures were taken every 20min for a duration of 12h20min during the dispersal of clusters. Videos were generated from the images obtained during the time course and can be found on the USB stick attached in the back of this thesis. Selected images of two of the myotubes are shown in Fig. 5.15. We chose not to perform a quantitative analysis of the clusters due to the surprising amount of movement observed among the cells. The images suggested that each cluster consists of smaller clusters (<5μm) which moved around when the myotubes contracted. The majority of clusters larger than ~5μm dispersed within 12h, however the smaller clusters stayed intact. Therefore, AChR clusters were found to be more dynamic than anticipated. A noteworthy finding is that there was variation in the dispersal of AChR clusters independent of whether ADRB2s were stimulated. A consistent trend towards

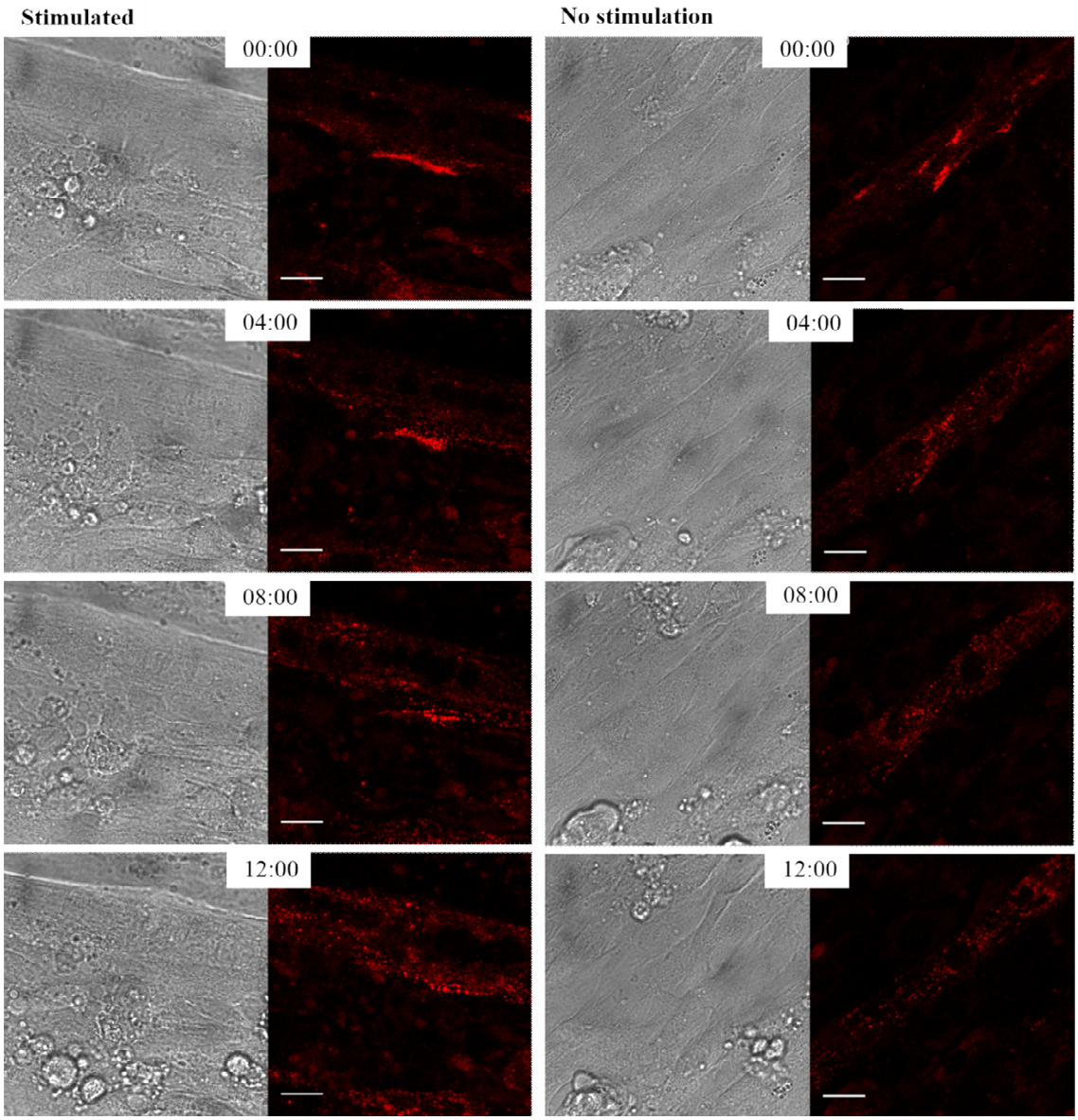

Figure 5.15 Representative microscopic images showing the effects of light-driven ADRB2 activation on AChR cluster stability. Myotubes overexpressing opto-ADRB2 were treated with short rat agrin for 16h to induce AChR cluster formation. Clusters were stained with Alexa Fluor-594 conjugated bungarotoxin. 10 myotubes with one or more AChR clusters were chosen, five of which were stimulated to activate ADRB2s adjacent to the cluster(s). Images of each position were acquired every 20min for a duration of 12h20min during the dispersal of clusters. A stimulated cell (left) and an unstimulated cell (right) are shown before stimulation, and 4h, 8h and 12h after stimulation. Videos of all cells are saved on the USB stick attached at the end of this thesis. No consistent trend towards reduced cluster dispersal after ADRB2 stimulation could be observed. In both conditions there was variability in cluster stability. Scale bar=20µm. Time stamp=h:min.

reduced dispersal after opto-ADRB2 stimulation could not be observed.

5.7 Discussion

By taking advantage of recent advances in the field of fluorescence microscopy, a novel experimental setup, which allows for the investigation of cAMP signalling in life single cells, was developed in the current chapter.

A FRET sensor was validated as a sensitive tool to detect dynamic changes in cAMP levels in C2C12 cells. A maximal increase of 0.48ns in the fluorescence lifetime could be detected in response to incubation of myotubes with 10µM salbutamol sulphate (Fig. 5.12C). Klarenbeek et al. (2015) validated the same FRET sensor construct in N1E-115 cells and reported a maximal increase in the lifetime of 1.46ns. Differences between the two cell lines might account for this variation. Moreover, the authors used a combination of 25µM forskolin, an activator of adenylyl cyclase, and 100µM IBMX, a phosphodiesterase inhibitor, to raise cAMP levels. We validated the FRET sensor in HEK293T cells (data not shown) and detected an increase in the fluorescence lifetime of 0.72ns in response to incubation of the cells with 25µM forskolin. Klarenbeek et al. (2011) reported a similar change in the lifetime (0.6ns) when validating a previous version of the here described sensor construct in HEK293T cells by treatment of cells with forskolin and IBMX.

The results show that treatment of C2C12 myotubes with an ADRB2 agonist causes an increase in cAMP production, and that within 3h, cAMP levels return to baseline levels. Since an increase in AChR clustering could be observed after incubation with an ADRB2 agonist for 22h (see chapter 4), in a future experiment, the FLIM time course could be extended beyond 3h. Moreover, as a comparison, a time course experiment could be performed on unstimulated cells. Improvements of the

FLIM acquisition software are desirable, so that multiple positions can be marked and lifetime measurements can be obtained for more than one cell at a time.

The effects of two ADRB2 agonists on cAMP levels were compared. At a concentration of 1μM, treatment with XA-01-NZ86 significantly increased the fluorescence lifetime by 0.42ns, whereas treatment with salbutamol sulphate caused a significant increase of 0.32ns. The finding in chapter 4 that XA-01-NZ86 causes an increase in the number of AChR clusters at lower concentrations than salbutamol might therefore be mediated by its ability to cause a larger increase in cAMP levels at low concentrations.

cAMP levels in response to XA-01-NZ86 and salbutamol treatment were investigated after 5min of agonist-incubation. A time course experiment could be devised in order to study whether XA-01-NZ86 causes a longer-acting response of ADRB2s than salbutamol.

For the interpretation of the results it is important that lifetime measurements are reproducible and can be compared between treatment conditions. The cells used for the experiment on the two agonists originated from the same culture flask. Two separate electroporations with the sensor construct were performed on the same day, and each population of cells was seeded into a culture dish. Myotubes from one of these dishes were incubated with salbutamol, whereas the other one was incubated with XA-01-NZ86. To test for potential variability in the results, the experiment should be replicated, in order to obtain results for cells that originate from multiple electroporations and culture dishes. It is unclear whether small differences in baseline cAMP levels might have an effect on the response of the cells to an ADRB2 agonist. If this was the case, cells from the same electroporation could be seeded into separate dishes and used for different experiments and conditions.

The variability in lifetime measurements between cell populations was tested in the absence of an agonist, and the results suggested that there is little variation between culture dishes prepared on the same day (Fig. 5.9C). Nevertheless, some variation was observed when comparing lifetime measurements obtained in different experiments on cells prepared on different days (e.g. compare the lifetimes in unstimulated cells in Fig. 5.9C with the lifetimes in Fig. 5.12B). Future experiments could investigate whether cAMP levels change with increasing passage number of myoblasts, in which case only results from experiments using age-matched cells should be compared.

Fluorescence lifetime imaging microscopy enabled us to validate an optogenetic variant of the *ADRB2* as a tool to study the effects of targeted ADRB2 activation on AChR cluster stability. It could be shown that 20s of 504nm laser stimulation by scanning a region of 10x10µm^2 on the myotube activates ADRB2s locally. For the first time it is possible to study the effects of ADRB2 activation on AChR cluster stability by comparing clusters on activated myotubes with clusters on un-activated cells. Marking positions on myotubes within the same cell culture dish allowed us to monitor the dispersal of several single AChR clusters. Based on the AChR dispersal experiments described in chapter 4, it was hypothesised that activation of ADRB2s adjacent to the cluster might partially prevent its breakdown. In all time-course experiments performed in the current chapter, it was found that the myotubes are surprisingly mobile and frequently contract. In some experiments, the cells moved significantly and/or were out of focus after several hours (minor myotube movement can be observed in Fig. 5.12D). The movement of both myotubes and AChR clusters during the time course makes the analysis of dispersing clusters challenging. Similar observations have been reported in earlier time course studies (Bruneau et al., 2005). Several alterations in the protocol may help to overcome this issue. In future

experiments, carbachol could be applied to the cells in order to accelerate cluster dispersal and minimise the duration of the time course experiment. Furthermore, images could be taken at lower magnification, such that cells are less likely to move out of the microscopic field. This would also allow for the analysis of a larger number of cells and clusters per microscopic field.

Clusters varied significantly in their stability independent of whether ADRB2s were previously activated. It was observed that larger clusters consist of smaller clusters (<5µm) which stay intact even after hours of dispersal. It is important to note that this novel experiment differs from the dispersal experiment described in chapter 4 in several ways. In the ADRB2 agonist experiments, the drug was added to the cells in excess and the treatment solution was not removed. In the optogenetics study, a region on the cell was subjected to 20s of laser stimulation only once. Using the FRET sensor, the increase in cAMP levels was found to be smaller than the changes achieved by agonist application. After 5min, 10µM salbutamol had increased the lifetime by 0.27ns and 1µM salbutamol by 0.32ns (Fig. 5.10A,C), whereas laser stimulation caused an increase of 0.22ns (Fig. 5.13B, 300s). Therefore, the effects of repeated laser stimulation could be investigated. Moreover, a future experiment could aim at testing cAMP levels in response to laser stimulation beyond 12min and to compare the results to the findings of the 3h time course experiments in response to agonist stimulation.

A further important difference is that the dispersal experiments in chapter 4 only gave a ’snapshot’ of the events taking place. Cells were incubated with Alexa Fluor-594 conjugated bungarotoxin and fixed at the end of the time course, whereas in the optogenetics experiments cells were incubated with Alexa Fluor-594 conjugated bungarotoxin before the start of the time course. Although agrin is washed off before the staining of AChR clusters in the optogenetics experiment, it is unclear whether

additional clusters form during the time course. These newly formed and therefore unstained clusters might even form larger aggregates together with the dispersing clusters that were stained before the start of the time course. Such dynamic events cannot be detected using the current experimental setup in the optogenetics experiment. To overcome this limitation, fluorescently tagged AChRs could be overexpressed in C2C12 cells. This would enable us to monitor not only the dispersal of preformed clusters but also the formation of emerging AChR aggregates throughout the time-course. First, optimisation experiments would have to aim at determining a suitable transfection and agrin-mediated AChR clustering protocol. Furthermore, it must be explored whether clusters formed on myotubes overexpressing tagged AChRs disperse at a similar rate as in the current experiments.

Future experiments on the dynamics of AChR cluster formation and dispersal in response to ADRB2 stimulation could take advantage of total internal reflection fluorescence microscopy (TIRFM). This technique enables imaging at the single molecule level in live cells with low background fluorescence and little exposure of the cell sample to light, and has been employed previously to visualise AChR clusters formed on cultured myotubes (Axelrod, 1981). In TIRFM, an excitation light beam is directed to the glass interface of a glass-bottom dish at a high angle larger than the critical angle of refraction. This angle depends on the ratio of the refractive indices of the glass of the culture dish and the medium solution that immerses the cell. Although at this critical angle the light beam is totally reflected by the glass-medium interface, a thin electromagnetic field is generated in the medium (<200nm). This so called evanescent wave decays exponentially with increasing distance from the surface and, if the cell expresses fluorescent-tagged proteins, excites only fluorophores located near the interface. This method results in high-contrast images with increased signal-to-

background ratio. TIRFM would provide a suitable imaging technique for long time-course experiments studying AChR cluster dispersal. Since the illumination is restricted to a small glass-medium interface region and does not penetrate the depth of the myotube, the resulting evanescent field only excites fluorescently labelled AChR aggregates immediately located at the substrate surface, whilst causing minimal photodamage to the cell (Wang and Axelrod, 1994). Using this technique, Wang and Axelrod (1994) conducted a TIRFM time-lapse experiment in which they imaged the dynamics of AChR clustering in aneural myotubes induced by substrate-contact (no agrin present) over a period of seven days. Since fluorophores present in the medium do not lead to background fluorescence in TIRFM, alpha-bungarotoxin may remain in the medium for the duration of the time course, which allows for the imaging of both pre-formed and newly aggregating AChRs in the substrate area. Alternatively, agrin-induced AChR clusters formed on salbutamol-treated or untreated myotubes could be visualised with a low concentration of alpha-bungarotoxin. This would enable us to study the effect of ADRB2 activation on the movement of single molecules within a cluster.

TIRFM can be combined with fluorescence recovery after photobleaching (FRAP). Using laser illumination, alpha-bungarotoxin labelled AChR clusters are photobleached which leads to the loss of fluorescence (Wang and Axelrod, 1994). Subsequently, the recovery of fluorescence in the bleached area can be monitored. In the study by Wang and Axelrod (1994), alpha-bungarotoxin was continuously present in the medium during the FRAP experiment. It was shown that the fluorescence intensity of some clusters recovered within several hours after photobleaching, suggesting that AChRs were newly incorporated into the membrane and/or that AChRs outside the bleached area moved towards the bleached cluster. In a more recent study,

AChR clusters induced through culturing of myotubes on laminin-substrate were labelled, and the alpha-bungarotoxin was removed (Bruneau et al., 2005). The clusters were then subjected to photobleaching, leaving only adjacent diffusible AChRs fluorescently labelled. The results indicated that lateral migration of these AChRs into the bleached cluster caused partial recovery of the original fluorescence intensity within 8h.

These results support the notion that in a dispersal study in which clusters are stained at the end of the experiments, some of the dynamic changes that AChR clusters undergo are missed. The above mentioned experiments could therefore be adapted to test the effects of ADRB2 activation on the dynamics on AChR clustering. One might speculate that salbutamol enhances the trapping of AChRs into existing clusters.

The mobility of AChRs can be studied in further detail by taking advantage of the phenomenon of photo-unbinding (Akaaboune et al., 2002). It was discovered in an *in vivo* study that laser stimulation of fluorescently tagged AChR clusters can result in the unbinding of alpha-bungarotoxin, and that the same AChRs can be relabelled with alpha-bungarotoxin of a different colour. This technique allows for the differential staining of subpopulations of AChRs and can therefore be used to track the migration of AChRs. Akaaboune et al. (2002) demonstrated that in synapses *in vivo*, extrasynaptic and synaptic AChRs are highly mobile and intermingle, and that synaptic AChRs are maintained for several days and remain in one location for no longer than about 8h. In the optogenetic experiment in the current study, AChR clusters dispersed into smaller clusters (<5µm) which appeared to travel along the myotube. Using the photo-unbinding technique could help to track their movement and to analyse cluster dispersal.

In summary, the development of a novel setup that gives optical control over ADRB2 activation in single myotubes has laid the ground work for future experiments on AChR cluster stability. Combination of this technique with other optical techniques such as TIRFM and FRAP may help to track smaller AChR clusters and single molecules.

CHAPTER 6

A novel cell culture model for studying *Dok7* mutations developed by utilising CRISPR/Cas9 genome editing

6.1 Introduction

By studying AChR clusters that form postsynaptically on C2C12 cultures, one can mimic some of the key events that take place at the neuromuscular synapse. The previous chapters investigated the effects of *DOK7* mutations on AChR clustering and the effects of ADRB2 agonists as potential treatment. Under physiological conditions, AChR clusters form on the muscle as a result of a complex signalling cascade, in which agrin, MuSK and DOK7 are key molecules. *In vitro*, it is possible to separate some of these signalling events: By using C2C12 WT myotubes, the effects of ADRB2 agonists on the agrin-mediated clustering pathway could be explored. By stable overexpression of WT or mutant DOK7, on the other hand, the effects of ADRB2 agonists on the agrin-independent AChR clustering pathway were investigated. While the overexpression model has significantly enhanced our understanding of neuromuscular functioning, it is also associated with certain disadvantages. As discussed in chapter 3, AChR clustering assays are conducted to help determine whether a *DOK7* variant found in a patient is pathogenic. The overexpression model is suitable for detecting large effects on AChR clustering, however, moderate effects of variants located towards the end of the DOK7 C-terminal domain may not be picked up in the current AChR clustering assay. A further drawback of the overexpression model is that endogenous wild type DOK7 is still present and might influence the results. Moreover, overexpression leads to non-physiological levels of the protein of interest, and despite standardised protocols, expression levels vary between transfections. Since infected C2C12 myoblasts often lose their ability to

differentiate into myotubes after freezing, new stable cell lines were generated regularly. Some variation was noticed in baseline AChR cluster numbers between transfected cell lines, even between cells infected with the same batch of virus. Finally, *in vivo*, AChR clustering does not occur in the absence of agrin, and therefore, a more physiological disease model of DOK7 CMS would be desirable.

In the last few years, some exciting discoveries advanced the field of targeted genome engineering, which provides a promising alternative to overexpression models. Gene editing takes advantage of the cells innate DNA repair mechanisms by which structural aberrations and mutations are corrected through nucleotide exchange. Although several studies demonstrated that single base-pair mutations can be corrected by transfection with short DNA nucleotides the success rate was very low (Hu et al., 2005). The development of programmable nucleases has revolutionised the field and significantly increased the frequency of targeted repair. These enzymes cause a double-stranded break in the chromosomal DNA at a specific site. In the absence of a DNA template, the repair occurs through nonhomologous end joining which disrupts the target location through deletions and/or insertions (indels) (Fig. 6.1). However, repair in the presence of a repair template homologous to the target site (homology-directed repair) can result in specific gene modifications.

Programmable nucleases possess a binding domain for a specific target site and a peptide domain or enzyme which cleaves the DNA. Zinc finger nucleases (ZFNs) were one of the first enzymes used for genome engineering and consist of a DNA-binding zinc-finger protein domain (usually three to six individual zinc-finger repeats) and a cleavage domain derived from the Fok1 restriction enzyme (Carroll, 2011). However, the target site selection is limited for ZNFs. Each zinc-finger binds to a 3bp sequence, but ZNFs have not been designed for all possible combinations, and novel ZNFs are not equally

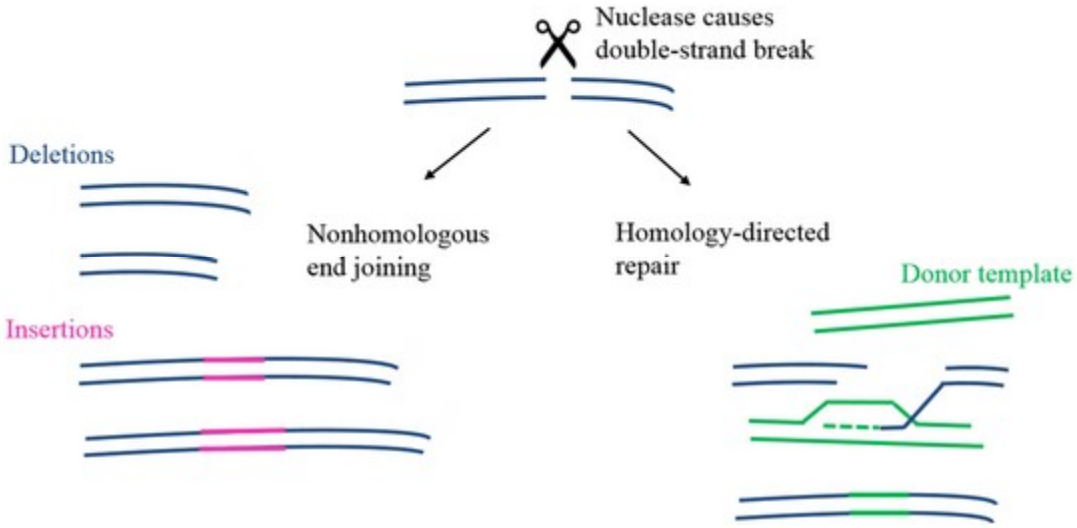

Figure 6.1 Schematic of gene editing after a nuclease-induced double-strand break. In the absence of a DNA template, repair occurs through nonhomologous end joining and results in deletions or insertions (indels) variable in size. In the presence of a homologous template, homology-directed repair allows for precise insertions or modifications at the target-locus.

effective in cutting the DNA. These restrictions led to the development of Transcription Activator-Like Effector Nucleases (TALENs) (Christian et al., 2010). TALENs differ from ZNFs only in their DNA binding domain. The so called TAL effectors, derived from phytopathogenic bacteria and composed of tandem arrays of 33 to 35 amino acid repeats, can easily be engineered to bind any desired sequence on the target DNA.

The newest generation of genome editing tools are clustered regularly interspaced short palindromic repeats (CRISPRs) coupled with CRISPR-associated (Cas) proteins (Mali et al., 2013). CRISPR/Cas was originally discovered in bacteria and archaea as an adaptive immune system against viruses and phages, that uses RNA-guided nucleases to cleave foreign DNA (Jinek et al., 2012). Non-coding short sequence repeats (SSRs) widely dispersed throughout the genome were identified in Escherichia coli K12 already in 1987 (Ishino et al., 1987) and later in other bacterial and archaeal species (Groenen et al., 1993, Mojica et al., 1995, Hoe et al., 1999). This class of repeats was then recognised as one family and called clustered regularly interspaced short palindromic repeats (Jansen et al., 2002). It was shown that CRISPRs are interspaced by similarly sized non-repetitive DNA. These spacers are the so called CRISPR associated genes, or short, *CAS* genes. Three subtypes of the CRISPR/Cas system were identified based on the structures and sequences of the Cas proteins involved. The type 2 CRISPR/Cas system relies on a single Cas protein, Cas9. Foreign DNA that enters bacteria or phages is cleaved by the Cas9 nuclease domain. The smaller DNA fragments are then incorporated into the CRISPR locus as spacers. A future infection causes the spacers to act as transcriptional templates to produce CRISPR RNA (crRNA). crRNA forms a complex with partially complementary transactivating crRNA (tracRNA) which then guides Cas9 to the DNA of the invading virus or phage for subsequent cleavage. Importantly, successful binding of Cas9 to the target DNA depends on the presence of a protospacer adjacent motif

(PAM) adjacent to target sequence. Only the spacer of the invading organism contains the PAM, which ensures that the CRISPR locus itself does not get targeted by the nuclease. Cas9 is known to cut 3bp 5' of the PAM.

Adaption of the CRISPR/Cas9 system revolutionised the field of genome engineering. In contrast to TALEN, where specific protein pairs have to be engineered for each target site, Cas9 can be targeted to new sequences easily (Jinek et al., 2012). So called guide RNA sequences have been designed which already contain the crRNA and tracrRNA (Fig. 6.2). By altering the guide RNAs and administering a DNA target, gene modifications can be made at almost any location.

The aim of the current chapter was to investigate whether CRISPR/Cas9 genome editing can be adapted to develop a novel cell culture model for CMS. The direct introduction of *DOK7* mutations into the genome of C2C12 cells would for the first time allow us to investigate the effects of *DOK7* mutations on agrin-mediated AChR clustering. In the current study, two different mutations in the C-terminal region of DOK7 were investigated, using CRISPR technology: *DOK7* c.1124_27dupTGCC and *DOK7* c.1504_1505insTA (Fig. 6.3). Investigating *DOK7* c.1124_27dupTGCC facilitates a comparison of the results with the findings from the overexpression model. The mutation *DOK7* c.1504_1505insTA located towards the end of the DOK7 C-terminal domain was found in one allele of one patient and predicts a region of additional C-terminal residues (Cossins et al., 2012). The corresponding stable cell lines with homozygous changes generated by CRISPR/Cas9 editing are henceforth referred to as C2C12$^{\text{CRISPR } Dok7 \text{ c.1124_27dupTGCC}}$ and C2C12$^{\text{CRISPR } Dok7 \text{ c.1504_1505insTA}}$.

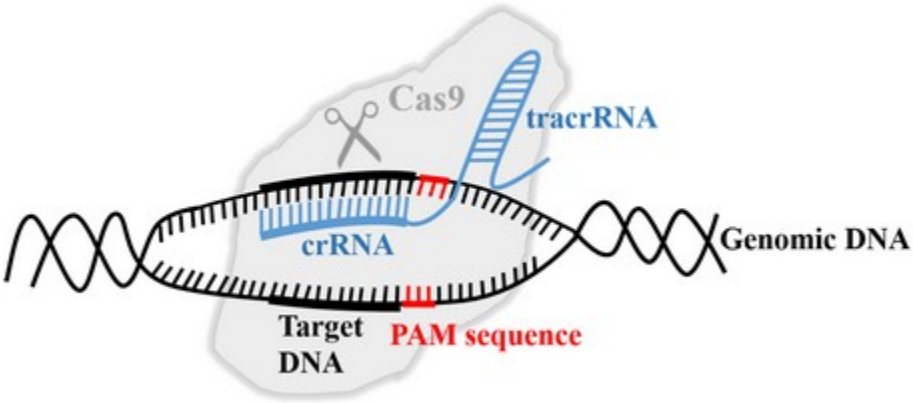

Figure 6.2 Basic principle of CRISPR/Cas9 genome engineering. The Cas9 nuclease is targeted to a sequence of genomic DNA by crRNA and tracrRNA, fused together to a chimeric single-guide RNA. The crRNA sequence is complementary to the target and in immediate vicinity of the PAM. Cas9 causes a double-strand break at the target locus, which allows for precise gene editing if a repair template is supplied (homology-directed repair). The CRISPR/Cas9 system allows the user to engineer guide RNAs to match almost any desired sequence on the genomic DNA. Suitable crRNAs can be cloned into a commercially available plasmid, which is then used together with a target sequence to transfect the cell system of interest.

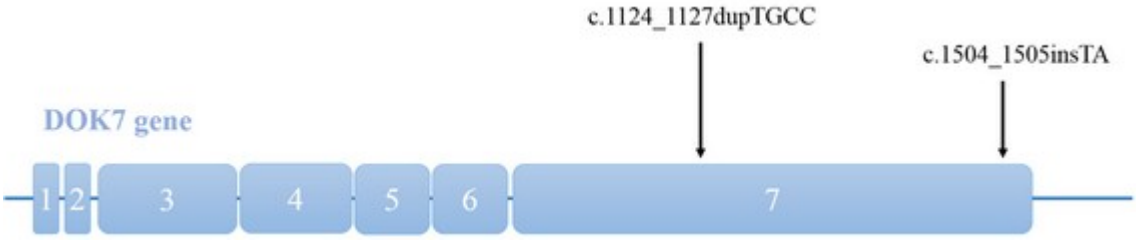

Figure 6.3 Location of mutations in the C-terminal region of DOK7 investigated by utilising CRISPR/Cas9 technology

6.2 CRISPR/Cas9 genome editing of *Dok7*

CRISPR/Cas9 genome engineering depends on the Cas9 protein being directed to the DNA target site through a guide RNA. The guide RNA contains a short oligonucleotide of 20 nucleotides complementary to the genomic site of interest. The target site has to be immediately followed by the PAM (NGG), which, however, must not be included in the guide oligonucleotide sequence. The guide oligonucleotide is followed by tracrRNA, which forms a hairpin. Plasmids which encode the Cas9 enzyme and also produce the guide RNA are commercially available. In the current study, C2C12 cells were transfected with a plasmid containing the Cas9 D10 nickase mutant, which has been shown to reduce the occurrence of off-target effects. While wild type Cas9 cuts both strands of the DNA, the nickase mutant only cuts one strand, and two independent guide RNAs are used to guide Cas9 to the top and to the bottom strands (Ran et al., 2013). Dr. Joey Riepsaame kindly provided us with a modified version of the plasmid pX335-U6-Chimeric_BB-CBh-hSpCas9n(D10A) developed by Zhang et al. (Cong et al., 2013). In this modified version, henceforth referred to as pX335, he inserted an EGFP and neo-resistance gene for selection (Fig. 6.4).

The first step in the current study was to design suitable guide oligonucleotides for the guide RNA. We used a freely available prediction software (http://crispr.mit.edu/) which determines possible sequences within a given genomic DNA sequence around the target locus. Top and bottom strand guide oligonucleotide sequences were chosen, that A) did not overlap, B) were maximal 20 nucleotides apart from each other and C) where one of the cleavage sites was within 50 nucleotides of the residue to be mutated. The last three residues (PAM) of the chosen sequences were removed, and overhangs were added to enable ligation of the annealed oligonucleotides with the BbsI-digested plasmid. Moreover, if the predicted guide oligonucleotide sequence did not begin with a G, a G

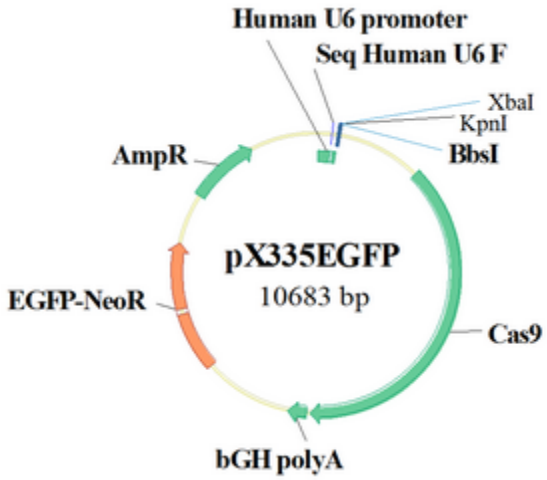

Figure 6.4 Map of the modified plasmid pX335-U6-Chimeric_BB-CBh-hSpCas9n(D10A). Using the BbsI, XbaI and KpnI restriction sites, any desired guide oligonucleotide sequences can be cloned into the plasmid which already encodes the Cas9 enzyme. The EGFP-neomycin resistance gene allows for selection of transfected cells.

was added to facilitate maximal transcription from the HU6 promoter (Table 6.1, Fig. 6.5). Next, target oligonucleotides were designed, in which the mutated residues are in the centre, flanked by 60 nucleotides on either side. The PAMs were removed from the target sequences by making silent changes when possible. The forward and reverse guide oligonucleotide strands were annealed for each of the two guides and cloned into the pX335 plasmid (see chapter 2.13.3 for details on the cloning and electroporation of cells).

To create a C2C12$^{\text{CRISPR } Dok7 \text{ c.1124_27dupTGCC}}$ and a C2C12$^{\text{CRISPR } Dok7 \text{ c.1504_1505insTA}}$ stable cell line, C2C12 myoblasts were electroporated with a mix of target DNA and pX335 plasmid containing the guide sequences and selected with neomycin for 72h. Off-target effects can occur during the DNA repair, and the desired genetic changes will not have occurred within every cell of the polyclonal cell population used for the transfection. Therefore, monoclonal populations of cells were obtained which could then be screened for the respective mutation.

Cloning by limiting dilution was performed by seeding the neomycin-selected cells into 96-well plates at a concentration of 0.5 cells/well. Cells were left to grow for at least one week until colonies formed, and each colony was then transferred into the well of a 6-well plate. An interesting observation was that the cell colonies differed considerably with respect to the shape and size of the cells. Many colonies had to be discarded because the cells did not grow as expected for C2C12 cells. DNA extract from each suitable colony was subjected to PCR reactions to screen for the mutations. In a first PCR reaction, a mutation-specific forward primer was used, which only binds to the DNA if the TGCC duplication or the TA insertion was successful (Fig.6.6 and Table 2.5). A reverse primer was chosen which binds to a region after the target locus. Only if the genome editing was successful, a band of ~120bp for c.1124_27dupTGCC and ~90bp for c.1504_1505insTA was expected. Importantly, the forward primer binds to either homozygous or

	c.1124_27dupTGCC	c.1504_1505insTA
Sequence suggested by prediction software		
Guide A	CACCGGCCCGCCACACGTCC**AGG**	CTGGAGGCGGCCCTGCATGG**GGG**
Guide B	TCTCTGCTCAGTCTGCCCCC**TGG**	TTCAATCTGTGGCGGACTC**AAG**
Final oligonucleotide sequence with overhangs		
Guide A forward	**CACC*G***CACCGGCCCGCCACACGTCC	**CACC*G***CTGGAGGCGGCCCTGCATGG
Guide A reverse	**AAAC**GGACGTGTGGCGGGCCGGTG***C***	**AAAC**CCATGCAGGGCCGCCTCCAG***C***
Guide B forward	**CACC*G***TCTCTGCTCAGTCTGCCCCC	**CACC*G***TTCAATCTGTGGCGGACTCA
Guide B reverse	**AAAC**GGGGGCAGACTGAGCAGAGA***C***	**AAAC**TGAGTCCGCCACAGATTGAA***C***
CRISPR target oligonucleotide sequence		
	ATGCCGGCAGCAATCTGGACGTGTGG CGGGCCGGTGAGGAATTCGGTTCTCT GCTCAGTCTGCCTGCCCCCTGGAGCC AGCGCACCTGAGCCCAGACTGTGTGC CTGCCCACCTGGGGCGGCCGAGTA	AGCAGGCAGTCCCCATGCAGGGCCGCCTC CAGCTTTCTTTTTGTCATGTTCAATCTGTGG CGGACTCAAAGTAAAGCTACCCCTCCCTG AGATAGCAGGCTGGCCGCTGCTAGATCCGC CCTTCCAGACAGGGGAAGAG

Table 6.1 Oligonucleotide sequences for CRISPR/Cas9 gene editing of *Dok7*. Suitable guide oligonucleotide sequences were determined, using a prediction software (PAM sequence in red). Overhangs were added (in bold) for cloning of the oligonucleotides into the modified pX335-U6-Chimeric_BB-CBh-hSpCas9n(D10A) plasmid, using the BbsI restriction site. Target sequences were designed with the mutated residues in the middle (underlined), flanked by 60 nucleotides on either side (PAM sequences, three of which were silently mutated are shown in red).

c.1124_27dupTGCC

c.1504_1505insTA

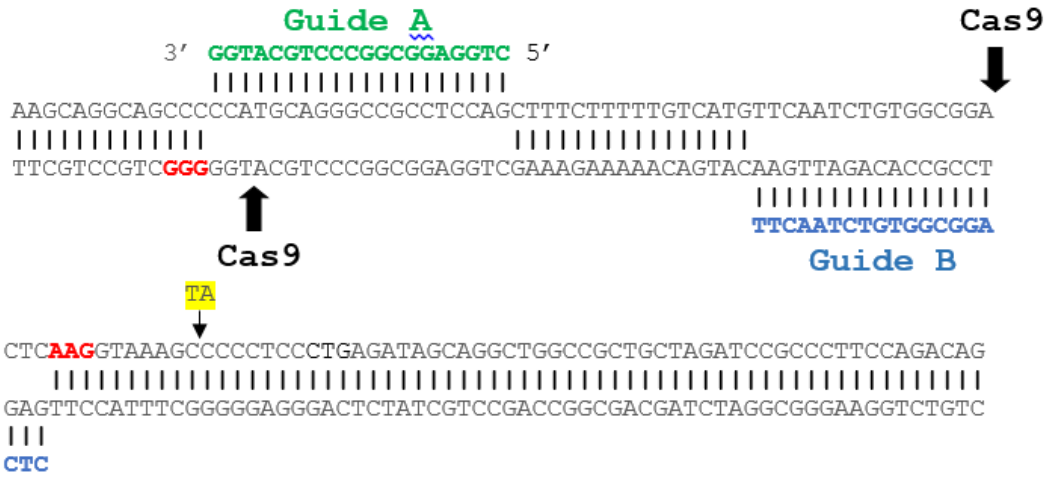

Figure 6.5 Schematic of CRISPR/Cas9 genome editing of *Dok7*. Two mutant cell lines were created: C2C12$^{\text{CRISPR } Dok7 \text{ c.1124_27dupTGCC}}$ (top) and C2C12$^{\text{CRISPR } Dok7 \text{ c.1504_1505insTA}}$ (bottom). The gene modifications at the target locus are highlighted in yellow (duplicated residues TGCC and the inserted residues TA, respectively). For each mutation, the location and sequence of the guide oligonucleotides are shown (green and blue). The PAMs in immediate vicinity of the guide sequences are shown in red. The Cas9 enzyme cuts 3bp 5' of the PAM.

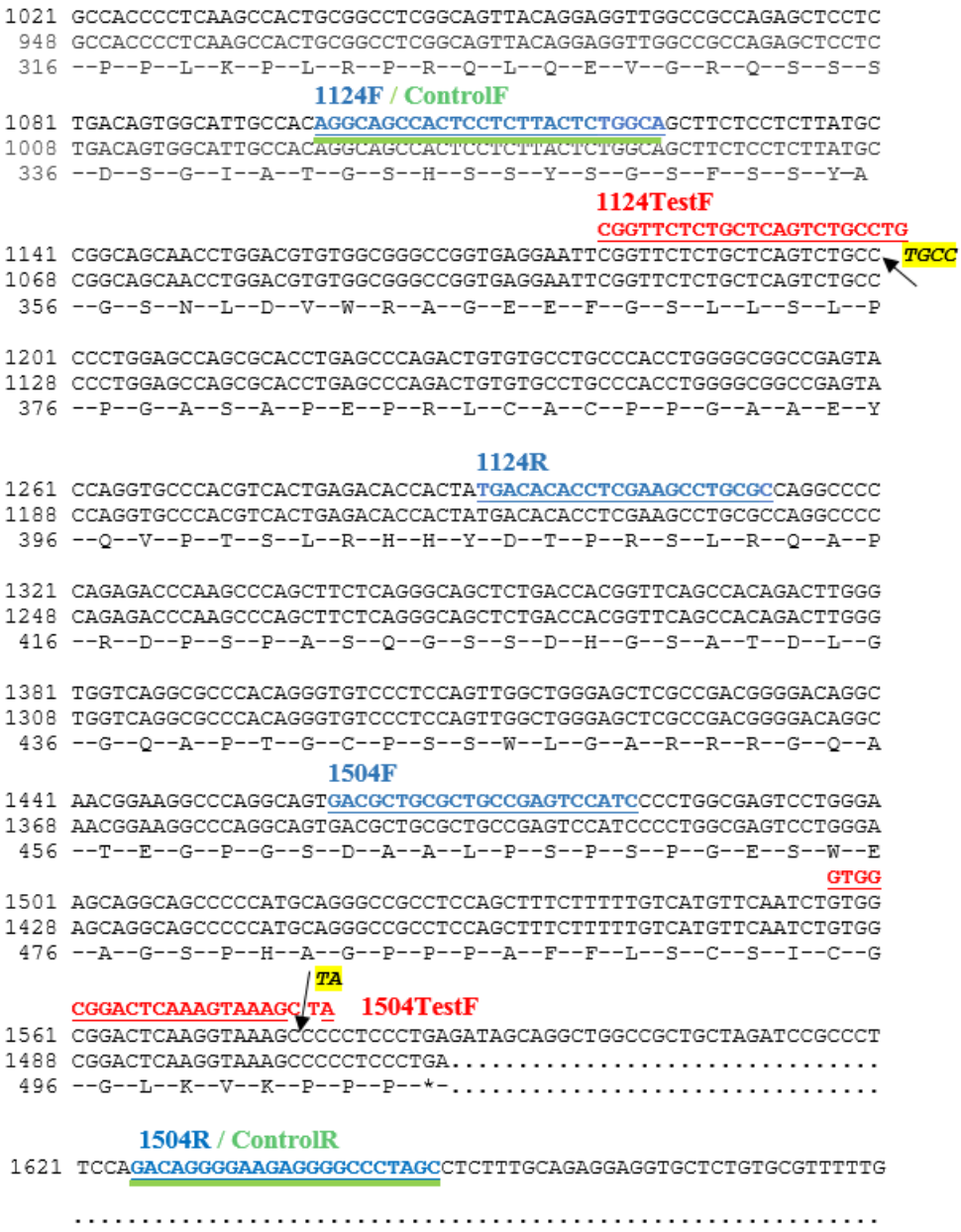

Figure 6.6 Location of primers for screening of cells for the *Dok7* c.1124_27dupTGCC and c.1504_1505insTA mutation. The duplicated/inserted residues at the target locus are highlighted in yellow. DNA extract from each cell colony was screened for the respective mutation by amplification and sequencing of the region around the target site. In a first PCR reaction, a forward primer was used which only binds to the DNA if the duplication/insertion was successful (primer sequences in red). In this case, a band size of ~120bp for c.1124_27dupTGCC and ~90bp for c.1504_1505insTA is expected. In a second PCR, a region of about 200bp around the target site was amplified and sequenced (primers in blue, used for both PCR and sequencing). Primers used for screening of controls are in green.

heterozygous changes. Since clones with homozygous changes were required, a second PCR was performed to amplify a region of about 200bp around the target site, and the resulting PCR product was sent for sequencing. This amplification often resulted in multiple bands, which could be an indicator of a mixed cell population or indels by non-homologous end joining (Fig. 6.7A). Sequencing of these PCR products either did not yield any result (the sequencing primers did not anneal) or showed overlapping sequences. Therefore, only single bands of ~200bp were sequenced, and only if the PCR reaction with the mutation specific primer had indicated that at least one allele harbours the mutation.

For the generation of the *Dok7* c.1124_26dupTGCC mutation, DNA of 41 clones was screened. One of these clones was a homozygous mutant (Fig. 6.7B,C). This clone was used for the AChR clustering experiments described below. The CRISPR/Cas9 protocol was later repeated twice: 45 clones were screened in the first repeat, none of which showed the mutation. In the second repeat, 63 clones were screened. Two clones were identified as homozygous mutants, but later did not differentiate into myotubes and had to be discarded. For the c.1504_1505insTA mutation, DNA from 42 clones was screened. One clone was a homozygous mutant and was used for AChR clustering experiments (Fig. 6.7B,C).

In order to be able to compare AChR clustering for the *Dok7* mutant cell lines with clustering for WT *Dok7* cell lines, CRISPR/Cas9 control cell lines were generated. C2C12 cells were electroporated with 10µg pX335 plasmid only (without the guides cloned in). Cloning by limiting dilution was performed as described earlier, and 10 healthy-looking monoclonal cell colonies were chosen. One further control colony (colony 11) was obtained from a separate transfection. Sequencing of a ~550bp region around the mutations confirmed that all controls were WT (see Fig. 6.6 and Table 2.5 for

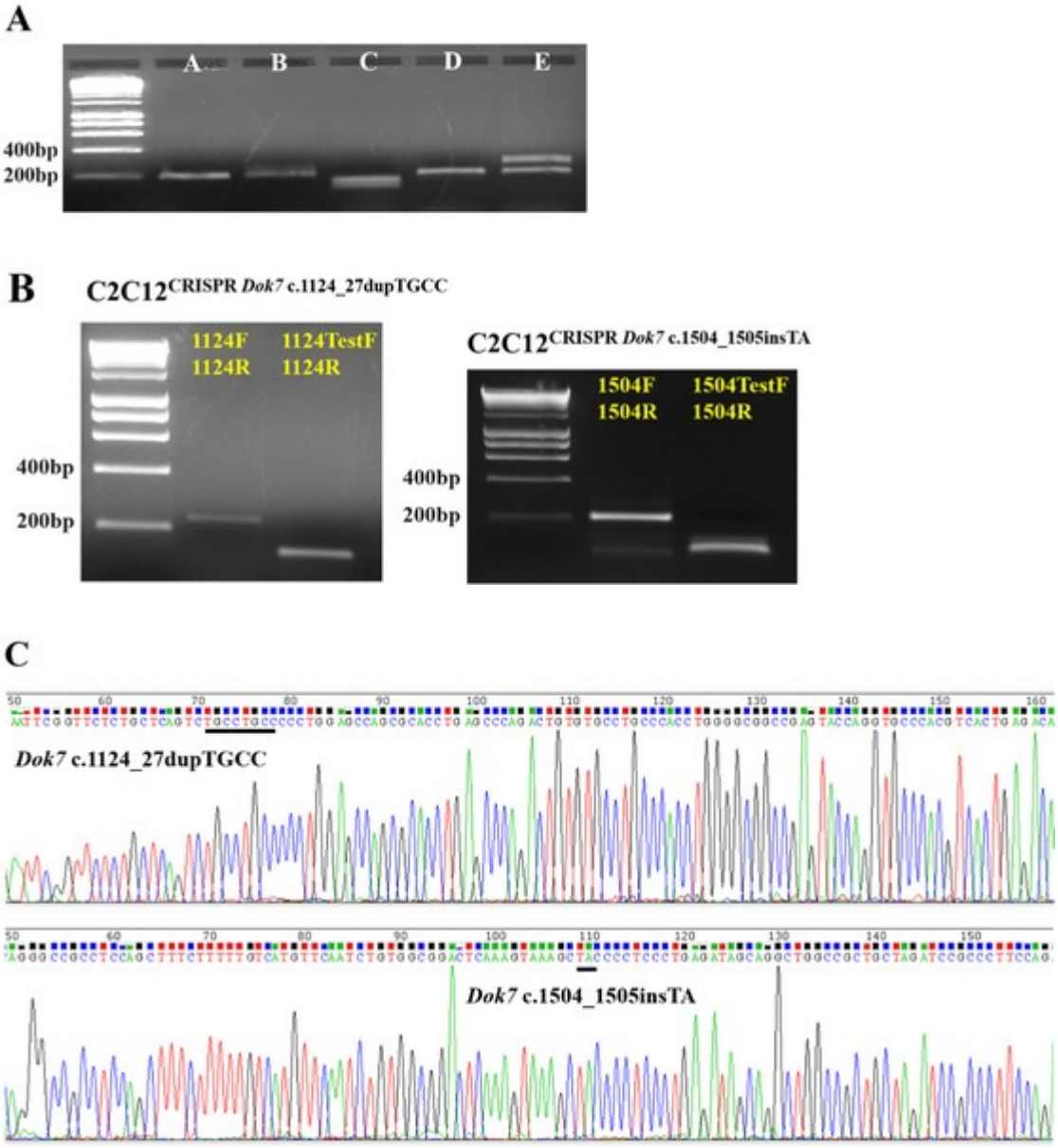

Figure 6.7 Screening of cell colonies. (A) Bands A-E correspond to PCR products from five of the 42 colonies screened for the c.1504_1505insTA mutation. A ~200bp region was amplified around the target region (primers 1504F and 1504R). Two bands were detected for colony E, which was excluded from sequencing. A-D did not yield a band, when a mutation-specific primer was used for a PCR (not shown), and were excluded from sequencing as well. (B) Cell colony screened positive for *Dok7* c.1124_27dupTGCC (left image) and *Dok7* c.1504_1505insTA mutation (right image). PCRs with a mutation-specific primer (right band) indicated the presence of the mutation in at least one allele. The PCR products from the DNA amplification around the target site (left band) were sent for sequencing. (C) The results confirmed successful CRISPR/Cas9 genome editing of *Dok7*.

information on the primers).

6.3 AChR clustering in CRISPR/Cas9 genome edited cells

6.3.1 Agrin titration study

Using CRISPR/Cas9 genome editing, *Dok7* mutant cell lines and *Dok7* controls were successfully generated. For future experiments, it was essential that myoblasts of these cell lines differentiate into myotubes and that AChR clusters form in response to incubation with agrin. Therefore, the culturing conditions for C2C12$^{\text{CRISPR } Dok7 \text{ c.1124_27dupTGCC}}$, C2C12$^{\text{CRISPR } Dok7 \text{ c.1504_1505insTA}}$ and each control cell line were optimised.

The culturing of all clonal cell lines was challenging. While C2C12 cells fuse easily into myotubes by serum starvation using 2% FCS, the CRISPR/Cas9 modified cell lines required a higher percentage of serum (often 10% HS + 2% FCS). Although the original polyclonal batch of C2C12 WT cells used for the generation of controls differentiated very well, control clones 1-6 did not fuse into myotubes under any of the cell culture conditions tested. Myotubes of controls 8-11 were treated with human full length agrin (1:100) or short rat agrin (1:100) for 16h to test whether AChR clusters would form (Fig. 6.8). Control 7 was excluded from further experiments due to abnormally shaped myotubes and a lack of AChR clusters. Controls 8-11 fused to myotubes comparable to C2C12 WT cells and formed AChR clusters in response to agrin. For further experiments, control 8, 10 and 11 were chosen.

We addressed the question whether there is variability in AChR clustering between control cell lines, and secondly whether the mutant cell lines differ from the controls with respect to cluster numbers. Therefore, an agrin titration experiment was conducted, where cells were treated for 16h with full length human agrin, diluted 1:100, 1:500, 1:1000 or 1:5000, or with short rat soluble agrin diluted 1:100 or 1:1000. For each agrin dilution,

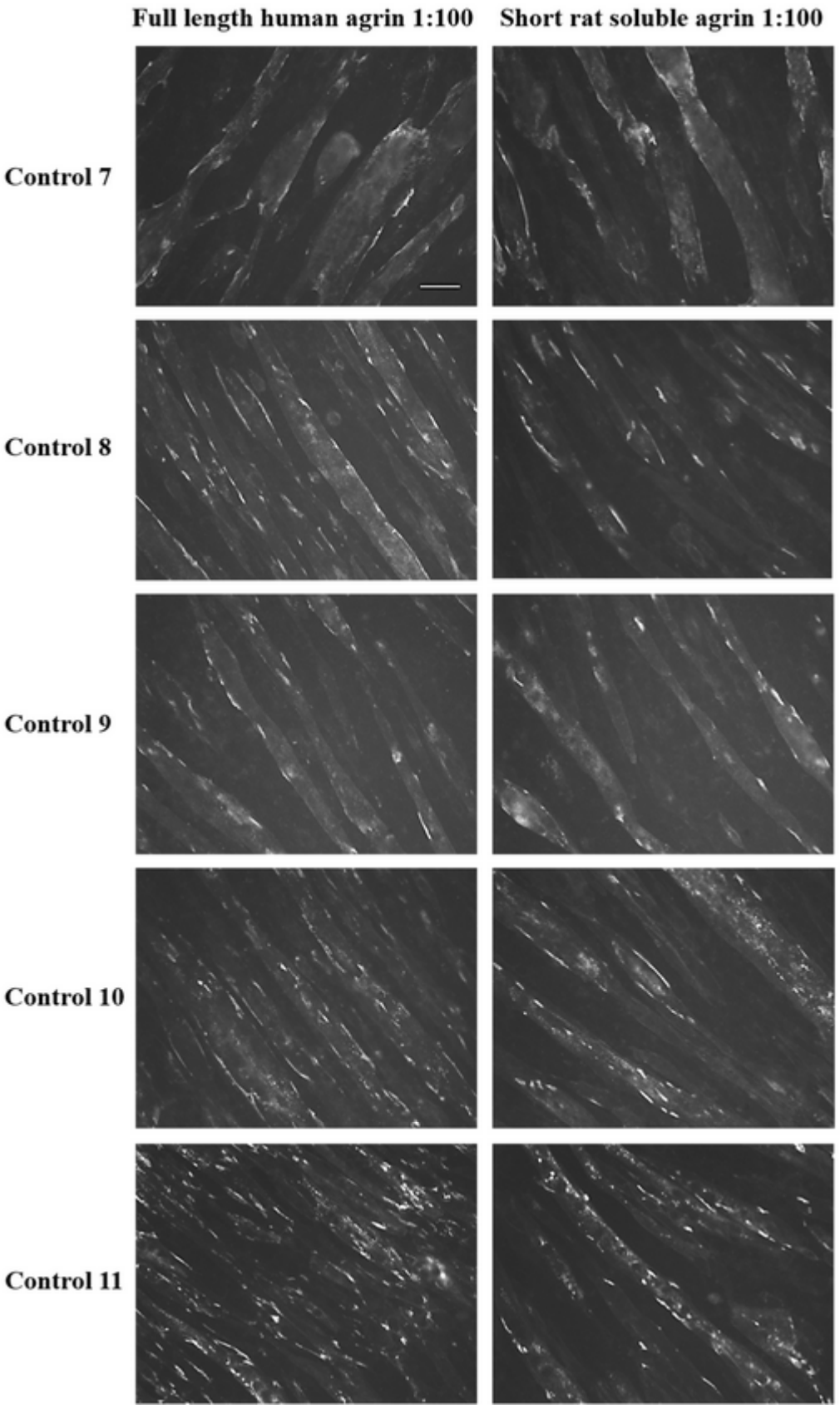

Figure 6.8 Representative microscopic images of CRISPR/Cas9 controls. Scale bar=50μm.

the number of AChR clusters for the different cell lines were compared to each other. Results are shown in Fig. 6.9. Statistical test details of all comparisons are shown in Table 6.2. due to space constraints. As expected from previous experiments, full length human agrin induced AChR clustering in a dose-dependent manner in all cell lines. Significant variability in the number of AChR clusters between control cell lines was observed. Of note, no significant differences in AChR cluster numbers occurred between the two *Dok7* mutant cell lines. Comparing the control cell lines to the mutants in response to full length agrin incubation, a trend occurred towards reduced cluster counts for the mutants (although not consistently found for all comparisons).

The more notable result was the difference in the number of AChR clusters between controls and mutants in response to incubation with short rat agrin. While clusters formed on all control cell lines (Fig. 6.8), no clustering was induced in C2C12$^{\text{CRISPR } Dok7 \text{ c.1124_27dupTGCC}}$ or C2C12$^{\text{CRISPR } Dok7 \text{ c.1504_1505insTA}}$ cells (Fig. 6.10). A preliminary experiment was conducted to explore this finding in greater detail. C2C12$^{\text{CRISPR } Dok7 \text{ c.1504_1505insTA}}$ cells were treated with 1:1000 full length human agrin or with 1:1000 short rat agrin for either 4h when clusters begin to form or for 24h (Fig. 6.11). The same experiment was conducted in C2C12 WT cells (not CRISPR/Cas9-edited). In the mutant, full length agrin incubation for 4h induced a large number of small freckle-like clusters (henceforth referred to as micro clusters). Cells stained after 24h showed that these then formed larger clusters. In contrast, after 4h incubation with short rat agrin, only very few micro clusters formed and no large clusters formed within 24h. In C2C12 WT cells, short rat agrin was sufficient to induce micro clusters after 4h and regular clusters within 24h.

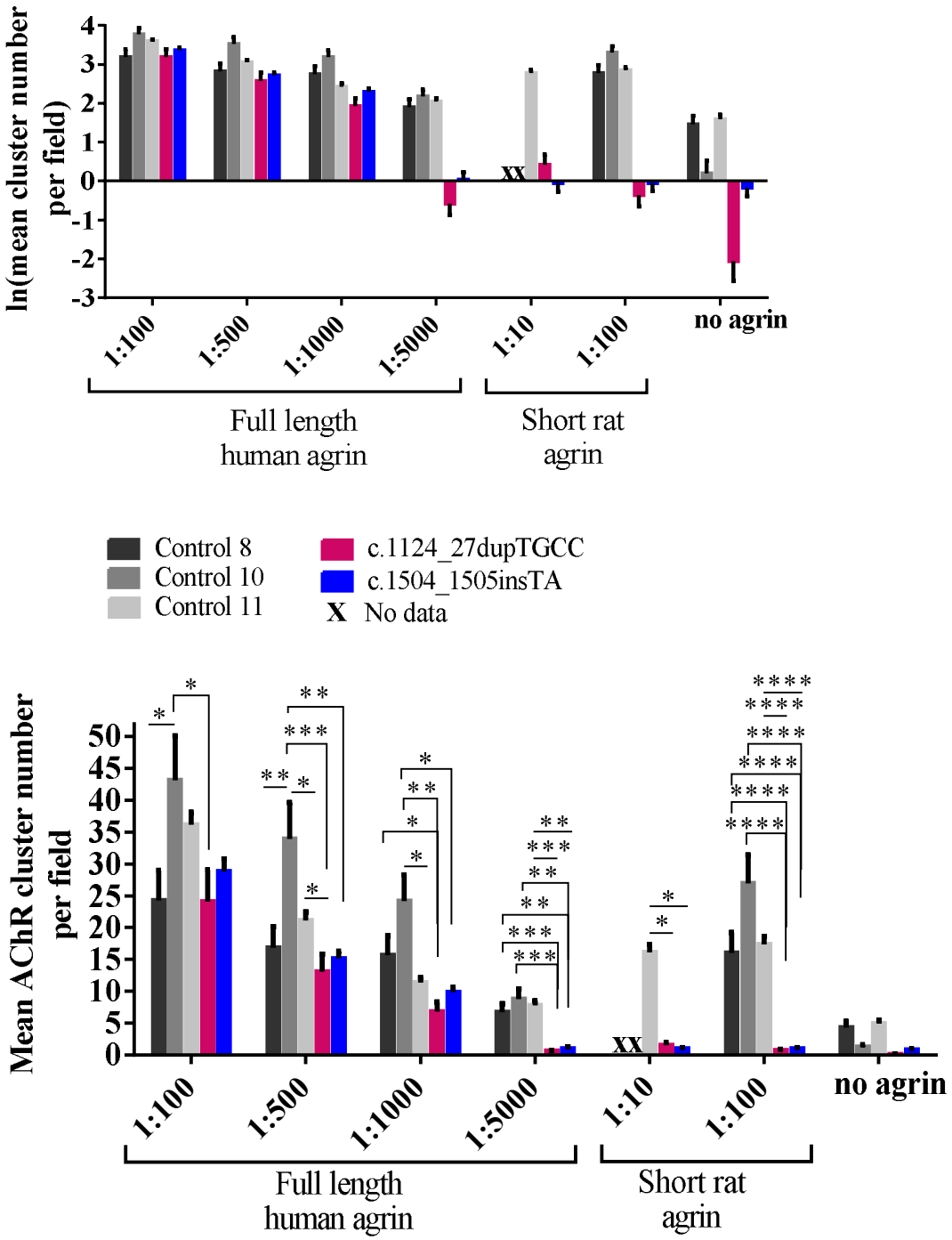

Figure 6.9 Agrin titration for CRISPR control cell lines, C2C12$^{CRISPR\ Dok7\ c.1124_27dupTGCC}$ and C2C12$^{CRISPR\ Dok7\ c.1504_1505insTA}$. Cells were incubated with 1:100, 1:500, 1:1000 or 1:5000 full length human or with 1:10 or 1:100 short rat agrin for 16h. AChR cluster numbers varied significantly between control cell lines, whereas the two mutants showed similar levels of clustering (see Table 6.2 for statistical test details). The controls differed significantly from *Dok7* mutants when AChR clustering was induced with short rat agrin. At 1:100, AChR clusters formed on control myotubes, whereas almost no clusters formed on mutant myotubes. N=3 (control 8, control 10, control 11, *Dok7* c.1124_27dupTGCC) and N=2 (*Dok7* c.1504_1505insTA). Error bars indicate the standard error of the mean. *p≤0.05, **p≤0.01, ***p<0.001, ****p≤0.0001. Only statistically significant differences are shown.

Full length human agrin				
	1:100	**1:500**	**1:1000**	**1:5000**
Control 8 vs. Control 10	d=0.6, SE=0.2, p=0.01	d=0.63, SE=0.18, p=0.007	d=0.58, SE=0.36, p=0.14	d=0.25, SE=0.45, p=0.59
Control 8 vs. Control 11	d=0.36, SE=0.2, p=0.1	d=0.2, SE=0.18, p=0.29	d=0.34, SE=0.32, p=0.33	d=0.21, SE=0.45, p=0.64
Control 8 vs. c.1124_27dupTGCC	d=0.01, SE=0.2, p=0.95	d=0.26, SE=0.18, p=0.19	d=0.92, SE=0.33, p=0.02	d=2.55, SE=0.5, p=0.0006
Control 8 vs. c.1504_1505insTA	d=0.17, SE=0.22, p=0.46	d=0.14, SE=0.2, p=0.52	d=0.45, SE=0.37, p=0.25	d=1.83, SE=0.54, p=0.008
Control 10 vs. Control 11	d=0.24, SE=0.2, p=0.25	d=0.42, SE=0.18, p=0.04	d=0.92, SE=0.36, p=0.03	d=0.04, SE=0.45, p=0.93
Control 10 vs. c.1124_27dupTGCC	d=0.58, SE=0.2, p=0.02	d=0.88, SE=0.18, p=0.0008	d=1.5, SE=0.36, p=0.003	d=2.8, SE=0.5, p=0.0003
Control 10 vs. c.1504_1505insTA	d=0.43, SE=0.22, p=0.08	d=0.76, SE=0.2, p=0.004	d=1, SE=0.4, p=0.03	d=2.09, SE=0.54, p=0.004
Control 11 vs. c.1124_27dupTGCC	d=0.34, SE=0.2, p=0.11	d=0.46, SE=0.18, p=0.03	d=0.58, SE=0.33, p=0.11	d=2.76, SE=0.5, p=0.0004
Control 11 vs. c.1504_1505insTA	d=0.19, SE=0.22, p=0.42	d=0.36, SE=0.2, p=0.13	d=0.11, SE=0.37, p=0.77	d=2.05, SE=0.54, p=0.004
c.1124_27dupTGCC vs. c.1504_1505insTA	d=0.16, SE=0.22, p=0.5	d=0.12, SE=0.2, p=0.57	d=0.47, SE=0.37, p=0.23	d=0.71, SE=0.58, p=0.25

Short soluble rat agrin		
	1:10	**1:100**
Control 8 vs. Control 10		d=0.5, SE=0.23, p=0.06
Control 8 vs. Control 11		d=0.05, SE=0.23, p=0.83
Control 8 vs. c.1124_27dupTGCC		d=3.15, SE=0.3, p<0.00005
Control 8 vs. c.1504_1505insTA		d=2.83, SE=0.37, p<0.00005
Control 10 vs. Control 11		d=0.45, SE=0.23, p=0.09
Control 10 vs. c.1124_27dupTGCC		d=3.65, SE=0.3, p<0.00005
Control 10 vs. c.1504_1505insTA		d=3.33, SE=0.37, p<0.00005
Control 11 vs. c.1124_27dupTGCC	d=2.5, SE=0.56, p=0.02	d=3.2, SE=0.3, p<0.00005
Control 11 vs. c.1504_1505insTA	d=2.8, SE=0.59, p=0.02	d=2.89, SE=0.37, p<0.00005
c.1124_27dupTGCC vs. c.1504_1505insTA	d=0.35, SE==0.61, p=0.61	d=0.32, SE=0.42, p=0.47

Table 6.2 Statistical test details for comparisons of AChR cluster numbers between cell lines for each agrin dilution. D=difference.

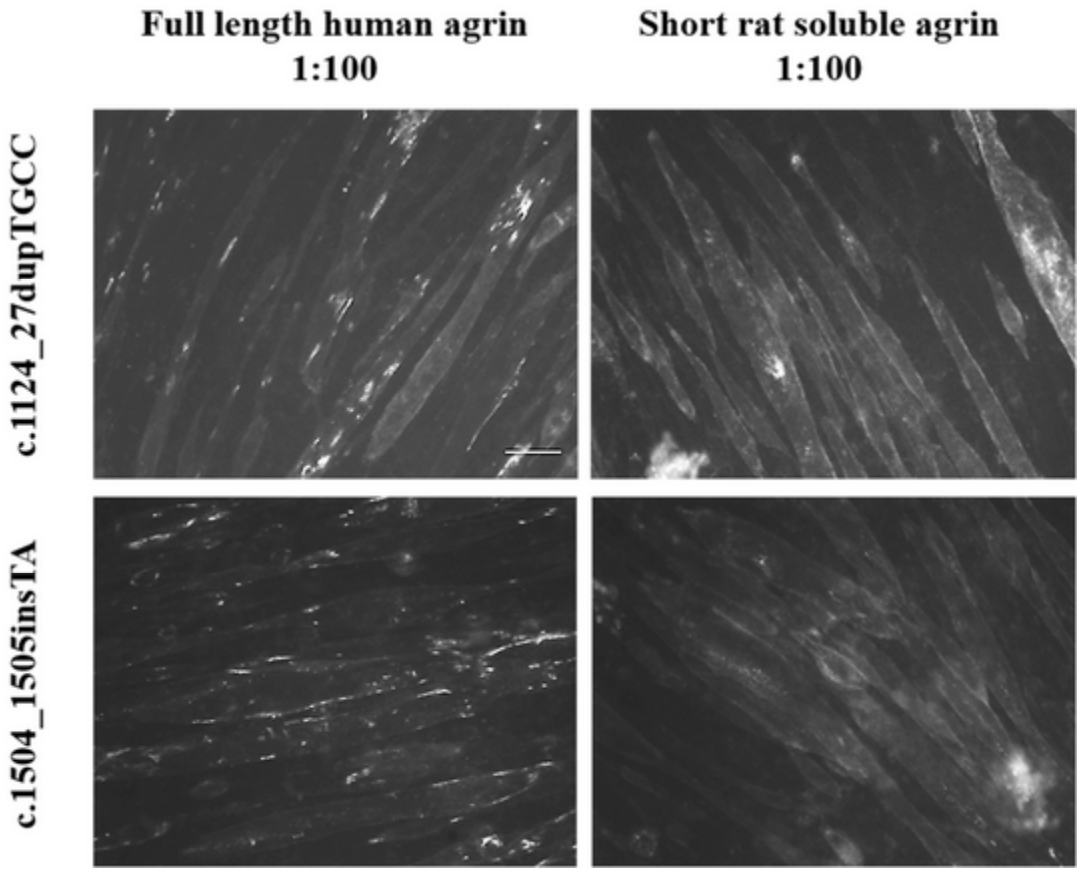

Figure 6.10 Representative microscopic images of C2C12$^{CRISPR\ Dok7\ c.1124_27dupTGCC}$ and C2C12$^{CRISPR\ Dok7\ c.1504_1505insTA}$ myotubes treated with 1:100 agrin for 16h. Clusters only formed with full length human agrin but not soluble short rat agrin. In control cells however, truncated agrin was sufficient to induce clustering (see Fig. 6.8). Scale bar=50µm.

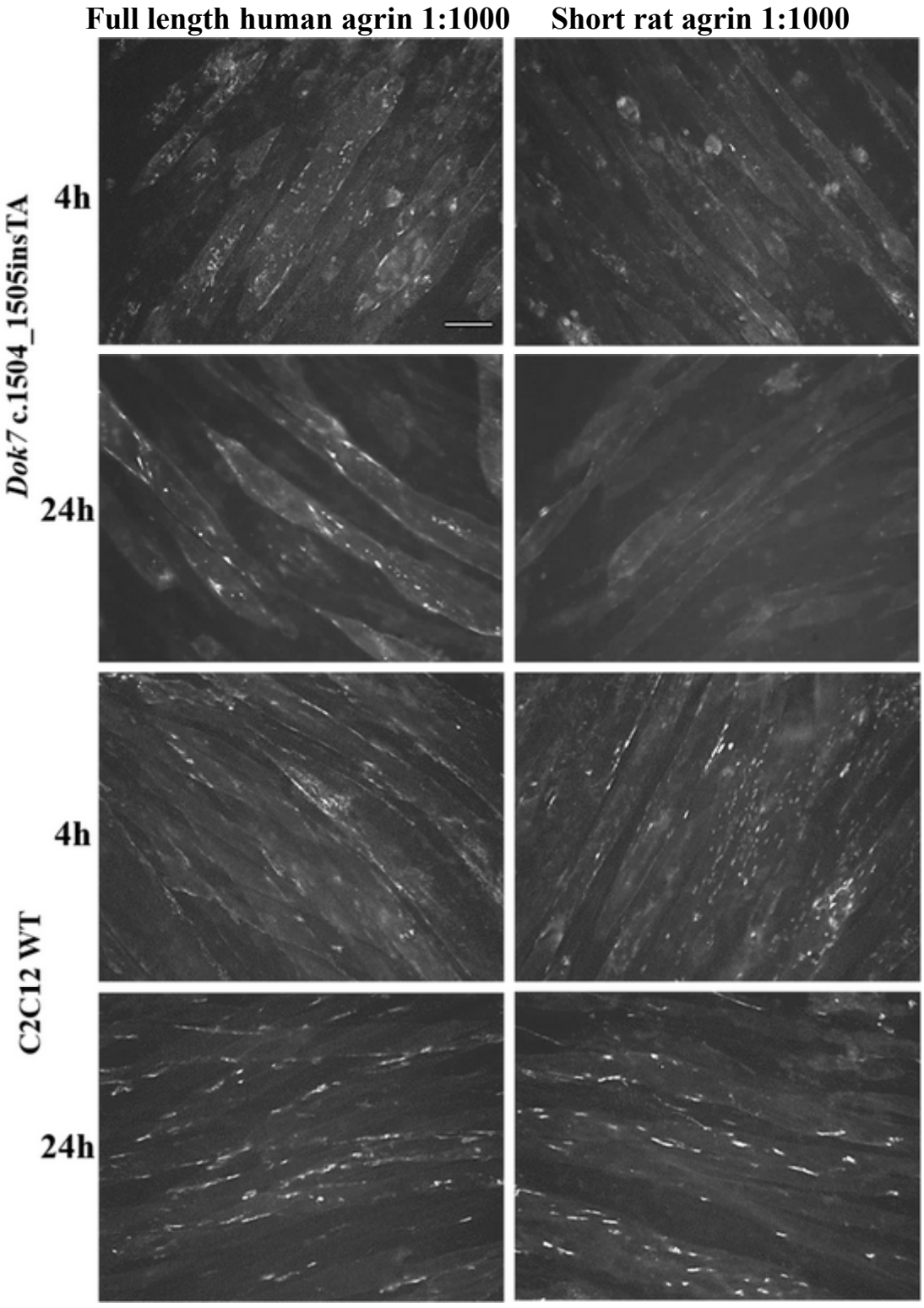

Figure 6.11 Representative microscopic images, showing the difference in AChR clustering between C2C12$^{CRISPR\ Dok7\ c.1504_1505insTA}$ and C2C12 WT cells. In the mutant, full length agrin incubation for 4h induced a large number of micro clusters, which by 24h formed average-sized clusters. However, after 4h incubation with short rat agrin, only very few micro clusters had formed and no average sized clusters formed within 24h. In C2C12 WT cells, short rat agrin was sufficient to induce micro clusters after 4h and larger clusters within 24h. Scale bar=50µm.

6.4 Effects of salbutamol on CRISPR/Cas9-edited cell lines

The experiments presented thus far show that mutant *Dok7* C2C12 cell lines can be generated by utilising CRISPR/Cas9 genome editing techniques. C2C12$^{\text{CRISPR } Dok7 \text{ c.1124_27dupTGCC}}$, C2C12$^{\text{CRISPR } Dok7 \text{ c.1504_1505insTA}}$ and *Dok7* WT CRISPR controls were characterised by performing agrin titrations. Next, experiments were conducted on the effects of salbutamol treatment on these cell lines.

6.4.1 Effects of salbutamol on AChR clustering

C2C12$^{\text{CRISPR } Dok7 \text{ c.1124_27dupTGCC}}$ and control 11 were treated with salbutamol sulphate for 16h simultaneously with 1:500 full length human agrin (Fig. 6.12). Full length agrin was chosen since the agrin titration experiment had shown that soluble agrin is not sufficient to induce AChR clustering in the mutant cell lines. In the mutant, 10µM salbutamol caused a small decrease in the number of clusters ($p=0.02$), while 50µM did not have an effect ($p=0.5$). No differences were observed in the control cell line ($p>0.99$ and $p=0.85$, respectively).

6.4.2 Effects of salbutamol on AChR beta-subunit tyrosine phosphorylation

In chapter 4, it was investigated in C2C12 WT and C2C12 $^{Dok7 \text{ c.1124\_27dupTGCC}}$ cells whether salbutamol incubation increases tyrosine phosphorylation of the AChR beta-subunit. These experiments were now repeated for the CRISPR/Cas9-edited cells (see chapter 2.10.1 for details on the protocol). First, CRISPR control 11, C2C12$^{\text{CRISPR } Dok7 \text{ c.1124_27dupTGCC}}$ or C2C12$^{\text{CRISPR } Dok7 \text{ c.1504_1505insTA}}$ myotubes were treated with 50µM salbutamol sulphate for 4h simultaneously with 1:1000 full length human agrin or in the absence of agrin (Fig. 6.13). In a further condition, C2C12$^{\text{CRISPR } Dok7 \text{ c.1504_1505insTA}}$ myotubes were treated with salbutamol sulphate simultaneously with 1:1000 short rat agrin (Fig. 6.13C(2)). No increase in AChR beta-subunit tyrosine-phosphorylation was

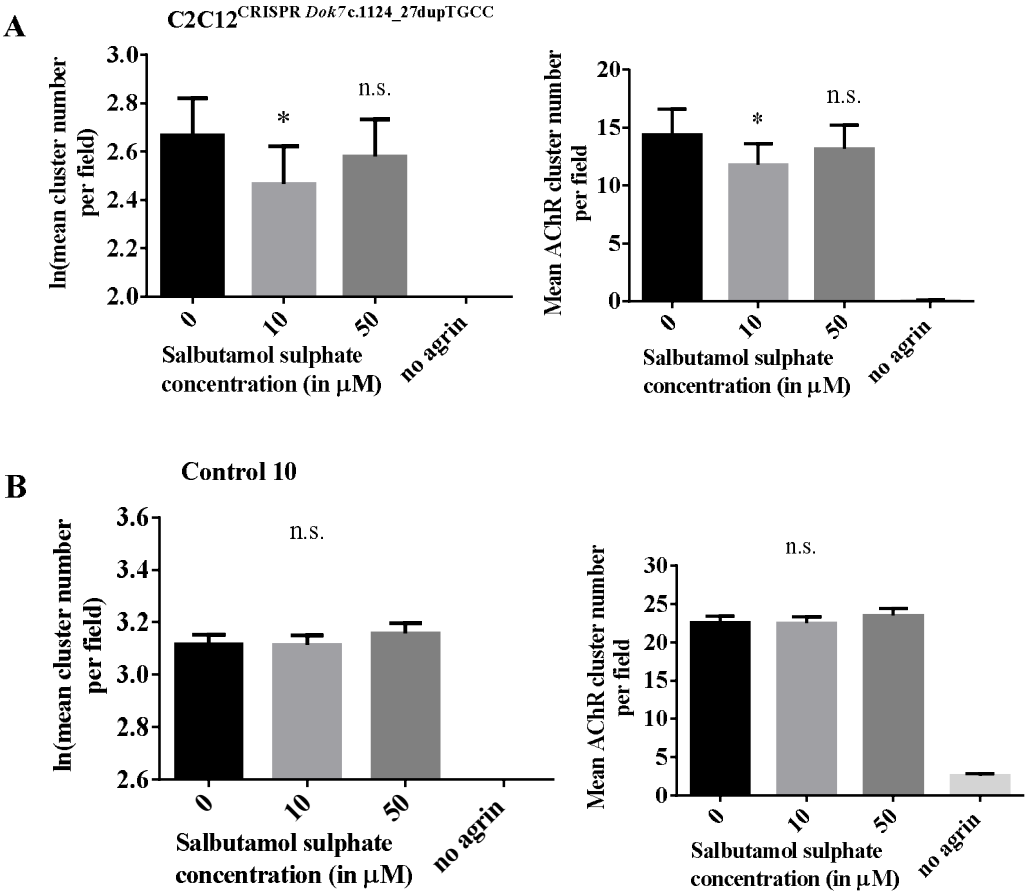

Figure 6.12 Effects of salbutamol on AChR clustering in CRISPR/Cas9-edited cells. Myotubes were treated with salbutamol sulphate for 16h simultaneously with AChR cluster induction with full length human agrin, diluted 1:500. (A) In C2C12$^{\text{CRISPR } Dok7 \text{ c.1124_27dupTGCC}}$ cells, 10μM salbutamol caused a small decrease in AChR cluster numbers, while 50μM did not have an effect (difference=0.2, SE=0.08, p=0.02, and difference=0.09, SE=0.08, p=0.5, respectively). (B) In control cell line 10, no difference occurred (difference=0.003, SE=0.05, p>0.99, and difference=0.04, SE=0.05, p=0.85). Error bars indicate the standard error of the mean. n.s.p>0.05, *p≤0.05. N=2.

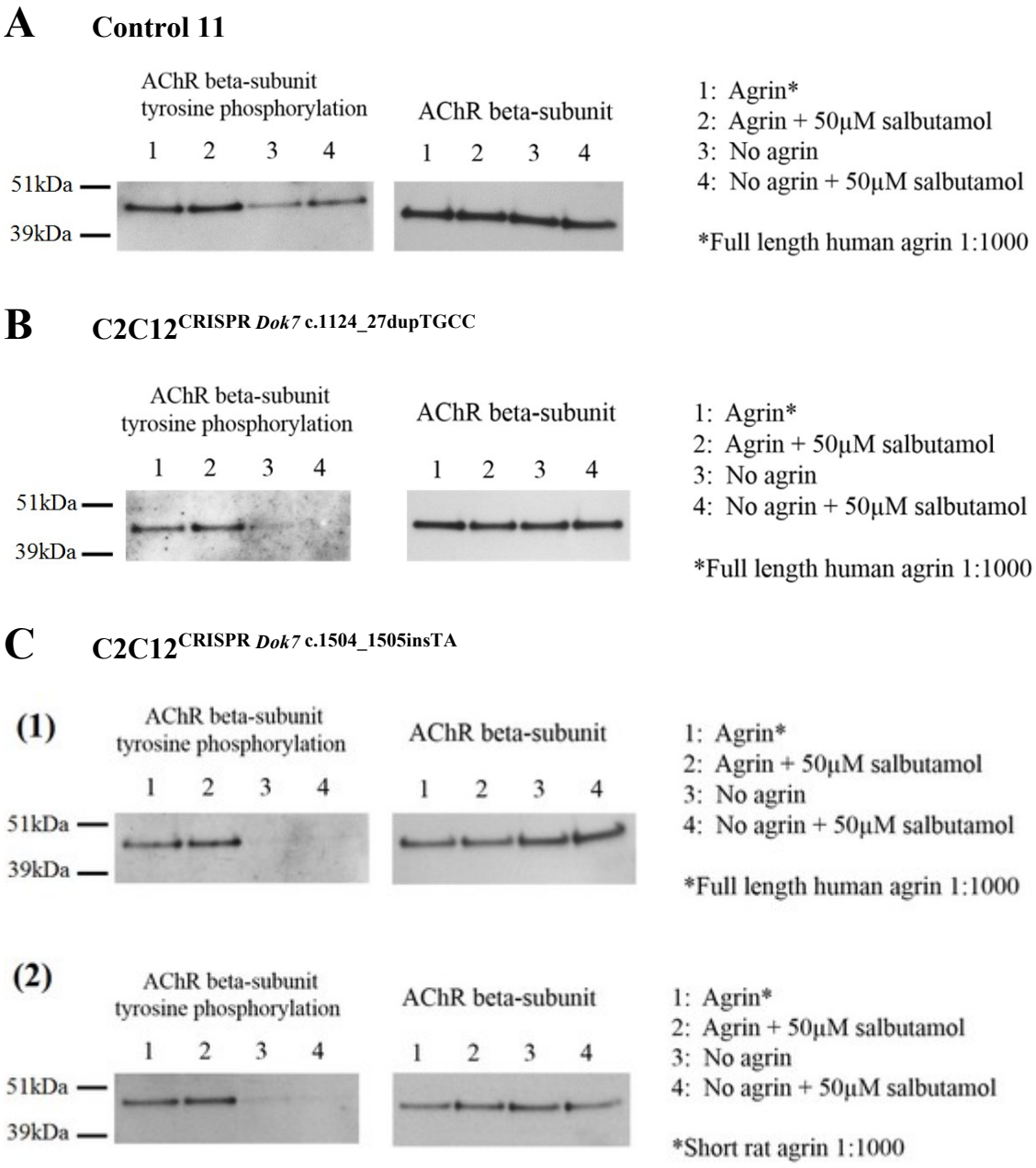

Figure 6.13 Effects of 4h salbutamol incubation on AChR beta-subunit tyrosine phosphorylation in CRISPR/Cas9-edited cells. (A) Control 11 myotubes, (B) C2C12$^{CRISPR\ Dok7\ c.1124_27dupTGCC}$ myotubes or (C(1)) C2C12$^{CRISPR\ Dok7\ c.1504_1505insTA}$ myotubes were treated for 4h with 1:1000 full length human agrin (band 1) or full length human agrin and 50µM salbutamol sulphate (band 2). The effects of salbutamol on baseline phosphorylation levels in the absence of agrin were tested by leaving the cells untreated (band 3) or by incubating them with 50µM salbutamol sulphate (band 4). In C2C12$^{CRISPR\ Dok7\ c.1504_1505insTA}$ myotubes, AChR beta-subunit tyrosine phosphorylation was also investigated in cells treated with short rat agrin (C(2)). AChRs were pulled down with biotin-XX α-bungarotoxin, and the samples were subjected to SDS Page. A band corresponding to the AChR beta-subunit (~48kDa) was detected with 1:3000 mAb124 anti-AChR beta, and phosphorylated AChR beta-subunit was detected using 1:100 p-AChRβ1 Tyr390 antibody. N=3 (A, C), N=2 (B).

observed in response to salbutamol treatment in the presence of absence of agrin.

Next, C2C12$^{\text{CRISPR } Dok7 \text{ c.1504_1505insTA}}$ myotubes were treated with full length human agrin or short rat agrin and salbutamol for 24h (Fig. 6.14A). It could be observed that significantly less phosphorylation occurred with short rat agrin compared to with full length agrin. Since not all cells had fused into 'high quality' myotubes, the experiment was repeated using myotubes of matching quality from CRISPR control 8 (Fig. 6.14B). Similar results were obtained, suggesting that the effect was not due to the *Dok7* mutation.

6.5 Discussion

The current chapter aimed at investigating CRISPR/Cas9 genome editing as a novel technique to model postsynaptic dysfunction at the NMJ. Being able to directly introduce mutations into genes encoding proteins located postsynaptically at the NMJ could help us understand mechanisms of CMS and determine the pathogenicity of variants identified in patients.

CRISPR/Cas9 editing was adapted to investigate DOK7 CMS by creating two stable mutant cell lines. This new cell culture model allowed us to study the effects of *Dok7* mutations on agrin-induced clusters. In response to full length human agrin, a large number of AChR clusters formed in cells harbouring the c.1124_27dupTGCC mutation. This contrasts with findings from the DOK7 overexpression model, where *DOK7* c.1124_27dupTGCC stimulated the formation of significantly fewer AChR clusters when overexpressed in C2C12 myotubes. The CRISPR/Cas9 cell culture model provides a more physiological disease model than the overexpression system. Although muscle biopsies from DOK7 patients reveal disruption of the endplate structures and small NMJs, the AChR clustering pathway is still partially functional (Beeson et al., 2006). Therefore,

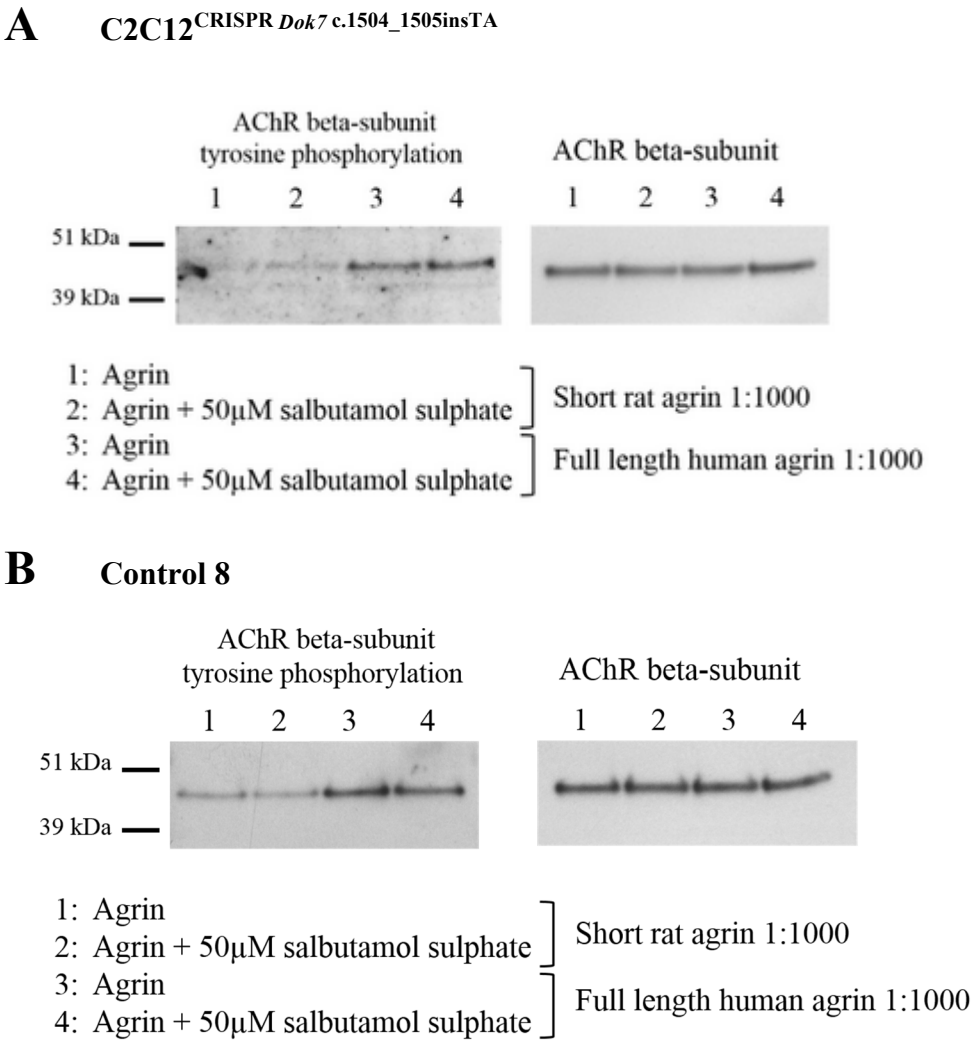

Figure 6.14 Effects of 24h salbutamol incubation on AChR beta-subunit tyrosine phosphorylation in CRISPR/Cas9-edited cells. (A) C2C12$^{\text{CRISPR } Dok7 \text{ c.1504_1505insTA}}$ or (B) control 8 myotubes were incubated for 24h with 1:1000 short rat agrin (band 1), 1:1000 short rat agrin and 50µM salbutamol sulphate (band 2), 1:1000 full length human agrin (band 3) or 1:1000 full length human agrin and 50µM salbutamol sulphate (band 4). AChRs were pulled down with biotin-XX α-bungarotoxin, and the samples were subjected to SDS Page. A band corresponding to the AChR beta-subunit (~48kDa) was detected with 1:3000 mAb124 anti-AChR beta, and phosphorylated AChR beta-subunit was detected using 1:100 p-AChRβ1 Tyr390 antibody. N=3 (1), N=3 (2).

one might not expect to see complete absence of AChR clusters when modelling the disease *in vitro*. Moreover, agrin treatment might 'overcome' the effects of the mutation. In the CRISPR/Cas9 model, agrin is applied exogenously in excess, and the interaction of agrin, MuSK and DOK7 is not as well regulated as in the *in vivo* situation. Subtle effects of the mutation on the AChR clustering pathway might not be detectable.

The *Dok7* mutants differed from the control cell lines in their ability to form AChR clusters in response to treatment with truncated rat agrin. In C2C12 WT cells and in the CRISPR controls, soluble agrin was sufficient to induce AChR clusters, which is in line with previous reports (Ferns et al., 1993). Almost no clusters formed in the CRISPR mutants. This difference between *Dok7* mutants and controls was apparent already after 4h of agrin treatment. In WT C2C12 cells, a large number of micro aggregates had formed, which preceded the formation of larger clusters. This finding is line with previous cell culture studies which showed that AChR micro clusters (2-5µm diameter) form within 2-4h after agrin incubation, which are then aggregated into larger clusters (15-20µm diameter) (Weston et al., 2003, Weston et al., 2007, Wallace, 1988). No such micro clusters formed in the mutant in response to soluble agrin. The full length agrin has a laminin-binding site in the N terminal region and attaches to the basal lamina (Denzer et al., 1998). Accordingly, we noticed in other experiments in our laboratory that full length agrin cannot be washed off the cells as easily as soluble agrin. One might speculate that the full length agrin sends a more constant signal than the potentially less constrained and more mobile soluble agrin. In the mutant cell lines where DOK7 functioning is impaired, a more continuous agrin signal might be required for sufficient stimulation of the AChR clustering pathway.

We observed robust AChR beta-subunit phosphorylation in the CRISPR mutants in response to incubation with short rat agrin despite the absence of cluster formation.

This supports the notion that although AChR beta-subunit phosphorylation precedes AChR clustering, it is neither required nor sufficient for cluster formation (Borges and Ferns, 2001).

A difference in the effect of the two agrin constructs was seen not only in C2C12$^{\text{CRISPR } Dok7 \text{ c.1124_27dupTGCC}}$ but also in C2C12$^{\text{CRISPR } Dok7 \text{ c.1504_1505insTA}}$ cells. Since gene screens using next-generation sequencing often result in the identification of rare variants, it is of great importance to be able to determine the pathogenicity of these variants. Many mutations identified in DOK7 CMS patients which are located towards the end of the C-terminal region do not impair AChR clustering if overexpressed in C2C12. The current results suggest that reduced AChR cluster formation in response to short rat agrin might be a feature that points towards pathogenicity of such variants. AChR clustering assays utilising CRISPR/Cas9 genome editing tools may therefore help in making a precise genetic diagnosis, with crucial implications for disease prognosis, prenatal diagnosis and treatment strategies. Further experiments will be performed in our laboratory to confirm and validate the current findings before this novel AChR clustering assay may find application in clinical practice.

No effect of salbutamol on tyrosine phosphorylation of the AChR beta-subunit could be observed. This finding is in line with the results from phosphorylation experiments on C2C12 WT and DOK7-overexpressing cells described in chapter 4.

The main aim of the current study was to conduct first experiments to test the suitability of the CRISPR/Cas9 genome editing technique for future use in CMS research. Despite the potential to identify pathogenic mutations located towards the end of the DOK7 C-terminal domain, certain concerns need to be addressed.

Overall, 191 monoclonal cell colonies were screened for mutant *Dok7*. Four clones could be identified as homozygous mutants. With 2.1%, the success rate was therefore

small. There is variation in the reported efficiency of CRISPR/Cas9 editing, however, in a recent study, in which prion protein knockout clones were generated from C2C12 cells, also a success rate of 2% was reported (Mehrabian et al., 2014). Further experiments could aim at optimising the transfection protocol, however, since C2C12 cells may be triploid (Baddeley et al., 2010), the success rate for creating homozygous mutants might remain low.

A concerning finding is the large number of cell populations which do not fuse into myotubes. Electroporation has not been found to affect the ability of myoblasts to differentiate in the past. The step of homology-directed repair can also be ruled out as an explanation, since 6 out of 11 control cell lines did not fuse. Instead, it is likely that the cloning of a polyclonal population of C2C12 cells accounts for this effect. The temperamental nature of the CRISPR/Cas9 colonies further reduces the number of mutant cell lines that can be used in experiments, since even when a correct clone is identified it might not be able to form myotubes.

Furthermore, it might be difficult to determine whether certain features of a mutant cell line result from the effects of the mutation or from the poor quality of the cells. This challenge could be addressed in further experiments by generating a suitable clone first and then subjecting it to CRISPR/Cas9 editing. This might also reduce the variability between cell lines. CRISPR control clone 8 and clone 10 originated from the same batch of C2C12 cells. Nevertheless, they differed significantly with respect to the number of AChR clusters. This variability complicates the comparison of mutant cell lines with each other and with controls. In the current study, a similar number of agrin-induced AChR clusters formed in C2C12$^{\text{CRISPR } \textit{Dok7} \text{ c.1124_27dupTGCC}}$ and C2C12$^{\text{CRISPR } \textit{Dok7} \text{ c.1504_1505insTA}}$ cells, although one might have expected a more severe effect of the c.1124_27dupTGCC

mutation. Further optimisation of the technique is necessary to overcome these challenges.

In future experiments, CRISPR/Cas9 editing could be utilised to create a stable *Dok7* knockout cell line. Subsequently, DOK7 mutations could be overexpressed in these cells by retroviral infection. This technique may provide an alternative model for testing rare *DOK7* variants that did not have an effect on AChR clustering in the current overexpression model.

One might consider alternatives to C2C12 cells for CRISPR/Cas9 gene editing. The time window in which C2C12 myoblasts fuse into myotubes and experiments can be conducted is limited. The CRISPR technique is time-consuming since all clones have to be maintained during the screening process. By the time a clone is identified as a homozygous mutant, it has already been cultured for several weeks. An alternative for future experiments may be the use of primary human muscle cells which were obtained through biopsies and cultured for a shorter period of time before the start of the experiment. This would also allow for a comparison of the effects of *DOK7* mutations on AChR clustering between human and mouse muscle cells. Results from animal models suggest that mice are more severely affected by *DOK7* mutations than humans (Arimura et al., 2014). *DOK7* knock-in mice homozygous for the c.1124_27dupTGCC mutation displayed features of DOK7 CMS observed in patients (smaller NMJs, reduced MuSK phosphorylation, disturbed gait) but were too weak for strength measurements and died between P13 and P20.

A further alternative to C2C12 cells for CRISPR/Cas9 genome editing could be the use of human pluripotent stem cells (hPSCs). Protocols for the generation of skeletal muscle cells from hPSCs are available and continuously improved (Abujarour and Valamehr, 2015). A major advantage of hPSCs is that they can be cultured for a longer

period of time than transformed or mortalised cells (Musunuru, 2013). WT and *DOK7*-mutant cell lines derived from the same parental cell line could then be compared.

CHAPTER 7

Discussion

7.1 ADRB2 agonists as novel treatment for CMS

The choice of treatment for CMS depends on the pathology underlying the disease. Drugs which reduce fatigable weakness in some CMS subtypes may be harmful in others. Acetylcholinesterase inhibitors, in some cases given in combination with 3,4-DAP, were, before the advent of modern molecular genetics, first line treatment for CMS. While they are beneficial in fast channel syndrome, rapsyn CMS and AChR deficiency due to mutations in *CHRNE*, they often worsen symptoms in DOK7 CMS, slow channel syndrome and COLQ CMS (Rodriguez Cruz et al., 2014). The observation that patients with DOK7 CMS respond dramatically to salbutamol and ephedrine sparked a revival of ADRB2 agonists as treatment for neuromuscular disorders. As a result, for many patients a combinational treatment approach is now chosen. ADRB2 agonists have been shown to provide benefit where destabilisation of NMJ structures is part of the underlying pathology, such as in DOK7, COLQ and MuSK CMS as well as in slow channel syndrome (Rodriguez Cruz et al., 2014). The finding that salbutamol maintains the treatment response to cholinesterase inhibitors in AChR deficiency due to mutations in *CHRNE* (Rodriguez Cruz et al., 2015) supports the notion that ADRB2 agonists exert a stabilising effect at the NMJ.

The results presented within this thesis provide first experimental evidence that ADRB2 agonists directly affect proteins located at the NMJ. The findings suggest that salbutamol and related agonists act via the AChR clustering pathway; however, further research is required to decipher the precise mechanisms underlying the effects on AChR

cluster formation and stability. The next step could be the investigation of kinase pathways involved in AChR aggregation, for which the AChR clustering experiments conducted in the current study may provide a useful framework.

Although to be interpreted with caution, the results on the novel ADRB2 agonist XA-01-NZ86 provide further evidence that this compound may in clinical practice provide an alternative to salbutamol. In CMS, salbutamol and ephedrine are currently used off-label, and XA-01-NZ86 is the first ADRB2 agonist specifically developed for the treatment of neuromuscular disorders. Due to its specific action on skeletal muscle and high potency it is expected to be associated with fewer side effects and could be superior to other agonists. Patient trials have to confirm whether the encouraging results from animal and cell culture studies transfer to the clinic.

Due to the differing response of CMS patients to the therapeutic agents available, a precise genetic diagnosis is of great importance for the tailoring of patient-specific treatment regimens.

7.2 Alternative CMS disease model systems

The availability of whole-exome capture, high through-put sequencing and bioinformatics tools has expedited the discovery of novel CMS subtypes. Within the last four years, five novel CMS-causative genes were identified affecting glycosylation (Senderek et al., 2011, Belaya et al., 2012, Cossins et al., 2013, Belaya et al., 2015). Moreover, next generation sequencing led to the discovery of mutations that underlie presynaptic CMS. Synaptostagmin 1 and 2 (SYT1 and SYT2) are calcium-binding synaptic vesicle proteins involved in the regulation of neurotransmitter release, and mutations in *SYTs* were shown to have multiple effects including presynaptic dysfunction at the NMJ (Baker et al., 2015, Herrmann et al., 2014). Prolyl-endopeptidase-like gene

(*PREPL*) encodes the protein PREPL which is ubiquitously expressed and belongs to a group of serine peptidases. PREPL deficiency was shown to underlie a case of CMS, with reduced filling of synaptic vesicles as a potential disease mechanism (Regal et al., 2014).

Therefore, the application of next generation sequencing raises hopes that within the next few years a genetic diagnosis can be made for most CMS patients where the disease-causing mutations are not yet determined. If rare variants are identified in established or novel CMS-causative genes, the next step is to establish their pathogenicity. This depends on the availability on sensitive disease model systems and *in vitro* assays.

While experiments on C2C12 cell cultures have significantly enhanced our understanding of how CMS-causing mutations affect the NMJ, they are associated with limitations (discussed in chapter 6), some of which could be overcome by the use of alternative disease models. Induced pluripotent stem cell technology (iPSC) could be exploited to generate disease- and patient-specific cell culture models for CMS research. These models could help with the investigation of disease mechanisms but could also be used for drug research. Besides unlimited proliferative capacity *in vitro*, a further advantage of iPSCs is that they can be used to generate cell types that are otherwise not easily available, such as neurons (Ellis and Bhatia, 2011). Hair root cells, which can be collected in a simple non-invasive procedure, are sufficient for the generation of iPSCs (Demestre et al., 2015). For CMS research, where it may not always be possible to obtain a muscle biopsy from a patient, iPSCs could be used to generate muscle fibres (Abujarour and Valamehr, 2015). Patient-derived muscle cultures could potentially provide a more physiological disease model than C2C12 mouse cells since they eliminate the need for gene editing or protein overexpression to mimic the disease. Moreover, they would

overcome the problem of interspecies differences, such as the observed differing disease severity between mice and humans carrying DOK7 mutations (Arimura et al., 2014).

There is no clear genotype-phenotype correlation in DOK7 CMS or other CMS subtypes, and there may be groups of patients within a CMS subtype who can be distinguished by a distinct early/late onset or mild/severe phenotype (Muller et al., 2007, Finlayson et al., 2013). iPSCs have the advantage that they can be generated from patients with differing disease phenotypes, which allows for the investigation of this variation *in vitro* and opens up the possibility to study the effects of drug treatment for differing patient groups. Furthermore, in the context of drug research, patient cell culture models could help reduce the number of animals used in the early stages of drug testing.

In a recent study, a co-culture model was developed by combining motoneurons and myotubes which were generated from the same donor iPS cell line (Demestre et al., 2015). In these co-cultures, AChRs aggregated after three weeks of culturing, and intact NMJs formed. A co-culture model has the advantage that neuromuscular disorders with presynaptic dysfunction could be investigated in greater detail. Moreover, AChR aggregation at these *in vitro* NMJs may be better regulated than AChR cluster formation induced in muscle monocultures. Muscle-nerve co-cultures could therefore provide an advanced model to investigate the effects of drug treatment on the AChR clustering pathway. Furthermore, in research on DOK7 CMS, mutations located towards the end of the gene which often have no clearcut effect on AChR clustering in C2C12 myotubes (Hamuro et al., 2008) could be investigated.

Besides many advantages, the application of iPSC technology, especially when combined with cell co-culturing, can be expensive, technically demanding and time consuming (Ellis and Bhatia, 2011). Whilst providing a novel and exciting tool for both

basic research and drug testing, it might not be suitable for routine pathogenicity testing of variants detected in patients.

7.3 Gene therapy as an alternative to drug treatment

Although still in its infancy, gene therapy might at some point in the future provide an alternative to drug treatment for some genetic diseases. In the last few decades, significant progress has been made in *in vivo* gene transfer using genetically engineered viruses. Adeno-associated viral (AAV) vectors have been used for gene delivery in numerous animal disease models, and the translation to the clinic has been successful for some genetic disorders (Nonnenmacher and Weber, 2012). In patients suffering from inherited retinal disorders and haemophilia B, gene delivery through AAVs led to long-term expression of the target genes at therapeutic levels (Mingozzi and High, 2011).

A recent study demonstrated the therapeutic potential of administration of an AAV vector encoding the human *DOK7* gene for treatment of DOK7 CMS, other forms of CMS and potentially other muscle disorders in which the NMJ may be involved in the pathogenic process (Arimura et al., 2014). The authors had previously created DOK7 transgenic (Tg) mice, which overexpressed DOK7 throughout the skeletal muscle (Inoue et al., 2009). The finding that these mice developed enlarged intact NMJs and did not reveal motoric abnormalities suggested that upregulation of DOK7 may provide a therapeutic approach for not only DOK7 CMS, where small NMJs are a hallmark feature of the disease, but also for other conditions in which the endplate structure is disrupted. Arimura et al. (2014) created an rAAV serotype 9 vector, encoding DOK7 under the control of the cytomegalovirus promotor. One week after a single intravenous injection with rAAV-DOK7, WT mice resembled the previously described DOK7 Tg mice. Treatment of knock-in mice homozygous for DOK7 c.1124_27dupTGCC, which usually

died before P20 and displayed severe weakness and NMJ disruption, led to prolonged survival of these mice, to increased muscle strength and enlargement of NMJs. Administration of rAAV-DOK7 had similar effects in an Emery-Dreifuss muscular dystrophy mouse model (Arimura et al., 2014).

In a different study, administration of an AAV serotype 8 carrying COLQ was shown to benefit COLQ-deficient mice by reducing fatigability, increasing the size of NMJ structures and normalising neuromuscular synaptic transmission (Ohno et al., 2013). These studies suggest that a gene delivery approach may have restorative effects in certain NMJ disorders, although effective systems for systemic delivery to human muscle have yet to be mastered.

RNA interference (RNAi) is a technology used for the manipulation of gene expression. Since it results in the downregulation of transcribed genes it has been explored in the context of the dominantly inherited slow channel CMS. Abdelgany et al. (2003) successfully employed allele-specific silencing by small interfering RNA and short hairpin RNAs for the downregulation of the pathogenic αS226F AChR mutant in HEK293 cells (Abdelgany et al., 2003). Similarly, a small interfering RNA was used to silence αC418W-AChR, another slow channel CMS-causing AChR allele (Shen et al., 2006).

Recent advances in the rapidly evolving field of genome engineering have raised hopes that gene correction may in the future be performed in patients in order to directly amend the disease-causing gene (Xiao-Jie et al., 2015). An advantage of this method is that mutations that result in either gain or loss of function could be corrected. CRISPR/Cas9 gene editing for the treatment of monogenic disorders has been studied in animals. Although highly controversial for the use in humans, CRISPR/Cas9-mediated germline correction was successful in an animal model of Duchenne muscular dystrophy,

where editing of the dystrophin gene *Dmd* produced genetically mosaic mice displaying 2-100% correction of *Dmd* (Long et al., 2014). A subset of corrected cells was sufficient to rescue normal muscle structure and function in the mice.

Application of CRISPR/Cas9 gene editing without embryo modification depends on effective delivery systems that direct the CRISPR/Cas9 components to the somatic cells of interest. These may include hydrodynamic injections (Suda and Liu, 2007, Yin et al., 2014) or AAVs (Senis et al., 2014), both of which have be developed further for potential use in humans.

An alternative is the application of CRISPR/Cas9 to iPSCs. After reprogramming of patient-derived somatic cells into iPSCs, they could be CRISPR/Cas9-modified *in vitro* and differentiated into the desired cells for subsequent autologous transplantation. In a recent study, iPS cells were generated from fibroblasts from a Duchenne muscular dystrophy patient and corrected by exon knock-in (Li et al., 2015). When the gene-edited iPSCs were differentiated into skeletal muscle cells, expression of full-length dystrophin protein could be detected.

Despite the growing number of *in vitro* and *in vivo* experiments demonstrating successful therapeutic gene editing, most of them were proof of principle studies, and there are challenges to be overcome before targeted gene modifications may be attempted in patients (Xiao-Jie et al., 2015). A serious concern is the safety of CRISPR/Cas9 genome engineering in humans due to potential off-target effects. Moreover, more effective tools for the delivery of Cas9 into the target cells are required to increase the editing efficiency.

7.4 Summary and contribution to the field

As opposed to gene therapy approaches which aim at curing genetic diseases and may find application in the more distant future, drug delivery systems can provide life-changing symptomatic treatment for patients. In order to be able to tailor effective drug treatment for an inherited condition it is of great importance to understand the molecular mechanisms that underlie the disease and the effects a compound has on the disease pathology.

CMS is one of few genetic diseases for which drug therapy is available. This is largely due to the detailed understanding of the functioning of the NMJ and the effects of mutations that cause its dysfunction. The current work aimed at investigating ADRB2 agonists as novel therapy for neuromuscular disorders. Within the course of this thesis the following issues were addressed:

- It was shown, using an overexpression model of DOK7 CMS, that ADRB2 agonists directly affect proteins located at the NMJ and may act via the AChR clustering pathway. Specifically, salbutamol and other ADRB2 agonists increased the number of forming AChR clusters in DOK7 mutant cells and exerted a stabilising effect on clusters.

  The novel compound XA-01-NZ86 as the first ADRB2 agonist developed specifically for the treatment of neuromuscular disorders was tested and shown to be effective at increasing the number of AChR clusters at low concentrations.
- It was demonstrated that overexpression of DOK7 variants in C2C12 cells provides a useful disease model for studying the pathogenicity of mutations and for studying the effects of drug treatment on the AChR clustering pathway. However, the limitations of the overexpression model were discussed, and alternative CMS

disease models were explored. CRISPR/Cas9 genome editing tools were adapted to directly introduce mutations to the genome of C2C12 cells.

- By combining optogenetics with FLIM, a novel experimental setup was developed in order to study the effects of ADRB2 activation on the AChR clustering pathway in greater detail. In this setup, optical control over ADRB2 signalling allows for the investigation of cAMP signalling and AChR cluster stability in single live myotubes.

The current results add to our understanding of how ADRB2 agonists affect NMJ functioning and exert beneficial effects in some CMS subtypes. The work on alternative cell culture models and experimental setups will underpin a framework for future research on both disease mechanisms and the effects of drug treatment. A precise understanding of the pathways that are activated by ADRB2 agonists and affect AChR clustering may help to develop further targeted compounds that allow for patient-tailored symptomatic drug treatment.

Bibliography

ABDELGANY, A., WOOD, M. & BEESON, D. 2003. Allele-specific silencing of a pathogenic mutant acetylcholine receptor subunit by RNA interference. Hum Mol Genet, 12**,** 2637-44.

ABOURASHED, E. A., EL-ALFY, A. T., KHAN, I. A. & WALKER, L. 2003. Ephedra in perspective--a current review. Phytother Res, 17**,** 703-12.

ABUJAROUR, R. & VALAMEHR, B. 2015. Generation of skeletal muscle cells from pluripotent stem cells: advances and challenges. Front Cell Dev Biol, 3**,** 29.

AKAABOUNE, M., GRADY, R. M., TURNEY, S., SANES, J. R. & LICHTMAN, J. W. 2002. Neurotransmitter receptor dynamics studied in vivo by reversible photo-unbinding of fluorescent ligands. Neuron, 34**,** 865-76.

ANTOLIK, C., CATINO, D. H., O'NEILL, A. M., RESNECK, W. G., URSITTI, J. A. & BLOCH, R. J. 2007. The actin binding domain of ACF7 binds directly to the tetratricopeptide repeat domains of rapsyn. Neuroscience, 145**,** 56-65.

ARIMURA, S., OKADA, T., TEZUKA, T., CHIYO, T., KASAHARA, Y., YOSHIMURA, T., MOTOMURA, M., YOSHIDA, N., BEESON, D., TAKEDA, S. & YAMANASHI, Y. 2014. Neuromuscular disease. DOK7 gene therapy benefits mouse models of diseases characterized by defects in the neuromuscular junction. Science, 345**,** 1505-8.

ARMAIZ-PENA, G. N., ALLEN, J. K., CRUZ, A., STONE, R. L., NICK, A. M., LIN, Y. G., HAN, L. Y., MANGALA, L. S., VILLARES, G. J., VIVAS-MEJIA, P., RODRIGUEZ-AGUAYO, C., NAGARAJA, A. S., GHARPURE, K. M., WU, Z., ENGLISH, R. D., SOMAN, K. V., SHAHZAD, M. M., ZIGLER, M., DEAVERS, M. T., ZIEN, A., SOLDATOS, T. G., JACKSON, D. B., WIKTOROWICZ, J. E., TORRES-LUGO, M., YOUNG, T., DE GEEST, K., GALLICK, G. E., BAR-ELI, M., LOPEZ-BERESTEIN, G., COLE, S. W., LOPEZ, G. E., LUTGENDORF, S. K. & SOOD, A. K. 2013. Src activation by beta-adrenoreceptors is a key switch for tumour metastasis. Nat Commun, 4**,** 1403.

ARREDONDO, J., LARA, M., NG, F., GOCHEZ, D. A., LEE, D. C., LOGIA, S. P., NGUYEN, J. & MASELLI, R. A. 2014. COOH-terminal collagen Q (COLQ) mutants causing human deficiency of endplate acetylcholinesterase impair the interaction of ColQ with proteins of the basal lamina. Hum Genet, 133**,** 599-616.

AUERBACH, A. 2015. Activation of endplate nicotinic acetylcholine receptors by agonists. Biochem Pharmacol.

AXELROD, D. 1981. Cell-substrate contacts illuminated by total internal reflection fluorescence. J Cell Biol, 89**,** 141-5.

BADDELEY, D., CHAGIN, V. O., SCHERMELLEH, L., MARTIN, S., POMBO, A., CARLTON, P. M., GAHL, A., DOMAING, P., BIRK, U., LEONHARDT, H., CREMER, C. & CARDOSO, M. C. 2010. Measurement of replication structures at the nanometer scale using super-resolution light microscopy. Nucleic Acids Res, 38**,** e8.

BAKER, K., GORDON, S. L., GROZEVA, D., VAN KOGELENBERG, M., ROBERTS, N. Y., PIKE, M., BLAIR, E., HURLES, M. E., CHONG, W. K., BALDEWEG, T., KURIAN, M. A., BOYD, S. G., COUSIN, M. A. &

RAYMOND, F. L. 2015. Identification of a human synaptotagmin-1 mutation that perturbs synaptic vesicle cycling. J Clin Invest, 125**,** 1670-8.
BANKS, G. B., FUHRER, C., ADAMS, M. E. & FROEHNER, S. C. 2003. The postsynaptic submembrane machinery at the neuromuscular junction: requirement for rapsyn and the utrophin/dystrophin-associated complex. J Neurocytol, 32**,** 709-26.
BARTOLI, M., RAMARAO, M. K. & COHEN, J. B. 2001. Interactions of the rapsyn RING-H2 domain with dystroglycan. J Biol Chem, 276**,** 24911-7.
BECKER, W. 2012. Fluorescence lifetime imaging--techniques and applications. J Microsc, 247**,** 119-36.
BEESON, D., HIGUCHI, O., PALACE, J., COSSINS, J., SPEARMAN, H., MAXWELL, S., NEWSOM-DAVIS, J., BURKE, G., FAWCETT, P., MOTOMURA, M., MULLER, J. S., LOCHMULLER, H., SLATER, C., VINCENT, A. & YAMANASHI, Y. 2006. Dok-7 mutations underlie a neuromuscular junction synaptopathy. Science, 313**,** 1975-8.
BELAYA, K., FINLAYSON, S., SLATER, C. R., COSSINS, J., LIU, W. W., MAXWELL, S., MCGOWAN, S. J., MASLAU, S., TWIGG, S. R., WALLS, T. J., PASCUAL PASCUAL, S. I., PALACE, J. & BEESON, D. 2012. Mutations in DPAGT1 cause a limb-girdle congenital myasthenic syndrome with tubular aggregates. Am J Hum Genet, 91**,** 193-201.
BELAYA, K., RODRIGUEZ CRUZ, P. M., LIU, W. W., MAXWELL, S., MCGOWAN, S., FARRUGIA, M. E., PETTY, R., WALLS, T. J., SEDGHI, M., BASIRI, K., YUE, W. W., SARKOZY, A., BERTOLI, M., PITT, M., KENNETT, R., SCHAEFER, A., BUSHBY, K., PARTON, M., LOCHMULLER, H., PALACE, J., MUNTONI, F. & BEESON, D. 2015. Mutations in GMPPB cause congenital myasthenic syndrome and bridge myasthenic disorders with dystroglycanopathies. Brain.
BEN AMMAR, A., SOLTANZADEH, P., BAUCHE, S., RICHARD, P., GOILLOT, E., HERBST, R., GAUDON, K., HUZE, C., SCHAEFFER, L., YAMANASHI, Y., HIGUCHI, O., TALY, A., KOENIG, J., LEROY, J. P., HENTATI, F., NAJMABADI, H., KAHRIZI, K., ILKHANI, M., FARDEAU, M., EYMARD, B. & HANTAI, D. 2013. A mutation causes MuSK reduced sensitivity to agrin and congenital myasthenia. PLoS One, 8**,** e53826.
BERGAMIN, E., HALLOCK, P. T., BURDEN, S. J. & HUBBARD, S. R. 2010. The cytoplasmic adaptor protein Dok7 activates the receptor tyrosine kinase MuSK via dimerization. Mol Cell, 39**,** 100-9.
BLOSSER, J. C. 1983. beta-Adrenergic receptor activation increases acetylcholine receptor number in cultured skeletal muscle myotubes. J Neurochem, 40**,** 1144-9.
BOLKER, B. M., BROOKS, M. E., CLARK, C. J., GEANGE, S. W., POULSEN, J. R., STEVENS, M. H. & WHITE, J. S. 2009. Generalized linear mixed models: a practical guide for ecology and evolution. Trends Ecol Evol, 24**,** 127-35.
BORGES, L. S. & FERNS, M. 2001. Agrin-induced phosphorylation of the acetylcholine receptor regulates cytoskeletal anchoring and clustering. J Cell Biol, 153**,** 1-12.
BORGES, L. S., YECHIKHOV, S., LEE, Y. I., RUDELL, J. B., FRIESE, M. B., BURDEN, S. J. & FERNS, M. J. 2008. Identification of a motif in the acetylcholine receptor beta subunit whose phosphorylation regulates rapsyn association and postsynaptic receptor localization. J Neurosci, 28**,** 11468-76.

BORNER, S., SCHWEDE, F., SCHLIPP, A., BERISHA, F., CALEBIRO, D., LOHSE, M. J. & NIKOLAEV, V. O. 2011. FRET measurements of intracellular cAMP concentrations and cAMP analog permeability in intact cells. Nat Protoc, 6**,** 427-38.

BRANDON, E. P., LIN, W., D'AMOUR, K. A., PIZZO, D. P., DOMINGUEZ, B., SUGIURA, Y., THODE, S., KO, C. P., THAL, L. J., GAGE, F. H. & LEE, K. F. 2003. Aberrant patterning of neuromuscular synapses in choline acetyltransferase-deficient mice. J Neurosci, 23**,** 539-49.

BRUNEAU, E. G., MACPHERSON, P. C., GOLDMAN, D., HUME, R. I. & AKAABOUNE, M. 2005. The effect of agrin and laminin on acetylcholine receptor dynamics in vitro. Dev Biol, 288**,** 248-58.

BURDEN, S. J., SARGENT, P. B. & MCMAHAN, U. J. 1979. Acetylcholine receptors in regenerating muscle accumulate at original synaptic sites in the absence of the nerve. J Cell Biol, 82**,** 412-25.

BURGES, J., WRAY, D. W., PIZZIGHELLA, S., HALL, Z. & VINCENT, A. 1990. A myasthenia gravis plasma immunoglobulin reduces miniature endplate potentials at human endplates in vitro. Muscle Nerve, 13**,** 407-13.

BURGESS, R. W., NGUYEN, Q. T., SON, Y. J., LICHTMAN, J. W. & SANES, J. R. 1999. Alternatively spliced isoforms of nerve- and muscle-derived agrin: their roles at the neuromuscular junction. Neuron, 23**,** 33-44.

BURKE, G., COSSINS, J., MAXWELL, S., ROBB, S., NICOLLE, M., VINCENT, A., NEWSOM-DAVIS, J., PALACE, J. & BEESON, D. 2004. Distinct phenotypes of congenital acetylcholine receptor deficiency. Neuromuscul Disord, 14**,** 356-64.

BURKE, G., HISCOCK, A., KLEIN, A., NIKS, E. H., MAIN, M., MANZUR, A. Y., NG, J., DE VILE, C., MUNTONI, F., BEESON, D. & ROBB, S. 2013. Salbutamol benefits children with congenital myasthenic syndrome due to DOK7 mutations. Neuromuscul Disord, 23**,** 170-5.

CAMPANELLI, J. T., HOCH, W., RUPP, F., KREINER, T. & SCHELLER, R. H. 1991. Agrin mediates cell contact-induced acetylcholine receptor clustering. Cell, 67**,** 909-16.

CARR, A. S., CARDWELL, C. R., MCCARRON, P. O. & MCCONVILLE, J. 2010. A systematic review of population based epidemiological studies in Myasthenia Gravis. Bmc Neurology, 10.

CARROLL, D. 2011. Genome engineering with zinc-finger nucleases. Genetics, 188**,** 773-82.

CARTAUD, A., COUTANT, S., PETRUCCI, T. C. & CARTAUD, J. 1998. Evidence for in situ and in vitro association between beta-dystroglycan and the subsynaptic 43K rapsyn protein. Consequence for acetylcholine receptor clustering at the synapse. J Biol Chem, 273**,** 11321-6.

CHAN, S. H., WONG, V. C. & ENGEL, A. G. 2012. Neuromuscular junction acetylcholinesterase deficiency responsive to albuterol. Pediatr Neurol, 47**,** 137-40.

CHANG, D., WOO, J. S., CAMPANELLI, J., SCHELLER, R. H. & IGNATIUS, M. J. 1997. Agrin inhibits neurite outgrowth but promotes attachment of embryonic motor and sensory neurons. Dev Biol, 181**,** 21-35.

CHAOUCH, A., MULLER, J. S., GUERGUELTCHEVA, V., DUSL, M., SCHARA, U., RAKOCEVIC-STOJANOVIC, V., LINDBERG, C., SCOLA, R. H., WERNECK, L. C., COLOMER, J., NASCIMENTO, A., VILCHEZ, J. J.,

MUELAS, N., ARGOV, Z., ABICHT, A. & LOCHMULLER, H. 2012. A retrospective clinical study of the treatment of slow-channel congenital myasthenic syndrome. J Neurol, 259**,** 474-81.

CHEN, F., QIAN, L., YANG, Z. H., HUANG, Y., NGO, S. T., RUAN, N. J., WANG, J., SCHNEIDER, C., NOAKES, P. G., DING, Y. Q., MEI, L. & LUO, Z. G. 2007. Rapsyn interaction with calpain stabilizes AChR clusters at the neuromuscular junction. Neuron, 55**,** 247-60.

CHEVESSIER, F., FARAUT, B., RAVEL-CHAPUIS, A., RICHARD, P., GAUDON, K., BAUCHE, S., PRIOLEAU, C., HERBST, R., GOILLOT, E., IOOS, C., AZULAY, J. P., ATTARIAN, S., LEROY, J. P., FOURNIER, E., LEGAY, C., SCHAEFFER, L., KOENIG, J., FARDEAU, M., EYMARD, B., POUGET, J. & HANTAI, D. 2004. MUSK, a new target for mutations causing congenital myasthenic syndrome. Hum Mol Genet, 13**,** 3229-40.

CHOI, K. R., BERRERA, M., REISCHL, M., STRACK, S., ALBRIZIO, M., RODER, I. V., WAGNER, A., PETERSEN, Y., HAFNER, M., ZACCOLO, M. & RUDOLF, R. 2012. Rapsyn mediates subsynaptic anchoring of PKA type I and stabilisation of acetylcholine receptor in vivo. J Cell Sci, 125**,** 714-23.

CHRISTIAN, M., CERMAK, T., DOYLE, E. L., SCHMIDT, C., ZHANG, F., HUMMEL, A., BOGDANOVE, A. J. & VOYTAS, D. F. 2010. Targeting DNA double-strand breaks with TAL effector nucleases. Genetics, 186**,** 757-61.

CONG, L., RAN, F. A., COX, D., LIN, S., BARRETTO, R., HABIB, N., HSU, P. D., WU, X., JIANG, W., MARRAFFINI, L. A. & ZHANG, F. 2013. Multiplex genome engineering using CRISPR/Cas systems. Science, 339**,** 819-23.

COSSINS, J., BELAYA, K., HICKS, D., SALIH, M. A., FINLAYSON, S., CARBONI, N., LIU, W. W., MAXWELL, S., ZOLTOWSKA, K., FARSANI, G. T., LAVAL, S., SEIDHAMED, M. Z., CONSORTIUM, W. G. S., DONNELLY, P., BENTLEY, D., MCGOWAN, S. J., MULLER, J., PALACE, J., LOCHMULLER, H. & BEESON, D. 2013. Congenital myasthenic syndromes due to mutations in ALG2 and ALG14. Brain, 136**,** 944-56.

COSSINS, J., LIU, W. W., BELAYA, K., MAXWELL, S., OLDRIDGE, M., LESTER, T., ROBB, S. & BEESON, D. 2012. The spectrum of mutations that underlie the neuromuscular junction synaptopathy in DOK7 congenital myasthenic syndrome. Hum Mol Genet, 21**,** 3765-75.

CRUZ, P. M., PALACE, J. & BEESON, D. 2014a. Congenital myasthenic syndromes and the neuromuscular junction. Curr Opin Neurol, 27**,** 566-75.

CRUZ, P. M. R., PALACE, J. & BEESON, D. 2014b. Inherited disorders of the neuromuscular junction: an update. Journal of Neurology, 261**,** 2234-2243.

DECHIARA, T. M., BOWEN, D. C., VALENZUELA, D. M., SIMMONS, M. V., POUEYMIROU, W. T., THOMAS, S., KINETZ, E., COMPTON, D. L., ROJAS, E., PARK, J. S., SMITH, C., DISTEFANO, P. S., GLASS, D. J., BURDEN, S. J. & YANCOPOULOS, G. D. 1996. The receptor tyrosine kinase MuSK is required for neuromuscular junction formation in vivo. Cell, 85**,** 501-12.

DEMESTRE, M., ORTH, M., FOHR, K. J., ACHBERGER, K., LUDOLPH, A. C., LIEBAU, S. & BOECKERS, T. M. 2015. Formation and characterisation of neuromuscular junctions between hiPSC derived motoneurons and myotubes. Stem Cell Res, 15**,** 328-336.

DENZER, A. J., SCHULTHESS, T., FAUSER, C., SCHUMACHER, B., KAMMERER, R. A., ENGEL, J. & RUEGG, M. A. 1998. Electron microscopic

structure of agrin and mapping of its binding site in laminin-1. EMBO J, 17**,** 335-43.
DOBBINS, G. C., LUO, S., YANG, Z., XIONG, W. C. & MEI, L. 2008. alpha-Actinin interacts with rapsyn in agrin-stimulated AChR clustering. Mol Brain, 1**,** 18.
DURANTI, G., LA ROSA, P., DIMAURO, I., WANNENES, F., BONINI, S., SABATINI, S., PARISI, P. & CAPOROSSI, D. 2011. Effects of salmeterol on skeletal muscle cells: metabolic and proapoptotic features. Med Sci Sports Exerc, 43**,** 2259-73.
EDGEWORTH, H. 1930. The effect of ephedrine in the treatment of myasthenia gravis. Journal of the American Medical Association 94.
ELLIS, J. & BHATIA, M. 2011. iPSC technology: platform for drug discovery. Point. Clin Pharmacol Ther, 89**,** 639-41.
ENGEL, A. G. 1984. Myasthenia gravis and myasthenic syndromes. Ann Neurol, 16**,** 519-34.
ENGEL, A. G. 2006. Light on limb-girdle myasthenia. Brain, 129**,** 1938-9.
ENGEL, A. G., LAMBERT, E. H., MULDER, D. M., TORRES, C. F., SAHASHI, K., BERTORINI, T. E. & WHITAKER, J. N. 1982. A newly recognized congenital myasthenic syndrome attributed to a prolonged open time of the acetylcholine-induced ion channel. Ann Neurol, 11**,** 553-69.
ENGEL, A. G., OHNO, K., BOUZAT, C., SINE, S. M. & GRIGGS, R. C. 1996a. End-plate acetylcholine receptor deficiency due to nonsense mutations in the epsilon subunit. Ann Neurol, 40**,** 810-7.
ENGEL, A. G., OHNO, K., MILONE, M., WANG, H. L., NAKANO, S., BOUZAT, C., PRUITT, J. N., 2ND, HUTCHINSON, D. O., BRENGMAN, J. M., BREN, N., SIEB, J. P. & SINE, S. M. 1996b. New mutations in acetylcholine receptor subunit genes reveal heterogeneity in the slow-channel congenital myasthenic syndrome. Hum Mol Genet, 5**,** 1217-27.
ENGEL, A. G., OHNO, K. & SINE, S. M. 1999. Congenital myasthenic syndromes: recent advances. Arch Neurol, 56**,** 163-7.
ENGEL, A. G., OHNO, K. & SINE, S. M. 2003. Congenital myasthenic syndromes: progress over the past decade. Muscle Nerve, 27**,** 4-25.
ENGEL, A. G., SHEN, X. M., SELCEN, D. & SINE, S. M. 2015. Congenital myasthenic syndromes: pathogenesis, diagnosis, and treatment. *Lancet Neurol,* 14**,** 461.
FERNS, M. J., CAMPANELLI, J. T., HOCH, W., SCHELLER, R. H. & HALL, Z. 1993. The ability of agrin to cluster AChRs depends on alternative splicing and on cell surface proteoglycans. Neuron, 11, 491-502.
FERNS, M., DEINER, M. & HALL, Z. 1996. Agrin-induced acetylcholine receptor clustering in mammalian muscle requires tyrosine phosphorylation. J Cell Biol, 132**,** 937-44.
FINLAYSON, S., BEESON, D. & PALACE, J. 2013a. Congenital myasthenic syndromes: an update. Pract Neurol, 13**,** 80-91.
FINLAYSON, S., SPILLANE, J., KULLMANN, D. M., HOWARD, R., WEBSTER, R., PALACE, J. & BEESON, D. 2013b. Slow channel congenital myasthenic syndrome responsive to a combination of fluoxetine and salbutamol. Muscle Nerve, 47**,** 279-82.
FINN, A. J., FENG, G. & PENDERGAST, A. M. 2003. Postsynaptic requirement for Abl kinases in assembly of the neuromuscular junction. Nat Neurosci, 6**,** 717-23.

FOYE, W. O., LEMKE, T. L. & WILLIAMS, D. A. 2008. Foye's principles of medicinal chemistry, Philadelphia, Lippincott Williams & Wilkins.
FÖRSTER, T. 1948. Zwischenmolekulare Energiewanderung und Fluoreszenz. Ann. Physik, 437**,** 55–75
FRAIL, D. E., MCLAUGHLIN, L. L., MUDD, J. & MERLIE, J. P. 1988. Identification of the mouse muscle 43,000-dalton acetylcholine receptor-associated protein (RAPsyn) by cDNA cloning. J Biol Chem, 263**,** 15602-7.
FRANK, E. & FISCHBACH, G. D. 1979. Early events in neuromuscular junction formation in vitro: induction of acetylcholine receptor clusters in the postsynaptic membrane and morphology of newly formed synapses. J Cell Biol, 83**,** 143-58.
FRIESE, M. B., BLAGDEN, C. S. & BURDEN, S. J. 2007. Synaptic differentiation is defective in mice lacking acetylcholine receptor beta-subunit tyrosine phosphorylation. Development, 134**,** 4167-4176.
FROEHNER, S. C., LUETJE, C. W., SCOTLAND, P. B. & PATRICK, J. 1990. The postsynaptic 43K protein clusters muscle nicotinic acetylcholine receptors in Xenopus oocytes. Neuron, 5**,** 403-10.
GALLENMULLER, C., MULLER-FELBER, W., DUSL, M., STUCKA, R., GUERGUELTCHEVA, V., BLASCHEK, A., VON DER HAGEN, M., HUEBNER, A., MULLER, J. S., LOCHMULLER, H. & ABICHT, A. 2014. Salbutamol-responsive limb-girdle congenital myasthenic syndrome due to a novel missense mutation and heteroallelic deletion in MUSK. Neuromuscul Disord, 24**,** 31-5.
GAUTAM, M., NOAKES, P. G., MOSCOSO, L., RUPP, F., SCHELLER, R. H., MERLIE, J. P. & SANES, J. R. 1996. Defective neuromuscular synaptogenesis in agrin-deficient mutant mice. Cell, 85**,** 525-35.
GAUTAM, M., NOAKES, P. G., MUDD, J., NICHOL, M., CHU, G. C., SANES, J. R. & MERLIE, J. P. 1995. Failure of postsynaptic specialization to develop at neuromuscular junctions of rapsyn-deficient mice. Nature, 377**,** 232-6.
GESEMANN, M., DENZER, A. J. & RUEGG, M. A. 1995. Acetylcholine receptor-aggregating activity of agrin isoforms and mapping of the active site. J Cell Biol, 128**,** 625-36.
GHAZANFARI, N., FERNANDEZ, K. J., MURATA, Y., MORSCH, M., NGO, S. T., REDDEL, S. W., NOAKES, P. G. & PHILLIPS, W. D. 2011. Muscle specific kinase: organiser of synaptic membrane domains. Int J Biochem Cell Biol, 43**,** 295-8.
GHAZANFARI, N., MORSCH, M., TSE, N., REDDEL, S. W. & PHILLIPS, W. D. 2014. Effects of the ss2-adrenoceptor agonist, albuterol, in a mouse model of anti-MuSK myasthenia gravis. PLoS One, 9**,** e87840.
GLASS, D. J., BOWEN, D. C., STITT, T. N., RADZIEJEWSKI, C., BRUNO, J., RYAN, T. E., GIES, D. R., SHAH, S., MATTSSON, K., BURDEN, S. J., DISTEFANO, P. S., VALENZUELA, D. M., DECHIARA, T. M. & YANCOPOULOS, G. D. 1996. Agrin acts via a MuSK receptor complex. Cell, 85**,** 513-23.
GLOERICH, M. & BOS, J. L. 2010. Epac: defining a new mechanism for cAMP action. Annu Rev Pharmacol Toxicol, 50**,** 355-75.
GODFREY, E. W., NITKIN, R. M., WALLACE, B. G., RUBIN, L. L. & MCMAHAN, U. J. 1984. Components of Torpedo electric organ and muscle that cause

aggregation of acetylcholine receptors on cultured muscle cells. J Cell Biol, 99**,** 615-27.

GOEDHART, J., VON STETTEN, D., NOIRCLERC-SAVOYE, M., LELIMOUSIN, M., JOOSEN, L., HINK, M. A., VAN WEEREN, L., GADELLA, T. W. J. & ROYANT, A. 2012. Structure-guided evolution of cyan fluorescent proteins towards a quantum yield of 93%. Nature Communications, 3.

GRADY, R. M., ZHOU, H., CUNNINGHAM, J. M., HENRY, M. D., CAMPBELL, K. P. & SANES, J. R. 2000. Maturation and maintenance of the neuromuscular synapse: genetic evidence for roles of the dystrophin--glycoprotein complex. Neuron, 25**,** 279-93.

GROENEN, P. M., BUNSCHOTEN, A. E., VAN SOOLINGEN, D. & VAN EMBDEN, J. D. 1993. Nature of DNA polymorphism in the direct repeat cluster of Mycobacterium tuberculosis; application for strain differentiation by a novel typing method. Mol Microbiol, 10**,** 1057-65.

HALLOCK, P. T., XU, C. F., PARK, T. J., NEUBERT, T. A., CURRAN, T. & BURDEN, S. J. 2010. Dok-7 regulates neuromuscular synapse formation by recruiting Crk and Crk-L. Genes Dev, 24**,** 2451-61.

HAMURO, J., HIGUCHI, O., OKADA, K., UENO, M., IEMURA, S., NATSUME, T., SPEARMAN, H., BEESON, D. & YAMANASHI, Y. 2008. Mutations causing DOK7 congenital myasthenia ablate functional motifs in Dok-7. J Biol Chem, 283**,** 5518-24.

HARCOURT, L. J., SCHERTZER, J. D., RYALL, J. G. & LYNCH, G. S. 2007. Low dose formoterol administration improves muscle function in dystrophic mdx mice without increasing fatigue. Neuromuscul Disord, 17**,** 47-55.

HEINEMANN, S., BEVAN, S., KULLBERG, R., LINDSTROM, J. & RICE, J. 1977. Modulation of acetylcholine receptor by antibody against the receptor. Proc Natl Acad Sci U S A, 74**,** 3090-4.

HERRMANN, D. N., HORVATH, R., SOWDEN, J. E., GONZALEZ, M., SANCHEZ-MEJIAS, A., GUAN, Z., WHITTAKER, R. G., ALMODOVAR, J. L., LANE, M., BANSAGI, B., PYLE, A., BOCZONADI, V., LOCHMULLER, H., GRIFFIN, H., CHINNERY, P. F., LLOYD, T. E., LITTLETON, J. T. & ZUCHNER, S. 2014. Synaptotagmin 2 mutations cause an autosomal-dominant form of lambert-eaton myasthenic syndrome and nonprogressive motor neuropathy. Am J Hum Genet, 95**,** 332-9.

HOCH, W., MCCONVILLE, J., HELMS, S., NEWSOM-DAVIS, J., MELMS, A. & VINCENT, A. 2001. Auto-antibodies to the receptor tyrosine kinase MuSK in patients with myasthenia gravis without acetylcholine receptor antibodies. Nat Med, 7**,** 365-8.

HOE, N., NAKASHIMA, K., GRIGSBY, D., PAN, X., DOU, S. J., NAIDICH, S., GARCIA, M., KAHN, E., BERGMIRE-SWEAT, D. & MUSSER, J. M. 1999. Rapid molecular genetic subtyping of serotype M1 group A Streptococcus strains. Emerg Infect Dis, 5**,** 254-63.

HOFF, J. M., DALTVEIT, A. K. & GILHUS, N. E. 2007. Myasthenia gravis in pregnancy and birth: identifying risk factors, optimising care. Eur J Neurol, 14**,** 38-43.

HU, Y., PAREKH-OLMEDO, H., DRURY, M., SKOGEN, M. & KMIEC, E. B. 2005. Reaction parameters of targeted gene repair in mammalian cells. Mol Biotechnol, 29**,** 197-210.

HUIJBERS, M. G., ZHANG, W., KLOOSTER, R., NIKS, E. H., FRIESE, M. B., STRAASHEIJM, K. R., THIJSSEN, P. E., VROLIJK, H., PLOMP, J. J., VOGELS, P., LOSEN, M., VAN DER MAAREL, S. M., BURDEN, S. J. & VERSCHUUREN, J. J. 2013. MuSK IgG4 autoantibodies cause myasthenia gravis by inhibiting binding between MuSK and Lrp4. *Proc Natl Acad Sci U S A,* 110**,** 20783-8.

HUM, J. M., SIEGEL, A. P., PAVALKO, F. M. & DAY, R. N. 2012. Monitoring biosensor activity in living cells with fluorescence lifetime imaging microscopy. Int J Mol Sci, 13**,** 14385-400.

INOUE, A., SETOGUCHI, K., MATSUBARA, Y., OKADA, K., SATO, N., IWAKURA, Y., HIGUCHI, O. & YAMANASHI, Y. 2009. Dok-7 activates the muscle receptor kinase MuSK and shapes synapse formation. Sci Signal, 2**,** ra7.

ISHINO, Y., SHINAGAWA, H., MAKINO, K., AMEMURA, M. & NAKATA, A. 1987. Nucleotide sequence of the iap gene, responsible for alkaline phosphatase isozyme conversion in Escherichia coli, and identification of the gene product. J Bacteriol, 169**,** 5429-33.

JACOBSON, C., COTE, P. D., ROSSI, S. G., ROTUNDO, R. L. & CARBONETTO, S. 2001. The dystroglycan complex is necessary for stabilization of acetylcholine receptor clusters at neuromuscular junctions and formation of the synaptic basement membrane. J Cell Biol, 152**,** 435-50.

JANSEN, R., EMBDEN, J. D., GAASTRA, W. & SCHOULS, L. M. 2002. Identification of genes that are associated with DNA repeats in prokaryotes. Mol Microbiol, 43**,** 1565-75.

JEPHSON, C. G., MILLS, N. A., PITT, M. C., BEESON, D., ALOYSIUS, A., MUNTONI, F., ROBB, S. A. & BAILEY, C. M. 2010. Congenital stridor with feeding difficulty as a presenting symptom of Dok7 congenital myasthenic syndrome. Int J Pediatr Otorhinolaryngol, 74**,** 991-4.

JINEK, M., CHYLINSKI, K., FONFARA, I., HAUER, M., DOUDNA, J. A. & CHARPENTIER, E. 2012. A programmable dual-RNA-guided DNA endonuclease in adaptive bacterial immunity. Science, 337**,** 816-21.

JOHNSON, M. 2006. Molecular mechanisms of beta(2)-adrenergic receptor function, response, and regulation. J Allergy Clin Immunol, 117**,** 18-24; quiz 25.

KIM, J. M., HWA, J., GARRIGA, P., REEVES, P. J., RAJBHANDARY, U. L. & KHORANA, H. G. 2005. Light-driven activation of beta 2-adrenergic receptor signaling by a chimeric rhodopsin containing the beta 2-adrenergic receptor cytoplasmic loops. Biochemistry, 44**,** 2284-92.

KIM, N. & BURDEN, S. J. 2008. MuSK controls where motor axons grow and form synapses. Nat Neurosci, 11**,** 19-27.

KIM, N., STIEGLER, A. L., CAMERON, T. O., HALLOCK, P. T., GOMEZ, A. M., HUANG, J. H., HUBBARD, S. R., DUSTIN, M. L. & BURDEN, S. J. 2008. Lrp4 is a receptor for Agrin and forms a complex with MuSK. Cell, 135**,** 334-42.

KIM, C. H., XIONG, W. C. & MEI, L. 2005. Inhibition of MuSK expression by CREB interacting with a CRE-like element and MyoD. Mol Cell Biol, 25**,** 5329-38.

KLEIMAN, R. J. & REICHARDT, L. F. 1996. Testing the agrin hypothesis. Cell, 85**,** 461-4.

KLEIN, A., PITT, M. C., MCHUGH, J. C., NIKS, E. H., SEWRY, C. A., PHADKE, R., FENG, L., MANZUR, A. Y., TIRUPATHI, S., DEVILE, C., JAYAWANT, S., FINLAYSON, S., PALACE, J., MUNTONI, F., BEESON, D. & ROBB, S.

A. 2013. DOK7 congenital myasthenic syndrome in childhood: early diagnostic clues in 23 children. Neuromuscul Disord, 23**,** 883-91.
KONECZNY, I., COSSINS, J. & VINCENT, A. 2014. The role of muscle-specific tyrosine kinase (MuSK) and mystery of MuSK myasthenia gravis. J Anat, 224**,** 29-35.
KONECZNY, I., COSSINS, J., WATERS, P., BEESON, D. & VINCENT, A. 2013. MuSK myasthenia gravis IgG4 disrupts the interaction of LRP4 with MuSK but both IgG4 and IgG1-3 can disperse preformed agrin-independent AChR clusters. PLoS One, 8**,** e80695.
KLARENBEEK, J. B., GOEDHART, J., HINK, M. A., GADELLA, T. W. J. & JALINK, K. 2011. A mTurquoise-Based cAMP Sensor for Both FLIM and Ratiometric Read-Out Has Improved Dynamic Range. Plos One, 6.
KLARENBEEK, J., GOEDHART, J., VAN BATENBURG, A., GROENEWALD, D. & JALINK, K. 2015. Fourth-Generation Epac-Based FRET Sensors for cAMP Feature Exceptional Brightness, Photostability and Dynamic Range: Characterization of Dedicated Sensors for FLIM, for Ratiometry and with High Affinity. PLoS One, 10**,** e0122513.
KRUPNICK, J. G. & BENOVIC, J. L. 1998. The role of receptor kinases and arrestins in G protein-coupled receptor regulation. Annu Rev Pharmacol Toxicol, 38**,** 289-319.
KUMMER, T. T., MISGELD, T. & SANES, J. R. 2006. Assembly of the postsynaptic membrane at the neuromuscular junction: paradigm lost. Curr Opin Neurobiol, 16**,** 74-82.
LASHLEY, D., PALACE, J., JAYAWANT, S., ROBB, S. & BEESON, D. 2010. Ephedrine treatment in congenital myasthenic syndrome due to mutations in DOK7. Neurology, 74**,** 1517-23.
LI, H. L., FUJIMOTO, N., SASAKAWA, N., SHIRAI, S., OHKAME, T., SAKUMA, T., TANAKA, M., AMANO, N., WATANABE, A., SAKURAI, H., YAMAMOTO, T., YAMANAKA, S. & HOTTA, A. 2015. Precise correction of the dystrophin gene in duchenne muscular dystrophy patient induced pluripotent stem cells by TALEN and CRISPR-Cas9. Stem Cell Reports, 4**,** 143-54.
LI, Z., FORESTER, N. & VINCENT, A. 1996. Modulation of acetylcholine receptor function in TE671 (rhabdomyosarcoma) cells by non-AChR ligands: possible relevance to seronegative myasthenia gravis. J Neuroimmunol, 64**,** 179-83.
LIEWLUCK, T., SELCEN, D. & ENGEL, A. G. 2011. Beneficial effects of albuterol in congenital endplate acetylcholinesterase deficiency and Dok-7 myasthenia. Muscle Nerve, 44**,** 789-94.
LIN, W., BURGESS, R. W., DOMINGUEZ, B., PFAFF, S. L., SANES, J. R. & LEE, K. F. 2001. Distinct roles of nerve and muscle in postsynaptic differentiation of the neuromuscular synapse. Nature, 410**,** 1057-64.
LIN, W., DOMINGUEZ, B., YANG, J., ARYAL, P., BRANDON, E. P., GAGE, F. H. & LEE, K. F. 2005. Neurotransmitter acetylcholine negatively regulates neuromuscular synapse formation by a Cdk5-dependent mechanism. Neuron, 46**,** 569-79.
LINDSTROM, J. M., SEYBOLD, M. E., LENNON, V. A., WHITTINGHAM, S. & DUANE, D. D. 1976. Antibody to acetylcholine receptor in myasthenia gravis. Prevalence, clinical correlates, and diagnostic value. Neurology, 26**,** 1054-9.

LONG, C., MCANALLY, J. R., SHELTON, J. M., MIREAULT, A. A., BASSEL-DUBY, R. & OLSON, E. N. 2014. Prevention of muscular dystrophy in mice by CRISPR/Cas9-mediated editing of germline DNA. Science, 345**,** 1184-8.

LUO, S., ZHANG, B., DONG, X. P., TAO, Y., TING, A., ZHOU, Z., MEIXIONG, J., LUO, J., CHIU, F. C., XIONG, W. C. & MEI, L. 2008. HSP90 beta regulates rapsyn turnover and subsequent AChR cluster formation and maintenance. Neuron, 60**,** 97-110.

LUO, Z. G., WANG, Q., ZHOU, J. Z., WANG, J., LUO, Z., LIU, M., HE, X., WYNSHAW-BORIS, A., XIONG, W. C., LU, B. & MEI, L. 2002. Regulation of AChR clustering by Dishevelled interacting with MuSK and PAK1. Neuron, 35**,** 489-505.

LYNCH, G. S. & RYALL, J. G. 2008. Role of beta-adrenoceptor signaling in skeletal muscle: implications for muscle wasting and disease. Physiol Rev, 88**,** 729-67.

MALI, P., YANG, L., ESVELT, K. M., AACH, J., GUELL, M., DICARLO, J. E., NORVILLE, J. E. & CHURCH, G. M. 2013. RNA-guided human genome engineering via Cas9. Science, 339**,** 823-6.

MARTIN, A. R. 1994. Amplification of neuromuscular transmission by postjunctional folds. Proc Biol Sci, 258**,** 321-6.

MARTINEZ-PENA Y VALENZUELA, I., MOUSLIM, C. & AKAABOUNE, M. 2010. Calcium/calmodulin kinase II-dependent acetylcholine receptor cycling at the mammalian neuromuscular junction in vivo. J Neurosci, 30**,** 12455-65.

MARTINEZ-PENA Y VALENZUELA, I., PIRES-OLIVEIRA, M. & AKAABOUNE, M. 2013. PKC and PKA regulate AChR dynamics at the neuromuscular junction of living mice. PLoS One, 8**,** e81311.

MASELLI, R. A., ARREDONDO, J., CAGNEY, O., NG, J. J., ANDERSON, J. A., WILLIAMS, C., GERKE, B. J., SOLIVEN, B. & WOLLMANN, R. L. 2010. Mutations in MUSK causing congenital myasthenic syndrome impair MuSK-Dok-7 interaction. Hum Mol Genet, 19**,** 2370-9.

MEHRABIAN, M., BRETHOUR, D., MACISAAC, S., KIM, J. K., GUNAWARDANA, C. G., WANG, H. & SCHMITT-ULMS, G. 2014. CRISPR-Cas9-based knockout of the prion protein and its effect on the proteome. PLoS One, 9**,** e114594.

METRICH, M., BERTHOUZE, M., MOREL, E., CROZATIER, B., GOMEZ, A. M. & LEZOUALC'H, F. 2010. Role of the cAMP-binding protein Epac in cardiovascular physiology and pathophysiology. Pflugers Arch, 459**,** 535-46.

MEYER, G. & WALLACE, B. G. 1998. Recruitment of a nicotinic acetylcholine receptor mutant lacking cytoplasmic tyrosine residues in its beta subunit into agrin-induced aggregates. Mol Cell Neurosci, 11**,** 324-33.

MIHAYLOVA, V., MULLER, J. S., VILCHEZ, J. J., SALIH, M. A., KABIRAJ, M. M., D'AMICO, A., BERTINI, E., WOLFLE, J., SCHREINER, F., KURLEMANN, G., RASIC, V. M., SISKOVA, D., COLOMER, J., HERCZEGFALVI, A., FABRICIOVA, K., WESCHKE, B., SCOLA, R., HOELLEN, F., SCHARA, U., ABICHT, A. & LOCHMULLER, H. 2008. Clinical and molecular genetic findings in COLQ-mutant congenital myasthenic syndromes. Brain, 131**,** 747-59.

MILONE, M. & ENGEL, A. G. 1996. Block of the endplate acetylcholine receptor channel by the sympathomimetic agents ephedrine, pseudoephedrine, and albuterol. Brain Res, 740**,** 346-52.

MINGOZZI, F. & HIGH, K. A. 2011. Therapeutic in vivo gene transfer for genetic disease using AAV: progress and challenges. Nat Rev Genet, 12**,** 341-55.
MISGELD, T., BURGESS, R. W., LEWIS, R. M., CUNNINGHAM, J. M., LICHTMAN, J. W. & SANES, J. R. 2002. Roles of neurotransmitter in synapse formation: development of neuromuscular junctions lacking choline acetyltransferase. Neuron, 36**,** 635-48.
MITTAUD, P., CAMILLERI, A. A., WILLMANN, R., ERB-VOGTLI, S., BURDEN, S. J. & FUHRER, C. 2004. A single pulse of agrin triggers a pathway that acts to cluster acetylcholine receptors. Mol Cell Biol, 24**,** 7841-54.
MIZE, C. W., KOEHLER, K. J. & COMPTON, M. E. 1999. Statistical considerations for in vitro research: II - Data to presentation. In Vitro Cellular & Developmental Biology-Plant, 35**,** 122-126.
MOJICA, F. J., FERRER, C., JUEZ, G. & RODRIGUEZ-VALERA, F. 1995. Long stretches of short tandem repeats are present in the largest replicons of the Archaea Haloferax mediterranei and Haloferax volcanii and could be involved in replicon partitioning. Mol Microbiol, 17**,** 85-93.
MORA, M., LAMBERT, E. H. & ENGEL, A. G. 1987. Synaptic vesicle abnormality in familial infantile myasthenia. Neurology, 37**,** 206-14.
MORANSARD, M., BORGES, L. S., WILLMANN, R., MARANGI, P. A., BRENNER, H. R., FERNS, M. J. & FUHRER, C. 2003. Agrin regulates rapsyn interaction with surface acetylcholine receptors, and this underlies cytoskeletal anchoring and clustering. J Biol Chem, 278**,** 7350-9.
MORGENSTERN, J. P. & LAND, H. 1990. Advanced mammalian gene transfer: high titre retroviral vectors with multiple drug selection markers and a complementary helper-free packaging cell line. Nucleic Acids Res, 18, 3587-96.
MULLER, J. S., HERCZEGFALVI, A., VILCHEZ, J. J., COLOMER, J., BACHINSKI, L. L., MIHAYLOVA, V., SANTOS, M., SCHARA, U., DESCHAUER, M., SHEVELL, M., POULIN, C., DIAS, A., SOUDO, A., HIETALA, M., AARIMAA, T., KRAHE, R., KARCAGI, V., HUEBNER, A., BEESON, D., ABICHT, A. & LOCHMULLER, H. 2007. Phenotypical spectrum of DOK7 mutations in congenital myasthenic syndromes. Brain, 130, 1497-506.
MUSUNURU, K. 2013. Genome editing of human pluripotent stem cells to generate human cellular disease models. Dis Model Mech, 6**,** 896-904.
NITKIN, R. M., SMITH, M. A., MAGILL, C., FALLON, J. R., YAO, Y. M., WALLACE, B. G. & MCMAHAN, U. J. 1987. Identification of agrin, a synaptic organizing protein from Torpedo electric organ. J Cell Biol, 105**,** 2471-8.
NOAKES, P. G., PHILLIPS, W. D., HANLEY, T. A., SANES, J. R. & MERLIE, J. P. 1993. 43K protein and acetylcholine receptors colocalize during the initial stages of neuromuscular synapse formation in vivo. Dev Biol, 155**,** 275-80.
NONNENMACHER, M. & WEBER, T. 2012. Intracellular transport of recombinant adeno-associated virus vectors. Gene Ther, 19**,** 649-58.
OHKAWARA, B., CABRERA-SERRANO, M., NAKATA, T., MILONE, M., ASAI, N., ITO, K., ITO, M., MASUDA, A., ITO, Y., ENGEL, A. G. & OHNO, K. 2014. LRP4 third beta-propeller domain mutations cause novel congenital myasthenia by compromising agrin-mediated MuSK signaling in a position-specific manner. Hum Mol Genet, 23**,** 1856-68.

OHNO, K., BRENGMAN, J., TSUJINO, A. & ENGEL, A. G. 1998. Human endplate acetylcholinesterase deficiency caused by mutations in the collagen-like tail subunit (ColQ) of the asymmetric enzyme. Proc Natl Acad Sci U S A, 95**,** 9654-9.

OHNO, K., ENGEL, A. G., SHEN, X. M., SELCEN, D., BRENGMAN, J., HARPER, C. M., TSUJINO, A. & MILONE, M. 2002. Rapsyn mutations in humans cause endplate acetylcholine-receptor deficiency and myasthenic syndrome. Am J Hum Genet, 70**,** 875-85.

OHNO, K., ITO, M., KAWAKAMI, Y., KREJCI, E. & ENGEL, A. G. 2013. Specific binding of collagen Q to the neuromuscular junction is exploited to cure congenital myasthenia and to explore bases of myasthenia gravis. Chem Biol Interact, 203**,** 335-40.

OHNO, K., QUIRAM, P. A., MILONE, M., WANG, H. L., HARPER, M. C., PRUITT, J. N., 2ND, BRENGMAN, J. M., PAO, L., FISCHBECK, K. H., CRAWFORD, T. O., SINE, S. M. & ENGEL, A. G. 1997. Congenital myasthenic syndromes due to heteroallelic nonsense/missense mutations in the acetylcholine receptor epsilon subunit gene: identification and functional characterization of six new mutations. Hum Mol Genet, 6**,** 753-66.

OHNO, K., TSUJINO, A., BRENGMAN, J. M., HARPER, C. M., BAJZER, Z., UDD, B., BEYRING, R., ROBB, S., KIRKHAM, F. J. & ENGEL, A. G. 2001. Choline acetyltransferase mutations cause myasthenic syndrome associated with episodic apnea in humans. Proc Natl Acad Sci U S A, 98**,** 2017-22.

OHNO, K., WANG, H. L., MILONE, M., BREN, N., BRENGMAN, J. M., NAKANO, S., QUIRAM, P., PRUITT, J. N., SINE, S. M. & ENGEL, A. G. 1996. Congenital myasthenic syndrome caused by decreased agonist binding affinity due to a mutation in the acetylcholine receptor epsilon subunit. Neuron, 17**,** 157-70.

OKADA, K., INOUE, A., OKADA, M., MURATA, Y., KAKUTA, S., JIGAMI, T., KUBO, S., SHIRAISHI, H., EGUCHI, K., MOTOMURA, M., AKIYAMA, T., IWAKURA, Y., HIGUCHI, O. & YAMANASHI, Y. 2006. The muscle protein Dok-7 is essential for neuromuscular synaptogenesis. Science, 312**,** 1802-1805.

OTERO-CRUZ, J. D., BAEZ-PAGAN, C. A., DORNA-PEREZ, L., GRAJALES-REYES, G. E., RAMIREZ-ORDONEZ, R. T., LUCIANO, C. A., GOMEZ, C. M. & LASALDE-DOMINICCI, J. A. 2010. Decoding pathogenesis of slow-channel congenital myasthenic syndromes using recombinant expression and mice models. P R Health Sci J, 29**,** 4-17.

PALACE, J., LASHLEY, D., BAILEY, S., JAYAWANT, S., CARR, A., MCCONVILLE, J., ROBB, S. & BEESON, D. 2012. Clinical features in a series of fast channel congenital myasthenia syndrome. Neuromuscul Disord, 22**,** 112-7.

PALACE, J., LASHLEY, D., NEWSOM-DAVIS, J., COSSINS, J., MAXWELL, S., KENNETT, R., JAYAWANT, S., YAMANASHI, Y. & BEESON, D. 2007. Clinical features of the DOK7 neuromuscular junction synaptopathy. Brain, 130**,** 1507-15.

PARR, J. R., ANDREW, M. J., FINNIS, M., BEESON, D., VINCENT, A. & JAYAWANT, S. 2014. How common is childhood myasthenia? The UK incidence and prevalence of autoimmune and congenital myasthenia. Arch Dis Child, 99**,** 539-42.

PONSIOEN, B., ZHAO, J., RIEDL, J., ZWARTKRUIS, F., VAN DER KROGT, G., ZACCOLO, M., MOOLENAAR, W. H., BOS, J. L. & JALINK, K. 2004. Detecting cAMP-induced Epac activation by fluorescence resonance energy transfer: Epac as a novel cAMP indicator. EMBO Rep, 5**,** 1176-80.

QIAN, Y. K., CHAN, A. W., MADHAVAN, R. & PENG, H. B. 2008. The function of Shp2 tyrosine phosphatase in the dispersal of acetylcholine receptor clusters. BMC Neurosci, 9**,** 70.

RAN, F. A., HSU, P. D., WRIGHT, J., AGARWALA, V., SCOTT, D. A. & ZHANG, F. 2013. Genome engineering using the CRISPR-Cas9 system. Nat Protoc, 8**,** 2281-308.

RASPE, M., KLARENBEEK, J. & JALINK, K. 2015. Recording intracellular cAMP levels with EPAC-based FRET sensors by fluorescence lifetime imaging. Methods Mol Biol, 1294**,** 13-24.

REGAL, L., SHEN, X. M., SELCEN, D., VERHILLE, C., MEULEMANS, S., CREEMERS, J. W. & ENGEL, A. G. 2014. PREPL deficiency with or without cystinuria causes a novel myasthenic syndrome. Neurology, 82**,** 1254-60.

REHMANN, H., ARIAS-PALOMO, E., HADDERS, M. A., SCHWEDE, F., LLORCA, O. & BOS, J. L. 2008. Structure of Epac2 in complex with a cyclic AMP analogue and RAP1B. Nature, 455**,** 124-7.

RODER, I. V., CHOI, K. R., REISCHL, M., PETERSEN, Y., DIEFENBACHER, M. E., ZACCOLO, M., POZZAN, T. & RUDOLF, R. 2010. Myosin Va cooperates with PKA RIalpha to mediate maintenance of the endplate in vivo. Proc Natl Acad Sci U S A, 107**,** 2031-6.

RODER, I. V., PETERSEN, Y., CHOI, K. R., WITZEMANN, V., HAMMER, J. A., 3RD & RUDOLF, R. 2008. Role of Myosin Va in the plasticity of the vertebrate neuromuscular junction in vivo. PLoS One, 3**,** e3871.

RODRIGUEZ CRUZ, P. M., PALACE, J. & BEESON, D. 2014. Inherited disorders of the neuromuscular junction: an update. J Neurol, 261**,** 2234-43.

RODRIGUEZ CRUZ, P. M., PALACE, J., RAMJATTAN, H., JAYAWANT, S., ROBB, S. A. & BEESON, D. 2015. Salbutamol and ephedrine in the treatment of severe AChR deficiency syndromes. Neurology.

RUDOLF, R., BITTINS, C. M. & GERDES, H. H. 2011. The role of myosin V in exocytosis and synaptic plasticity. J Neurochem, 116**,** 177-91.

RUFF, R. L. 2011. Endplate contributions to the safety factor for neuromuscular transmission. Muscle Nerve, 44**,** 854-61.

RYALL, J. G., SILLENCE, M. N. & LYNCH, G. S. 2006. Systemic administration of beta2-adrenoceptor agonists, formoterol and salmeterol, elicit skeletal muscle hypertrophy in rats at micromolar doses. Br J Pharmacol, 147**,** 587-95.

SADASIVAM, G., WILLMANN, R., LIN, S., ERB-VOGTLI, S., KONG, X. C., RUEGG, M. A. & FUHRER, C. 2005. Src-family kinases stabilize the neuromuscular synapse in vivo via protein interactions, phosphorylation, and cytoskeletal linkage of acetylcholine receptors. J Neurosci, 25**,** 10479-93.

SANES, J. R. & LICHTMAN, J. W. 2001. Induction, assembly, maturation and maintenance of a postsynaptic apparatus. Nat Rev Neurosci, 2**,** 791-805.

SCHAAF, C. P. 2014. Nicotinic acetylcholine receptors in human genetic disease. Genet Med, 16**,** 649-56.

SCHARA, U., BARISIC, N., DESCHAUER, M., LINDBERG, C., STRAUB, V., STRIGL-PILL, N., WENDT, M., ABICHT, A., MULLER, J. S. & LOCHMULLER, H. 2009. Ephedrine therapy in eight patients with congenital

myasthenic syndrome due to DOK7 mutations. Neuromuscul Disord, 19**,** 828-32.

SEKAR, R. B. & PERIASAMY, A. 2003. Fluorescence resonance energy transfer (FRET) microscopy imaging of live cell protein localizations. J Cell Biol, 160**,** 629-33.

SELCEN, D., MILONE, M., SHEN, X. M., HARPER, C. M., STANS, A. A., WIEBEN, E. D. & ENGEL, A. G. 2008. Dok-7 myasthenia: phenotypic and molecular genetic studies in 16 patients. Ann Neurol, 64**,** 71-87.

SELCEN, D., OHKAWARA, B., SHEN, X. M., MCEVOY, K., OHNO, K. & ENGEL, A. G. 2015. Impaired Synaptic Development, Maintenance, and Neuromuscular Transmission in LRP4-Related Myasthenia. JAMA Neurol, 72**,** 889-96.

SENDEREK, J., MULLER, J. S., DUSL, M., STROM, T. M., GUERGUELTCHEVA, V., DIEPOLDER, I., LAVAL, S. H., MAXWELL, S., COSSINS, J., KRAUSE, S., MUELAS, N., VILCHEZ, J. J., COLOMER, J., MALLEBRERA, C. J., NASCIMENTO, A., NAFISSI, S., KARIMINEJAD, A., NILIPOUR, Y., BOZORGMEHR, B., NAJMABADI, H., RODOLICO, C., SIEB, J. P., STEINLEIN, O. K., SCHLOTTER, B., SCHOSER, B., KIRSCHNER, J., HERRMANN, R., VOIT, T., OLDFORS, A., LINDBERGH, C., URTIZBEREA, A., VON DER HAGEN, M., HUBNER, A., PALACE, J., BUSHBY, K., STRAUB, V., BEESON, D., ABICHT, A. & LOCHMULLER, H. 2011. Hexosamine biosynthetic pathway mutations cause neuromuscular transmission defect. Am J Hum Genet, 88**,** 162-72.

SENIS, E., FATOUROS, C., GROSSE, S., WIEDTKE, E., NIOPEK, D., MUELLER, A. K., BORNER, K. & GRIMM, D. 2014. CRISPR/Cas9-mediated genome engineering: an adeno-associated viral (AAV) vector toolbox. Biotechnol J, 9**,** 1402-12.

SHEN, X. M., DEYMEER, F., SINE, S. M. & ENGEL, A. G. 2006. Slow-channel mutation in acetylcholine receptor alphaM4 domain and its efficient knockdown. Ann Neurol, 60**,** 128-36.

SHER, E. & CLEMENTI, F. 1984. Agonist-induced internalization of the beta adrenergic receptor in a smooth muscle cell line. Biochem Biophys Res Commun, 124**,** 863-70.

SHI, L., FU, A. K. & IP, N. Y. 2012. Molecular mechanisms underlying maturation and maintenance of the vertebrate neuromuscular junction. Trends Neurosci, 35**,** 441-53.

SIEB, J. P. & ENGEL, A. G. 1993. Ephedrine: effects on neuromuscular transmission. Brain Res, 623**,** 167-71.

SLATER, C. R., FAWCETT, P. R., WALLS, T. J., LYONS, P. R., BAILEY, S. J., BEESON, D., YOUNG, C. & GARDNER-MEDWIN, D. 2006. Pre- and post-synaptic abnormalities associated with impaired neuromuscular transmission in a group of patients with 'limb-girdle myasthenia'. Brain, 129**,** 2061-76.

SMITH, C. L., MITTAUD, P., PRESCOTT, E. D., FUHRER, C. & BURDEN, S. J. 2001. Src, Fyn, and Yes are not required for neuromuscular synapse formation but are necessary for stabilization of agrin-induced clusters of acetylcholine receptors. J Neurosci, 21**,** 3151-60.

SUDA, T. & LIU, D. 2007. Hydrodynamic gene delivery: its principles and applications. Mol Ther, 15**,** 2063-9.

TATTERSFIELD, A. E. 2006. Current issues with beta2-adrenoceptor agonists: historical background. Clin Rev Allergy Immunol, 31**,** 107-18.

TEZUKA, T., INOUE, A., HOSHI, T., WEATHERBEE, S. D., BURGESS, R. W., UETA, R. & YAMANASHI, Y. 2014. The MuSK activator agrin has a separate role essential for postnatal maintenance of neuromuscular synapses. Proc Natl Acad Sci U S A, 111**,** 16556-61.

TINTIGNAC, L. A., BRENNER, H. R. & RUEGG, M. A. 2015. Mechanisms Regulating Neuromuscular Junction Development and Function and Causes of Muscle Wasting. Physiol Rev, 95**,** 809-52.

UNWIN, N. 2005. Refined structure of the nicotinic acetylcholine receptor at 4A resolution. J Mol Biol, 346**,** 967-89.

VALENZUELA, D. M., STITT, T. N., DISTEFANO, P. S., ROJAS, E., MATTSSON, K., COMPTON, D. L., NUNEZ, L., PARK, J. S., STARK, J. L., GIES, D. R. & ET AL. 1995. Receptor tyrosine kinase specific for the skeletal muscle lineage: expression in embryonic muscle, at the neuromuscular junction, and after injury. Neuron, 15**,** 573-84.

VINCENT, A., WATERS, P., LEITE, M. I., JACOBSON, L., KONECZNY, I., COSSINS, J. & BEESON, D. 2012. Antibodies identified by cell-based assays in myasthenia gravis and associated diseases. Ann N Y Acad Sci, 1274**,** 92-8.

WAHL, M., RAHN, H. J., ROHLICKE, T., KELL, G., NETTELS, D., HILLGER, F., SCHULER, B. & ERDMANN, R. 2008. Scalable time-correlated photon counting system with multiple independent input channels. Rev Sci Instrum, 79**,** 123113.

WALLACE, B. G. 1988. Regulation of agrin-induced acetylcholine receptor aggregation by Ca++ and phorbol ester. J Cell Biol, 107**,** 267-78.

WALLACE, B. G. 1989. Agrin-induced specializations contain cytoplasmic, membrane, and extracellular matrix-associated components of the postsynaptic apparatus. J Neurosci, 9**,** 1294-302.

WALLACE, B. G. 1994. Staurosporine inhibits agrin-induced acetylcholine receptor phosphorylation and aggregation. J Cell Biol, 125**,** 661-8.

WALLACE, B. G., QU, Z. & HUGANIR, R. L. 1991. Agrin induces phosphorylation of the nicotinic acetylcholine receptor. Neuron, 6**,** 869-78.

WANG, M. D. & AXELROD, D. 1994. Time-lapse total internal reflection fluorescence video of acetylcholine receptor cluster formation on myotubes. Dev Dyn, 201**,** 29-40.

WATTY, A., NEUBAUER, G., DREGER, M., ZIMMER, M., WILM, M. & BURDEN, S. J. 2000. The in vitro and in vivo phosphotyrosine map of activated MuSK. Proc Natl Acad Sci U S A, 97**,** 4585-90.

WEATHERBEE, S. D., ANDERSON, K. V. & NISWANDER, L. A. 2006. LDL-receptor-related protein 4 is crucial for formation of the neuromuscular junction. Development, 133**,** 4993-5000.

WEBB, B. A., ZHOU, S., EVES, R., SHEN, L., JIA, L. & MAK, A. S. 2006. Phosphorylation of cortactin by p21-activated kinase. Arch Biochem Biophys, 456**,** 183-93.

WEBSTER, R. G., COSSINS, J., LASHLEY, D., MAXWELL, S., LIU, W. W., WICKENS, J. R., MARTINEZ-MARTINEZ, P., DE BAETS, M. & BEESON, D. 2013. A mouse model of the slow channel myasthenic syndrome: Neuromuscular physiology and effects of ephedrine treatment. Exp Neurol, 248**,** 286-98.

WESTON, C., GORDON, C., TERESSA, G., HOD, E., REN, X. D. & PRIVES, J. 2003. Cooperative regulation by Rac and Rho of agrin-induced acetylcholine receptor clustering in muscle cells. J Biol Chem, 278**,** 6450-5.

WESTON, C. A., TERESSA, G., WEEKS, B. S. & PRIVES, J. 2007. Agrin and laminin induce acetylcholine receptor clustering by convergent, Rho GTPase-dependent signaling pathways. J Cell Sci, 120**,** 868-75.

WESTON, C., YEE, B., HOD, E. & PRIVES, J. 2000. Agrin-induced acetylcholine receptor clustering is mediated by the small guanosine triphosphatases Rac and Cdc42. J Cell Biol, 150**,** 205-12.

WITTING, N. & VISSING, J. 2014. Pharmacologic treatment of downstream of tyrosine kinase 7 congenital myasthenic syndrome. JAMA Neurol, 71**,** 350-4.

WOOD, S. J. & SLATER, C. R. 2001. Safety factor at the neuromuscular junction. Progress in Neurobiology, 64**,** 393-429.

WU, H., XIONG, W. C. & MEI, L. 2010. To build a synapse: signaling pathways in neuromuscular junction assembly. Development, 137**,** 1017-33.

XIAO-JIE, L., HUI-YING, X., ZUN-PING, K., JIN-LIAN, C. & LI-JUAN, J. 2015. CRISPR-Cas9: a new and promising player in gene therapy. J Med Genet, 52**,** 289-96.

YAFFE, D. & SAXEL, O. 1977. Serial passaging and differentiation of myogenic cells isolated from dystrophic mouse muscle. Nature, 270, 725-7.

YANG, X., ARBER, S., WILLIAM, C., LI, L., TANABE, Y., JESSELL, T. M., BIRCHMEIER, C. & BURDEN, S. J. 2001. Patterning of muscle acetylcholine receptor gene expression in the absence of motor innervation. Neuron, 30**,** 399-410.

YANG, Z. X., XU, K. L. & XIONG, H. 2015. Clinical characteristics and therapeutic evaluation of childhood myasthenia gravis. Exp Ther Med, 9**,** 1363-1368.

YIN, H., XUE, W., CHEN, S., BOGORAD, R. L., BENEDETTI, E., GROMPE, M., KOTELIANSKY, V., SHARP, P. A., JACKS, T. & ANDERSON, D. G. 2014. Genome editing with Cas9 in adult mice corrects a disease mutation and phenotype. Nat Biotechnol, 32**,** 551-3.

YOUNG, H. S., HERBETTE, L. G. & SKITA, V. 2003. Alpha-bungarotoxin binding to acetylcholine receptor membranes studied by low angle X-ray diffraction. Biophys J, 85, 943-53.

ZHANG, B., LUO, S., DONG, X. P., ZHANG, X., LIU, C., LUO, Z., XIONG, W. C. & MEI, L. 2007. Beta-catenin regulates acetylcholine receptor clustering in muscle cells through interaction with rapsyn. J Neurosci, 27**,** 3968-73.